Numerical Studies on Mass Transfer Enhancement by Vortex Generators

A Thesis submitted

in partial fulfilment for the degree of

Doctor of Philosophy

by

Aravind G P

Department of Aerospace Engineering

INDIAN INSTITUTE OF SPACE SCIENCE AND TECHNOLOGY

THIRUVANANTHAPURAM - 695 547

February 2020

CERTIFICATE

This is to certify that the thesis titled *Numerical Studies on Mass Transfer Enhancement by Vortex Generators* submitted by **Aravind. G. P**, to the Indian Institute of Space Science and Technology, Thiruvananthapuram, in partial fulfillment for the award of the degree of **Doctor of Philosophy**, is a bonafide record of the original work carried out by him under my supervision. The contents of this thesis, in full or in parts, have not been submitted to any other Institute or University for the award of any degree or diploma.

Dr. Deepu. M
Research Supervisor
Associate Professor
Department of Aerospace Engineering

Dr. Manoj T. Nair
Head of the department
Department of Aerospace Engineering
IIST

Place: IIST, Thiruvanathapuram
Date: 28 February 2020

Declaration

I declare that this thesis titled *Numerical Studies on Mass Transfer Enhancement by Vortex Generators* submitted in partial fulfillment for the award of the degree of **Doctor of Philosophy** is a record of the original work carried out by me under the supervision of **Dr. Deepu. M.** and has not formed the basis for the award of any degree, diploma, associateship, fellowship, or other titles in this or any other Institution or University of higher learning. In keeping with the ethical practice in reporting scientific information, due acknowledgments have been made wherever the findings of others have been cited.

Place: IIST, Thiruvanathapuram
Date: 28 February 2020

Aravind. G. P.
SC15D024

Acknowledgements

First of all, I would like to thank my guide Dr.Deepu M. for his constant support and guidance. This research work would not have been possible without the constant encouragement and advice extended to me by him. I will forever be grateful to you sir.

Besides my advisor, I would like to thank the rest of my Doctoral Committee: Dr. A. Sameen (Professor, Department of Aerospace ,IIT Madras), Dr. Manoj T Nair (DC chairman, HOD Department of Aerospace, IIST), Dr. Praveen Nair (Scientist Engineer, ISRO), Dr. Sudheesh Chethil (Associate Professor, Department of Physics, IIST) and Dr. P. Pradeep Kumar (Associate Professor, Department of Aerospace ,IIST), for their insightful comments and encouragement, but also for the hard question which incented me to widen my research from various perspectives. I sincerely thank to Dr. A. Salih (former DC chairman, Professor, Department of Aerospace ,IIST) for his valuable valuable support and technical guidance throughout the research.

I also express my gratitude and thanks to Director, IIST, Dean academics, and Dean R & D for providing me the research ambience during my tenure in IIST.

I express my thanks and wishes to my colleagues, Ms. G.S. Athira, Ms. V.C. Swetha, Ms. Soumya Asokan, Mr. K.M. Muhammad Rafi, Mr. S. Jayakrishnan, Mr. S. L. Nandakrishnan, Mr. S.Kiran, Mr. S. Gokul, Mr. R. Rajesh, Mr. M. Deepak, Mr. K. Prabith, Mr. Aryadutt Oamjee, Mr. K.M. Muhammad Shiyas, Mr. A. Dhanesh, Mrs. Anuja Vijayan, Ms. M. Aswathy, Mr. K.P. Sarath, Mr. C.M. Prasoon, Mr. Gaurab Khanra, Mr. A. R. Renjith, Mr. Renjith Thomas and also my other friends for sharing their knowledge with me and comfort they provided me by giving a good association to me during the college days.

I would also like to thank my parents and my younger sister for their constant encouragement that kept me motivated through various phases of my research. Last but not the least; Thank You, God Almighty for your grace.

Abstract

Limited exchange time available for transfer processes in high speed flows calls for energy-efficient enhancement methods. Passive heat/mass transfer enhancement techniques such as flow or surface manipulations are widely preferred owing to its simplicity. Mass transfer enhancement methods by vortex generators with minimal pressure loss find applications in the field of chemical processing systems, aerospace, hybrid rocket propulsion systems, industrial gas turbines etc. Engineered surfaces, rough surfaces, extended surfaces, swirl flow generators, coiled tubes, etc. are used in conventional passive enhancement methods. Mass transfer enhancement is often achieved by generating secondary flows, and reducing boundary layer thickness that develops favorable gradients. Passive mass transfer enhancement from the surface of a liquefying substance using Lateral Sweep Vortex Generators (LSVG) alone and its combination with dimpled surface placed in high-speed flow are analyzed. Numerical simulation of three-dimensional turbulent compressible flow field involving species transport has been carried out using Advection Upstream Splitting Method (AUSM) scheme based Finite Volume solver. A temperature dependent mass efflux boundary condition has been developed and implemented in the computational procedure for updating the boundary mass flux as a function of the temperature of adjoining fluid mass. The computational procedure has been well validated using the experimental wall pressure profile and heat transfer coefficients reported for similar vortex generators placed in high-speed flow. Computations could capture the complex flow features resulted by the vortex-boundary layer interactions. Convective mass transfer of species is found to get improved in the wake region of the LSVG by the horseshoe vortices and further get transported downstream by the counter-rotating vortex pair. Extensive numerical simulations have been carried out with several lateral sweep angles of LSVG to explore the role of vortices in promotion of the convective mass transfer. It has been observed that the mass efflux enhances with an increase in sweep angle of the vortex generator due to the vorticity augmentation in the wake region. Analysis of the vortex trajectories could figure out the influence of vortex interactions leading to the peak mass efflux. An analysis using the method of images and potential flow theory establishes a coherence between vortex trajectory and location of peak mass transfer enhancement in the flow field. Further, an exponential-power law based correlation between relative Sherwood number and relative

streamwise vorticity has also been developed for various configurations analyzed. Intensity and strength of the asymmetrical vortices attributes to further mass transfer augmentation in the wake region. Placement of a Variable Sweep Vortex Generator (VSVG) in high-speed flow results in asymmetrical vortex interaction on the mass transferring surface. VSVG has a wedge shape with different sweep angles on its lateral sides and a slant top surface. This novel geometrical features induce large-scale asymmetrical transverse vortices in its wake region as the compressible freestream spills and expand over it. Thus, VSVG realizes larger gradients on associated boundaries that promote transfer effects. Oscillatory nature of the transverse counter-rotating vortex pair interaction enables the evolved mass to convect further into the free stream. Mass transport profile in the entire flow field is found to strongly depend on the vortical fluid motion. Combination of passive mass transfer enhancers is emerging due to the inherent limitations of flow manipulation that a single surface feature can perform. These methods can sustain sharp gradients on the solid-fluid interface for wider expanse, thereby the effectiveness of mass/heat transfer process can be augmented considerably. Convective mass transfer augmentation systems call for the requirement of not only the enhancement near the surface but also the evolved mass should be carried away to the farther locations in adjoining free stream. Therefore, the sustenance of the strength of the evolved vortex system in the wake of the vortex generator is a key objective while selecting combinational convective mass transfer augmenting system. Unsteady RANS method could accurately describe the unsteady vortex boundary layer interactions effects attributed by LSVG-dimple combination. Extensive numerical simulations have been performed to analyze the nature of the evolution of secondary flow structures and their role in the promotion of mass advection for various geometry and flow conditions. Q Criterion estimates have been used for identifying region of intense vortex fluid motion and its role in the promotion of mass transfer. Present vortex generator dimple combination can enhance mass transfer for the wider expanse of the domain. Unsteady numerical computations have been extended to derive correlations for the estimation of spatiotemporal convective mass transfer effects.

Table of contents

List of figures

List of tables

Nomenclature

English Letters

B Length of LSVG, mm

D Dimple foot print diameter, mm

d Distance from the trailing edge of LSVG to the dimple center, mm

D_{AB} Diffusion coefficient m^2/s

e Enthalpy, J

H Height of LSVG, mm

q Heat flux, W/m^2

h Heat transfer coefficient, W/m^{2}K

k Thermal Conductivity, W/m.K

M Molecular weight g/mol

m Mass flux kg/m^2s

Nu Nusselt number

p Pressure, Pa

r Radial distance,m

Re Reynolds number

Sh Sherwood number

Sh_R Relative Sherwood number

c Specific heat, J/KgK

T Temperature, K

t Time, s

Tu Turbulence intensity

W Width of LSVG, mm

b Width of the annulus, m

x x-coordinate, m

u Velocity in x direction, m/s

Y Mass fraction of species

y y-coordinate, m

v Velocity in y direction, m/s

z z-coordinate, m

w Velocity in z direction, m/s

Greek symbols

α, β Coefficients used in correlation for Sh

Γ Circulation

λ Depth of layer, m

μ Dynamic Viscosity, Pa.s

ω Specific dissipation rate, 1/s

ϕ Char fraction, mm

ψ Lateral sweep angle of vortex generator, $\circ$

ρ Density, kg/m^3

ξ_R Relative Vorticity, 1/s

ξ Vorticity, 1/s

Subscripts

a ambient

b base solid

c char

g vapour

k species

l liquid

s surface

Abbreviations

ASB Arc Shaped Baffles

AUSM Advection Upstream Splitting Method

BVG Baffle Vortex Generator

CFD Common Flow Down

CFU Common Flow Up

CTWH Curved Winglet Type Vortex Generators with punched holes

CTWP Curved Trapezoidal Winglet Pair

DWP Delta Winglet Pair

DWVG Delta Winglet Vortex Generator

IPWP Inclined Projected Winglet Pair

LSVG Lateral Sweep Vortex Generator

LVG Longitudinal Vortex Generators

PR Pitch Ratio

PR-W Punched Rectangular Winglet

RWP Rectangular Winglet Pair

RWVG Rectangular Winglet Vortex Generator

TDME Temperature Dependent Mass Efflux

TWP Trapezoidal Winglet Pair

VSVG Variable Sweep Vortex Generator

WPT Winglet Perforated Tape

WTT Winglet non-Perforated Tape

Chapter 1

Introduction

Passive heat and mass transfer enhancement methods are inevitable in the development of felicitous energy-efficient transfer process enhancement devices. The deliberate placement of flow manipulators sets in large scale secondary flows that can improve heat and mass transfer enhancement. Recent technology progress towards miniaturization fostered the development of effective transfer processes involving high energy density. Effective energy-efficient enhancement techniques are essential in high speed transfer processes. Passive transfer process augmentation methods are quite ideal to use in conjunction with almost all facets of heat transfer endeavors owing to its simplicity in implementation and usage. At the outset, convective heat transfer enhancement is often achieved by using a flow manipulator which itself acts as a source of increased exposure of the heat transfer surface to the adjoining fluid medium. The same surface shall also play a pivotal role in the creation of secondary flow structures which shall inject a part of the mainstream in the boundary layer in order to disturb its development. Streamwise vortices, secondary flows, and enhanced turbulence levels sustain sharper gradients in the vicinity of the heat/mass exchanging surface. Surface extensions, protrusions, swirl flow devices, and depressions are widely used for this purpose (Dewan et al. (2004)). Often an array of such surface manipulations are employed for the sustenance of amplification for a broader expanse. Compound enhancement methods are also emerging due to the inherent limitation of the transfer process intensification that an independent flow manipulator can perform in isolation. Present work focuses on passive convective mass transfer augmentation facilitated by lateral sweep vortex generators and its further modification with the introduction of surface depression, using numerical simulation. Incessant advances in research on heat and mass transfer augmentation has been witnessing over these years that attempts the exposition of the mechanism of transfer process. The advent of sophisticated visualization tools and high fidelity computational techniques have realized a paradigm shift in the research approach in recent years in elucidating the physics of secondary

flow generation and its role promotion of mass transfer. Flow past vortex generators realizes complex flow features and their interaction. Present work is a systematic exposition of the evolution of flow past lateral sweep vortex generators and resulting convective mass transfer effects. Extensive numerical simulations have been performed to bring about the physics of secondary flow generation and associated transfer process enhancement for various geometry and flow conditions. Studies are extended to investigate the possibility of combinational enhancement techniques that can be used in conjunction with lateral sweep vortex generators. Illustration of spatiotemporal aspects of the convective mass transfer process using vortex generator and dimple combination has also been carried out. Computational techniques have now matured to portray the unsteady three-dimensional turbulent flow field development over the flow manipulators with species transport. Computations in the present study have been carried out using Advection Upstream Splitting Method (AUSM) scheme based Finite Volume solver. An improvised temperature-dependent mass efflux boundary condition has been worked out and made available in the computational framework for simulating the participative boundary mass flux as a function of the temperature of co-flow. Characteristics that mark the region of intense vortex fluid motion and its correspondence in the promotion of mass transfer are established. Correlations are worked out from the extensive set of data for the use of design and implementation in real-life systems.

1.1 Single-phase transfer enhancement process using vortex generators

Work described in this thesis deals with the single-phase passive mass transfer enhancement using lateral sweep vortex generators in isolation or in coexistence with surface depression. The transfer process enhancement using flow manipulators is realized by the creation of secondary flows and its interaction with the developing boundary layer formed over the surface which exchanges heat or mass (Jacobi and Shah (1995)). Swirling motion can develop favorable gradients in developing boundary layer as it possesses high tangential velocity than in the mainstream which can laterally inject fluid mass. The nature of vortices induced by a typical vortex generator is shown in Fig 1.1. Secondary vortices are generated as a result of strong swirling fluid motion, flow separation, and friction while the fluid flow past a manipulator. These flow manipulators set in oscillation and unsteadiness that promote heat/mass transfer from the adjoining boundary. Though this enhancement technique has the advantage of low cost and ease of implementation, is usually accompanied by a modest

pressure drop penalty. Physics of fluid motion and associated mass transfer effects of various flow geometries considered for the present work are described subsequently.
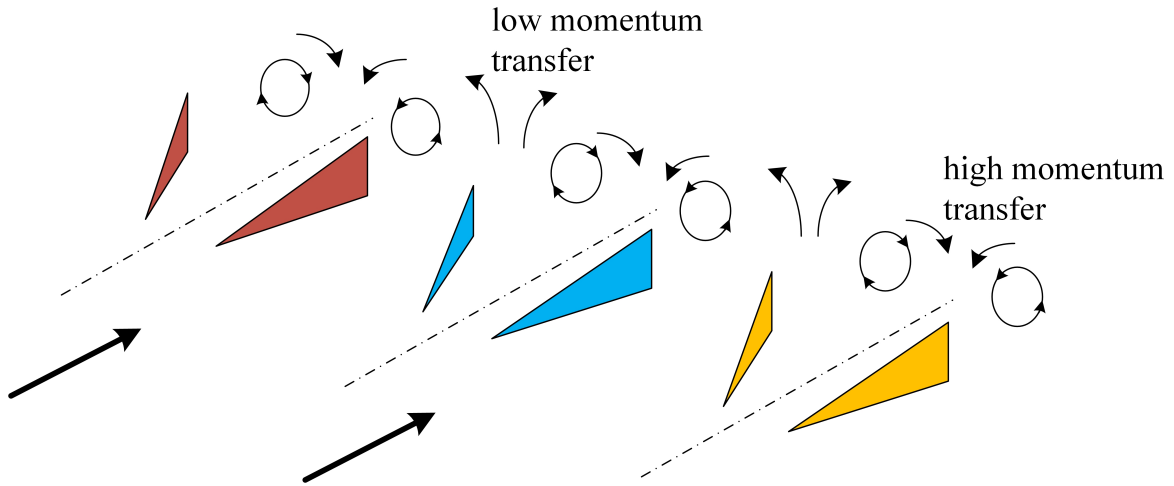
Fig. 1.1 Conceptual sketch of flow generated by longitudinal vortex generators (concept adapted from Luo et al. (2017))

1.1.1   Lateral Sweep Vortex Generator (LSVG)

Primary focus of the presentwork is to explore the passive mass transfer enhancement from the surface of a liquefying substance using a Lateral Sweep Vortex Generators (LSVG) placed in high-speed flow. The lateral sweep provided on the vortex generator is found to develop large scale vortices in its wake region as shown in Fig 1.2. The interaction of flow with the sidewalls of LSVG generates horseshoe vortices near its bottom surface as the flow expands and spills over the vortex generator. Low-pressure regions are formed at the wake of LSVG, which advects more fluid in the lateral free stream to the center. Species evolved by the liquefaction of solid substance gets transported to the mixing zone initially by the horseshoe vortices and later carried by streamwise counter-rotating vortex pair. In this process, evolved mass from the boundary adjacent to the vortex generator gets mixed-up well with the high-speed free stream as it creates low-velocity region to promote molecular diffusion. Convective mass transfer enhances with the increase in lateral sweep provided on the vortex generator, which helps to have a precise control over mass transfer augmentation. This part of the study focuses on the augmentation of mass transfer from a mass evolving boundary using an LSVG so as to explore the role of lateral sweep angle and associated dynamics of vortex system in mass transfer enhancement.
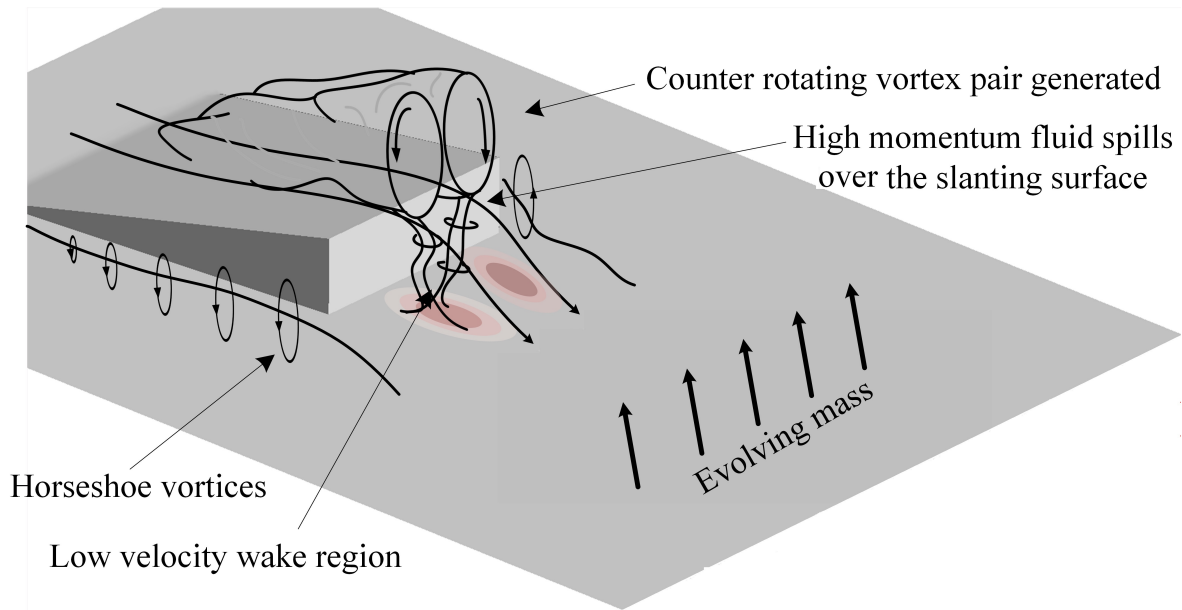
Fig. 1.2 Vortex system associated with an LSVG

1.1.2   Variable Sweep Vortex Generators (VSVG)

Variable Sweep Vortex Generators (VSVG) is a geometric modification of its parental counterpart (LSVG). This is a unique type of vortex generator with a wedge shape, with lateral sweep on its edges and an inclination on its slanting surface (VSVG) as shown in Fig 1.3 Flow separation at the lateral walls of the vortex generator generates asymmetric horse show vortices. Low-velocity regions are formed in the wake region downstream of the vortex generator, which advects more fluid in the lateral free stream to the center. The different lateral sweep provided on the vortex generator is intended to develop large-scale asymmetrical vortices in its wake region. The asymmetrical vortex system can induce much sharper gradients in the developing boundary layer than its symmetrical counterpart. Thus, VSVG realizes larger gradients on associated boundaries that promote transfer effects. Active unsymmetrical and oscillatory vortex systems is playing crucial role in convective mass transfer in this case. Mass efflux due to the liquefaction of solid substance gets transported to the mixing zone initially by the horseshoe vortices and later carried by periodically shedding asymmetric counter-rotating vortex pair. The oscillatory nature of the transverse counter-rotating vortex pair interaction enables the evolved mass to convect further into the free stream. Convective mass transfer found to get consistently enhance with the increase in the asymmetry provided to the vortex generator geometry.
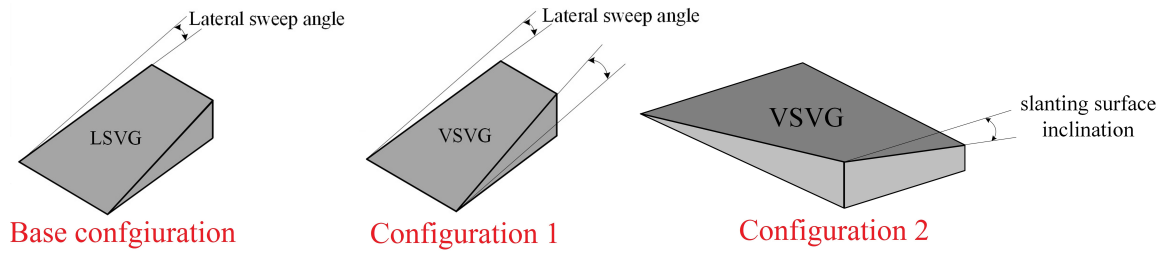
Fig. 1.3 Geometric modifications carried out for VSVG

1.1.3   Role of dimple cavity downstream of LSVG

There exist inherent spatial limitations of the extent of flow manipulation and resulting transfer process augmentation that a single surface feature can perform. Hence a combinational passive mass transfer enhancer is envisaged in the present study by placing a hemispherical depression (dimple) downstream of a lateral sweep vortex generator. Dimple alter the wake flow field, thereby it is expected to sustain sharp gradients on the solid-fluid interface for wider expanse. LSVG creates dominant vortex systems such as horseshoe vortices and
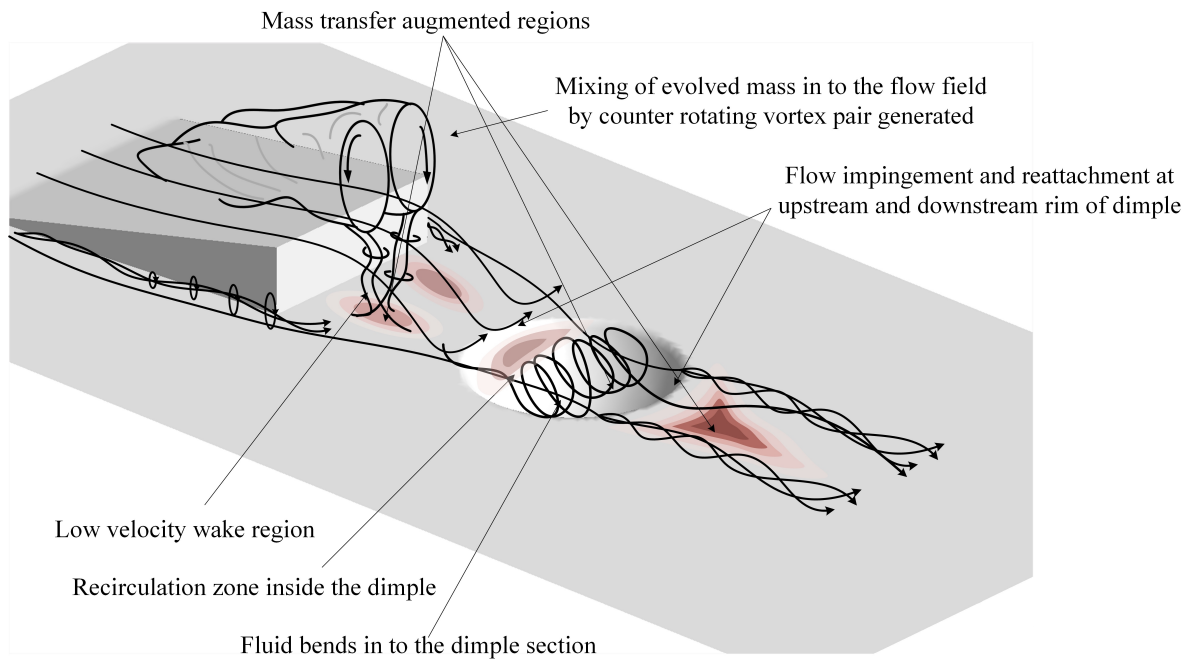
Fig. 1.4 Vortex system associated with an LSVG-dimple combination

counter-rotating vortex pairs due to the lateral surface interactions and spillage over its top slanting surface respectively. Dimple placed downstream in the wake of the vortex generator alter the reattachment process as it laterally advects the fluid free-stream as shown in Fig 1.4. This results in the active sustenance of the vortex strength for farther downstream locations

as well. Hence the combinational flow manipulation method by placing dimple in the wake of LSVG can maintain sharper gradients on the surface for a larger extend of the domain due to the presence of large scale vortical structures downstream of the dimple.

1.2 Application areas

The development of energy-efficient devices calls for heat and mass transfer enhancement methods (Siddique et al. (2010)).Mass transfer enhancement methods are essential in performance agmentation of various industrial processes and devices such as hybrid propulsion systems, chemical reactors, vapor extractors, solid fuel burners, bio-medical devices, etc. An effective mass transfer method requires creation of sharp gradients that facilitates convective mass transport and transfer of the evolved mass to the free stream at a minimal pressure loss.

1.2.1 Hybrid rocket propulsion

A typical hybrid propulsion system makes use of a solid fuel grain in contact with vaporizing oxidizer medium in which a turbulent diffusion flame is maintained (Fig 1.5) to generate thrust. Though the hybrid rocket system is believed to be safe when compared to its conventional counterparts, there are many challenges in establishing stable combustion. This is due to the low regression rate of solid fuel such as wax when oxidizer flows over it as the residence time is less. Hence the fuel grain of hybrid rocket system is designed to have maximum regression rate. Convective mass transfer enhancement endeavors can augment the performance of combustion and propulsive performance of a hybrid rocket system.
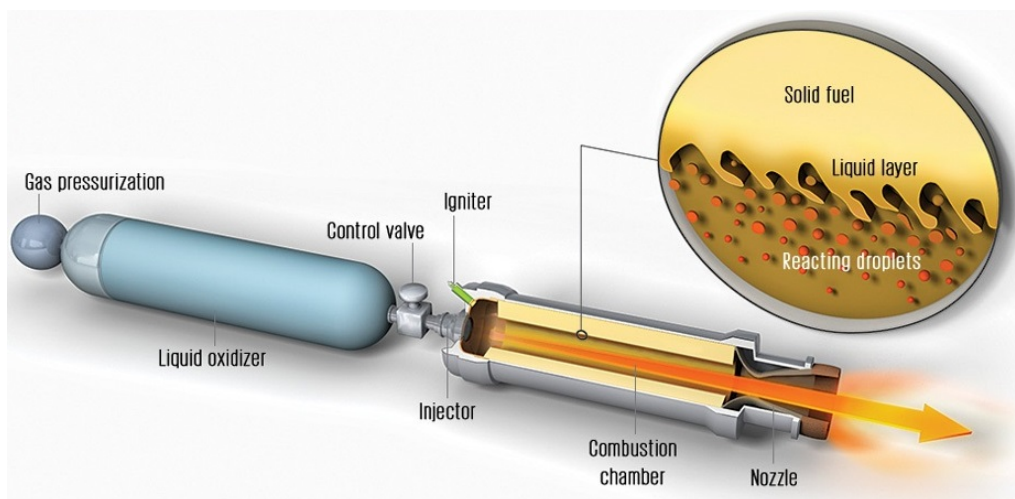
Fig. 1.5 Architecture of a typical hybrid propulsion system (adapted from Shah (2016).)

1.2.2 Vortex combustors

Vortex combustors are preferred in solid-fuel burners due to its improved residence time and lean combustion capability (Eiamsa-Ard et al. (2008)). Active recirculation zones facilitates heat and mass transfer, creates a hot pool of active reactants that can sustain stable combustion with less pollutant formation. This finds application in gas turbines, industrial burners, incinerators, etc. A dual-staging vortex-combustor (DSVC) making use of rice husk as fuel is shown in Fig 1.6. The snail entry mounted at the bottom of the combustion chamber creates the vortex/swirl flow into the combustor.
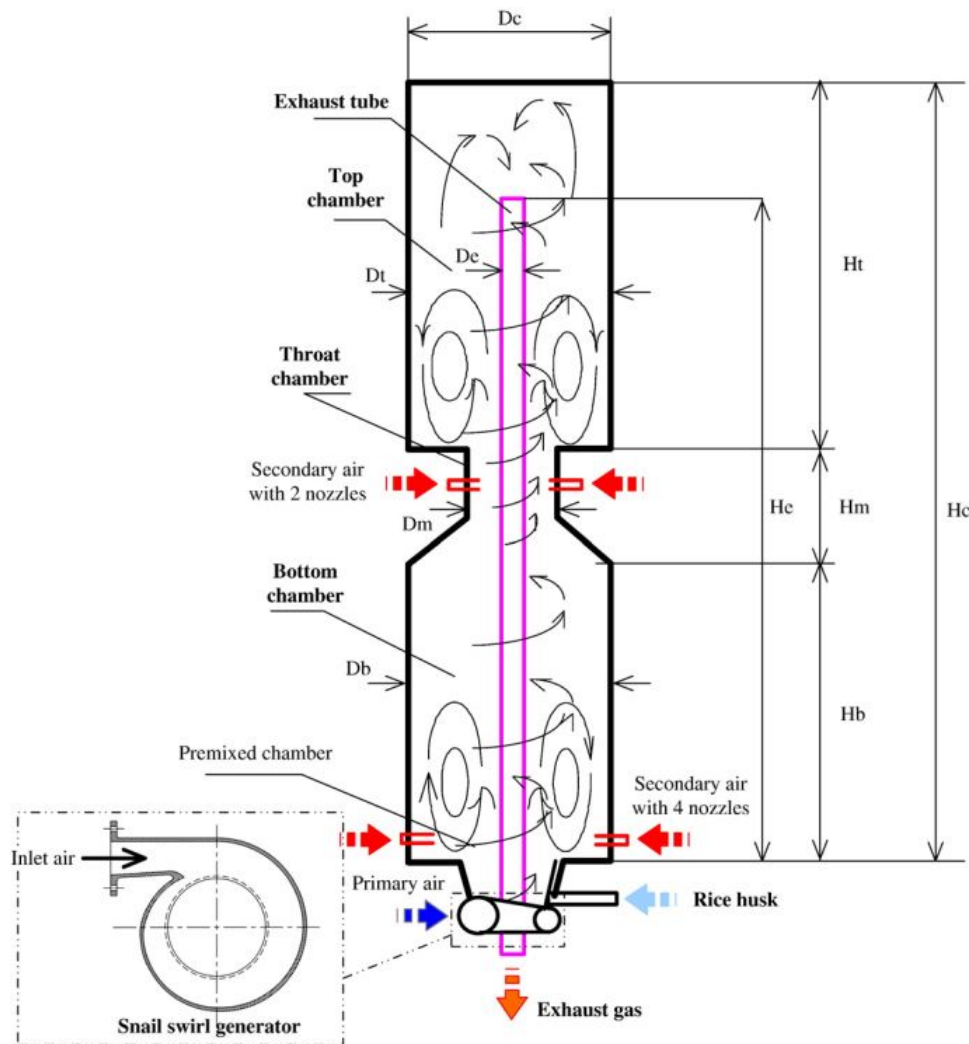
Fig. 1.6 Configuration of dual-staging vortex-combustor with snail entrance (adapted from Eiamsa-Ard et al. (2008))

Vortex combustors integrates many advantages of cyclone combustor, multistage combustor, swirl burner, pulverized coal fired combustor, and fluidized-bed combustor while

eliminates most of their inherent disadvantages. The increased swirling intensity generated by the snail at the combustor entrance results in lower pollutant formation and enlargement of recirculation region. The use of secondary air injection is found to be inefficient for the combustor with snail entrance because the split air causes lower strength of vortex flow inside.

1.3   Organization of the thesis

Numerical study of passive mass transfer enhancement expedited by lateral sweep vortex generators and its promotion with a surface depression is presented in this thesis. The research theme is outlined in this chapter. A detailed survey of established practices in flow manipulators/vortex generators with a focus on heat and mass transfer enhancement is elaborated in Chapter 2. Physics of the problem dealt here involves the flow past vortex generator placed in a liquefying substance and consequent mass transfer effects. Mathematical modeling of fluid flow, heat and mass transfer is described in Chapter 3. A temperature-dependent mass efflux boundary condition has been developed and implemented for simulating the mass evolving boundary. Well-validated numerical procedure has been subsequently used to simulate a wide variety of mass transfer enhancement options. Numerical modeling, simulation, and analysis of mass transfer enhancement adjoining the surface of a liquefying substance, using Lateral Sweep Vortex Generators (LSVG) is elaborated in Chapter 4. LSVG develops secondary flow structures. Extensive numerical studies are performed to explore the role of lateral sweep angles of LSVG in developing vortices that promotes the convective mass transfer. Studies are extended to map the unique relation of vortex trajectory and resulting peak convective mass transfer effects in the domain. The presence of variable lateral sweep provided on lateral sweep vortex generator is found to provide unsteadiness and asymmetry of vortices. Chapter 5 deals with mass transfer enhancement by asymmetrical vortex interactions. Studies are aimed to explore the precise control over mass enhancement with the variable lateral sweep provided on lateral sweep vortex generator. The slanting surface inclination provided promotes additional asymmetry to the vortices generated and observed a strong up wash and downwash of flow. A hemispherical depression (dimple) is a geometric feature capable of modifying the spectral characters of large scale flow structures thereby a unique fluctuation is imparted for the wider extent of the domain. Hence a dimple placed in the wake of LSVG circumvents the inherent limitation of vortex generator augmenting transfer effects towards the wider and farther extent of the domain. Chapter 6 discusses the role of the dimpled cavity in modification of mass transfer characteristics. Detailed numerical studies are carried out to explore the apt location of the dimple in front of the vortex generator as it is a vital factor

that decides the nature of asymmetry of wake vortices that head towards the fore-edge of the dimple. Spatiotemporal convective mass transfer characteristics in all these endeavors are summarized in the form of empirical correlations. Salient aspects of the exploration of the physics, assessment of convective mass transfer enhancement, and major contributions are summarized in Chapter 7, with some relevant remarks on possible future research extensions.

Chapter 2

Literature Review

The modern developments and energy dearth call for efficient compact heat/mass exchange processing devices. In performance viewpoint, industrial applications such as petrochemical processing systems, aerospace, hybrid rocket propulsion systems, thermal power plants, refrigeration systems, etc. calls for the tranfer process augmentation to be carried out at minimal pressure loss. Generally, heat transfer enhancement methods are classified as passive, active, and compound. Passive methods require some special surfaces to generate flow manipulations. Conventionally passive enhancement is often achieved using engineered surfaces, rough surfaces, extended surfaces, swirl flow generators, coiled tubes, etc. Webb and Kim (2005) present the novelty of these special surfaces or surface manipulations can augment heat-transfer. Vortex Generators (VGs), dealt in the present study, fall in the category of passive methods that do not require any external power. These type of methods have received wide research attention (He and Zhang (2012)) in the recent years. This unique technique can generate vortices with axes parallel to the primary flow field. Secondary vortices are generated as a result of strong swirling fluid motion, flow separation, and friction. Vortex generators can take advantage of all the aforementioned mass transfer enhancement features. Hence the longitudinal vortex generators can significantly increase the mass transfer coefficient on mass evolving boundary with minimal pressure drop, compared to the traditional mass transfer enhancement techniques. In general, passive methods have a low-pressure loss penalty, compared to active methods (Bergles and Manglik (2013)). Flow manipulators generates secondary flows, boundary layer thickness reduction, and swirling motion that develops favorable gradients for mass tranfer improvement Novel methods for improving convective mass transfer in high-speed flows are essential due to its inherent shortage of residence time. One among the celebrated comprehensive reviews of earlier era, Bergles et al. (1983) proposed more than a dozen of basic techniques for the heat transfer enhancement. This includes surface coatings, extended surfaces like fins, rough

surfaces, coiled tubes, square and helical ribs, electrostatic fields, mechanical aids, and surface vibration. The last few decades have witnessed unprecedented exploration of novel transfer enhancement techniques. A systematic survey of the exhaustive literature available in this field is presented in this chapter.

2.1 Single-phase passive enhancement methods and their classification

Research on the single-phase enhancement heat and mass transfer attained paramount interest due to the overwhelming demand for the effectiveness augmentation of various devices used in thermal science and engineering. Existing literature on heat and mass transfer enhancement run through thousands of experimental and numerical research works on various types of methods. Heat/mass transfer enhancement methods can be classified as active, passive, or compound (Bergles (2001)). Active methods require external power, such as electric or acoustic fields, mechanical devices, or surface vibration, whereas passive methods do not require external power but make use of a special surface geometry or fluid additive. Enhancement methods that simultaneously make use of more than one method are referred to as compound methods. A pictorial overview of the available single-phase passive heat/mass transfer enhancement methods is given in Fig 2.1.

Surface modifications are often used to achieve enhanced heat transfer, resulting in a transformation in flow dynamics and performance of augmentation of thermal systems. Passive heat/mass transfer enhancement can be achieved either by main flow manipulation or by introducing secondary flows. Elements such as protuberances and winglets can be intentionally placed in the flow field for generating secondary flows. The main flow field characteristics itself can be altered by bringing in flow manipulations, geometric features, etc. There are many critical reviews by Bergles and Manglik (2013), Jacobi and Shah (1995), and Gentry and Jacobi (2002) which presents various methods that can generate longitudinal vortices deliberately by means of flow manipulators.

Even though there exist many passive methods proposed by many researchers over these years, following are the popular passive enhancement techniques used in different applications (Liu and Sakr (2013)) ;

1. *Treated surfaces* – Heat transfer surface is provided with fine-scale alteration to surface finish or coating.

2. *Rough surfaces* - Surface modifications that promote turbulence in the flow field without an appreciable increase in the surface area.
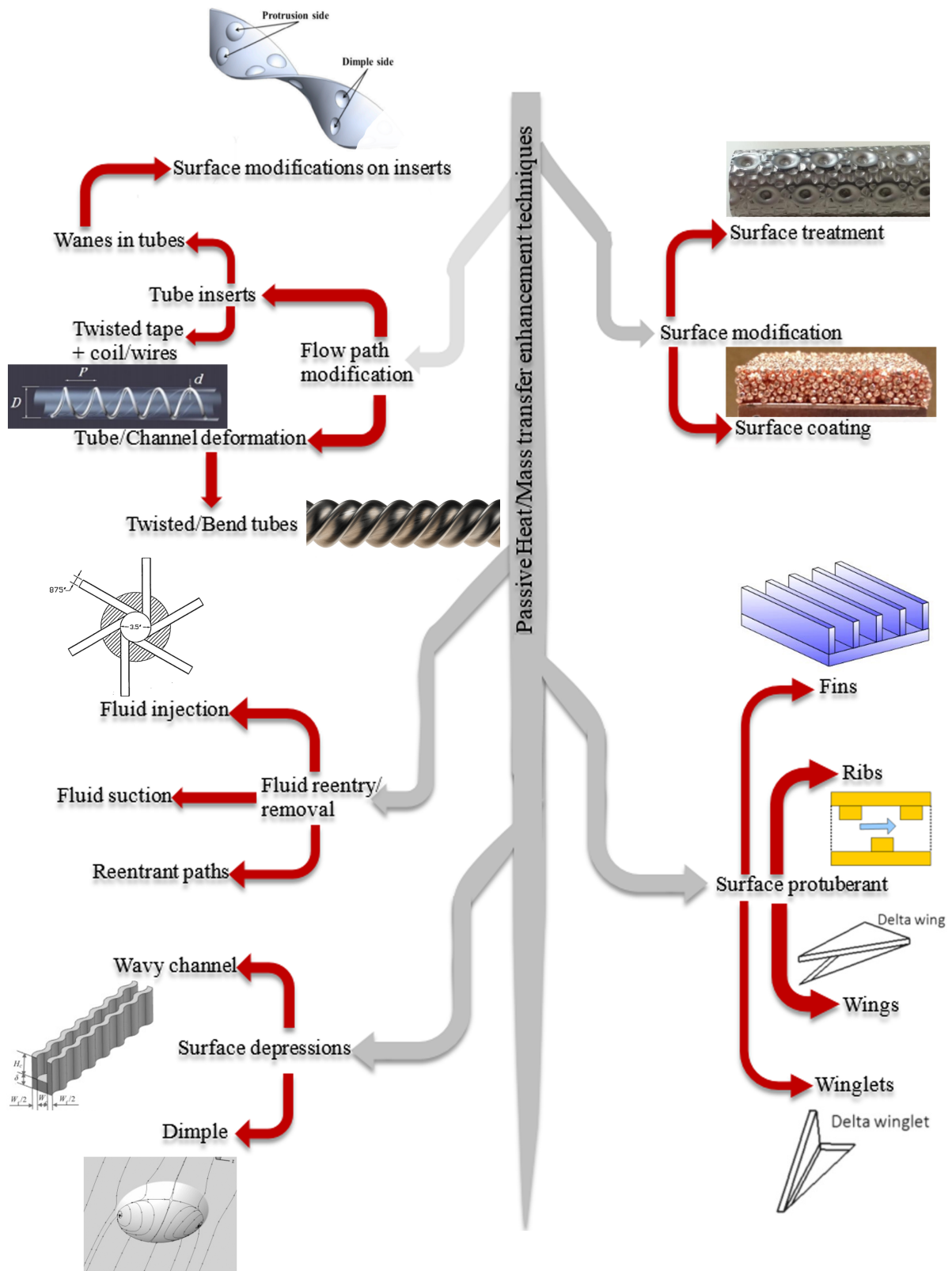
Fig. 2.1 An overview of single-phase passive heat/mass transfer enhancement methods

3. *Extended surfaces* - Improve the heat transfer coefficients by disturbing the flow field in addition to the inherent increase in the surface area.

4. *Displaced enhancement devices* – Inserts provided in confined forced convection which indirectly improves the heat transfer by displacing the fluid from the heated or cooled surface of the duct/pipe with bulk fluid to the core flow.

5. *Swirl flow devices* - Induces swirl flow or secondary recirculation axially on the flow.

6. *Coiled tubes* – Produces vortices and secondary flows that promote high heat transfer coefficients.

7. *Additives*- Additives in the form of solid particles, liquid droplets, soluble trace additives, and gas bubbles into single-phase flows for improving heat transfer.

Often there exists limitations on the transfer process enhancement that a single flow manipulator can perform. Advanced energy-efficient heat/mass transfer enhancement application aspire augmentation effects beyond the expanse of the flow manipulator. A unique combination of different passive transfer enhancement can be employed to achieve the effects towards far vicinity (Bhuiyan et al. (2014)). Such a configuration involving lateral sweep vortex generator and dimple cavity has experimented in the present work.

2.2   An overview of surface protuberant based enhancement methods and flow physics

Surface protuberances are widely used for the passive heat and mass transfer enhancement which itself is a secondary transfer surface for increased surface area. These extended surfaces generate secondary flow that leads to reduction in boundary layer thickness and favorable gradient generation for transport processes. Fins form one of the simple and primitive approaches in this category. Various types of fins used for transfer process augmentations are wavy fins (Wang et al. (1997)), offset strip fins (Manglik and Bergles (1995)), louver fins (T'Joen et al. (2009), Lyman et al. (2002), Jabardo et al. (2006), Cuevas et al. (2011),DeJong and Jacobi (2003)), sinusoidal fins (Oviedo-Tolentino et al. (2009), Gschwind et al. (1995)), herringbone wavy fins (Sarmadian et al. (2017)), plane fins (Bhuiyan et al. (2011)), perforated fins and micro fin tube (Rush et al. (1999)), etc. Extended surface in the form of cube or diamond shape Chyu et al. (2007) are also found effective. Helical/spiral fin geometries (Naphon (2007)) are also widely experimented during these years as they can be easily implemented in the form of twisted inserts in confined internal flow passage. Though fins
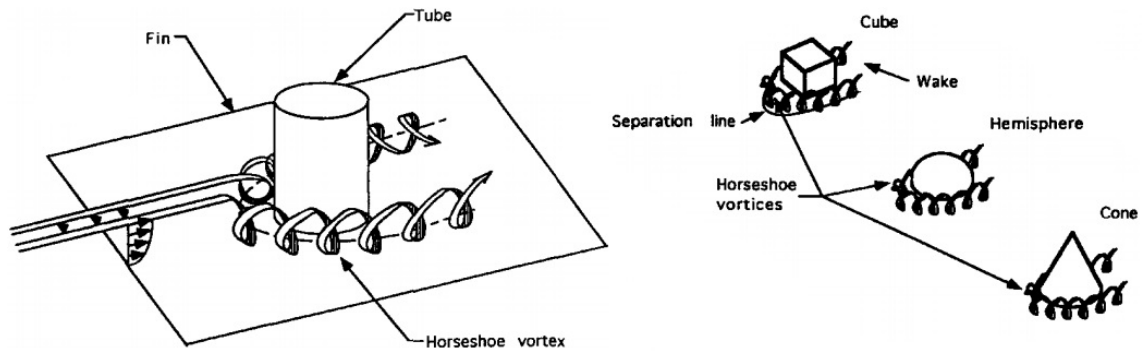
Fig. 2.2 Horseshoe vortices formed by different boundary layer protrusions (adapted from Jacobi and Shah (1995))

realize considerable enhancement, high level of pressure drop remains as an unresolved concern. Flow manipulators develop transverse vortices and longitudinal (streamwise) vortices that are widely used for improving air-side heat transfer coefficients in industrial heat exchangers. A comparison of flow features developed by different types of surface protuberances are shown in Fig 2.2. (Jacobi and Shah (1995)).

Longitudinal vortices have axis parallel to the stream wise flow direction whereas transverse vortices rotate in an axis normal to the flow direction. Longitudinal vortices are more effective in heat/mass transfer enhancement than transverse vortices because of the strong upwash and downwash generated. Interaction of these secondary flows leads to the local thinning of the thermal boundary layer as shown in Fig 2.3.
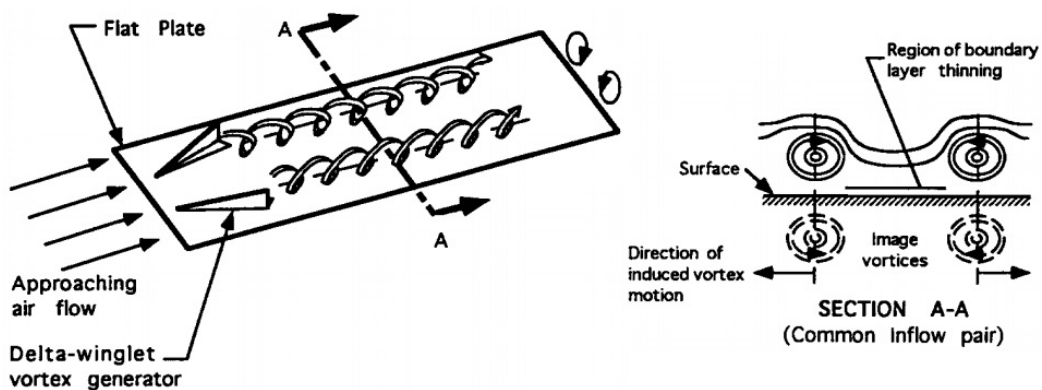
Fig. 2.3 Vortex pair interaction with boundary layer leading to its thinning and heat transfer enhancement (adapted from Jacobi and Shah (1995))

Vortex generator based mass transfer devices are capable of realizing transfer effects at minimal pressure loss (Henze et al. (2011)) and are envisaged in this thesis. Hence a detailed survey of passive enhancement options in this category are given in subsequent sections.
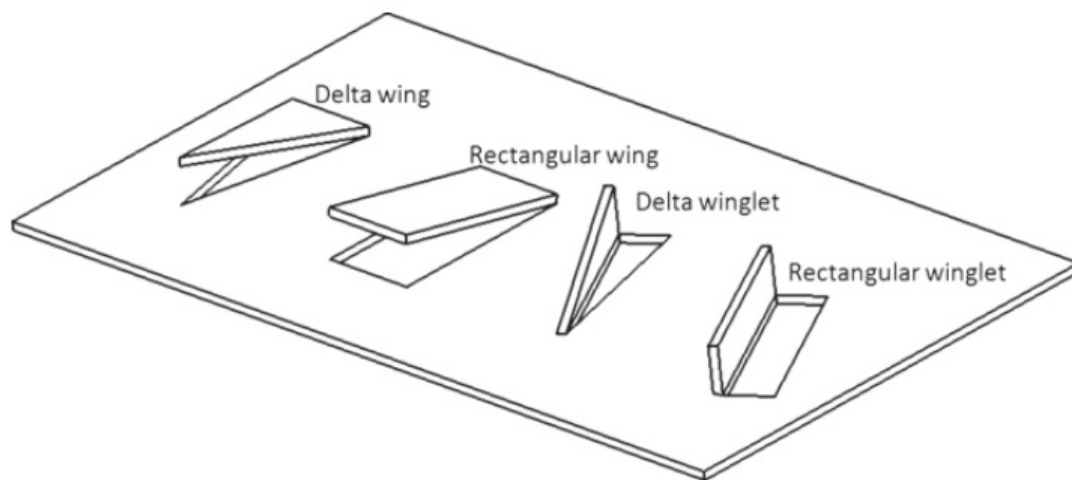
Fig. 2.4 Schematic of few common types of longitudinal vortex generators (adapted from He and Zhang (2012))

2.2.1 Longitudinal vortex generator based enhancement methods

Longitudinal Vortex Generators (LVG) are effective in creating the longitudinal vortices that are more ideal in heat/mass transfer enhancement than transverse vortices due to the presence of strong upwash and downwash. A simple schematic of the LVGs that are commonly used in practice is shown in Fig 2.4. Following are the major categories of wing/winglet type of longitudinal vortex generators and their application

1. *Delta wing*

2. *Rectangular wing*

3. *Delta winglet*

4. *Rectangular winglet*

In recent years, several numerical and experimental investigations have been reported the impact of vortex generators in the performance of heat exchangers. The influences of different types of VGs on heat transfer and friction characteristics of compact heat exchanger is documented based on the recent works reported by scientific researchers . Numerical studies performed by Biswas and Chattopadhyay (1992), Biswas et al. (1994) and Tiwari et al. (2003) describes the role of winglet type VGs on heat transfer enhancement in fin-tube heat exchanger and reportes most promising attachment methods of VGs on heat transfer surface, influence of number of winglets with position and geometry etc. When oval tubes are installed without VGs, Nu is very high at the leading edge of the passage. This is because, the hot fluid encounters with the cold fin surface. Then Nu starts decreasing as the boundary

layer thickness starts growing on the channel. However, a swirling motion caused by an oval tube intensifies the fluid mixing and hence Nu rises. While in downstream region, due to dead water zone and low fluid velocity, Nu reduces. This problem can be rectified by mounting a winglet protrusion on the fin surface. The corner or horseshoe vortex induced by the winglet pair at the upstream side swept downstream of the winglet. As a result, wake region is reduced behind the oval tubes hence enhances the heat transfer performance. It is found that for plane channel span-averaged Nu decreases in downstream direction because of the growth of the boundary layer along the channel wall and finally it becomes constant. For channel with combination of one oval tube and winglet pair 81% higher heat transfer is achieved as compared to the plane channel.Similarly, by making further improvement adding an additional winglet pair resluts in 147% higher span-averaged Nu as compared to the plane channel. Wu and Tao (2007) demonstrated the comparison between plain fin and fin with DWVGs ($\alpha = 30°$) in the presence of two aligned tube rows number at 800 $\leq$ Re $\leq$ 2000. Heat transfer augmentation is found 13-18% and corresponding pressure drop reduction is 9-11% due to the formation of longitudinal vortices and highly turbulent flow. Wall et al. (2009) conducted numerical study to verify the influence of RWVGs on heat transfer enhancement of plate fin heat exchanger and found 13% enhancement in heat transfer rate as compared to baseline case. Furthermore Hiravennavar et al. (2007) also stated the effectuality of DWVGs on heat transfer performance through numerical study and found that channel with single winglet and winglet pair lead to 33% and 67% heat transfer enhancement as compared to the channel without winglets.

He et al. (2012) numerically investigated the effect of punched winglet vortex generators in fin and tube heat exchangers. Performance of arrays of large, continuous and discontinuous punched winglets are compared in this work. Longitudinal vortices are generated when the flow past the winglet VGs due to the pressure difference created at the upstream and downstream of VG. The main vortex is formed when the fluid flow encounters with the punched delta winglet due to the flow separation at the leading edge of winglet. A part of fluid flows through the punched hole and mixes with the fluid bypassing the trailing edge of the winglet. This mixing leads to the formation of a corner vortex which is different from the conventional corner vortex reported by Biswas et al. (1996). More disturbance in the flow field can be induced by these corner vortex (Fig 2.5) as it has same characteristics and same rotation axis as of the main vortex. The strength of these corner vortex is generally weaker than the main vortex. The use of punched delta winglets allow a considerable amount of fluid stream to pass through the punched hole. This fluid stream causes reduction in the pressure difference and reduces the quantity of fluid to form main vortex.
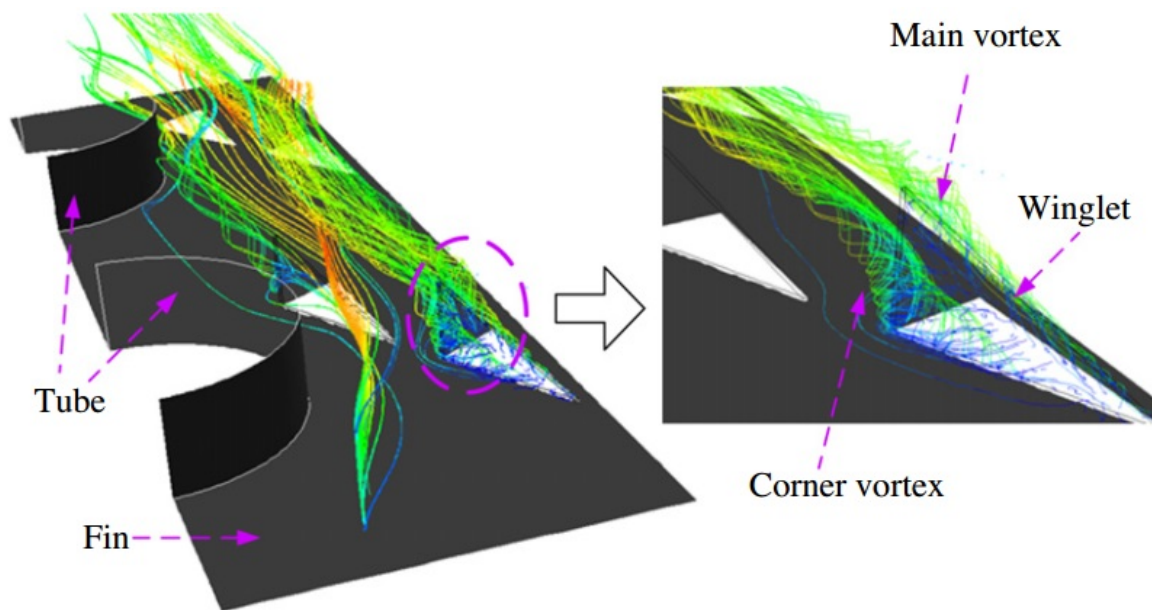
Fig. 2.5 Path lines around the delta winglet array (Figure adapted from He et al. (2012))

An array of discontinuous winglets offer best heat transfer among all kinds of vortex generators due to its unique flow organization. Larger winglets show a lower pressure drop due to a better wake region management and resulting reduction in form drag. The heat transfer coefficient and pressure drop in comparison with plain fin increases by 28.7 – 68.3% and 35.2–74.6%, respectively for a larger winglet arrangement. Whereas, a typical continuous smaller winglet arrays offer enhancement about 29.9–59.1% and discontinuous smaller winglet arrays offer 42.6–89.6%. But overall volume goodness factor for the winglet configurations shows an increment in comparison with plain fin case. Larger winglets and discontinuous winglet array show better performance than continuous array winglets. Gholami et al. (2014) carried out investigations on the effect of wavy-up and wavy-down rectangular winglets to reveal the flow features and heat transfer characteristics when it is used in a fin and tube heat exchanger. A recirculation region is created in the wake of each tube in an array of tube banks. The flow separates at the downstream portion of a tube and reattaches at the upstream portion of the subsequent tube. This forms a larger stationary recirculation region between two neighboring inline tubes. In comparison with the conventional winglet, both the wavy forms of rectangular winglets show a relative decrease in size of the wake region. This consistent decrease in wake region can be used as a better controlling measure of the form drag. Introducing high momentum fluid delays the wake separation downstream of the tube surface. An average temperature difference of inlet and outlet fluid for both wavy-up and wavy-down rectangular winglets is found to be larger than conventional rectangular winglets. The wavy-up configuration is found to
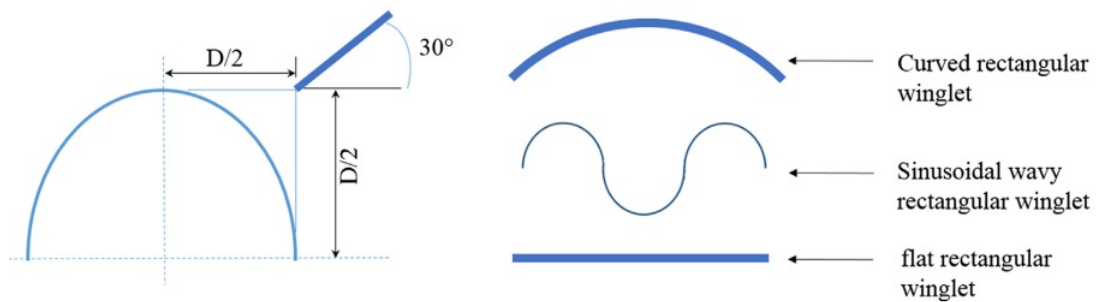
Fig. 2.6 Position of flat and wavy rectangular winglet (adapted from Modi and Rathod (2019))

offer better heat transfer performance. The wavy-down winglets show lesser pressure drop than the wavy-up and conventional rectangular winglets. Different modifications given to the winglet vortex generators have distinct effects on heat transfer performance. Modi and Rathod (2019) numerically examined the effects of sinusoidal wavy and elliptical curved type rectangular winglet vortex generator (RWVG). The different types of RWVGs analyzed in this study are shown in Fig B.3. These vortex generators are placed in both flow-up and flow-down orientation. Heat transfer characteristics of different Common Flow Down (CFD) configurations of wavy-up, wavy-down, curved-up, curved down and flat rectangular winglets are compared with baseline configuration (non-winglet case). Flow structure, temperature distribution, and pressure distribution for fin-and-tube compact heat exchanger are compared with seven inline circular tube arrangement. Appreciable improvement in heat transfer characteristics is obtained for wavy and curved rectangular winglets with a moderate loss in pressure.

Du et al. (2013) performed experiments to find the influence of LVGs on the performance of air-cooled condenser in the range 1500<Re<4500. Winglet vortex generators were installed on wavy fins around flat tubes. Wavy finned tubes with LVGs augment heat transfer significantly when compared to the traditional wavy finned flat tubes. This is attributed to the longitudinal vortices induced by delta winglet pairs that disrupt the thermal boundary layer. The sharper velocity gradient enables the mixing of cold and hot fluid streams. The enhancement in Nusselt number is found to be about 21-60% at the expense of considerable friction effects. Kwak et al. (2002), (Kwak (2005)) experimentally analyzed the heat transfer enhancement and pressure loss reduction of transverse rows of winglets on a finned-tube heat exchanger (inline and staggered arrangement of tubes). It is observed that winglets with 2 transverse rows and staggered arrangement of tubes provide 6-15% higher heat transfer performance as compared to the winglets having single row configuration. Two transverse rows of winglets are responsible for intensifying the turbulence intensity than realized by winglets with one transverse rows. Often higher heat transfer rate is achieved at the expense of larger
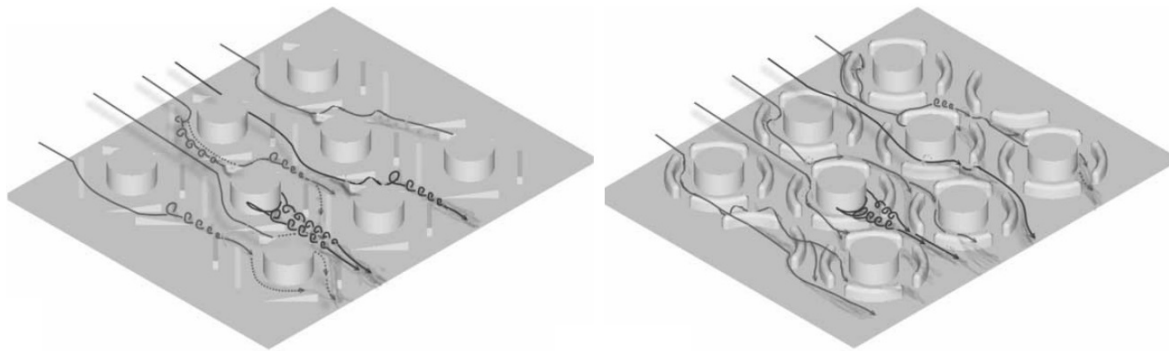
Fig. 2.7 Formation of vortices due to (a) delta VGs (b) annular VGs (adapted from Wang et al. (2002))

pressure drop. Pressure drop for 2 transverse rows of winglets in this type of configuration is found to be 61-117% higher than a single transverse row of winglets. In comparison with the single transverse rows of winglets, a typical inline arrangement of tubes with two transverse rows of winglets found to provide 7-9% higher heat transfer enhancement with an increase in pressure drop of 3-9%. Staggered arrangement always leads to a higher mixing of flow. Experimental studies of Joardar and Jacobi (2008) investigate the influence of one and three rows of winglets on fin-and-tube heat exchanger in the range 220<Re<960. Single and three pairs of vortex generators are found to increase air-side heat transfer coefficient by 16.5-44% and 30-68.8% respectively. Moreover, winglets with three arrays yield higher heat transfer performance than a single array. However, this higher transfer rate is achieved with higher-pressure drop penalty. Formation of longitudinal vortices induced by winglet arrays can significantly reduce the boundary layer thickness, enhance turbulence intensity and finally augment flow mixing between hot and cold fluid which leads to a higher heat transfer performance. Studies of Wang et al. (2002) demonstrate the influence of annular and delta winglet vortex generators on heat transfer performance of heat exchangers of fin-and-tube heat exchanger at Re=1000. The strength of horseshoe vortices induced by tubes diminishes in the downstream region. The formation of longitudinal vortices appeared behind the tubes due to staggered winglet arrangement is as shown in Fig 2.7. The annular height seemed to have significant impact on counter-rotating longitudinal vortex strength.

Eiamsa-Ard and Promvonge (2011) experimentally investigated the impact of backward and forward wing types of vortex generators on heat transfer performance and friction factor. Fig 2.8a and Fig 2.8b depict geometry of typical forward wing and backward wing vortex generators. Forward wing VGs provide higher heat transfer performance than backward wing VGs at the penalty of a larger friction factor. The forward wing VGs disrupt the continuous boundary layer development, thereby augment turbulent flow intensity and increase mixing
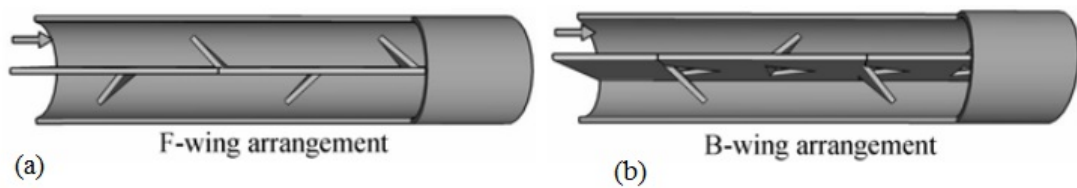
Fig. 2.8 (a) Forward wing arrangement (b) Backward wing arrangement (adapted from Eiamsa-Ard and Promvonge (2011))

flow. This results in greater augmentation of heat transfer rate when compared to backward VGs.

Zhou and Ye (2012) introduce a novel enhancement technique by curving the sidewalls of a winglet vortex generator. Experimental investigation of heat transfer enhancement by curved trapezoidal winglet has been performed and compared with traditional winglet vortex generators. The curved winglet has a streamline-curved configuration that found to offer better performance in fully turbulent region at a relatively lower pressure drop. Better thermal performance is obtained for a larger inclination angle and smaller attack angle of the vortex generator. Rectangular winglet pair (RWP) achieve a higher heat transfer enhancement compared to curved trapezoidal winglet pair (CTWP), delta winglet pair (DWP) and trapezoidal winglets (TWP) (Zhou and Ye (2012)). This comparison has been done for the same attack angle and height to length ratio. The rectangular winglet has the largest face area and can induce strong longitudinal vortices. Correspondingly, RWP has the highest pressure loss followed by TWP. Delta winglet pair has a lower pressure loss in the laminar and transitional flow region. The CTWP has a minimal pressure loss in fully turbulent region due to its streamlined surface and hence it can provide the best overall thermal performance. CTWP has a better thermal performance at lower angles of attack. This is because, the face area of vortex generator facing the flow is maximum at higher angles of attack. CTWP shows maximum overall performance for zero angle of attack when used at higher Reynolds number of 18000. The ellipticity or the curvature of the CTWP describes the width to length ratio. The traditional trapezoidal winglet is CTWP with no curvature. Offer 50% more heat transfer performance than a CTWP of semi-cylindrical shape. This is due to the ideal streamlined shape of CTWP, which leads to the lowest pressure drop.

The mixed orientation of CFU and CFD also attributes significant effects on heat transfer enhancement. Ke et al. (2019) introduced this unique mixed-orientation in a rectangular channel fitted with delta-shaped winglet vortex generators. Channel height and aspect ratio of the vortex generators have significant influence on heat transfer enhancement. The unique mixed configuration is more promising in mixing enhancement and heat transfer augmentation when the channel height is relatively small. The CFD orientation over performs
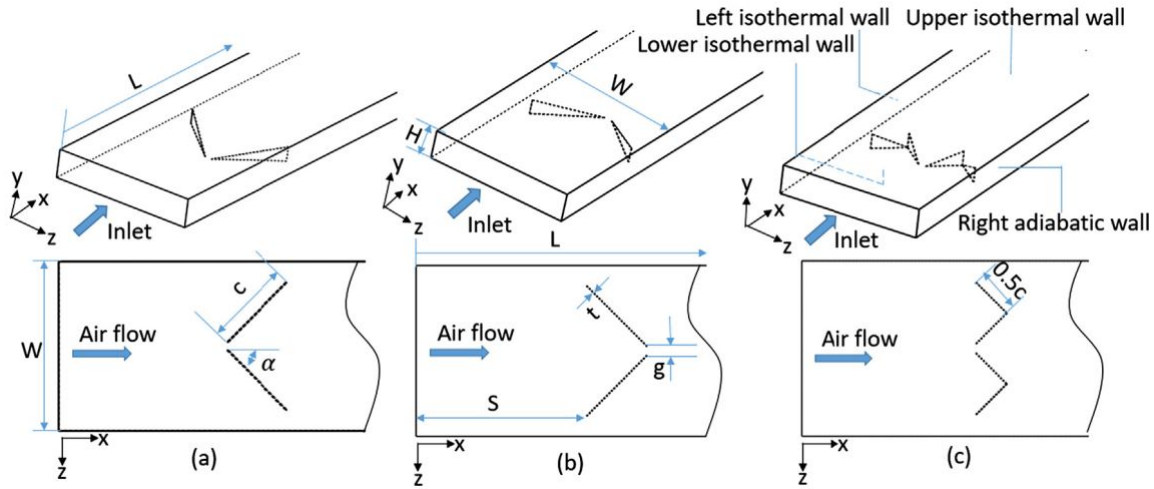
Fig. 2.9 Physical model and relevant geometrical parameters of a channel with LVGs: (a) common-flow-down configuration, (b) common-flow-up configuration, and (c) mixed configuration (adapted from Ke et al. (2019))

the CFU with larger vortex generator aspect ratios. Apart from the common flow-down (Fig 2.9a) and the common-flow-up (Fig 2.9b) configurations that have been investigated previously by other researchers, a unique mixed configuration (Fig 2.9c) is recommended. The fluid flows over the CFD oriented delta winglet vortex generators and generates a strong counter-rotating vortex pair downstream of the VG. Left side vortex rotates in clockwise direction and right side vortex in the counterclockwise direction. These vortices create a strong upwash flow from side wall of the channel towards upper wall and another downwash flow from middle of the channel to the lower wall of the channel. Secondary flow velocities are found to be higher when the flow washes down the lower channel wall. The strength of these vortices decreases further downstream, wherein the vortex core moves away from each other.

The vortex cores move closer to each other and they create an upwash flow to the upper channel for a typical CFU orientation. These vortices induce a weak interaction with the sidewalls. Mixed configuration generates two groups of counter-rotating vortex pairs. Flow patterns generated by both common flow up and common flow down orientations are realized with the mixed configuration. Mixed configuration generates weak vortices as the size of vortex generator is rather small. These vortices shift to the upper side of the channel rather than spreading in the spanwise direction. This is a major distinction of the flow pattern created by mixed configuration. The strength and position of longitudinal vortices strongly affect the thermal boundary layer thickness, which influences the heat transfer performance of LVG channels. The movement of the vortices in the channel can be explained qualitatively

by the method of images. When the channel height is relatively small (3 mm or 4 mm as in this investigation), the mixed configuration generates two groups of counter-rotating vortex pairs, which help with fluid mixing across the whole channel cross-section and enhance heat transfer. The common-flow-down and common-flow-up configurations induce fluid mixing on the sides or in the center of the channel. There exist an optimal transverse distance of VGs that offer the best heat transfer performance of heat exchangers (Song and Tagawa (2018)). The selected minimum domain of the fin is the region ABCD, as shown in Fig 2.10a. All the numerical results are obtained in the fin region ABCD. The schematic view of the simulation domain with VGs is shown in Fig 2.10b. The transverse distance of VGs has a slight effect on the interaction of co-rotating longitudinal vortices in the region around the same tube. The co-rotating longitudinal vortices around the same tube side interact with each other and merge into a new vortex with a larger intensity. The transverse distance of VGs has a significant effect on the interaction of counter-rotating longitudinal vortices. The interaction of longitudinal vortices is higher for an optimal transverse distance between two VGs around tube. The maximum differences in the increments of intensity of longitudinal vortices, Nusselt number and friction factor for different transverse distance of VGs are 34.0%, 33.9% and 18.5%, respectively.

Chamoli et al. (2018) have investigated the effect of tip to edge ratio as the geometric parameter for a modified winglet type VG. A schematic of the physical domain along with functional parameters are shown in Fig 2.11. Heat transfer performance has been significantly improved by the modification provided to the conventional winglet VG. Heat transfer was found to be maximum for an angle of attack 60°. Other researchers who used winglet VG also obtained maximum heat transfer at an angle of attack 60° and beyond which the heat transfer effect reduces. Winglet VGs obstruct the mainstream flow and secondary flow structures are generated. These secondary flow structures propagate along the walls of winglet VG and generate longitudinal vortices. This provides the adequate contact time for better mixing of cold and hot fluid. The turbulence intensity and heat transfer performance increases with edge to tip ratio. Optimal heat transfer performance is found to obtain for a edge to tip ratio value of unity and angle of attack 60° as it creates strong vortex structures.

It is already established that the secondary flows plays an important role in enhancement in heat transfer. Song and Wang (2013) numerically investigated the effectiveness of secondary flow produced by vortex generators mounted on a fin and tube heat exchanger.A non-dimensional parameter, *Se* has been used to specify the intensity of secondary flow intensity. *Se* is the ratio of inertial force to viscous force induced by secondary flowThe Nusselt number variations have a good consistency with the secondary flow intensity for the different Reynolds numbers investigated. There exists a correlation between the peak values of volume-
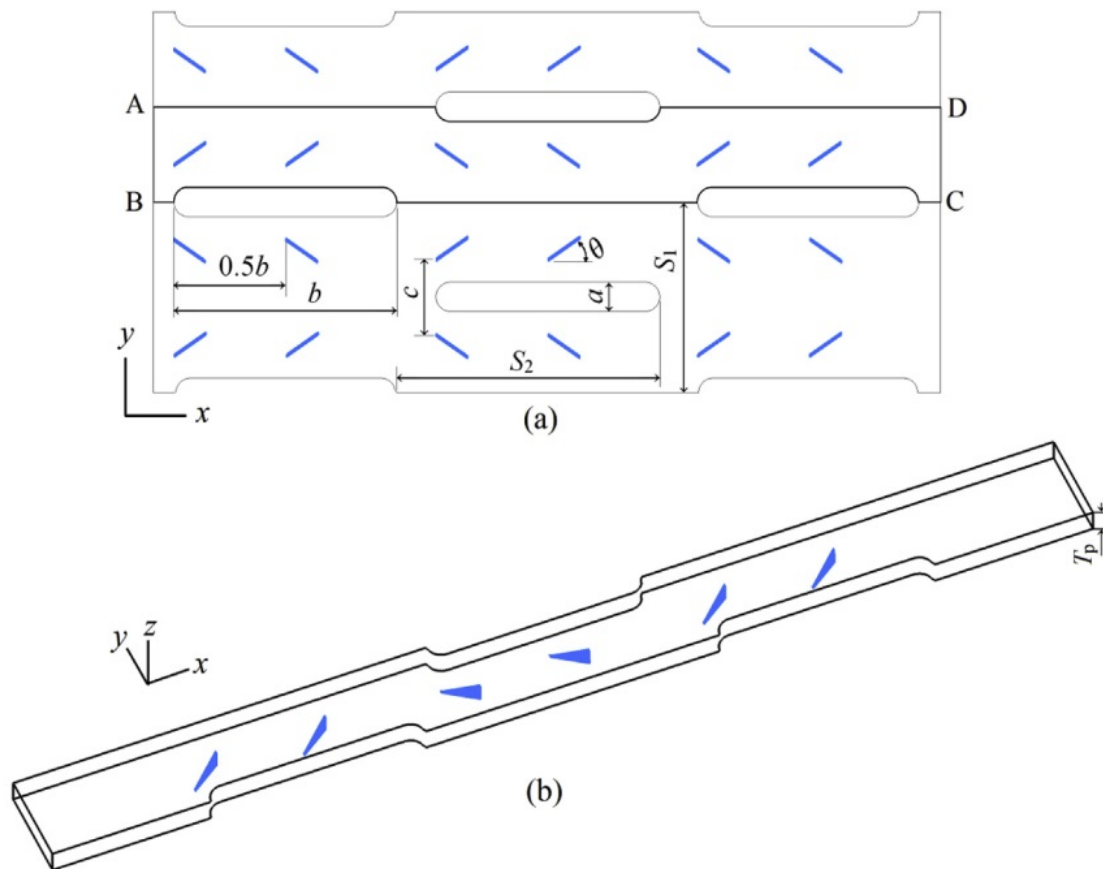
Fig. 2.10 Configuration of the fin, (a) fin, (b) Schematic view of the simulation domain (adapted from Song and Tagawa (2018))
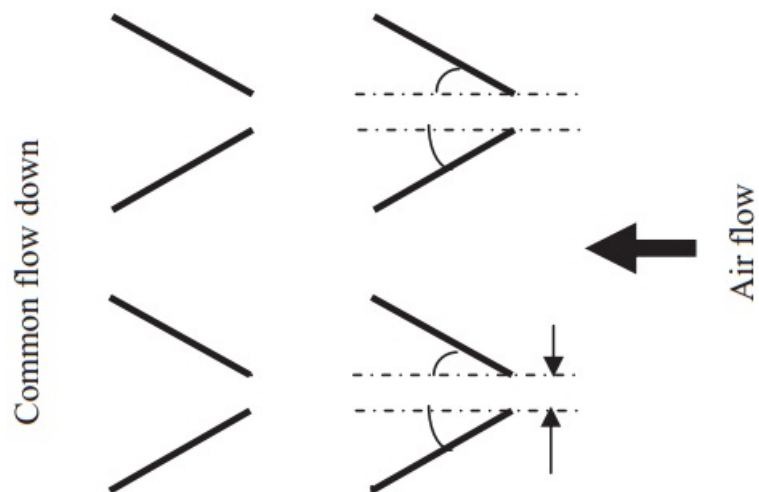
Fig. 2.11 Schematic of the physical domain along with functional parameters. (adapted from Chamoli et al. (2018))
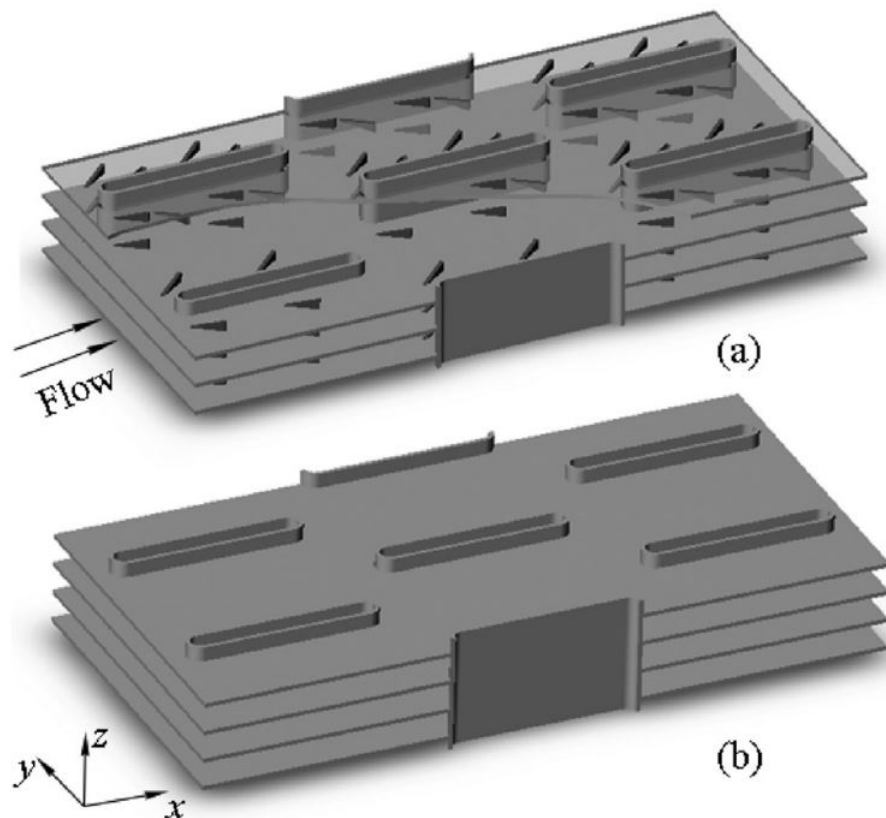
Fig. 2.12 Schematic view of a flat tube bank fin heat exchanger.(a) VGs mounted on both surfaces. (b) Without VGs, plain (adapted from (Song and Wang (2013))

averaged Se and area-averaged Nusselt number. Largest values of secondary flow intensity and Nusselt number are obtained at the leading edge of each tube. Fluid flows along the narrow semicircle flow crosssection of the tube. A vortex generator of delta winglet shape placed in a flat tube bank fin heat exchanger shown in Fig 2.12.

The vortex generators mounted in flat tube bank fin heat exchanger (Fig 2.12) generate longitudinal vortices. This creates a strong secondary flow around the front portion of the tube. Both secondary flow intensity and Nusselt number values decrease downstream of the leading edge of tube along the streamwise direction. The other vortex generators mounted around the side of tube generates also secondary flows, which counterbalance the reduction in intensity of secondary flow coming from upstream. The decrease of intensity of secondary flows around the tube slows down due to the existence of VG around the tube. There is peak values of secondary flow intensity at leading edge of VG around the tubes. At the upstream half of the tube the value of secondary flow intensity caused by VG is not so large compared to value at leading edge for first and second VGs. The decrement in the secondary flow intensity is the novelty of these VGs and is primarily controlled by the tube rather than the

VGs. Whereas, at downstream half of tube, the intensity of secondary flows caused by the VGs around downstream half of tube is higher than that around the upstream half of tube. Peak values of secondary flow intensity generated by VGs are also observed in this region. Similarly, a decrement in the Nusselt number is also observed in these regions. Hence similar distributions of secondary flow intensity and Nusselt number distribution are attributed by the contribution of secondary flow on heat transfer enhancement in these types of VGs.

2.2.2   Various types of vortex generators and enhancement effects

Many varieties of longitudinal vortex generators have experimented over these years. A review on various types of vortex generators and their typical enhancement effects are presented in this section. The selection of a typical type of VG is quite crucial in realizing the necessary heat transfer augmentation. Delta Winglet Vortex Generator (DWVG) is a common type of VG installed in industrial heat exchangers. Kwak (2005) demonstrate the effect of VGs type on heat transfer by performing an experimental study on finned-tube heat exchanger having winglet type of VG installed on fins with common flow up (CFU) configuration. An inline arrangement of tubes is found to augment heat transfer rate by 10% to 20% with a reduction in pressure drop of 8 to 15%. Whereas, a staggered arrangement of tubes with similar geometric arrangements of test core is found enhance heat transfer rate by 10 to 30% with a pressure loss reduction of 34 to 55%. It is observed that the staggered arrangement of tubes and DWVG eliminate the weak heat transfer zone in the wake region by delaying the flow separation. The CFU configuration of delta winglet with staggered arrangement in low Reynolds number application provides enhancement as much as twice of that of an inline due to the typical difference in wake interaction with the subsequent row. Prasopsuk et al. (2016) experimentally investigated the effect of rectangular winglet tape vortex generators (RWT) on the thermal performance of tubular heat exchanger for the range 4100<Re<26000. Rectangular winglet type of vortex generator yields higher heat transfer performance as compared to baseline case (plain tubes) at the expense of finite pressure drop. Chomdee and Kiatsiriroat (2006) and Gentry and Jacobi (2002) experimentally evaluated the influence of delta winglet type vortex generators on heat transfer performance and found that delta winglets play significant role in reducing thermal wake region that results in a higher heat transfer coefficient. Skullong et al. (2016) experimentally investigated the influence of staggered arrangement of winglet perforated tape (WPT) and winglet non-perforated tape (WTT) on heat transfer and friction factor in the range 4000<Re<30000. Fig 2.13 adepicts geometry of WPT used in tubular heat exchanger.

It could be seen that both WPT and WTT arrangement yield higher Nu as compared to smooth tube at same angle of attack 30°. Both winglets induce secondary flow and vortices
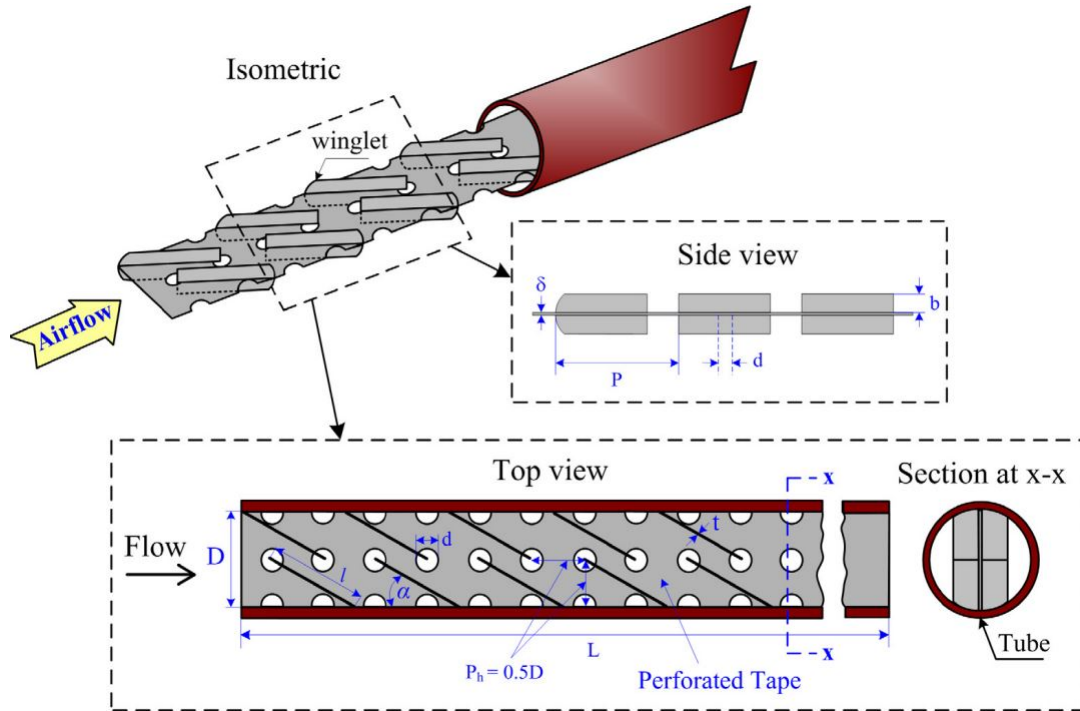
Fig. 2.13 Winglet perforated tape (WPT) used in tubular heat exchanger (figure adapted from Skullong et al. (2016))

in the flow stream that leads to the augmentation of turbulent flow intensity and better flow mixing. However, WTT provides better heat transfer rate than WPT. As perforated winglets tends to fix the flow leakage which results in the reduction of temperature gradient in radial direction. Furthermore, the corresponding friction factor for WTT is higher than WPT. Promvonge and Skullong (2019) experimentally investigated modified perforated/punched rectangular winglet (P-RW) on heat transfer enhancement in a solar air duct. Both forward and backward-facing winglets are considered. Fig 2.14 shows the vortex generator geometry of punched rectangular wing (P-RW). Backward facing perforated winglet shows better performance than forward type. Porosity ratio is termed as the area ratio of hole to wing and relative pitch is the ratio of longitudinal pitch spacing of wing to duct height. Three porosity ratios and three numbers of pitch ratios are considered in this study. Smaller porosity ratioes and relative pitch ratios can generate stronger vortices, which disrupts the thermal boundary layer development. Forward-facing winglet gives higher heat transfer as well as higher pressure losses as it creates more flow obstruction. However, the overall thermal performance is higher for backward-facing winglets and optimal thermal performance is obtained for porosity ratio of 0.34 and relative pitch ratio of 1.5 at an angle of attack 45°.
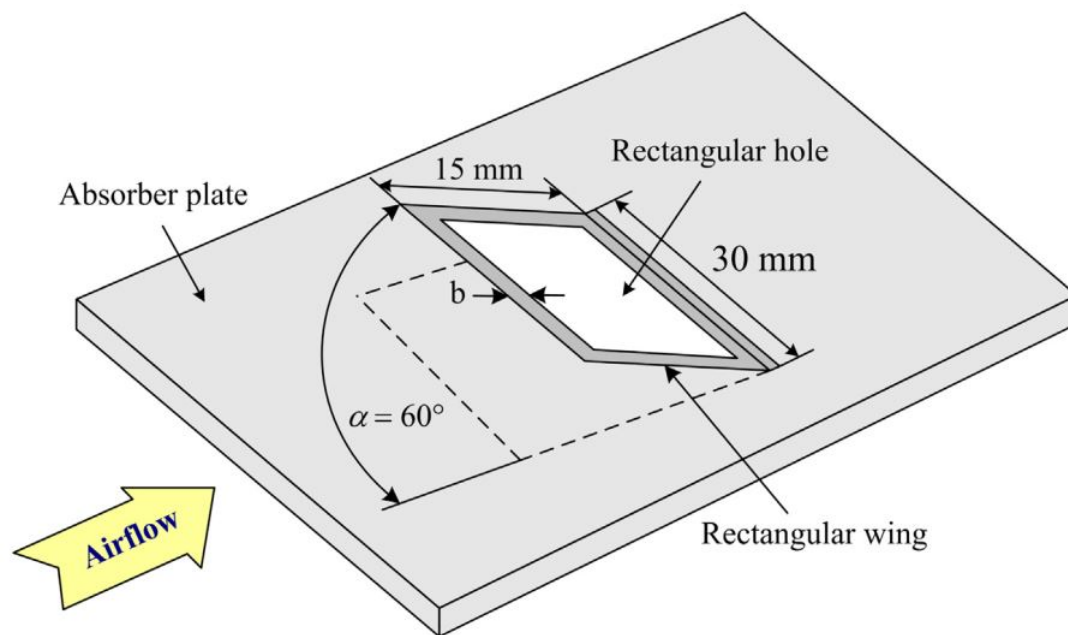
Fig. 2.14 Absorber plate with forward P-RW geometry (adapted from Promvonge and Skullong (2019))

Arc shaped baffles (ASB) placed on a heated channel can significantly influence on heat transfer. Koolnapadol et al. (2014) experimentally reported thermal behavior of placing baffles on a solar-heated channel. ASB with three pitch ratios is compared with a smooth channel. The ASB placed in the channel promotes creation of strong turbulence intensity. The ASB induces longitudinal vortex flow that leads to thinning of boundary layer. The heat transfer rate increases with both Reynolds number and pitch ratio. Assessment of heat transfer characteristics and friction losses in a channel fitted with 60° V-baffle turbulators has been experimentally performed by Promvonge (2010). Effect of three baffle pitch ratios (e/H = 0.1, 0.2,0.3) and three baffle pitch spacing ratios (P/H=1,2 and 3) has been investigated. Formation of secondary flows and better mixing induced by V baffle results increment in Nusselt number and pressure loss. V baffle turbulators interrupt the turbulent boundary layer and increase the degree of turbulence on the flow field. The baffle with lower pitch spacing ratio provides maximum heat transfer by interrupting and diverting the flow and promoting high levels of mixing. The heat transfer enhances by 118% and 134% in comparison with higher pitch ratios of 2 and 3. For PR = 1, the usage of turbulators leads to substantial increment in pressure loss also due to the blockage to the flow by the placement of baffles. Placement of baffles attributes to flow blockage, higher contact area, and occurrence of reverse flow. Maximum heat transfer is obtained for PR =1 and as expected friction loss is also highest for PR =1 due to the higher blockage ratio. The increase in pressure loss

is considerably high (146% to 180%) obtained for PR = 1 in comparison with PR =2 and 3. The higher surface area, dissipation of dynamic pressure, and the forces exerted by the reverse flow etc. are reasons for maximum heat transfer as well as higher-pressure loss. A higher blockage ratio induces stronger vortex strength and leads to higher heat transfer rate. The blockage ratio e/H = 0.30 provides maximum heat transfer rate. Nusslet number values are incremented by 1.46 and 1.21 times for e/H = 1 and 2. Similarly the pressure loss is maximum as expected for blockage ratio e/H = 0.3. The average hike in friction losses of the V-baffles with e/H=0.30, 0.20 and 0.10 are, respectively, around 29.44, 16.10 and 7.31 times compared to a smooth channel. There is a substantial increment in friction loss in the channel fitted with baffles. The pressure loss is maximum with higher blockage ratio. Overall performance evaluation of all blockage ratios and pitch spacing ratios of 60° V-baffle turbulators suggests that better performance is obtained for e/H = 0.10 and PR = 1.

Tamna et al. (2014) performed heat transfer augmentation studies in a solar air heater channel fitted with V baffle vortex generators (BVG). This baffle VG generates multiple longitudinal vortices in the flow field. This increases strong mixing and turbulence intensity in the flow field. Relative baffle height is termed as blockage ratio, b/H. Baffle pitch to channel height ratio is termed as PR. The influence of three PR at an attack angle of 45° and blockage ratio of 0.25 has been reported. Three baffle vortex generator arrangements, namely, single BVG, in-line and staggered BVGs on two opposite walls are investigated. Inline BVG arrangement creates flow circulation and flow separation and increases the turbulence intensity than staggered and single BVG arrangement. The presence of the BVG with inline arrangement at PR = 0.5 provides a considerable heat transfer augmentation of about 3.91 to 7.53 times. Smaller PR induces more interruption to boundary layer and stronger vortex strength. This leads to higher heat transfer rate for small PR baffle VG. It is evident that the use of baffles also creates substantial pressure drop. Inline arrangement provides more disturbances to the flow and hence more pressure drop. For single BVG, friction factor increases by about 8 to 38 times for inline arrangement as compared with staggered arrangement. Most of the losses occurred by the recirculating flow downstream of VG and due to presence of higher surface area.

Yongsiri et al. (2014) investigated the effect of inclined detached ribs of different angle of attack on heat transfer enhancement in a heated channel. The inclined ribs provided in the channel (Fig 2.15) induces recirculation zones behind the rib section. Some small recirculation regions are generated upstream of the ribs as well. The recirculation zones are found to be weak at smaller attack angles as well as at larger attack angles,. These induced recirculation zones has significant influence on heat transfer as it possess better fluid mixing of hot and cold fluid. This leads to the development of favorable temperature
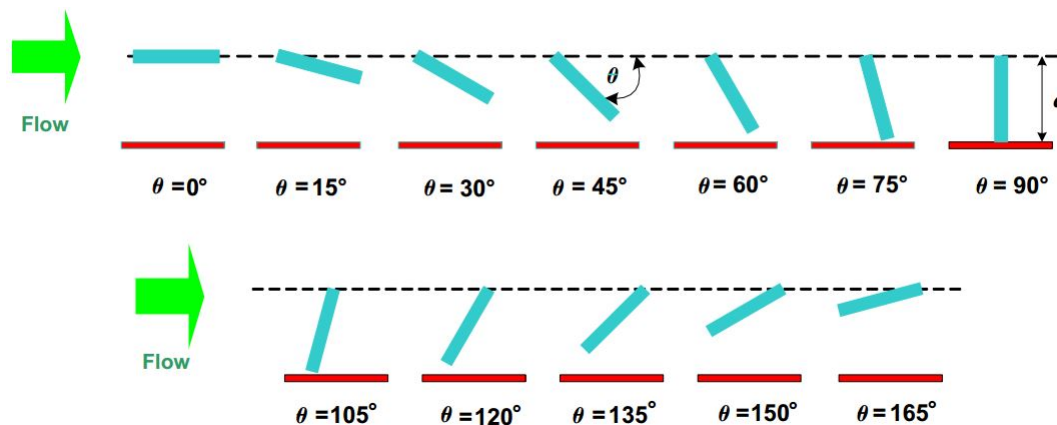
Fig. 2.15 Channel geometry and Ribs with different attack angles (adapted from Yongsiri et al. (2014))

gradient in the channel. Ribs with moderate angles of attack offer better mixing and lead to the thinning of boundary layer than for a smaller or larger angles of attack of 60° and 120°. Resulting pressure loss is also more at moderate angle of attacks due to the presence of higher recirculation. The pressure loss mounts to 2.79 to 3.49 times increase when compared to that of a smooth channel. Overall thermal performance shows the effect of rib angle is more prominent at higher Reynolds numbers. 60° and 120° angle of attack give favorable thermal performance factor of more than unity. Whereas, the lower and higher angle of attacks shows thermal performance factor less than unity. Experimental studies by Skullong et al. (2015) show that rib size and arrangement also has significant effect on heat transfer in a heated channel. The effect of square ribs and thin ribs are compared. Three configurations are studied; a ribbed wall, inline and staggered rib arrangements on two opposite walls. Arrangement of ribs and rib size have significant influence on heat transfer and friction loss in comparison with smooth channels. Both square and thin ribs considerably enhance the heat transfer in a similar manner. The thin ribs provide better performance than square ribs. The thin rib turbulators disturbs the thermal boundary layer and increase the turbulence intensity inside the channel. Inline arrangement provides better heat transfer performance of all the arrangements. High levels of mixing and strong flow interruption attributes to a higher heat transfer performance with inline arrangement. Inline arrangement of thin rib enhances Nusselt number by 213-216% in comparison with a typical smooth channel. The staggered and single rib configures gives 204-211% and 164-165% than the smooth channel. Higher contact surface area, blockage effect and the reverse flow by the ribs etc. attribute to significant pressure drop. Pressure losses for thin ribs is more than that for square ribs. There is about 3 to 7 times increase of pressure loss for smooth channel with ribs. Pressure loss

for inline arrangement gives rise to 17% more pressure loss than a staggered arrangement. Therefore the tin ribs staggered arrangement provides better overall thermal performance

Geometry, arrangement, and type of VGs has a significant influence on transfer characteristics of heat/mass exchange devices. Intensity and strength of vortices induced by each VGs dependent on flow parameters, height, and angle of attack. Researchers investigated to find the optimal flow and geometrical parameters of winglets. Following discussion summarize the major numerical and experimental investigations carried out by several researchers for innovative designing of compact heat/mass exchange devices.

2.2.3   Influence of geometrical parametrs on performance of vortex generators

Major geometrical parametrs that influence the performance of vortex generator in improving heat and mass transfer effects are its angle of attack and height. Vortex generators are attached to the heat transfer surfaces (fins/channels) at a specified or optimum angle, as vortices induced by these VGs are certainly dependent on its inclination The formation of circulation zone and turbulence intensity, hence the heat transfer enhancement and pressure drop is largely affected by how the vortex are induced on the fins of compact heat exchangers. The last few years have witnessed considerable research attention for finding the effect of angle of attack of VGs in heat transfer augmentation. The selection of angle of attack of VGs plays an important role in compact heat exchangers, as heat transfer and friction characteristics are crucial in such applications. The choice of the angle of attack of Delta Winglet Vortex Generator (DWVG) should be moderate, as larger attack angle can lead to pressure drop penalty. Larger attack angle yields vortices with greater strength until transverse vortex formation and breakdown of longitudinal vortex occur. Researchers have arrived at an optimum attack angle of 30° for VGs after performing exhaustive systematic experiments and numerical simulations for which the heat transfer performance is significant with moderately lo pressure loss. Wu and Tao (2007) illustrate the influence of attack angle of DWVGs in the presence of three tube rows number on the heat transfer performance of fin and tube heat exchanger. Heat transfer enhancement obtained is about 20-25 and 16-20% for angle of attack 45° and 30° respectively when compared to a baseline case. Corresponding pressure drop is more for a higher angle of attack. Fin surface as well as protrusions leads to a higher pressure drop in this type of heat transfer enhancement option. The impact of the different angle of attacks of LVGs on heat transfer performance and friction factor for various Reynold number (500, 1000, 1500 and 2500) is shown in Fig 2.16. As the angle of attack increases Nu number rises due to the formation of longitudinal vortices. Whereas, Nu
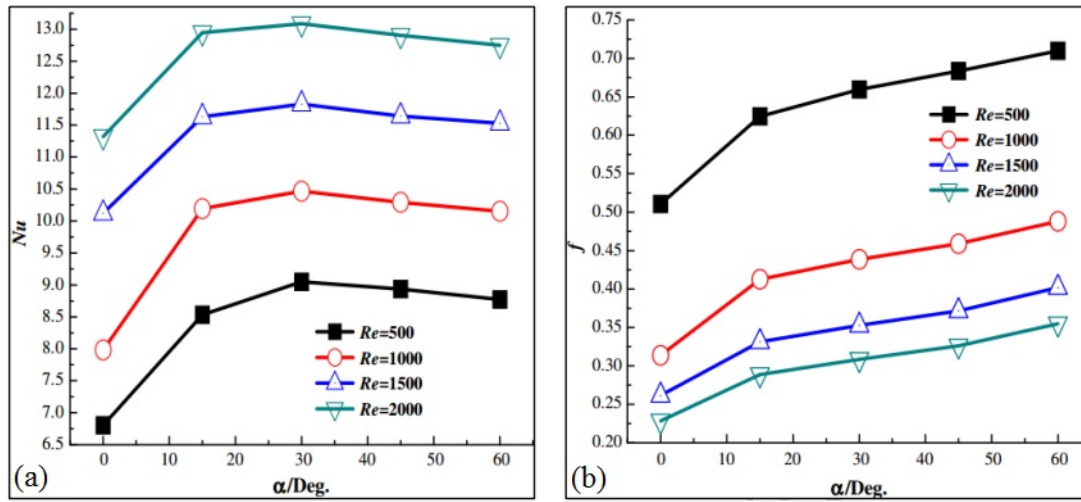
Fig. 2.16 Influence of angle of attack on (a) Nu (b) friction factor f (adapted from Chu et al. (2009))

starts decreasing for $\alpha > 30°$ due to the formation of transverse vortices and breakdown of longitudinal vortices. For all Reynold numbers, the influence of angle of attack shows same behavior. The corresponding friction factor is also increased as the LGV's angle of attack increases due to the enhanced form drag at higher angle of attack (Chu et al. (2009),Chen et al. (2000), Gong et al. (2013)) .

Numerical investigation performed by Ke et al. (2006) describes the influence of the angle of attack DWVGs on heat transfer and friction characteristics of a fin-and-tube type of heat exchanger. Maximum heat transfer was found at 40° optimum attack angle. A similar study was performed by Wu and Tao (2012) also arrived at 45° as the optimum angle of attack for better heat transfer augmentation with minimal pressure drop. He et al. (2010) demonstrated the impact of two different attack angles viz, 10° and 30° on a delta- winglet pairs on the thermal performance of fin-and-tube heat exchanger for $1400 \leq Re \leq 3400$. A significant heat transfer performance is obtained for an angle of attack 30° than at 15° . The influence of various attack angles on heat transfer performance varies with other parameters too such as, inclination angle of vortex, attachment method, Reynold number etc.

Zhou and Feng (2014) experimentally investigated the heat transfer enhancement of a plane and curved winglet type vortex generators with punched holes (CTWH). This study acknowledges the impact of curve winglets on heat transfer performance with different angles of attack and for $650 \leq Re \leq 21000$. Angle of attack 60° yielded the best heat transfer performance. The height of vortex generator also has a significant role in creation of longitudinal vortices and thereby enhancing the heat transfer. Torii and Yanagihara (1989) experimentally studied the impact of longitudinal vortices induced by DWVGs on heat
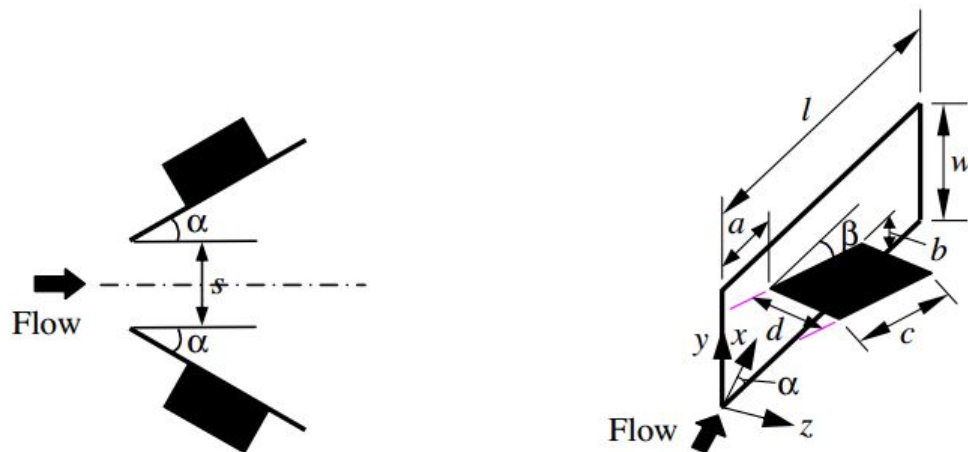
Fig. 2.17 Schematic of longitudinal vortex generators (adapted from Min et al. (2012)

transfer characteristics of laminar boundary layer. The height of DWVG is varied from 3 to 30 mm by keeping the angle of attack 15° with a constant free stream velocity. The enhanced region grows while the peak Stanton number ratio remains unaffected. This is due to the transition of laminar to turbulent boundary layer created by variation of the VG height. The influence of internal and external vortices on heat transfer performance is also found to be varying with the vortex height. It is noticed that internal vortices affect the transition of boundary layer while external vortices influence development pattern of the transition to the turbulence. Min et al. (2012) numerically analyzed the turbulent flow characteristics of a novel combined longitudinal vortex generator (LVG), comprising a rectangular wing mounted with an accessory rectangular wing as shown in Fig 2.17. The combined RWP generates vortices with larger area and lower core. The accessory wings generate vortices that swirl downward towards the channel bottom and disturb the boundary layer growth more effectively. The accessory wings mounted on the front surface of the main wings can increase heat transfer and pressure drop more than that mounted on the back surface. Nu and friction factor for CRWP and RWP are more in comparison with the flat plate channel. Attack angle of main winglet also effected in increased heat transfer. An angle of attack of 60° is found to be optimal for maximum heat transfer. An increase of Nu by 28.0–51.1% and friction factor by 150.3–391.7% for RWP configuration is achieved in comparison with a flat plate channel.

The effect of angle of attack for RWP and CRWP is more or less identical. But there are other factors contributing to enhancement in heat transfer by the addition of an accessory wing. Increasing the length of accessory wing attributes additional disturbance to the boundary layer. The larger accessory wing length invokes a shorter route for the accessory wing

vortices to travel along the main wing lengthwise direction. Hence, the local heat transfer gets enhanced. With CRWP, the Nu and friction factor gets increased by 6.2–10.7% and 15.0–33.0%, respectively at a wing length of 15mm. Similar effects of larger boundary layer disturbance and more effective mixing can be observed when the accessory wing width is increased. Nu and friction factor of the channel with CRWP are increased by 2.7–7.0% and 5.6–14.5%, respectively for a wing width of 10 mm. Nu and friction loss found to be maximum for a secondary attack angle of 60°. Accessory wings can effectively generate longitudinal vortices at larger angles of attack. The Nu and friction factor of the channel with CRWP are increased by 2.1–5.0% and 4.7–13.9%, respectively at secondary angle of attack of 60°.

Oneissi et al. (2019) recently introduced a novel vortex generator (Fig 2.18) , known as Inclined Projected Winglet Pair (IPWP). Effect of the inclination angle of IPWP on heat transfer enhancement as well as on pressure drop has been numerically investigated. Nu increases with the Reynolds number and is found to be almost independent of the inclination angle. However, the friction factor is sensitive to the inclination angle. Both forms of drag (skin friction drag and pressure drag) account for the total pressure loss increases with increase in inclination angle of this type of VG. Flow separation from the vortex generator body results in pressure drag and viscous shear boundary layer over the vortex generator cause skin friction drag. Changes the inclination angle, for the same frontal area of vortex generator, can minimize the pressure losses due to the creation of a streamlined flow. An optimal inclination angle of about 30° − 35° is obtained which provides maximum heat transfer. IPWP is suggested to have a higher overall thermal performance compared to a traditional delta winglet vortex generators.

Wu and Tao (2008), numerically studied the impact of longitudinal vortex generators (LVGs) on heat transfer and pressure drop by varying the crucial parameters of LVGs such as area, length, height and location. Attack angle of 45° and increase in area provides enhancement in Nu. Moreover, it is deduced that for rectangular winglets longitudinal vortex generators (RWLVGs) with greater height tends to provide higher heat transfer performance and pressure drop. It could be explained as augmentation in height of LVGs yield lower cross-sectional flow area of the channel, which in result leads to the higher flow velocity and hence strong induction of vortices. The winglet height and longitudinal pitch distance have strong influence on the size and strength of vortices generated by a winglet VG. Large Eddy Simulations performed by Bjerg et al. (2019) detailed the flow and heat transfer mechanisms with various geometrical configurations of winglet height and longitudinal pitch distance (Fig 2.19). Rectangular winglets often generate the main vortex, corner vortex, and an induced vortex. Winglet height has significant impact on nature of vortices generated and provides
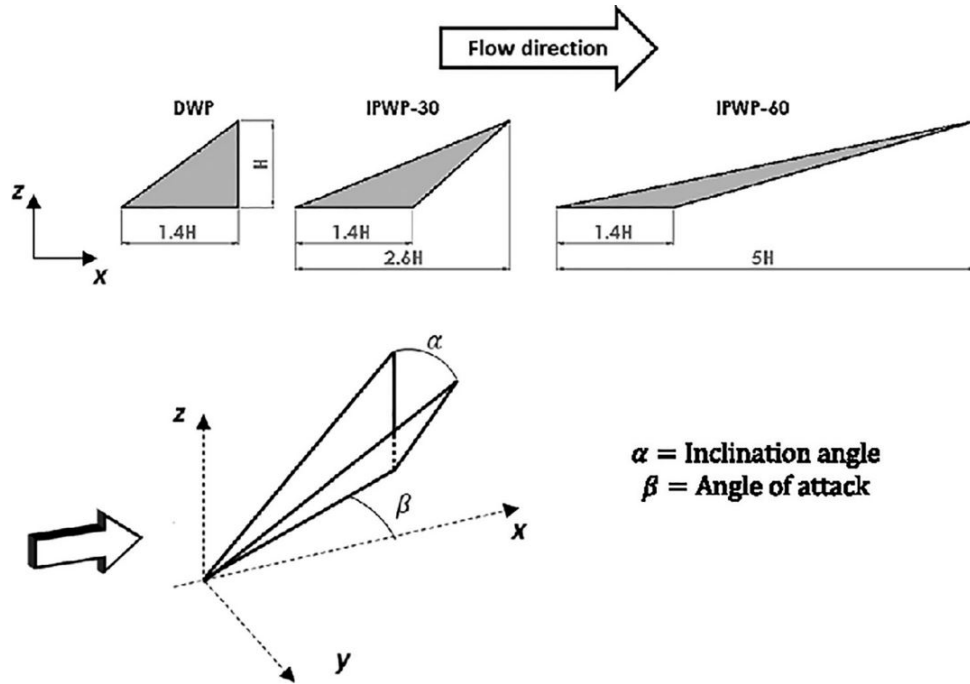
Fig. 2.18 Delta winglet pair (DWP), 30° inclined delta winglet pair (IPWP-30), and 60° inclined delta winglet pair (IPWP-60) vortex generators (Oneissi et al. (2019))

heat transfer characteristics and pressure losses. A pair of corner vortices are formed due to the adverse pressure gradient formed near the lower wall at the lower part of the winglet. Pair of corner vortices are generated at the lower part of leading edge of the winglets due to the adverse pressure gradient formed near the lower wall. Longitudinal vortices are formed due to the flow separation around the winglets. These are larger vortices and have greater influence on heat transfer enhancement. Longitudinal counter rotating vortices moves further towards the sidewalls. This phenomenon is common in all common flow down orientation of winglets. Longitudinal vortices has a positive relation with the winglet height, however, its persistence while moving downstream seizes with increase in size and strength. As the size of the vortices generated are higher, its interaction with the thermal boundary layer are more and leads to increased dissipation. Hence the heat transfer enhancement is strongly influenced by the longitudinal pitch distance for higher winglet heights. Persistence of main vortices downstream are longer with smaller winglet heights which leads to a uniform heat transfer at a reasonably lower pressure loss than larger winglet heights. Smaller winglets heights generally result in a higher local heat transfer enhancement on the fin side. However, winglets with larger height and smaller longitudinal height are more viable if the pressure loss increase is acceptable. Along with the geometrical variations, novel placement of longitudinal vortex generators also has a role in heat transfer enhancement. Liu et al. (2019) numerically and
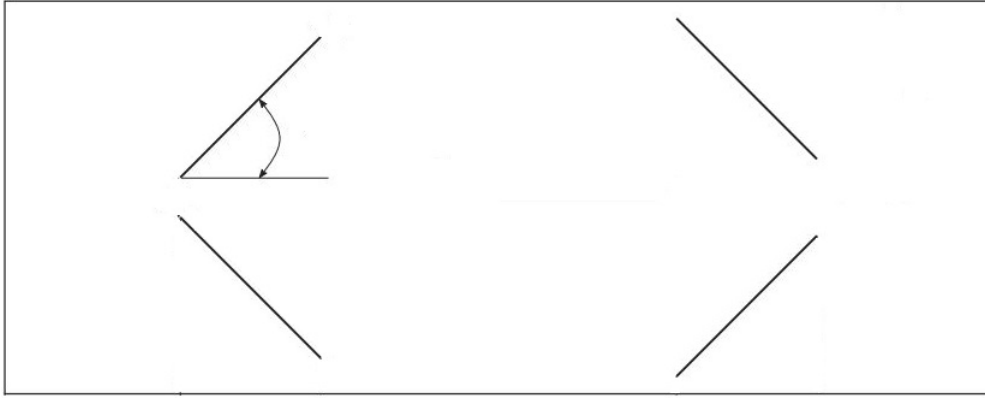
Fig. 2.19 Schematic of the computational domain with staggered rectangular winglet pair vortex generators (adapted from Bjerg et al. (2019))
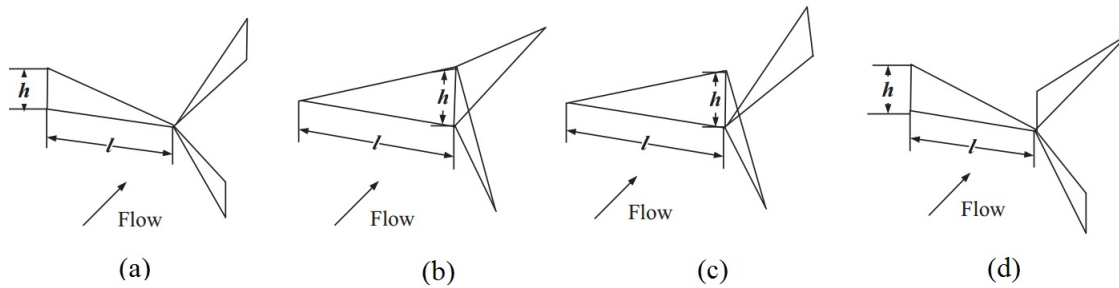
Fig. 2.20 Physical model of four kinds of composite winglets used by Liu et al. (2019) (a) delta winglets connected by their vertices (b) three winglets connected by their edges (c),(d) mixed arrangement of winglets
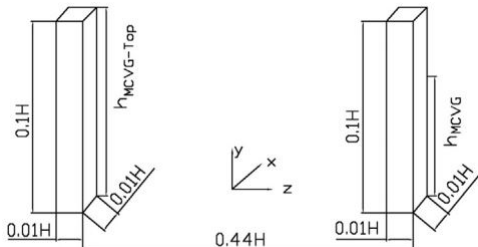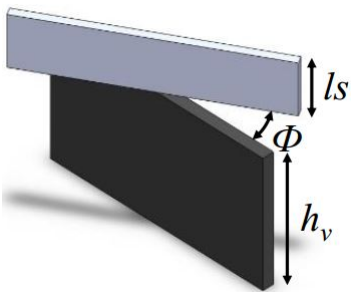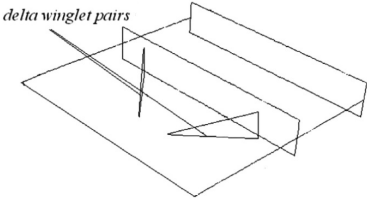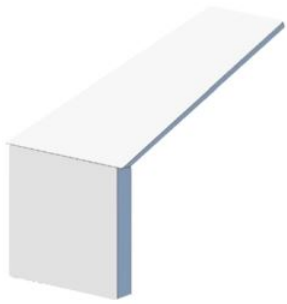
experimentally studied the effect of combined delta winglet vortex generators (2.20). The different arrangements of delta winglets, spacing between a single winglet and winglet pair, and rotation angles of winglets have significant influence on heat transfer. Recent years have witnessed unprecedented growth in the literature of heat transfer enhancement using vortex generators. An abstract of the recent technological developments in the field of LVG on heat /mass transfer enhancement is summarized in Table 2.1

2.3   Role of surface depressions in enhancing transfer effects and associated flow physics

Present research invokes both surface protuberant as well as depression for mass transfer enhancement. Surface depressions are preferred over surface protrusions owing to their capability to enhance transfer effects with minimal pressure loss in high-speed flows. Surface

Table 2.1 Recent technological developments in the field of LVG on heat /mass transfer enhancement

Author (year)/Vortex generator used	Flow conditions	Major observations
Jiansheng et al. (2019) Miniature cuboid vortex generators (MCVGs)	Re = 3745	1. Nu and performance coefficient increases by 5.17% and 8.15%, respectively
Uddip Kashyap (2019) Secondary Surfaces fixed over a Rectangular Vortex Generator	Re = 350	1. Secondary surfaces fixed parallel to the heated plate over the vortex generator significantly augments the heat transfer rate to about 13.4%. However, it enhances the drag by 5.7%. 2. Linear regression analysis predicts the suitable placement of the secondary surface
Xiaoze Du (2014) Delta winglet pair with attack angle 25°	1 m/s<velocity<5 m/s	1. Average performance evaluation criteria (PEC) of 1.23 has been obtained with a single row of delta winglets at the middle of wavy fin surface and is recommended for practical applications.
Jeongmoon Park (2017) (Tab induced CVP)	Re = 2000	1. Taper angle of the vortex generator has direct effects on the path of the CVP, the onset location of Kelvin–Helmholtz (K-H) instabilities, and the circulation strength. 2. Linear relation between VG taper angle and the onset of instability was obtained
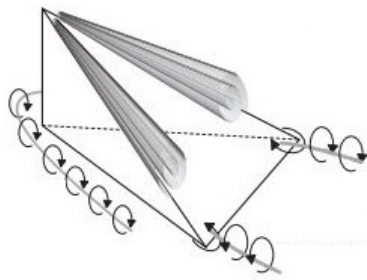
Henze et al. (2011)		
Tetrahedral full body vortex generators	150000<Re<550000	1. Heat transfer significantly affected by the ratio between the height of the VG and the hydrodynamic boundary layer thickness. 2. Correlation between vortex trajectories and the heat transfer distribution was obtained by potential flow theory
Chunhua Min (2010)		
Modified rectangular wing pairs (MRWPs)	5000<Re<17500	1. For RWP, the average Nu increases with the attack angle and a 55^\circ attack angle shows the highest average Nu number in the range of the present study. 2. MRWPs have better heat transfer characteristics than RWP
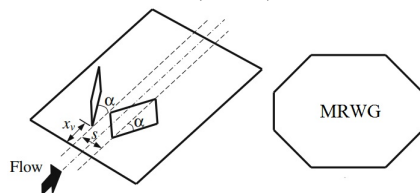
depression advects fluid free stream into it and consequent ejection from it promotes turbulent mixing into the bulk fluid flow. Often an escalation in approach velocity attributes a further growth in flow structures. Hemispherical and oval surface depressions are widely used in transfer augmentation applications. It is quite interesting to explore the local flow structures and mechanisms responsible for heat/mass transfer enhancement. An overview of the local flow structures inside the dimples and mechanisms responsible for heat transfer improvement by dimples are shown in Fig 2.21. Flow is found to separate near to the fore wall of the depression and later get reattaches on aft wall. Heat/mass transfer is found to be low near separation region and high near aft wall. An upwash effect is generated due to the interaction of advection of free stream and flow impingement inside the cavity (Ligrani et al. (2001), Mahmood et al. (2000)).

Turnow et al. (2018) performed a numerical study on heat transfer enhancement realized by dimples placed in high Re flows. Fig 2.22 shows the streamlines around a single dimple at Reynolds number of 105,000. A large recirculating region with an unsteady asymmetric monocore structure and predominant transversal direction are formed inside the dimple as shown in Fig 2.22. It is observed that the fluid that enters directly within the dimple is made to rotate inside the recirculating region before it finally leaves it. Recirculating regions and the organized self-sustained oscillations created due ot it are responsible for heat transfer enhancement.
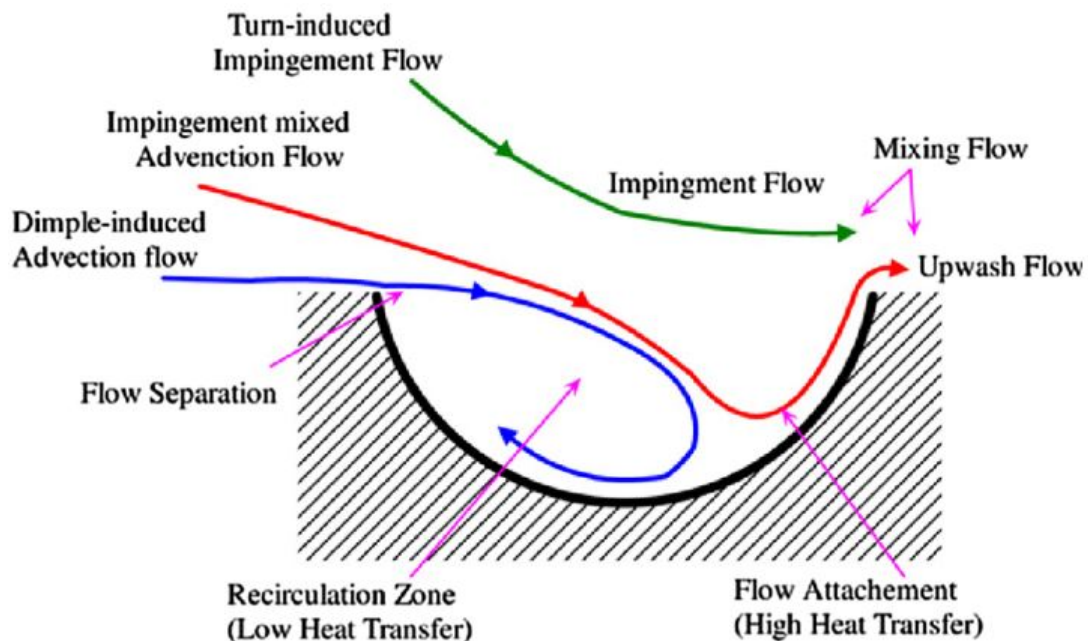
Fig. 2.21 Conceptual plot of a dimple, and mechanisms responsible for heat transfer improvement (adapted from Xie et al[109]

Isaev et al. (2000) analyzed the formation of vortices in a stalled turbulent flow streaming over a deep spherical and asymmetric holes on a surface. It is observed that an asymmetric hole creates only one vortex structure, whereas two large scale vortex cells are created by a spherical hole. This change in vortex structure is due to the influence of vortex intensification due to asymmetry of the hole. Isaev et al. (2002) performed numerical simulations to study the vortex aided intensification of heat transfer in a duct with a set of deep spherical dimples. This method of heat transfer has resulted significant hydraulic resistance in the dimpled duct. Isaev and Leont'ev (2003) performed a numerical study on the flow structure over a spherical dimple placed on the surface of a narrow duct for the turbulent regime with a focus on the effects of dimple depth in heat transfer enhancement. It is observed that the separation zone occupies a bigger space in the dimple and the maximum longitudinal velocity of the return flow increases with increase in depth of the dimple. Isaev and Mityakov (2003) performed a numerical study to investigate the effect of the shape of an asymmetric hole with moderate depth, on the convective heat transfer in turbulent regime. These results also indicate that providing an asymmetric shape to the shallow hole causes restructuring of the flow near it. In another study by Isaev and Sergey (2003), the rearrangement of the flow separation from symmetric to monotornado is found to create a considerable intensification in heat transfer both inside the spherical dimple as well as in the wake region. Effects of dimple depth on heat transfer improvement is also taken up in another study by Isaev et al. (2016).
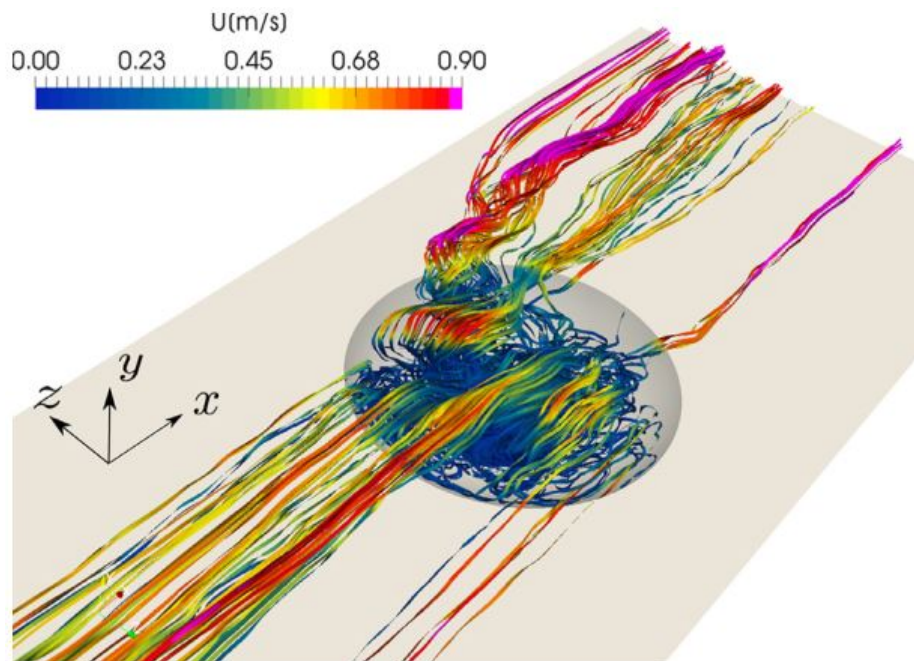
Fig. 2.22 Streamlines over a single dimple at Re = 105,000 (adapted from Turnow et al. (2018))

Results showed that the performance of vortex heat transfer is augmented consistently from moderate-depth to large depth dimples.

2.3.1 Effect of the geometry and spatial arrangements of dimple on heat/mass transfer

Geometrical features of the dimple cavities such as depth, ovalty, symmetry, footprint diameter to depth ratio and its spatial arrangement have significant effect in heat/mass transfer enhancement. Aforementioned aspect has received much research attention during the last few years. A systematic review of the available literature is presented in this section. Khalatov et al. (2004) presents the analysis of flow over spherical and cylindrical dimples for the Re< 25,000 in both the laminar and turbulent regimes. In general, the cylindrical dimples provide longer separation zones when compared with spherical dimples at similar flow conditions. The in-dimple separation zone of both cylindrical and spherical dimple are found to be almost identical for Re< 10,000. However, a shallower cylindrical dimple can provide lengthy separation zone for Re>10,000. Turnow et al. (2011) investigated the flow structures and heat transfer improvement in a channel with oval and spherical dimples. Heat transfer is found to enhance significantly by smoothing the dimple edge and employing oval dimples. Elyyan and Tafti (2009) used a novel split-dimples as the surface roughness on an

interrupted plate fin. The split-dimples continuously perturb the boundary layer formed on the fin surface and generate energetic shear layers, which provide an additional mechanism for heat transfer enhancement. Fig 2.23 shows the streamlines at a stream-wise plate for different values of Reynolds number. The recirculating flows formed inside the split-dimple cavity disrupt the thermal boundary layer formed on the fin surface and improve the turbulence intensities in the flow field and heat transfer from the fin. The sizes of these recirculating flows are smaller for laminar flow at a Re=240. Usage of the split-dimple fin improves the heat transfer in the range of 60–175% as compared with a plain interrupted plate fin.
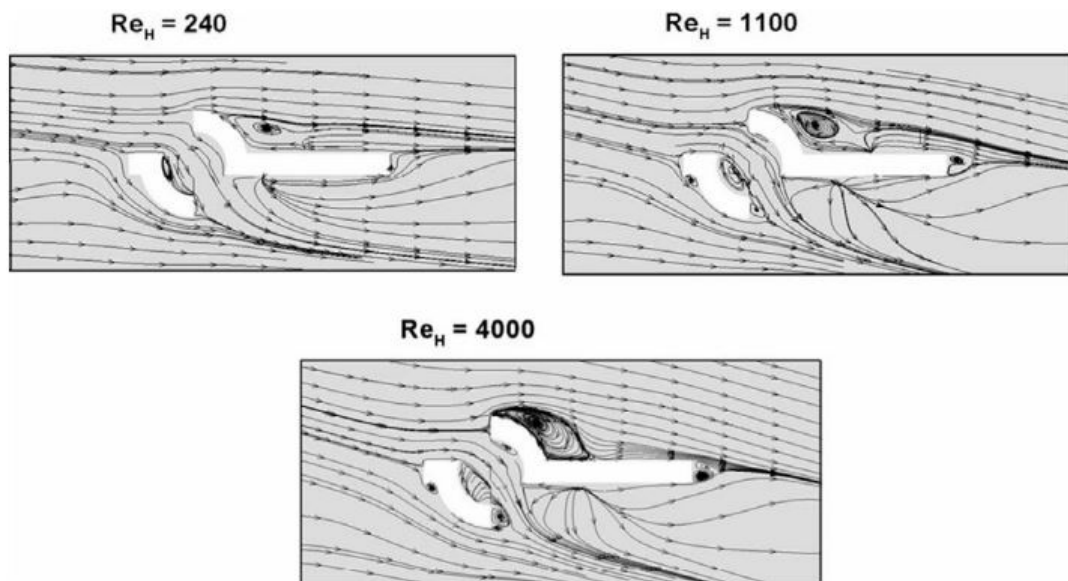
Fig. 2.23 The streamlines inside and around the split-dimple fn at a stream-wise plate for various Reynolds number (adapted from Elyyan and Tafti (2009))]

Chen et al. (2012) presents the effects of asymmetric and symmetric (spherical) dimples on the heat transfer improvement in a channel. The skewing of the core of the dimple towards the downstream side while keeping the spherical shaped print diameter is found to provide a noticeable improvement in heat transfer with almost the same pressure drop. Xie et al. (2013) performed a numerical work to study the fluid flow and heat transfer in square ducts with various inner-protruded dimple geometrics. These are special dimpled surface having a regular dimple cavity with a protrusion structure placed inside it. It can be viewed as a protrusion structure within the dimple cavity to improve the fluid mixing and the heat transfer, particularly in the recirculation flow area in which the heat transfer is negligible. Recirculation flows can be suppressed and the heat transfer rate can be augmented inside the upstream sections of the dimples by using a protrusion structure within the dimple cavity. Moreover, the pressure drop can be decreased by using a protrusion structure within the

dimple cavity in comparison with the regular dimples as the drag formed in the upstream and the friction drag in the downstream sections of the dimple are reduced. Chen et al. (2014) investigated the heat transfer and turbulent flow structure in a channel with periodically patterned surfaces having dimple and protrusion. Maximum heat transfer effects are obtained at the upstream portion of protrusion and the downstream portion of dimple. Isaev et al. (2015) increased the heat transfer in a narrow channel with one row of oval dimples. Stepwise and zigzag arrangements of the dimples was provided to analyze the heat transfer effects. An arrangement with a zigzag relief and shifted dimples provides heat transfer intensification of 90% at the expense of 25% increment in the hydraulic loss as compared with the plane-parallel channel. Borisov et al. (2004) investigated the heat transfer and pressure drop of flow through a duct. Two kinds of heat transfer enhancement methods have been investigated; viz, dimple concavities and combining dimples on one side with concentrically arranged toroidal banks protruding into the duct on another side. Significant improvement in heat transfer is achieved for both types of arrangement (73% for the duct with one dimpled side and 67% for double-sided dimpled passage).

Rao et al. (2015) studied the thermal characteristics of flow in a channel with one dimpled surface with rows of spherical or teardrop dimples in the turbulence regime. Two types of dimples having identical depth is considered. The teardrop dimples provided up to 18% higher heat transfer rate in comparison with the spherical ones. Moreover, the teardrop dimples created about 15% to 35% larger pressure drop as compared with the spherical dimples. Fig 2.24 shows the streamlines around teardrop and spherical dimples at Re = 50,500.

Spherical dimple   Teardrop dimple
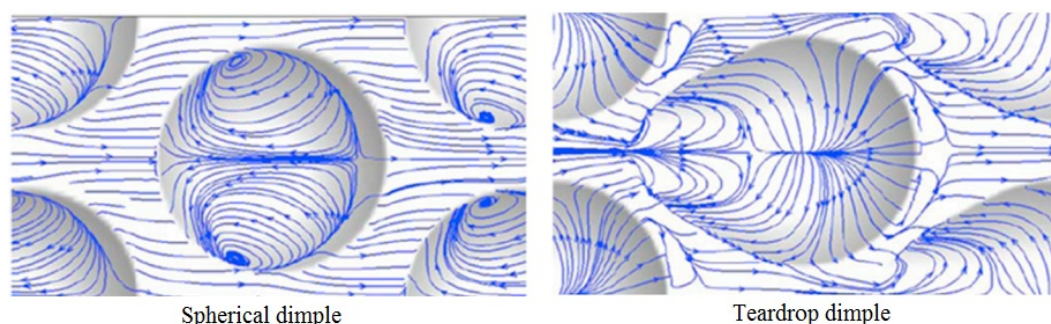
Fig. 2.24 The streamlines around teardrop and spherical dimples at Re = 50,500 (Rao et al. (2015))

Yoon et al. (2015) investigated the geometrical aspects of tear-drop dimples on a plate. Recirculating flows created by the teardrop dimples are found to reach out of the dimple and improves the turbulent mixing that realize more improvement in heat transfer rate. The size of the recirculation flow, which is formed at the upstream region of the dimple, decreases

with increasing the length of the upstream dimple. Xie et al. (2015) compared the flow and heat transfer parameters of hemispherical and teardrop dimples used in a rectangular channel in the range 3000<Re<9000. Results shows that the flow can cover the teardrop surface easily and can impinge on the rear part with higher energy as compared with the hemispherical one. This is due to the typical curvature of the front edge of the teardrop shape which is smaller compared to the hemispherical one. The teardrop dimples have a good efficiency for heat transfer for 3000<Re<9000. Tsynaeva and Nikitin (2016) investigated the flow structures in a rectangular duct with dimples in the turbulent regime with two shapes for dimples including dumbbell and spherical shapes. Head loss in a channel with dumbbell-shaped dimples is found to be less compared with the spherical dimples. The inclination of dumbbells towards the flow direction leads to the development of laminar zones with lower speeds. Isaev et al. (2017) compared the potentials of three types of dimples to improve the heat transfer inside a narrow plane-parallel duct. These dimples are spherical, 10°-truncated conical, and oval dimples. The thermo hydraulic performances are found to be 1.79, 0.98, and 1.07 for the oval-trench, spherical dimple, and conical dimples, respectively. The formation of a vortex structure in the oval-trench (consists of two semi-spherical dimples, which are connected by a cylindrical insert) is found to be stable as compared with spherical and conical dimples. Moreover, for the oval-trench dimple, a large extend of the upstream surface of the dimple can be streamlined without separating the flow.

Wang et al. (2018) simulated the flow and heat transfer in a converging channel with a dimpled wall having a bleed hole inside the cavity. The installation angles of the bleed hole are varied in the range of $-30°$ to $30°$. Fig 2.25a shows the bleed hole with different installation angles in the dimple. A large recirculation flow in the dimple cavity is found to diminish the heat transfer efficiency. However, a cooling fluid flow can be guided towards the outlet of the dimple by considering a bleed hole in the dimple cavity. In this case, the heat transfer rate can be improved because the total flow rate of the cooling fluid in the dimple cavity increases. The streamlines and the turbulent kinetic energy distributions for two cases of dimples with and without a bleed hole at Re = 36,750 are shown in Fig 2.25b. The flow structure within the dimple is altered with a bleed flow through a hole. The low-speed-recirculating zone is reduced and the region with higher turbulent kinetic energy is developed by using a bleed hole in the dimple.The local heat transfer is enhanced due to the bleed hole in a dimpled channel.

Xie et al. (2018) simulated a pipe with transverse and longitudinal dimples at each cross-plane. Here the transverse and longitudinal dimples create downward flows and enhance the fluid mixing. Moreover, this dimple arrangement intercepts the boundary layer and generates periodic impinging flows. These effects cause better heat transfer improvement compared
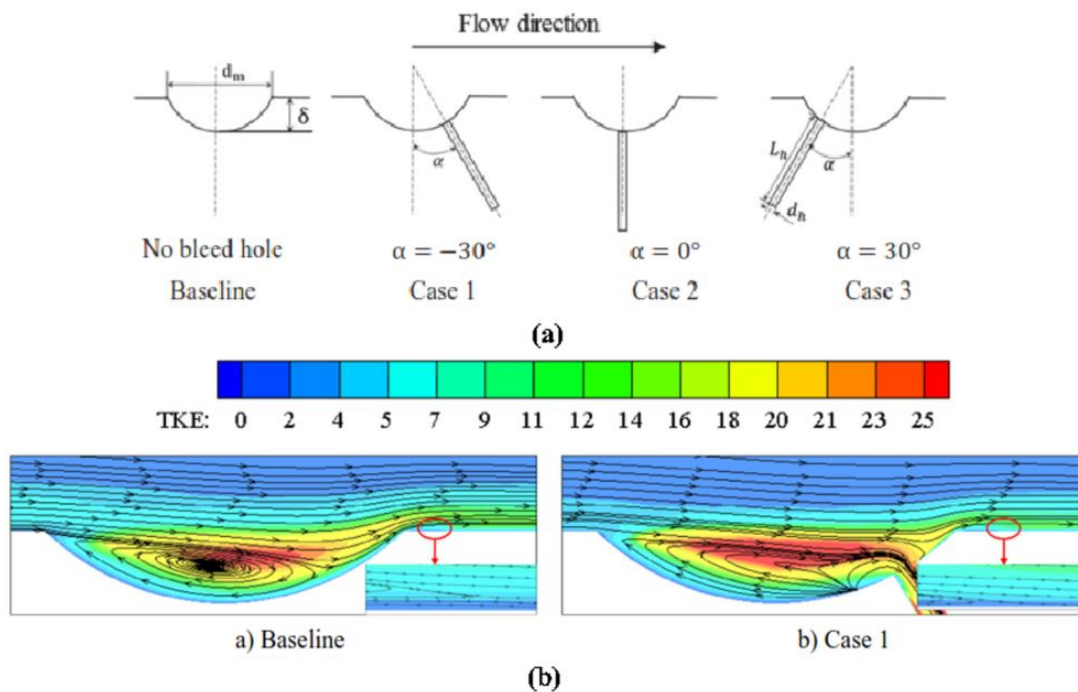
Fig. 2.25 (a) The bleed hole with different installation angles; (b) Streamlines and the turbulent kinetic energy distributions for two cases of a dimple with and without a bleed hole at Re = 36,750 (Wang et al. (2018))

with other dimples. It is observed that the strength and size of the vortices created by the transverse dimples are higher than those of longitudinal dimples. The dimple shapes and their arrangements against the flow affect considerably the flow structures and heat transfer enhancement achieved by dimples. Often a shallower dimple improves the heat transfer more than with a deeper one.

Katkhaw et al. (2014) used 45° ellipsoidal dimples on a flat plate with staggered and in-line arrangements. The dimpled plate with staggered arrangement is found to provide up to better thermal performance 21.7% as compared with the smooth plate. Moreover, the usage of a dimpled plate with in-line arrangement provides 18.5% more thermal performance than a smooth plate. In a similar work, Vorayos et al. (2016) experimented with spherical dimples created on a flat plate with staggered and in-line arrangements. Now the dimpled plate with staggered arrangement provided up to 26% higher heat transfer coefficient as compared with the smooth plate, while the usage of dimpled plate with in-line arrangement could improve heat transfer coefficient about 25% higher than a smooth plate. Sangtarash and Shokuhmand (2015) performed both experimental and numerical studies on the heat transfer and pressure loss in a regular louver fin bank, dimpled louver fin bank, and perforated dimpled louver fin bank. Two arrangements are employed, viz. staggered and in-line arrangements, for dimpled
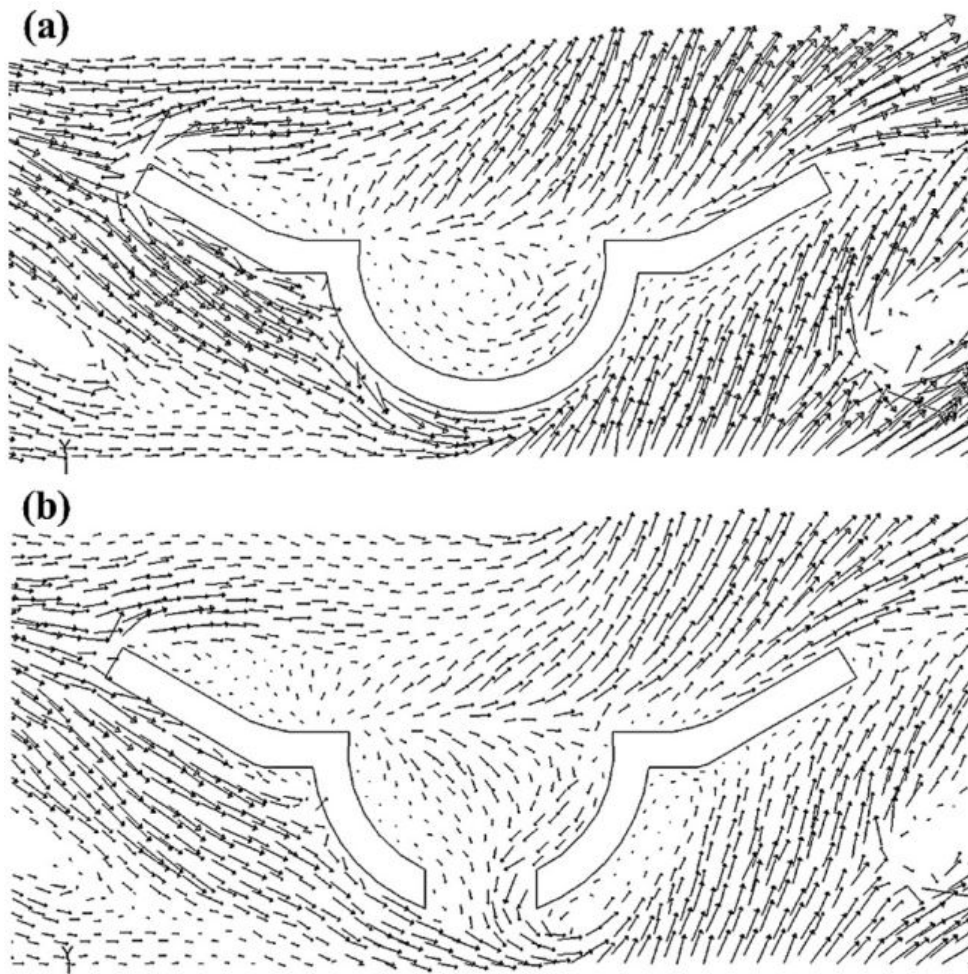
Fig. 2.26 Velocity vector for fluid around (a) regular dimple; (b) perforated dimple at Re = 600 (Sangtarash and Shokuhmand (2015))

louver fin bank and perforated dimpled louver fin bank. Note that the louver fin banks can be used in multi-louvered heat exchangers. It is found that both the heat transfer rate and friction factor increase by using dimples on the louver. Moreover, they observed that the perforated dimpled louver fin bank provides a better heat transfer rate as compared with other cases. Fig 2.26 shows the velocity vector for the fluid flow around the regular and perforated dimples at Re = 600. This figure indicates that the trap zones can be removed and the flow efficiency is enhanced by implementing the perforations on the dimples. This increases the heat flux, which leads to improved heat transfer from the fin to the fluid flow. The trapping and circulation of the hot fluid in the dimple cavity for a long time can also reduce the thermal efficiency. The staggered arrangement for both dimples and perforated dimples gives a better heat transfer rate than the in-line one as the staggered arrangement creates more turbulence in the flow.

Leontiev et al. (2017) performed an experimental study to investigate the influence of dimple shapes on heat transfer and drag coefficients on surfaces. Six dimples with different shapes are used in this study. These include spherical dimples (model 1), oval dimples (model 3), teardrop dimples aligned with the flow direction (model 6), turned teardrop dimples placed with 45° angle respect to the flow direction (model 4), spherical dimples with rounded edges (model 5), and dimples created by milling a sphere along a circular arc (model 2). These dimples are shown in Fig 2.27. Spherical dimples and dimples with rounded edges have smaller amount of drag than the other type of dimples. For these two dimples, the drag ratio remains almost constant with increasing Reynolds number and they have a slightly larger drag coefficient compared with the smooth surface. Teardrop dimples have the lowest values of the mean thermo hydraulic performance because they have the highest values of the drag being significantly larger than the related heat transfer coefficient. Table 2.2 gives a brief summary of exhaustive set of results related to dimple assisted heat/mass transfer enhancement.
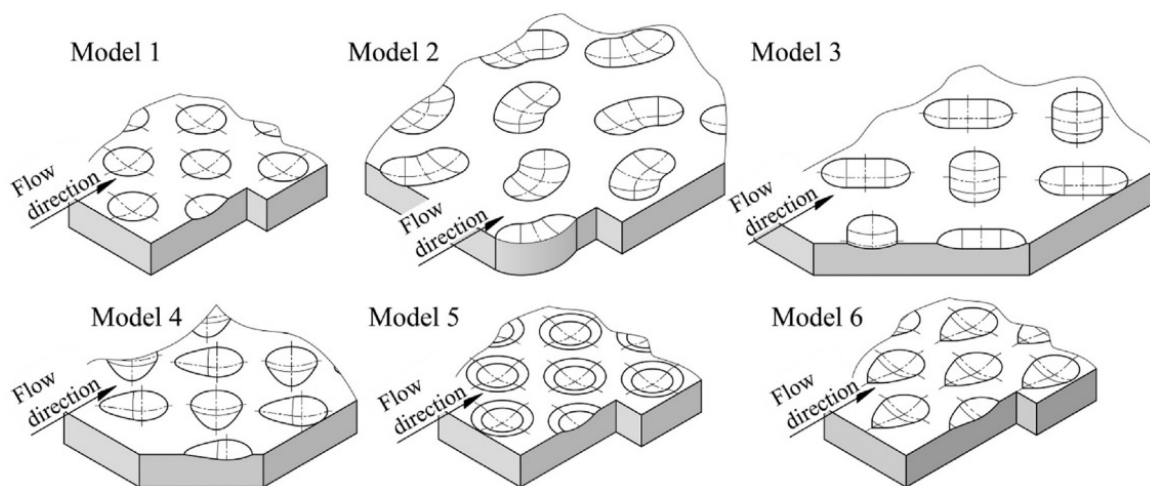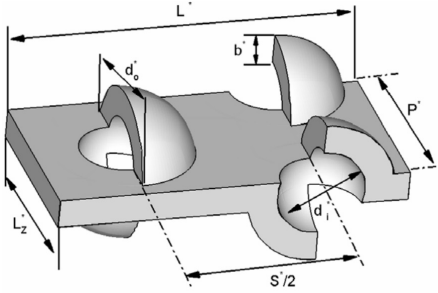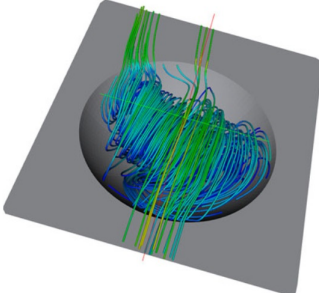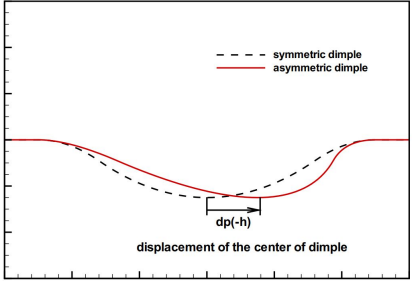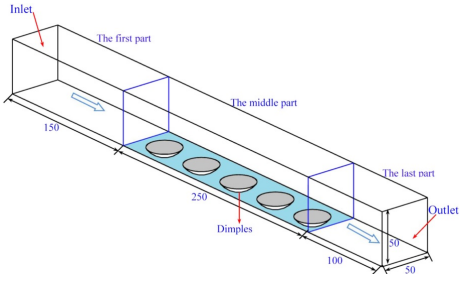
Fig. 2.27 Six dimples with different shapes analyzed by Leontiev et al. (2017)

2.4 Combinational transfer process enhancement methods

A major limitation of either surface protrusions or depressions is that they cannot sustain the enhancement effect for wider expanse beyond their vicinity. Rao et al. (2012) studied both experimentally and numerically the simultaneous usage of pin fins and dimples on heat transfer improvement in a channel. Du et al. (2018) studied heat transfer and flow structure in a rotating pin finned duct with various dimple placements. It is concluded that the dimple placement has a considerable influence on the flow structure and heat transfer. As the dimple

Table 2.2 Summary of the recent advances in dimple assisted heat/mass transfer enhancement

Author/Dimple geometry used (year)	Flow conditions	Major observations
Elyyan and Tafti (2009) Novel split-dimple interrupted fin	240–4000	1. Protruding geometry of the split dimple also aids in augmenting heat transfer from the fin surface by generating unsteady or turbulent wakes. 2. 60–175% higher heat transfer than a plain interrupted plate fin, but at a cost of 4–8 times the frictional losses.
Turnow et al. (2011) Spherical and Oval dimples	20,000 and 40,000	1. Heat transfer increases by rounding the dimple edge and use of oval dimples. 2. Presence of coherent vortex structure inclined to the mean flow
Chen et al. (2012) Asymmetric dimples	4000–6000	1. Heat transfer enhancement is by ejection with counter-rotating flow, intensified secondary flow and vortex structures at the downstream rim of asymmetric dimple. 2. Asymmetric dimpled surface presents a viable means of enhancing heat transfer compared to the symmetric dimple.
Xie et al. (2013) Internal protruded dimples	7500–27,500	1. Internal-protruded dimple structures suppress recirculation flows in the upstream parts of the dimples. 2. Internal-protruded dimples greatly improve the average local heat transfer of dimple curved surface by suppressing the recirculation flows and enhancing heat transfer in the upstream parts of dimples.
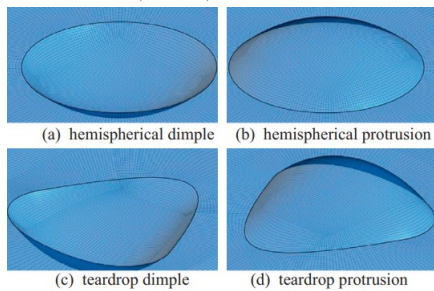
Xie et al. (2015) Tear drop dimples	3000–9000	1.Flow covers the teardrop surface easily and impinges onto the rear section with more energy in the teardrop dimple/protrusion compared with hemispherical dimple/protrusion. 2. Teardrop dimple/protrusion shows good performance for lower Reynolds number
Sangtarash and Shokuhmand (2015) Dimpled louver fin banks	100–1200	1. Continuous temperature gradients have been observed over the louver surface with the highest temperature at the base of the louver and the lowest temperature at the middle of the louver. 2. Adding dimples on the louver surface and adding perforation increases the heat transfer and pressure loss.
Isaev et al. (2017) Oval-trench dimple	10000	1. Abrupt increase of heat transfer in the vicinity of the spherical dimple due to the restructuring of the flow structure in the dimple 2. Vortex structure with oval dimple separated by cylindrical insert is rather stable and intense in comparison to spherical dimple.
Xie et al. (2018) Cross ellipsoidal dimples	5000–30,000	1. Transverse and longitudinal dimples cause downward flow, improve the flow mixing and reattachment, interrupt the boundary layer and form periodic impingement flows, which greatly improve the heat transfer. 2. Nu increases with the increase of depth and axis ratio, and decrease with increase of pitch.
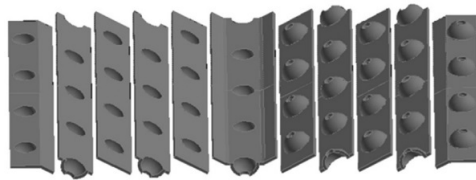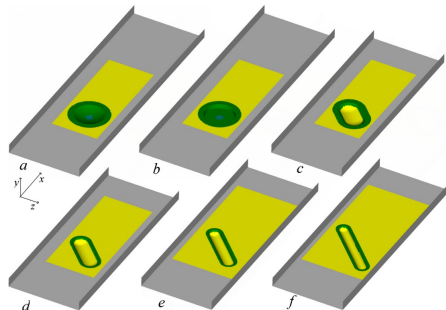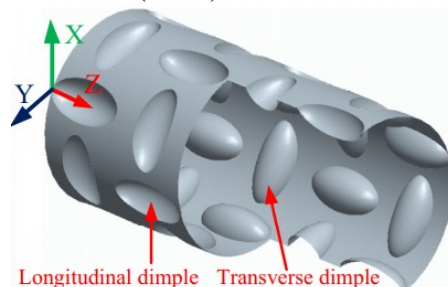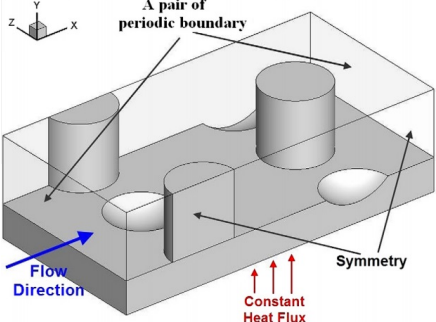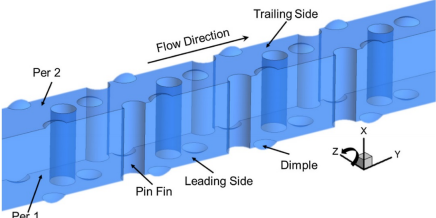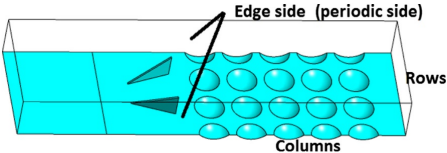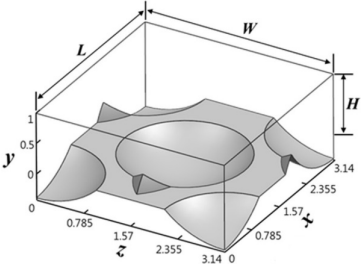
is placed downstream of the pin fin, a small impingement region, that beneficial for the heat transfer enhancement, is formed at the rear section of the dimple. Singh et al. (2017) used rib turbulators along with cylindrical dimples of various configurations in a two-pass square channel. Four ribs with various shapes including 45° angled, M, V, and W shapes are considered. For each rib shape, three different cases including rib alone, dimple alone, and a combination of ribs and dimples are investigated. The simultaneous usage of ribs and dimples that are arranged in the shape of the rib follow the direction of the secondary flows created by the ribs. The dimples are accommodated within the rib pitch. The combined usage of ribs and dimples gives the maximum heat transfer rate for the 45° angled and V configurations, compared with that when rib alone and dimple is alone used. However, for the M and W configurations, the usage of a rib alone gives the minimum heat transfer rate compared with the corresponding cases of dimple alone and simultaneous usage of ribs and dimples. Luo (2016) attempted a combination of pin fin wedge and different dimple arrangements for turbine blade cooling applications and found significant enhancement for end-wall heat transfer. A combination of grooves and ribs with delta-winglet vortex generator (Luo and Wen (2016)) also provided a higher thermal performance in a solar receiver. A multi-objective optimization (Luo (2017)) based on various geometrical aspects of such a combination could figure out apt thermal performance enhancement scheme. Direct numerical simulations of Yang et al. (2019) revealed the flow structure and associated heat transfer enhancement of a typical wedge-shaped vortex generator and a dimple in a cooling channel. In a similar manner, Yoon et al. (2015) simulated fluid flow and heat transfer associated with a tear-drop dimple combinational enhancement option. Such a combination is found to perform better than a simple dimple surface. Jang et al. (2018) presents transient heat transfer measurements indicated a higher thermal performance of rib-dimple configuration as compared to a rib-protrusion system. Recent research trend indicates that combinational transfer enhancement is gaining interest among research community. A summary of this category of augmentation methods is given in Table 2.3. Present work analyses a typical combinational mass transfer process enhancement method in which a vortex generator is used along with a dimple placed at its downstream.

Table 2.3 Recent advances in combined passive methods for heat/mass transfer enhancement

Author (year)/Dimple geometry used	Flow conditions	Major observations
Rao et al. (2012) Pin fins and dimple	8200–50,500	1. Improved convective heat transfer performance by up to 19.0% 2. Pin fin-dimple channel with deeper dimples shows relatively higher Nu number
Du et al. (2018) Dimple location on pin finned channel	7000	1. Counter-rotating vortex, which is induced by the Coriolis force, is found at the back of the pin fin and transports wake fluid from the trailing side to leading side. 2. As the dimple moves close to the leading edge of the pin fin, Nu increases remarkably at both the leading side and trailing side.
Luo et al (2017) Dimple combined with DWVG	4000 - 40,000	1. Adoption of dimples significantly impacts the flow structure by interacting with the vortex which is generated by the DWVGs 2. Inline arrangement dimples provides the best mixing and the highest heat transfer performance.
Yang et al. (2019) Dimple with a wedge-shaped vortex generator	2800	1. Main design parameter is the width ratio between the cooling channel and vortex generator (W*). 2. When W* increases, the heat transfer on the surface is enhanced because of the main counter-rotating vortex downstream of the computational domain.

2.5   Summary of literature review

Detailed survey has been performed on established and recent developments in passive
heat/mass transfer enhancement methods. Relative performance of different vortex generators
are analyzed in detail. Different passive/combinational methods studied are compiled and its
graphical representation is given in Fig 2.28. The performance aspects depends on various
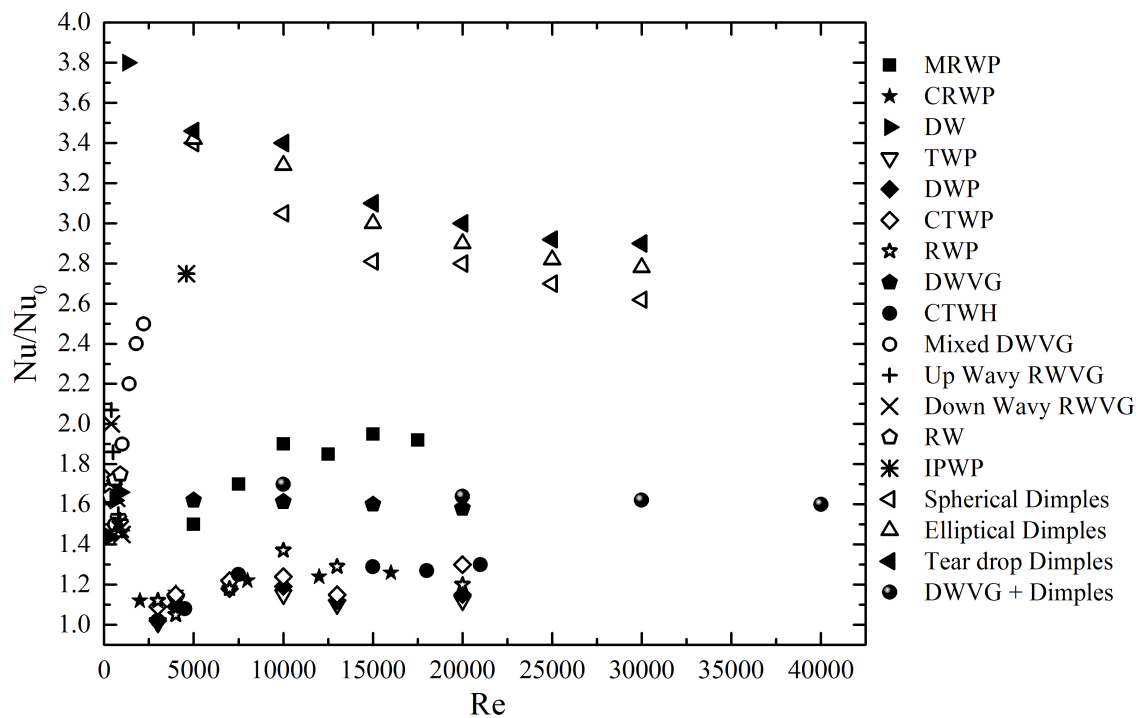
Fig. 2.28 Relative Nu comparison for different flow manipulators

parameters such as flow conditions, geometry etc. Hence, a unique performance character is
not observed for the entire flow regime envisaged in this comparison.

Out of all the geometric aspects covered from the literature, the surface depressions
provides relatively higher heat transfer enhancement. In comparison with spherical dimples,
its modifications like tear drop dimples and elliptical dimples are more effective. In addition,
modifications provided to the conventional surface flow manipulators shows more transport
properties. Examples are Mixed Delta Winglet Pairs (MWDP) and IPWP. Conventional
vortex generators like DWP, RWP etc. shows relatively lesser heat transfer enhancement than
the surface depressions and with modifications. Of the various flow conditions approached
by several authors, surface depressions is a better aspect for transfer enhancement than a
surface protrusion. It is well established in the figure 2.28.

2.6   Research gap

Research on the enhancement of heat and mass transfer parameters attained paramount interest due to the overwhelming demand for the effectiveness augmentation of various devices used in thermal science and engineering. Existing literature work on heat and mass transfer enhancement run through thousands of experimental and numerical research works on various active and passive methods. Most of the aforementioned literature on the heat and mass transfer enhancement is for low Reynolds number applications. Studies on convective mass transfer enhancement need to be extended to high Reynolds numbers in order to make them applicable for the analysis of various combustors of practical interest in nonconventional propulsion arena. Mixing process in high-speed fuel–air mixing devices has shorter residence time. Higher Reynolds number flows essentially develops a turbulent boundary layer over the fuel surface, which generates larger gradients of velocity, temperature, and species normal to the surface. Experimental assessment of convective mass transfer in the flow field from a liquefying or sublimating boundary is inherently difficult. Hence, numerical studies can provide useful information for surface mass efflux and gradients that can enhance its evolution. Many passive transfer process enhancement methods have been experimented in the recent past. These devices can be either a single vortex generator or a combination of vortex generators or their arrays. Recent advances in high fidelity numerical/experimental visualization and measurements could portray the fluid dynamics of transfer process enhancement using vortex generators. A major limitation of either surface protrusions or depressions is that they cannot sustain the enhancement effect for wider expanse beyond their vicinity. Combinational mass transfer enhancement studies are not abundant in the literature. Convective mass transfer augmentation systems call for the requirement of not only the enhancement near the surface but also the evolved mass should be carried away to the farther locations in adjoining fluid free stream. Therefore, the sustenance of the strength of the evolved vortex system in the wake of the vortex generator is a key objective while selecting combinational convective mass transfer augmenting system.

2.7   Research objectives

Modeling and simulation of passive mass transfer enhancement from the surface of a liquefying substance, using vortex generator alone and its combination with dimpled surface placed in high-speed flow are envisaged in this thesis. The flow field is inherently three-dimensional, turbulent, and compressible with species transport. Simulations have been carried out using Advection Upstream Splitting Method (AUSM) scheme based Finite Volume solver with an

objective of capturing the complex flow features resulted from the vortex-boundary layer interactions and associated convective mass transfer of species. The mass efflux is computed by taking care of all typical features of the flow field. Focus of the present work is to relate vorticity with mass transfer enhancement created by vortex generators, hence the other effects created by compressibility are not discussed in detail. Flow features typical to the compressibility are invariant in the wake region close to the vortex generators and its combination examined in the present study. Major objectives of the research are the following

- To develop a computational model for analyzing mass transfer from a surface in high-speed applications

- To develop a special Temperature-Dependent Mass Efflux condition (TDME) to simulate mass efflux from the boundary as a function of fluid temperature at the interface.

- To resolve the spatial and temporal features of flow past flow manipulators.

- To investigate the effect of geometry and flow conditions in mass transfer enhancement.

- To obtain a relation between vortex trajectory and location of maximum mass transfer

- To perform time-resolved analysis for identifying the signature of instabilities in the promotion of transfer effects.

- To develop correlations for mass transfer as a function of flow and geometry parameters involved in the present analysis

Chapter 3

Numerical Methodology and Validation

3.1 Introduction

Passive mass transfer augmentation device can be used in fuel regression rate enhancement in hybrid rocket motors making use of solid fuels. The Reynolds number range in typical hybrid rocket motors of practical interest (Zilliac and Karabeyoglu (2006)) is of the order 10^4 to 10^6. Reynolds number used for the present research is in this range. A finite volume density based solver is used to study the flow and turbulent convective mass efflux from a mass evolving substance in front of vortex generator. A detailed description of governing equations, turbulence equations and numerical schemes, employed in the present study is given in the beginning of the chapter. A temperature dependent mass efflux (TDME) condition is worked out and invoked to the mass evolving boundary as a user-defined function (UDF). Detailed derivation of TDME is also explained. Air is taken as the working fluid. To simulate mass evolution from the surface, properties of Naphthalene is implemented at the mass evolving boundary. Numerical methods used in the current work has been validated using the experimental wall pressure as well as heat transfer profiles reported for an identical vortex generator placed in high Reynolds number flows.

3.2 Governing Equations

For simulating the turbulent convective mass flux evolution from the liquefying substance, following transport equations are solved in Cartesian coordinate systems.

1. Mass conservation - Continuity equation

$$\frac{\partial \rho}{\partial t} + \frac{\partial \rho u_i}{\partial x_i} = 0 \tag{3.1}$$

2. Momentum balance equation

$$\frac{\partial \rho u_i}{\partial t} + \frac{\partial \rho u_i u_j}{\partial x_i} = -\frac{\partial p}{\partial x_i} + \frac{\partial \tau_{ij}}{\partial x_i} \tag{3.2}$$

3. Energy balance equation

$$\frac{\partial (\rho e)}{\partial t} + \frac{\partial (\rho u_i e)}{\partial x_i} = \frac{\partial (p)}{\partial t} + \frac{\partial (\mu(\frac{1}{Sc_k} - \frac{1}{Pr}) \sum_{k=1}^{N} e_k \frac{\partial Y_k}{\partial x_i} + \frac{\mu}{Pr} \frac{\partial e}{\partial x_i})}{\partial x_i} \tag{3.3}$$

4. Species transport equation

$$\frac{\partial (\rho Y_k)}{\partial t} + \frac{\partial (\rho u_i Y_k)}{\partial x_i} = \frac{\partial (\rho D \frac{\partial Y_k}{\partial x_i})}{\partial x_i} \tag{3.4}$$

5. Equation of state

$$p = \rho RT \sum_{k=1}^{N} \left(\frac{Y_k}{M_k} \right) \tag{3.5}$$

The turbulence is modeled using Menter's Shear Stress Transport $\kappa - \omega$ two equation model (Menter et al. (2003)). This model combines both $\kappa - \varepsilon$ and $\kappa - \omega$ turbulence models, in such a way that $\kappa - \omega$ model is used in inner boundary layer regions whereas, $\kappa - \varepsilon$ model is used in free shear regions.

The turbulent kinetic energy equation is,

$$\frac{\partial (\rho \kappa)}{\partial t} + \frac{\partial (\rho u_i \kappa)}{\partial x_i} = \tilde{P}_\kappa - \beta^\star \rho \omega \kappa + \frac{\partial (\mu + \sigma_\kappa u_t) \frac{\partial \kappa}{\partial x_i}}{\partial x_i} \tag{3.6}$$

The specific dissipation rate equation is,

$$\frac{\partial (\rho \omega)}{\partial t} + \frac{\partial (\rho u_i \omega)}{\partial x_i} = \gamma \rho S^2 - \beta \rho \omega^2 + \frac{\partial (\mu + \sigma_\omega u_t) \frac{\partial \omega}{\partial x_i}}{\partial x_i} + 2(1 - F_i) \frac{\rho \sigma_{\omega 2}}{\omega} \frac{\partial \kappa}{\partial x_i} \frac{\partial \omega}{\partial x_i} \tag{3.7}$$

where the closure coefficients are $\beta^* = 0.09$

$\beta = 0.075, \sigma_{\omega 1} = 0.65, \sigma_{\kappa 1} = 0.85$ for $\kappa - \omega$

$\beta = 0.0828, \sigma_{\omega 2} = 0.856, \sigma_{\kappa 2} = 1$ for $\kappa - \varepsilon$

F_1 is the blending function μ_t is the turbulent eddy viscosity, S is the invariant measure of the strain rate, and $\widetilde{P}_k$ is the production limiter used in the SST model.

The averaged continuity, momentum, energy, and species transport equations are:

Continuity

$$\frac{\partial \bar{\rho}}{\partial t} + \frac{\partial}{\partial x_i} \bar{\rho} \tilde{u}_i = 0 \tag{3.8}$$

Momentum

$$\frac{\partial}{\partial t} \left(\bar{\rho} \tilde{u}_i \right) + \frac{\partial}{\partial x_j} \left(\bar{\rho} \tilde{u}_i \tilde{u}_j \right) = -\frac{\partial \bar{p}}{\partial x_i} + \frac{\partial}{\partial x_j} \left(\bar{\tau}_{ij} - \overline{\rho u_i'' u_j''} \right) \tag{3.9}$$

Enthalpy

$$\frac{\partial}{\partial t} \left(\bar{\rho} \tilde{h} \right) + \frac{\partial}{\partial x_j} \left(\bar{\rho} \tilde{u}_j \tilde{h} \right) = \frac{\partial}{\partial x_j} \left[\chi_h \frac{\partial \tilde{h}}{\partial x_j} \right] + \bar{S}_h \tag{3.10}$$

Species transport

$$\frac{\partial}{\partial t} \left(\bar{\rho} \tilde{Y}_k \right) + \frac{\partial}{\partial x_j} \left(\bar{\rho} \tilde{u}_j \tilde{Y}_k \right) = \frac{\partial}{\partial x_j} \left[\chi_k \frac{\partial \tilde{Y}_k}{\partial x_j} \right] + \frac{\partial}{\partial x_j} \left[\bar{\rho} D_k \overline{\frac{\partial Y_k''}{\partial x_j}} \right] \tag{3.11}$$

where, $\chi_h = \mu/\sigma + \mu_t/\sigma_h$ and $\chi_k = \mu/\sigma + \mu_t/\sigma_k$

σ_h = turbulent Prandtl number and σ_k = turbulent Schmidt number

3.3 Temperature Dependent Mass Efflux condition (TDME)

A mathematical model for species mass efflux[1] from the liquefying substance is developed based on energy balance at its boundary. A liquefying substance develops a melt layer on its surface when an external heat flux is applied. A fraction of the external heat flux is absorbed into the liquefying substance and the remaining is lost to the surroundings as convective and radiative losses. The net normal heat flux in to the boundary surface is obtained by subtracting surface losses from the heat flux from external ambient, wherein radiation losses can be modelled along with convective losses.

$$q_n = q_a - h_{eff}(T_s - T_a) \tag{3.12}$$

where h_{eff} is the effective heat transfer coefficient for combined convective and radiative heat losses and the ambient temperature T_a is obtained from the solution of the external compressible turbulent ambient flow field.

---

[1] *Aravind G P, Deepu M*, "Implementation of Temperature Dependent Mass Flux Boundary Condition for Convective Mass Transfer Enhancement Computations". 6th International and 43rd National Conference on Fluid Mechanics and Fluid Power December 15-17, 2016, MNNITA, Allahabad, U.P., India
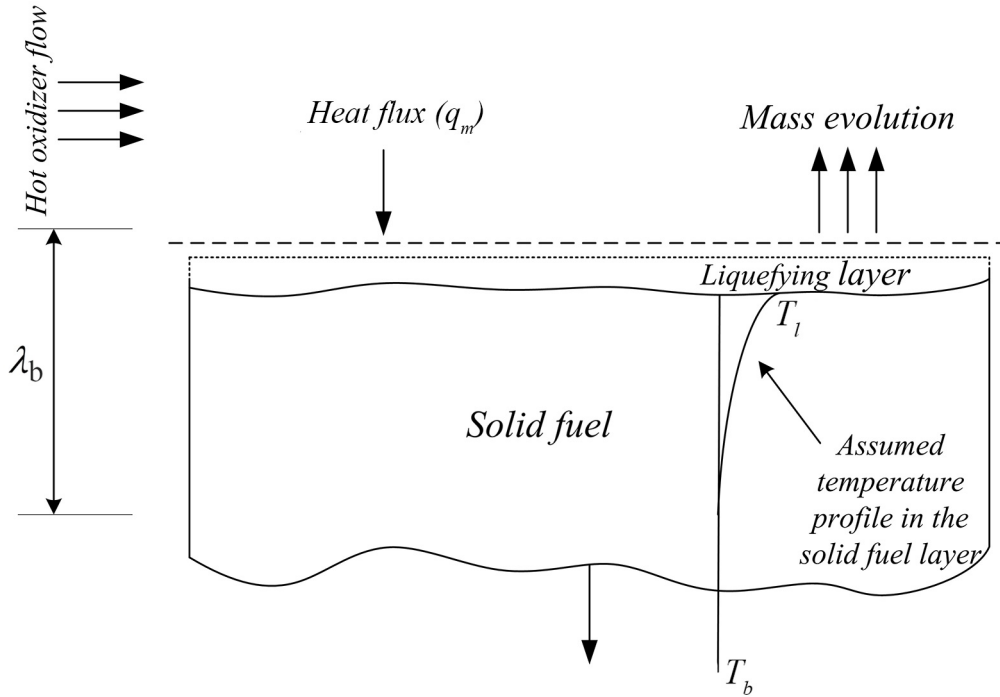
Fig. 3.1 Control volume for the analysis of heat transfer in to solid boundary and mass efflux

As a result of this absorbed flux on the surface, its temperature increases gradually with time. Liquefaction of the fuel starts when it attains the melting temperature. It is assumed that the heat conduction in to the boundary is only one-dimensional and its thermal properties are remaining constant. In case of liquefying substance like paraffin wax or frozen methane, there will be a melt layer formation above it. As a general case, model for the decomposition of a charring material is developed initially and subsequently modified for a simple non-charring liquefying substance. Decomposition process of the charring materials is due to heat transfer towards its char layer, melt layer and base solid layer.

Conservation of energy on the char layer is calculated as

$$\rho_c c_c \frac{d}{dt} \int_0^{\lambda_c} (T - T_l)dx + mc_g(T_s - T_l) = q_s - q_c \tag{3.13}$$

where λ_c is the depth of char layer formed on the boundary and q_c is the heat conducted in to the subsequent melt layer below the char layer. Conservation of energy on the melt layer is calculated as

$$\rho_l \frac{d\lambda_c}{dt}\Delta H = q_c - q_m \tag{3.14}$$

where ΔH is the latent heat of fusion of the solid material and q_m is the heat conducted in to the subsequent solid layer below the melt layer.

Conservation of energy on the base solid material is calculated as

$$\rho_b c_b \frac{d}{dt} \int_0^{\lambda_b} (T(x',t) - T_b)dx' + \rho_b c_b \frac{d\lambda_b}{dt}(T_m - T_b) = q_m \tag{3.15}$$

where λ_b is the depth of the base solid layer and T_b is the temperature at the bottom of the base solid layer.

Assuming a parabolic temperature profile in the base solid layer, the equation 2.10 can be modified as

$$\frac{m}{1 - \phi}\Delta H = \frac{k_c(T_s - T_l)}{\lambda_c} - \frac{2k_b(T_l - T_b)}{\lambda_b} \tag{3.16}$$

where ϕ is the char fraction and k_c, k_b are the thermal conductivities of char and base solid respectively. Surface will be attaining the melting temperature during the process and it leads to the mass entrainment of liquefying substance. There is no need to consider char fraction for a liquefying substance as it does not develop a char layer. Therefore, equation (2.12) reduces to

$$m = \frac{2k_b(T_b - T_l)}{\Delta H \lambda_b} \tag{3.17}$$

This is the expression for mass efflux in gaseous form from the boundary towards the flow field, in terms of temperature gradient developed in the solid substance, when it is exposed to a hot ambient (Fig 3.1). The implementation aspects of this boundary condition in the solution procedure is given in Fig 3.2 as a flow chart (detailed explanation is given in Appendix A).

3.4   Numerical Scheme

Advection Upstream Splitting Method (AUSM) scheme (Liou (1996), Liou (2006)) available in an explicit Finite Volume Method (FVM) based commercial package (Fluent (2012)), has been made use for the inviscid flux computations in the present study. Every inviscid flux is split in to convective flux and pressure flux as

$$F = F_{con} + P \tag{3.18}$$

The convective flux, F_{con} for the present three dimensional compressible turbulent flow field involving species transport is given by,

$$F_{con} = M_{1/2}\begin{bmatrix} \rho a & \rho au & \rho av & \rho aw & \rho aH & \rho a\kappa & \rho a\omega & \rho aY_i \end{bmatrix}^T \tag{3.19}$$
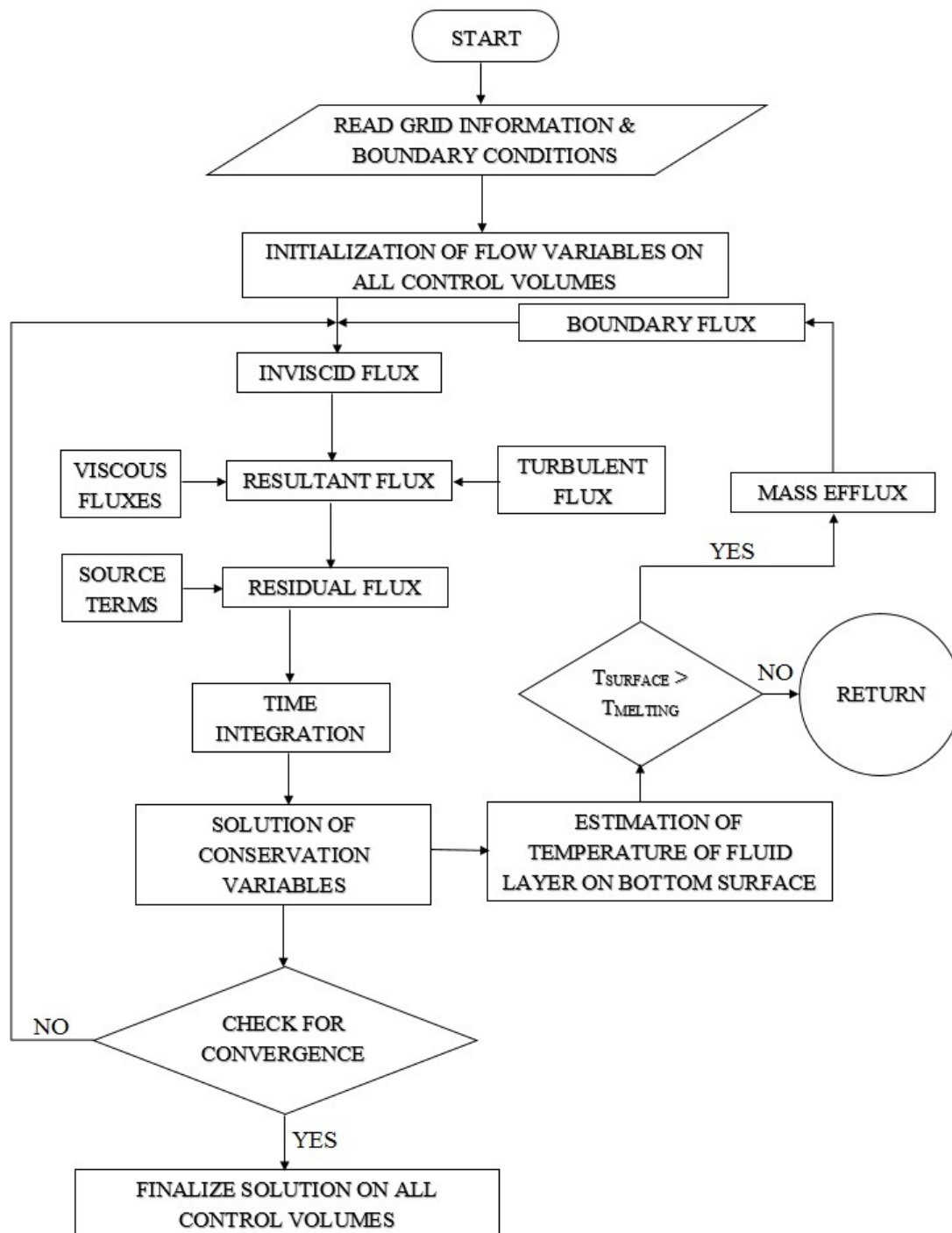
Fig. 3.2 Control volume for the analysis of heat transfer in to solid boundary and mass efflux

where $M_{1/2}$ is called convective Mach number which has been taken out from the convective flux term, that defines the effective convective potential of flow, given by

$$M_{1/2} = M_L^+ + M_R^- \tag{3.20}$$

where M_L^+ and M_R^- are the split Mach number functions. Similarly, the pressure flux term is also split in to split pressure terms are defined by using second order polynomial functions of the acoustic speeds given by

$$P = P_L^+ + P_R^- \tag{3.21}$$

Therefore, the flux at any cell boundary for the present computations become

$$F = (M_L^+ + M_R^-) \begin{Bmatrix} \rho a \\ \rho a u \\ \rho a v \\ \rho a w \\ \rho a H \\ \rho a \kappa \\ \rho a \omega \\ \rho a Y_i \end{Bmatrix} + \begin{Bmatrix} 0 \\ P_x \\ P_y \\ P_z \\ 0 \\ 0 \\ 0 \\ 0 \end{Bmatrix} = m_{1/2} \begin{Bmatrix} 1 \\ u \\ v \\ w \\ H \\ \kappa \\ \omega \\ Y_i \end{Bmatrix} + \begin{Bmatrix} 0 \\ P_x \\ P_y \\ P_z \\ 0 \\ 0 \\ 0 \\ 0 \end{Bmatrix} \tag{3.22}$$

The viscous terms are discretized using a second-order-accurate central differencing scheme and the solution is driven to a steady-state using an explicit second order upwind scheme. Hence the converged results provide the profile of evolved species in the compressible turbulent flow field at a steady state based on the temperature dependent mass efflux condition imposed on liquefying surface in front of vortex generator.

3.5   Data reduction

Fluid flow and associated mass transfer effects dealt in the present study make use of few dimensionless parameters for the description of the results.

Reynolds number estimated based on vortex generator length (B), defined as,

$$Re_B = \frac{\rho V B}{\mu} \tag{3.23}$$

Reynolds number estimated based on dimple diameter (D), defined as,

$$Re_D = \frac{\rho V D}{\mu} \tag{3.24}$$

The entire boundary at the bottom in front of the vortex generator will not be affected by the vortices. The area affected by the induced vortices in the flow field by vortex generators are obtained from the numerical solution. Gentry and Jacobi (2002) , introduced a relative Sherwood number for the quantification of the mass transfer.

Relative Sherwood number, which is the ratio of Sherwood number in the vortex affected area ($\overline{Sh}_{af}$) to Sherwood number in the in vortex unaffected area ($\overline{Sh}_{uf}$), is used in the present analysis to signify the mass transfer enhancement in the vortex affected area. This is calculated based on an area weighting scheme as

$$\overline{Sh}A_L = \overline{Sh}_{af}A_{af} + \overline{Sh}_{uf}A_{uf} \tag{3.25}$$

where A_L is the total area of the bottom wall in front of the vortex generator, and A_{af} and A_{uf} are the area of vortex affected and vortex unaffected regions respectively.

Hence, the relative Sherwood number

$$Sh_R = \overline{Sh}_{af}/\overline{Sh}_{uf} \tag{3.26}$$

Similar to the definition of the relative Sherwood number, a relative vorticity term also used in the present analysis, which is the ratio of vorticity magnitude at vortex affected areas (ξ_{af}) to that in the vortex unaffected areas (ξ_{uf}) as,

$$\xi_R = \xi_{af}/\xi_{uf} \tag{3.27}$$

The growth of instabilities in the flow leads to the shedding of vortices with a natural frequency characterized by Strouhal Number (St), defined as,

$$St = \frac{fL}{V} \tag{3.28}$$

Where V is the mean free stream velocity, f is the characteristic frequency, and L is the characteristic length *(In this thesis, characteristic length may be length of vortex generator (B) or dimple diameter (D))*

Q criterion is used the present study for the detection of vortex dominant portions in transient flows

$$Q_{criterion} = \frac{1}{2}\left(\left|\Omega^2\right| - \left|R^2\right|\right) \tag{3.29}$$

where R and Ω are the shear strain rate tensor and vorticity tensor respectively.

3.6   Validation test cases

3.6.1   Vortex generator placed in high speed compressible flow

Vortex generator placed in high speed compressible flow generates complex three-dimensional flow features. Donohue and cDaniel (1996) used planar based iodine fluorescence to map a high-speed mixing flowfield introduced by an unswept vortex generator. Computational procedure used in the present convective mass transfer study is used to simulate this flow situation reported in the experiment. The wall pressure distribution essentially follows the interaction of generated vortex system with the bottom surface. Wall pressure profile obtained in computations is in agreement with the centerline wall pressure data from this experiment (Fig 3.3). Though the validation test case does not deal with convective mass transfer, this result can be used to compare the wall pressure distribution, which essentially is a true descriptor of the resulting compressible turbulent flow field. Hence this experimental results can benchmark the accuracy of the solver to predict salient flow structures. Similarly, the temperature at bottom wall resulting from the solution of compressible turbulent flow field is also a typical characteristic of the complex flow field. The temperature gradient at the bottom wall resulting from the solution of compressible turbulent flow field is used to compute the mass evolution from boundary using the temperature dependent mass efflux condition developed for the present analysis.
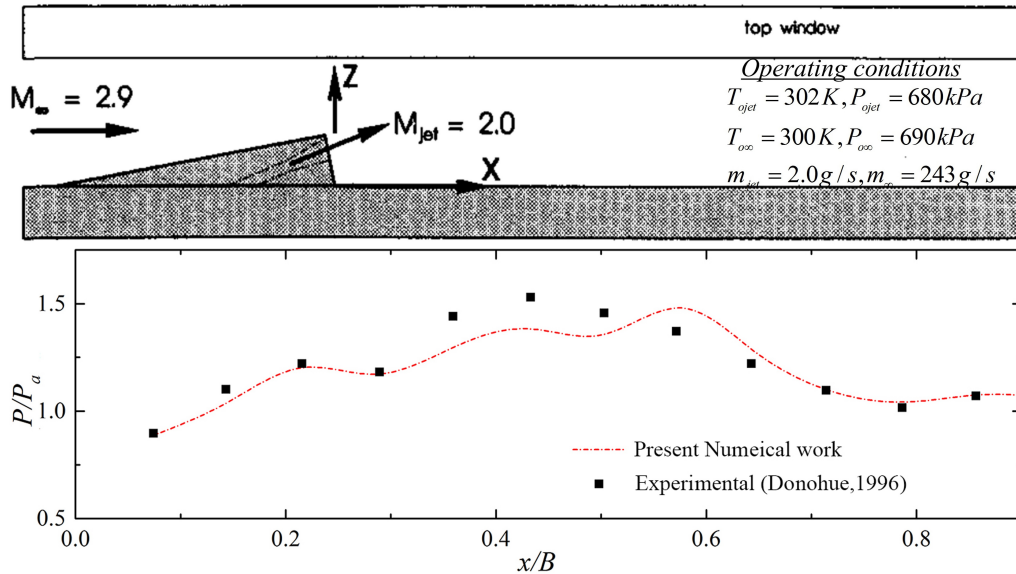
Fig. 3.3 Comparison of computed wall pressure profile with experiment Donohue and cDaniel (1996)

3.6.2 Flow characteristics downstream of tetrahedral vortex generators

Transfer process on a surface placed in the immediate vicinity of vortex generators is a true depicter of vortical fluid motion in its wake region. Henze et al. (2011) measured heat transfer characteristics of a flow field generated by tetrahedral vortex generators. Thermochromic liquid crystals were used for obtaining the heat transfer distribution downstream of the vortex generator. Three component PIV captured the longitudinal vortices generated in the flow field. Aforementioned experimental flow situation is numerically simulated Heat transfer pattern on the surface and the computed area-averaged Nusselt number on the heat plate are well in agreement with experimental data (Fig 3.4). Simulated Nusselt number profile and turbulent intensity (Fig 3.5) is in good agreement with the experimental results.
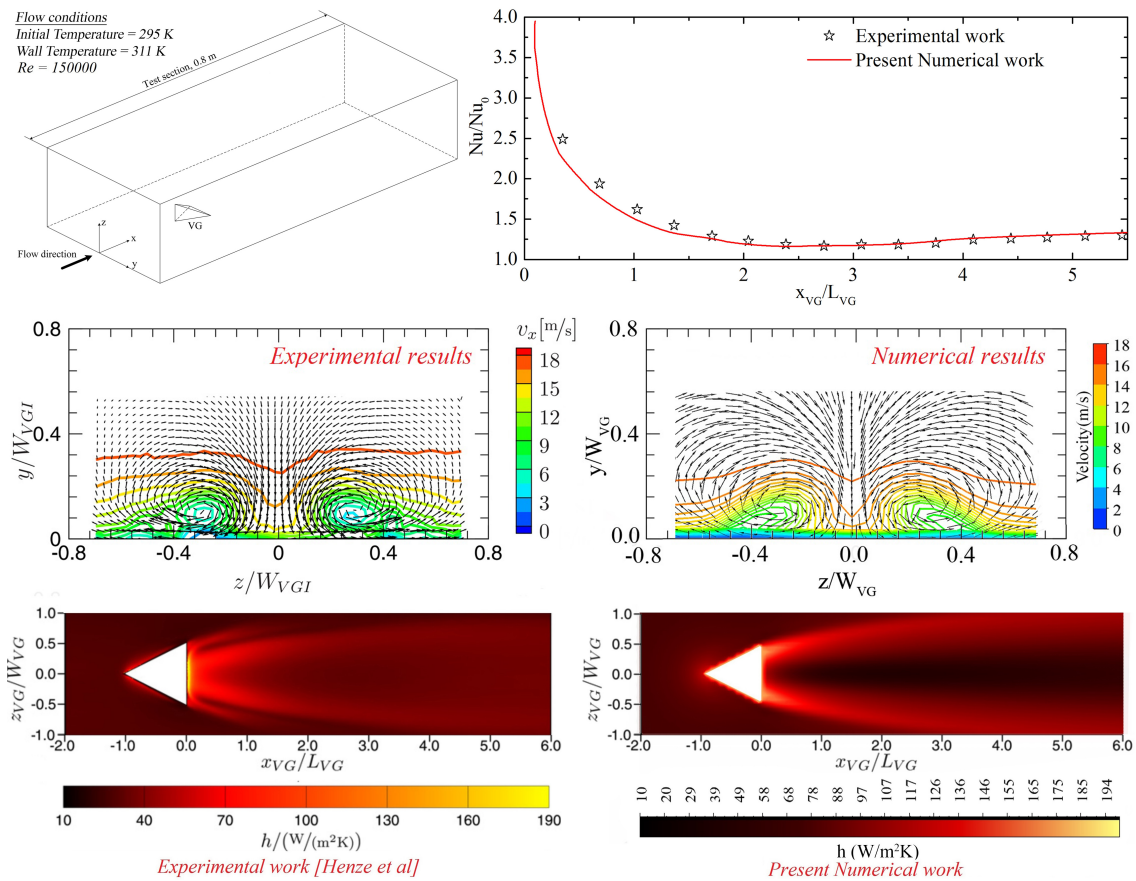
Fig. 3.4 Validation study on heat transfer profiles of flow past a vortex generator (Henze et al. (2011))
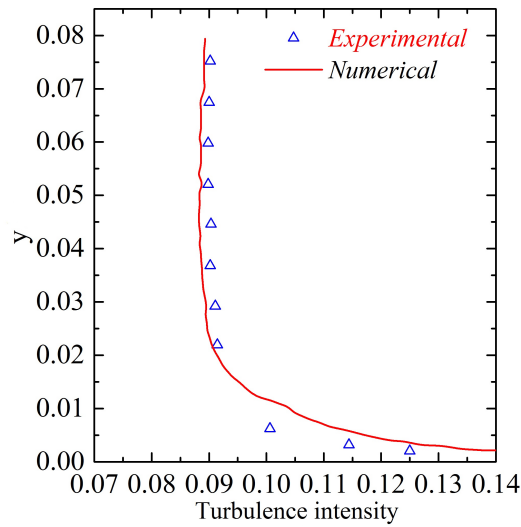
Fig. 3.5 Validation study on turbulent intensity of flow past a vortex generator (Henze et al. (2011))

3.6.3 Heat transfer and flow structure on and above Dimpled surface

Mahmood et al. (2001), Mahmood and Ligrani (2002) carried out infrared thermography mapping of spatially-resolved temperature distributions on a dimpled surface which sheds vortices periodically.
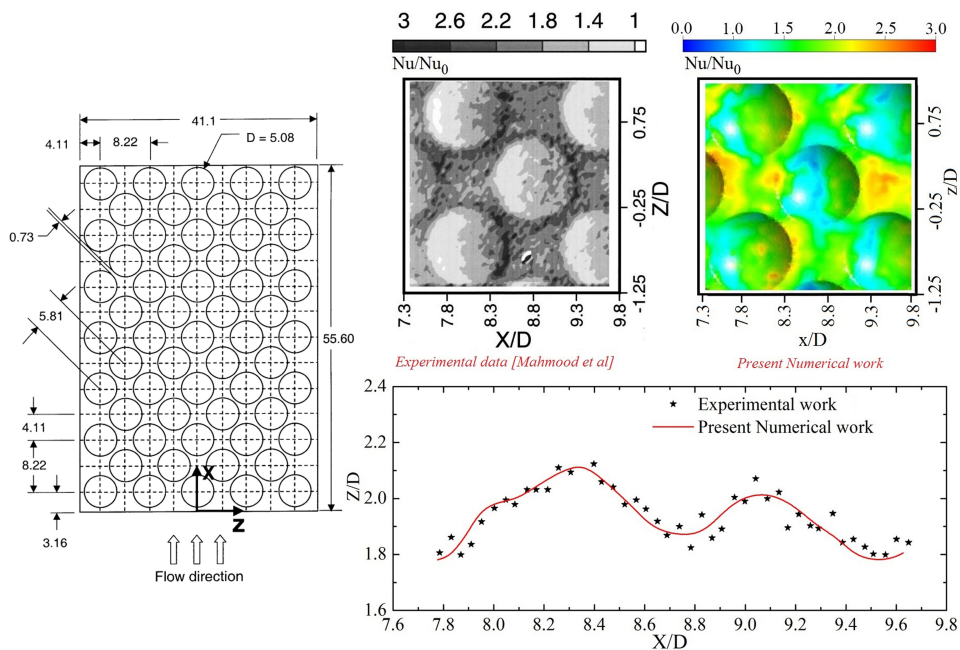
Fig. 3.6 Validation study on heat transfer profiles of the dimpled surface (Mahmood and Ligrani (2002))

Experimental data of the spanwise averaged relative Nusselt number obtained for a typical inflow condition corresponding to Re= 61500 is used to ascertain the accuracy of the present numerical procedure. Nusselt number profile obtained using the aforementioned numerical scheme are in good agreement with experimental observations and could accurately portray the flow and heat transfer characteristics around the dimple surface (Fig 3.6). Heat transfer enhancement is attributed by the recirculation zone generated inside the dimple cavity and reattach of the flow aft rim of the dimple wherein spanwise vortices are being periodically evolved.

3.7   Summary

A temperature dependent mass efflux boundary condition is formulated and implemented in an AUSM based FVM solver. This could successfully update the mass entrainment from the boundary based on the evolution of complex turbulent flow field resulted by the placement of vortex generator in a high speed flow. Computational procedure has been validated using the experimental wall pressure as well as heat transfer profiles reported for a similar vortex generator placed in high Reynolds number flows.

Chapter 4

Mass transfer enhancement using Lateral Sweep Vortex Generators

The basic flow make overs such as secondary flows, reduction of boundary layer thickness, and swirling motion develops favorable gradients for mass transfer enhancement. Novel methods for improving convective mass transfer in high speed flows are essential due to its inherent shortage of residence time.

LSVG [2] creates vortices so as to bring in the effect of vortex boundary layer interaction on the surface of a liquefying substance, as given in Fig 4.1. The surface of the liquefying substance placed downstream of LSVG undergo mass transport in convective boundary layer formed on it. The interaction of flow with the side walls of LSVG generates horseshoe vortices near bottom surface as the flow expands and spills over the vortex generator. Low-pressure regions are formed at the wake of LSVG, which advects more fluid in the lateral free stream to the center. Species evolved by the liquefaction of solid substance gets transported to the mixing zone initially by the horseshoe vortices and later carried by streamwise counter-rotating vortex pair. In this process, evolved mass from the boundary adjacent to the vortex generator gets mixed up well with the high speed free stream as it creates low velocity region to promote molecular diffusion. Convective mass transfer is found to consistently enhance with the increase in lateral sweep provided on the e vortex generator, which helps to have precise control over mass transfer augmentation.

Simulations have been performed for a three dimensional computational domain to compare the mass transfer enhancement due to secondary vortex interaction set in by a Lateral Sweep Vortex Generator (LSVG). Geometry and dimensions of the vortex generator are given in Fig 4.2. Boundary conditions are given in Table 4.1. Reynolds number based

[2]*Aravind G P, Deepu M*, "Numerical Study on Convective Mass Transfer Enhancement by Lateral Sweep Vortex Generators". International Journal of Heat and Mass Transfer, 115, (2017)pp.809-825.
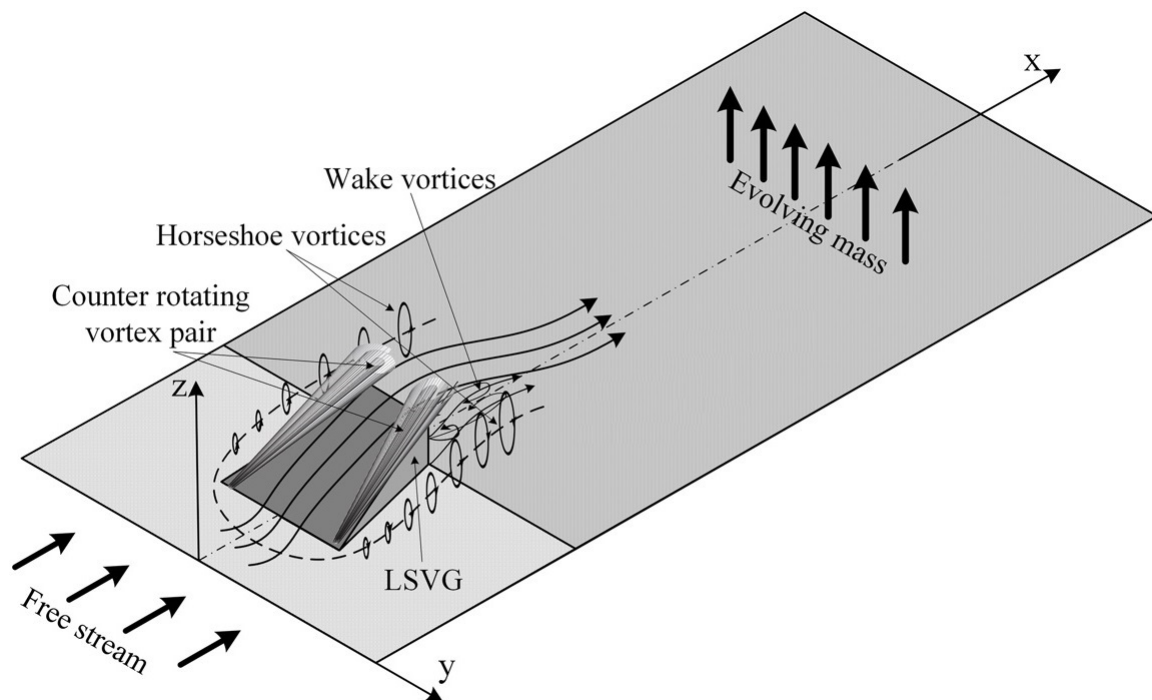
Fig. 4.1 Vortex-boundary layer interaction downstream of LSVG
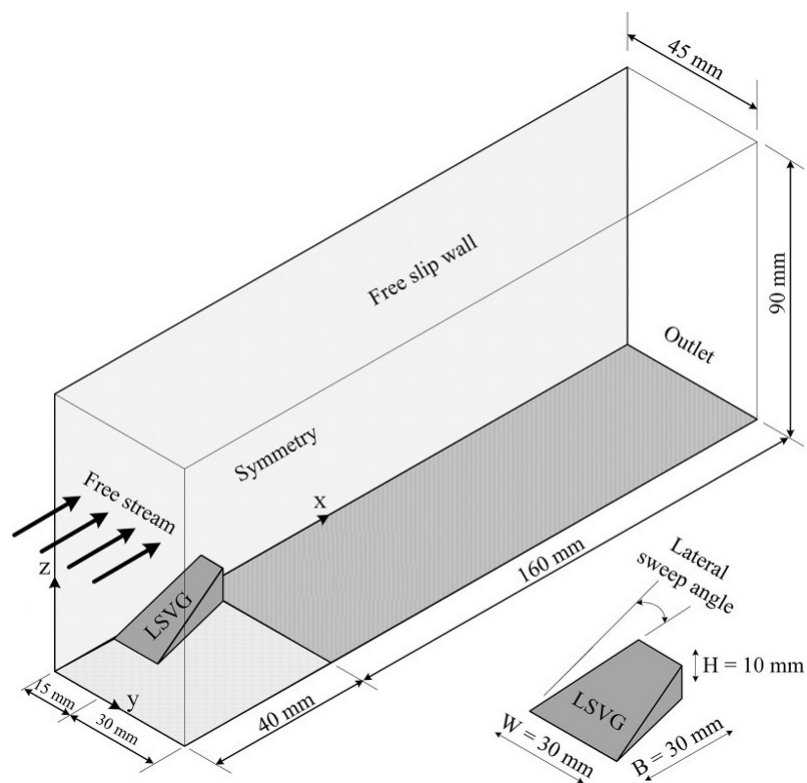
Fig. 4.2 Computational domain and boundary conditions

Table 4.1 Boundary conditions

Inlet	$T = 800K$, $P = 1bar$, $Y_{O2} = 0.23$
Plate	Isothermal wall, $Y_S = f(T_S)$
Outlet	Pressure outlet
Side walls	Symmetry

on the LSVG length (B) is $Re_B = 400000$. A grid independency study has been conducted for computations performed on three-dimensional domain shown in Fig 4.2. The entire computational domain is initialized with free stream conditions. Grid is refined near all no-slip walls and regions close to the LSVG by giving bias in the direction normal to no-slip walls, maintaining a $y^+ \leq 1$. For the present density based solver using an explicit time integration, convergence of the order of 10^{-6} for all residuals has been achieved after about 140000 iterations with a CFL of 0.5. Results are compared for the three levels of grid refinement as given in Table 4.2. The computational domain is initially discretized with 0.7 million control volumes and later refined to 1.4 million and 2.8 million control volumes for which convergence of average dimensionless mass transfer coefficient and wall pressure distribution (Fig 4.3) have been attained. Final grid refinement could converge the first peak in normalized wall pressure distribution within the acceptable limit. Hence the grid size corresponding to the second level of refinement (1.4 million) has been selected for the further simulations. A summary of results of grid independency tests is also given in Table 4.2, the differences in the average values of Sherwood number and normalized pressure are within 1 percentage error.
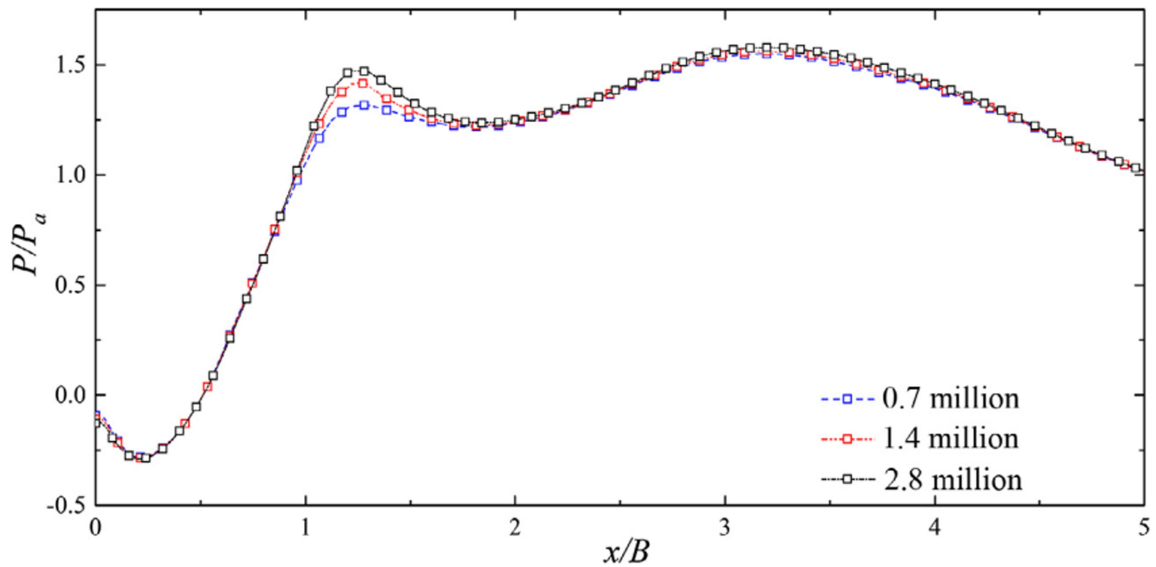
Fig. 4.3 Wall pressure distribution along the stream wise direction for various grids

Table 4.2 Summary of the grid independency test

Grid refinement	No of grid (million)	First peak value of the normalized wall pressure along the centreline	Average Sherwood number
Coarse	0.7	1.33	2.21
Fine	1.4	1.47	2.28
Very fine	2.8	1.48	2.29

4.1   Effect of lateral sweep of vortex generator on mass transfer

It is well established that the longitudinal vortices generated in a flowfield can significantly improve heat/mass transfer effects. A vortex generator with lateral sweep deliberated in the present analysis can set in vortex system that can favor mass transfer enhancement. A temperature dependent mass efflux condition given on the bottom surface creates mass entrainment to the flowfield. This effect gets properly rationalized based on the flow variables in boundary layer as the flow develops. Mass fraction of the evolved substance in the adjoining flowfield is shown in Fig 4.4. Large scale turbulent structures are observed in the developing boundary layer but they are found to get realigned when advected with the downstream vortices. Enhancement in mass transfer is observed more at the wake region downstream of the vortex generator. Strong secondary flows are generated when the high-speed fluid passes over the LSVG introduced in the flowfield. The tangential velocity of these vortices can be as much as double that of the free stream velocity. The advantages of this high velocity secondary flows is that it promotes mixing of the evolving mass from the solid boundary with the incoming fluid. Also it can inject the high energy fluid to the turbulent boundary layer. This injection phenomena delays the growth of the boundary layer and also suppresses the separation of boundary layer. Enhancement in mass transfer is due to longitudinal and horse shoe vortices formed in the flowfield by the LSVGs.

Four LSVG configurations are used in the present study by providing various amounts of lateral sweep ranging from $3°$ to $9°$ and compared its effects with a base VG, which do not have a lateral sweep. Longitudinal counter rotating vortex pairs are generated as the flow attracts more fluid laterally from the free-stream due to pressure difference in flowfield created by the LSVG. Lateral vortices are induced by the flow attachment towards the side wall of the vortex generator. Plots of streamlines and mass fraction field (at z/H = 0.01 above the surface) for different lateral sweep angles analyzed in the present work are given in Fig 4.5. It is clearly visible from the streamline plots that the lateral sweep generates more
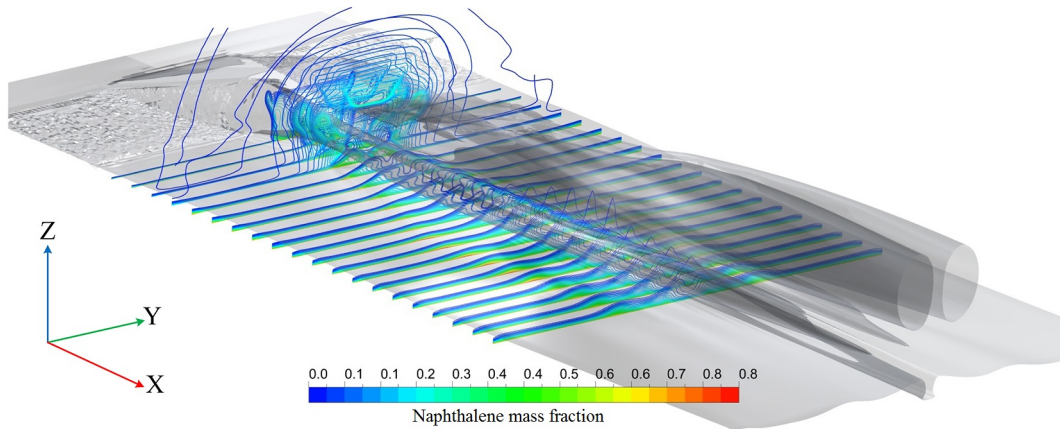
Fig. 4.4 Species profiles of evolved mass in flow field

dominant vortices (Figs 4.5 (b) to 4.5 (e)) when compared to vortices generated by the base VG (Fig 4.5 (a)). Magnitude of velocity at the wake region of the LSVG is less compared to the main stream velocity. These low velocity recirculation regions are also observed in the pattern of streamlines downstream of the LSVG. The axis of this recirculation region is perpendicular to the free stream flow. Similar to the longitudinal vortices, these transverse vortices also rotate in an axis perpendicular to the main flow. These transverse vortices are formed due to the flow separation of fluid from the boundary surface. Transverse vortices are isolated from main flow, and it independently circulates in the wake region. It can also be observed that the size of the wake region decreases when a high momentum fluid passes by the laterally swept vortex generators (Figs 4.5 (b) to 4.5 (e)). The size of this wake region further gets reduced with increase in sweep angle as the longitudinal vortices get intensified. Further in this region, the temperature gradient increases results in increase of mass efflux and results in further enhancement of the mass transfer.

Secondary flows generate strong temperature and density gradients in the flow which favor the mass transfer from an adjoining surface. Enhancement of mass transfer with vorticity augmentation due to the lateral sweep of vortex generator is quantified along the streamwise direction and presented in Fig 4.6 Enhancement in mass transfer is observed from the aft end of the vortex generator (x/B = 0) due to the secondary vortices generated in the flowfield by the LSVG. After a distance of about x/B = 2, the induced vortex pair disappears and hence the effect of mass transfer also dies out.Cross stream normalized velocity profiles adjacent to the vortex generator is given in Fig 4.7. Velocity profiles typical to separated flows can be observed in this study also.

Near wall velocity gradients increases with increase in sweep angle due to strong interference of horseshoe vortex and this effect differ for various angle of sweep. These gradients further enhances near the reattachment point of the shear layer (x/B=1.15). Mass transfer
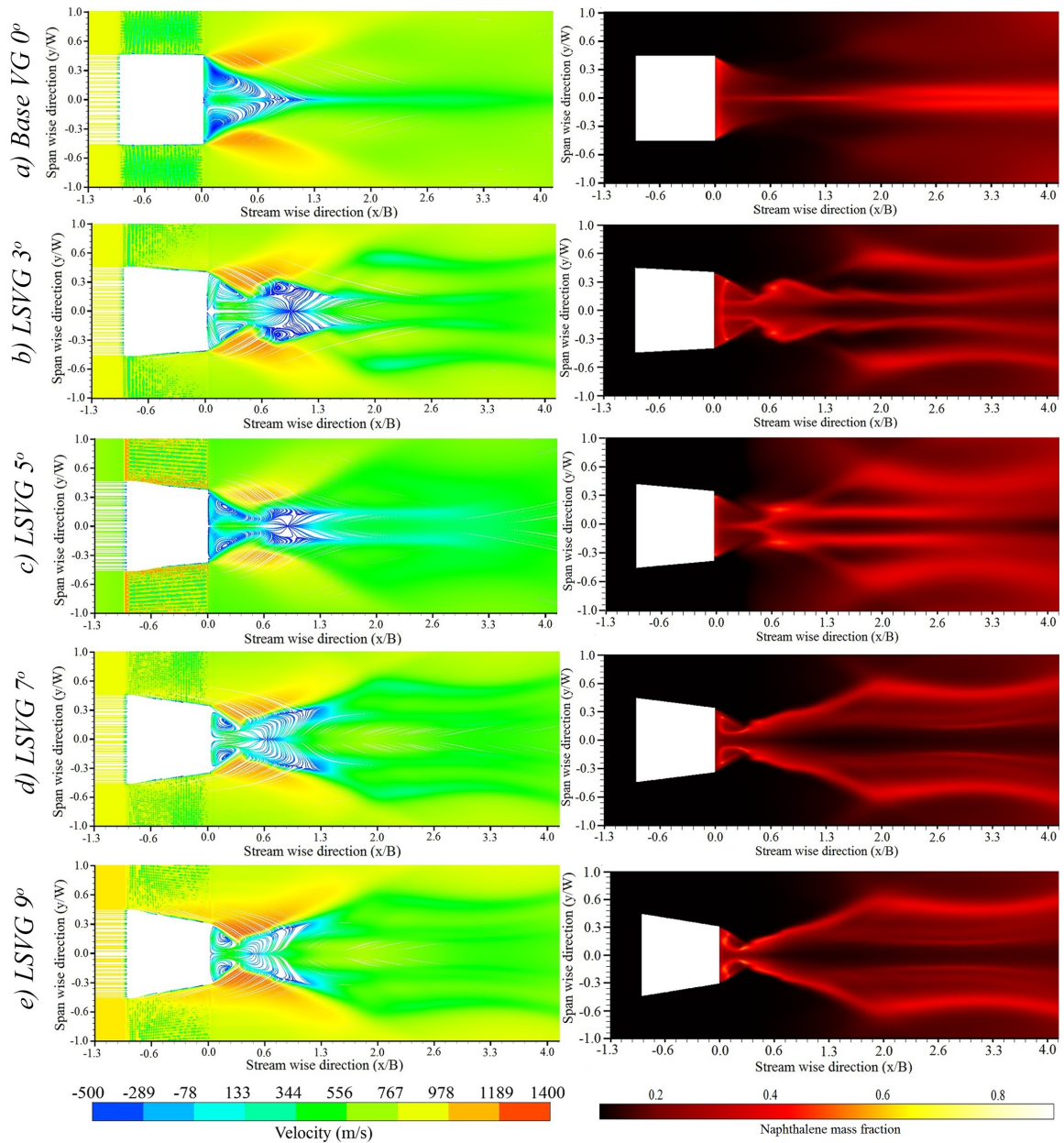
Fig. 4.5 Plots of velocity streamlines and mass fraction field (at z/H = 0.01) for different lateral sweep angles,
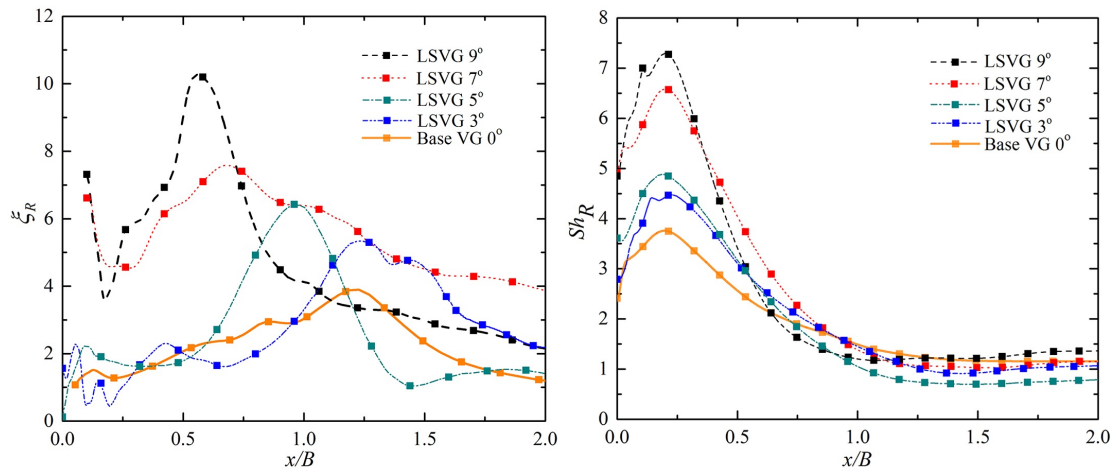
Fig. 4.6 Variation of relative vorticity and relative Sherwood number along stream wise direction
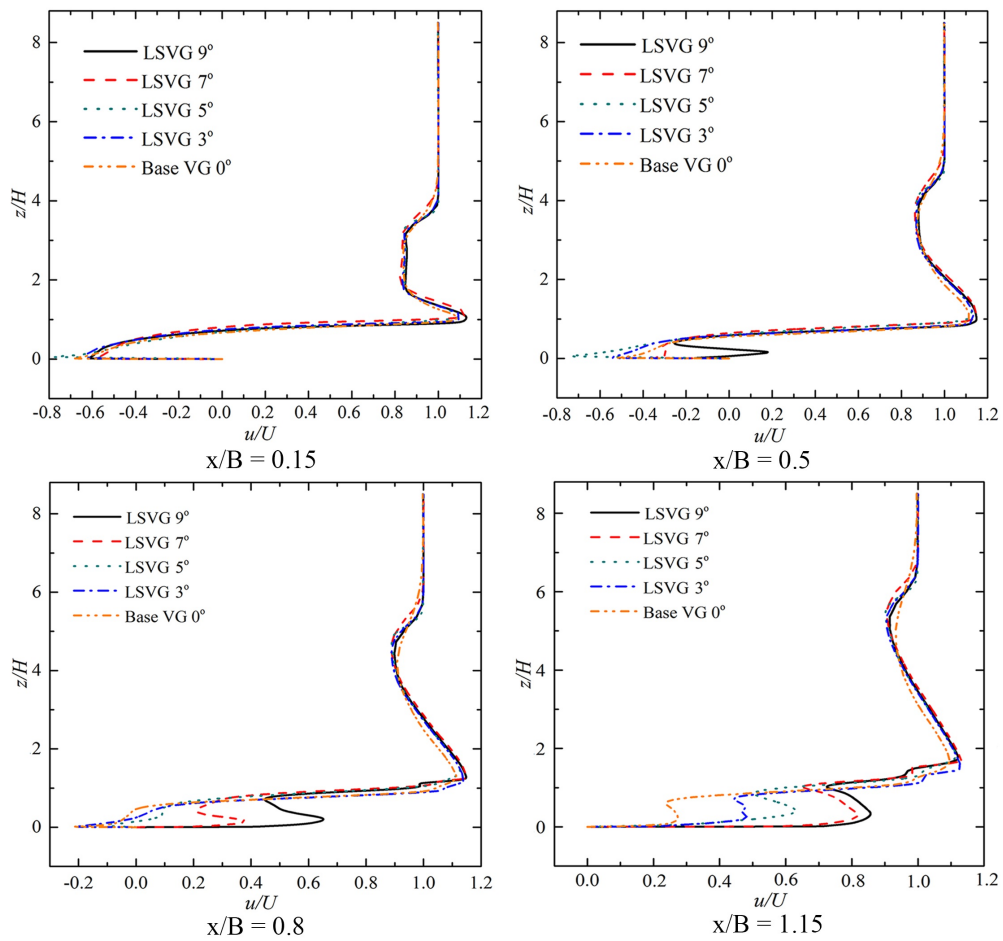
Fig. 4.7 Cross stream normalized velocity profiles at various streamwise locations downstream of LSVGs
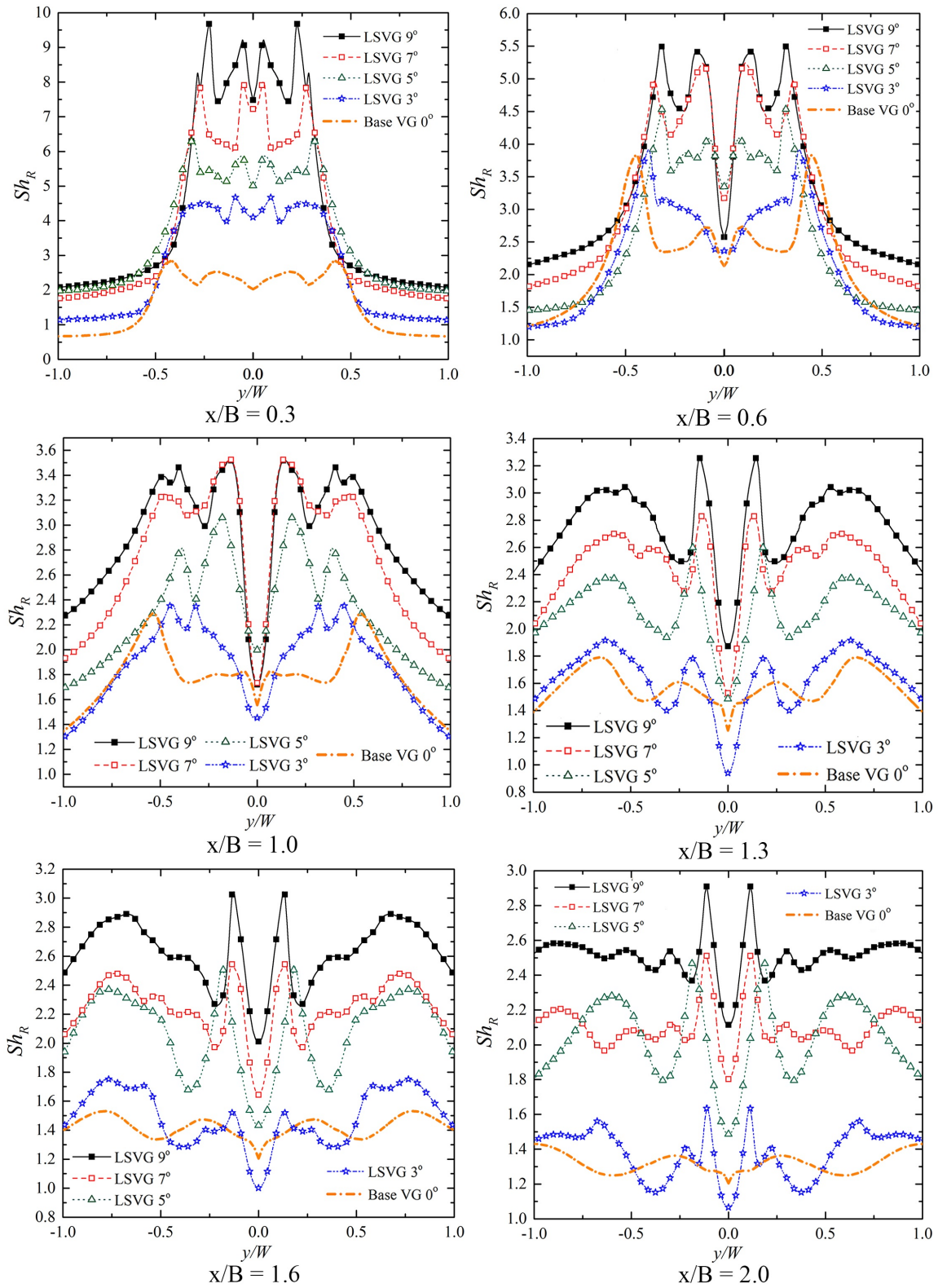
Fig. 4.8 Mass transfer profiles at various streamwise locations downstream of LSVGs

from the bottom surface is significantly influenced by the flow features induced by LSVGs. Sherwood number profiles along the spanwise direction, at various streamwise locations, for different sweep angles analyzed in the present study are given in Fig 4.8. The variation of Sherwood number in spanwise direction depends on the vortex path. A sudden mass transfer enhancement occurs in front of the vortex generator (x/B=0.3) due to the vortices formed by the lateral sweep near to the plane of symmetry. Thereafter, the interaction of longitudinal vortices brings the enhancement in the Sherwood number again. Counter rotating vortex pair approaches towards the center as the lateral sweep increases, which in turn brings the peak mass efflux points to move closer to the centerline. This phenomenon is more predominant in the wake region in front of the vortex generator and becomes insignificant as moved further downstream (x/B=1.6 and 2.0).

4.2 Relation between vortical fluid motion and position of maximum mass efflux

It has been already established from the preceding discussions that mass efflux enhances with vortices with axes parallel to primary flowfield, which is influenced by the sweep angle of the vortex generator. Now the vortex trajectories are obtained based on the numerical solution of the flowfield are analyzed in detail.

This analysis gives the locations of peak mass efflux from the surface and its relation with vortices generated. Fig 4.9 shows the superimposed image of mass efflux on a plot of vortices generated at different stream wise axial locations for the base vortex generator without lateral sweep. It is evident that the counter rotating vortex pair gets lifted off from the boundary surface as it moves away from the vortex generator, thereby its interaction with mass evolving.

The superimposed images of mass efflux on a plot of vortices generated at various streamwise axial locations obtained for LSVG with 9° sweep is given in Fig 4.10. Mass transfer enhancement by the LSVGs are evidently more than that of vortex generators without lateral sweep. This enhancement is due to the presence of horseshoe vortices generated close to the boundary by the interaction of lateral surface of LSVG with the freestream. The first peak in the plot of mass transfer coefficient, along spanwise direction from the center of the LSVG, occurs due to the interaction of horseshoe vortices with boundary. Whereas the second peak in the plot of mass transfer coefficient occur at the interface of this lateral inflow and vortex pairs in the core region as observed in the previous case. Also, this effect of interaction of the lateral inflow and vortex pairs in the core region dominates in farther
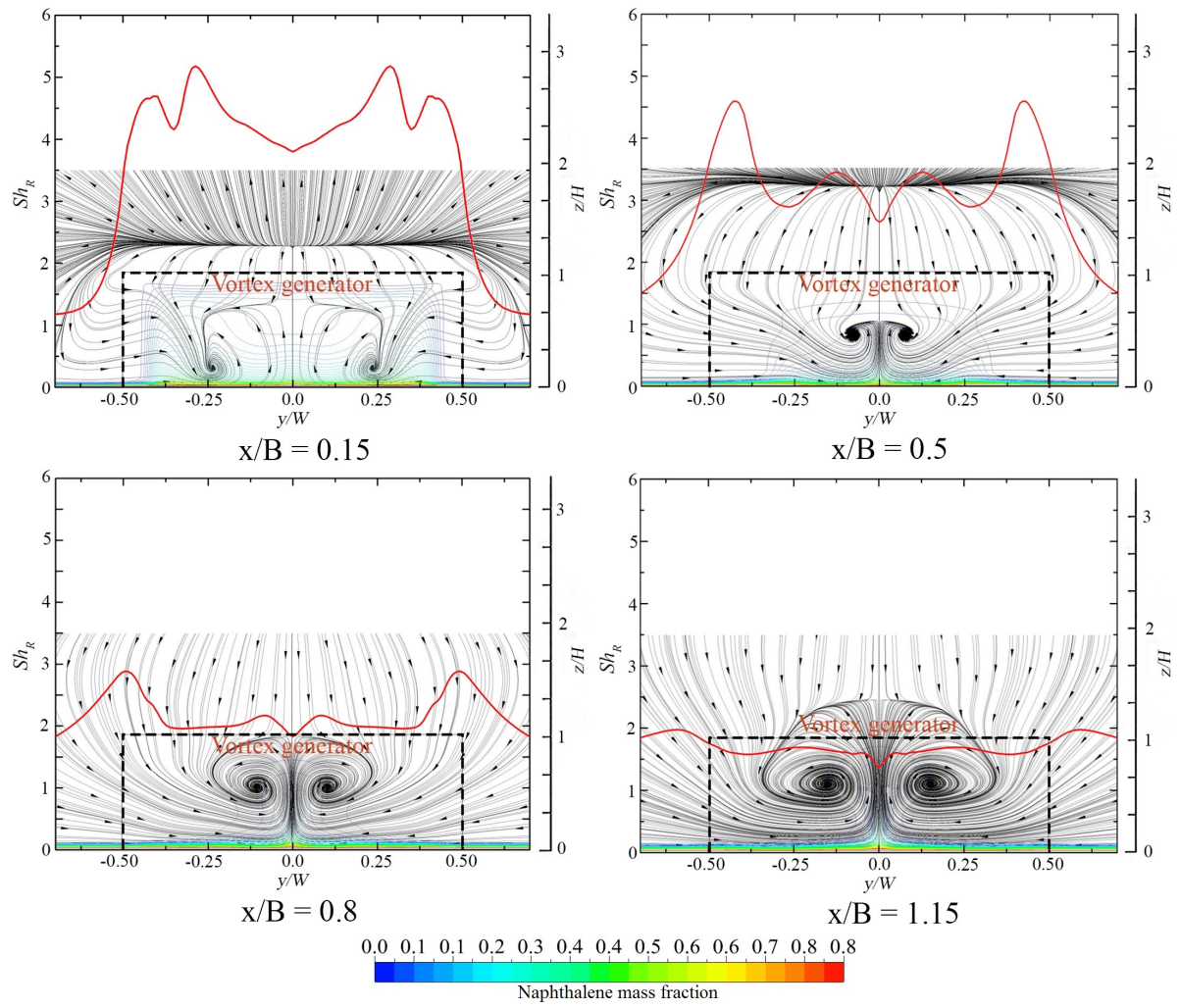
Fig. 4.9 Field plot of species mass fraction superimposed on plot of streamlines for base VG. Red curves indicate the Sherwood number profiles and black dotted lines indicate the position of VG
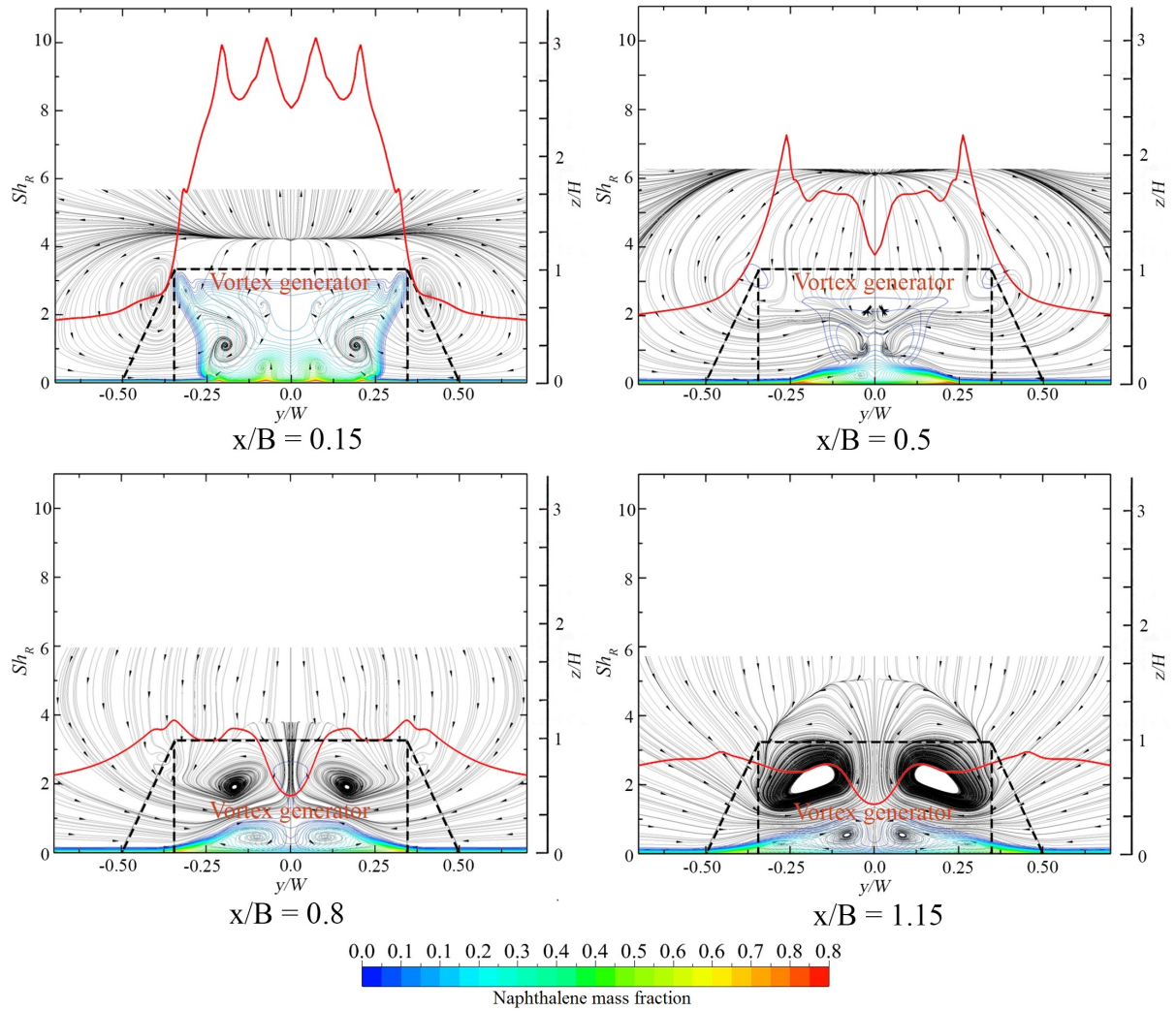
Fig. 4.10 Field plot of species mass fraction superimposed on plot of streamlines for the 9° LSVG. Red curves indicate the Sherwood number profiles and black dotted lines indicate the position of VG
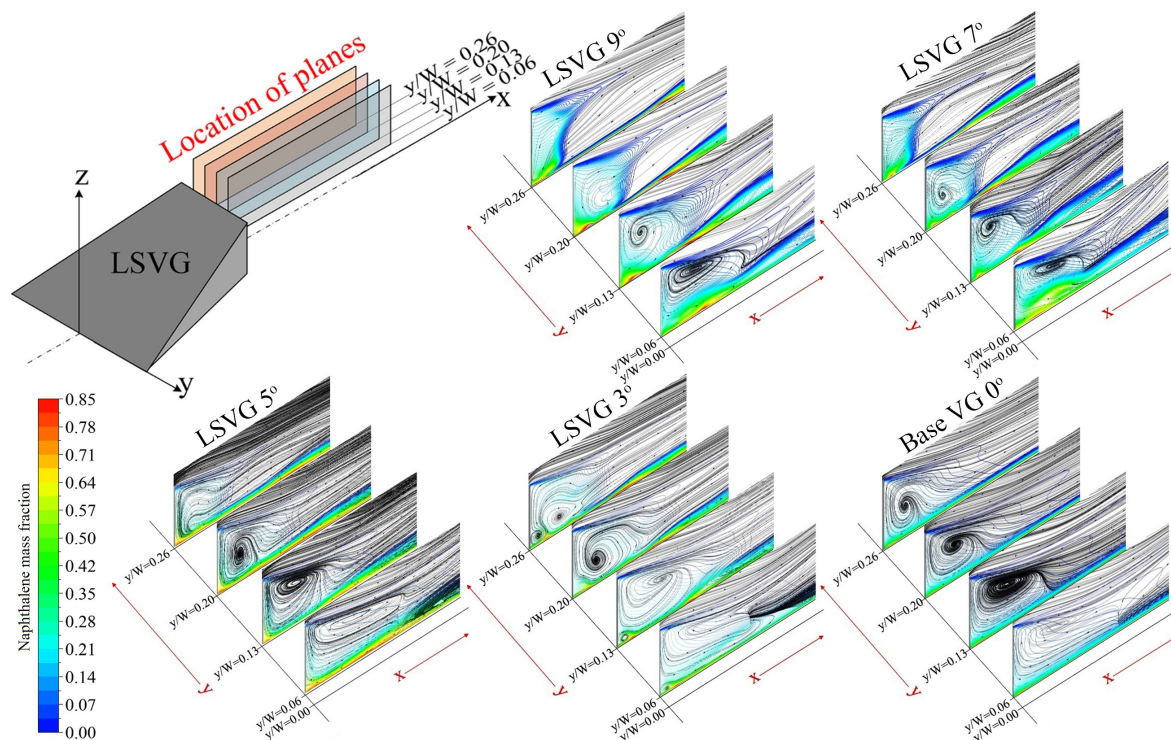
Fig. 4.11 Field plot of species mass fraction superimposed on plot of streamlines in various transverse planes in trapped vortex region

locations (x/B=0.5 and x/B=0.8) from the aft face of the vortex generator. Effect of vortex interactions in the core region diminishes along the streamwise direction as the lateral inflow towards the core lifts these vortices from the boundary. Mass transfer enhancement patterns become almost identical with that of the previous case in regions where the vortices in core region become totally lifted off from the boundary (for the axial location x/B=1.15 in Figs 4.9 and 4.10).

Structure of the three-dimensional trapped vortex in the separation region formed by the reattachment of fluid stream flowing over the vortex generator is shown in Fig 4.11. Contours of mass efflux is superimposed over the streamlines in trapped vortex region. Structure of trapped vortex in the separation region is affected by the interaction of the horseshoe vortices near to the boundary. This interaction significantly affect the streamwise reattachment location of the shear layer. Extent of this interaction varies with the sweep angle of the LSVG. Mass transfer enhancement created by the interaction of horseshoe vortices near to the boundary allows more species to be carried along with fluid streams in trapped vortex inside separation region. Therefore, the trapped vortex can hold more amount of the species evolved from the boundary. In addition to this, the effect of lifting experienced by the core region of counter rotating vortices are also observed for the vortex generators with lateral

sweep. Since the base vortex generator do not generate sufficient interaction of horseshoe vortices, mass transfer enhancement pattern observed in other cases are not observed for them.

4.3   Correlation for relative Sherwood Number (Sh_R) and relative vorticity (ξ_R)

Variation of relative vorticity and relative Sherwood number along the streamwise direction for various sweep angles of the LSVG has been discussed in the preceding section. Now a correlation between relative Sherwood Number (Sh_R) and relative vorticity (ξ_R) is developed. It is evident from the variation of relative vorticity and Sherwood number along streamwise direction that the vortex path can be divided into two zones as shown in the Fig 4.12.

Zone 1:- From the aft end of LSVG to a location where vorticity is maximum. Here the Sherwood number also shows an increasing trend (0<x/B<max vorticity)

Zone 2:- Downstream from the location where vorticity is maximum to a position where effect of vorticity vanishes in the domain (max vorticity<x/B<1)
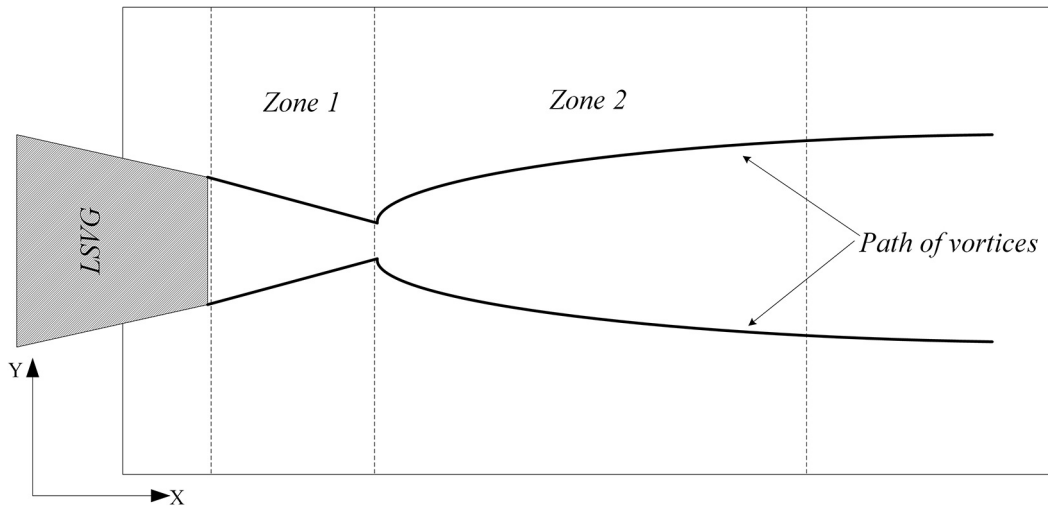
Fig. 4.12 Path of vortices downstream of LSVGs

Both relative vorticity and relative Sherwood number shows an increasing trend in the first zone, in the immediate downstream of the LSVG, whereas these parameters shows a decreasing trend in the second zone. Habchi et al used a similar power law formulation for relating heat transfer effects with vorticity in flowfield. Variation of streamwise relative
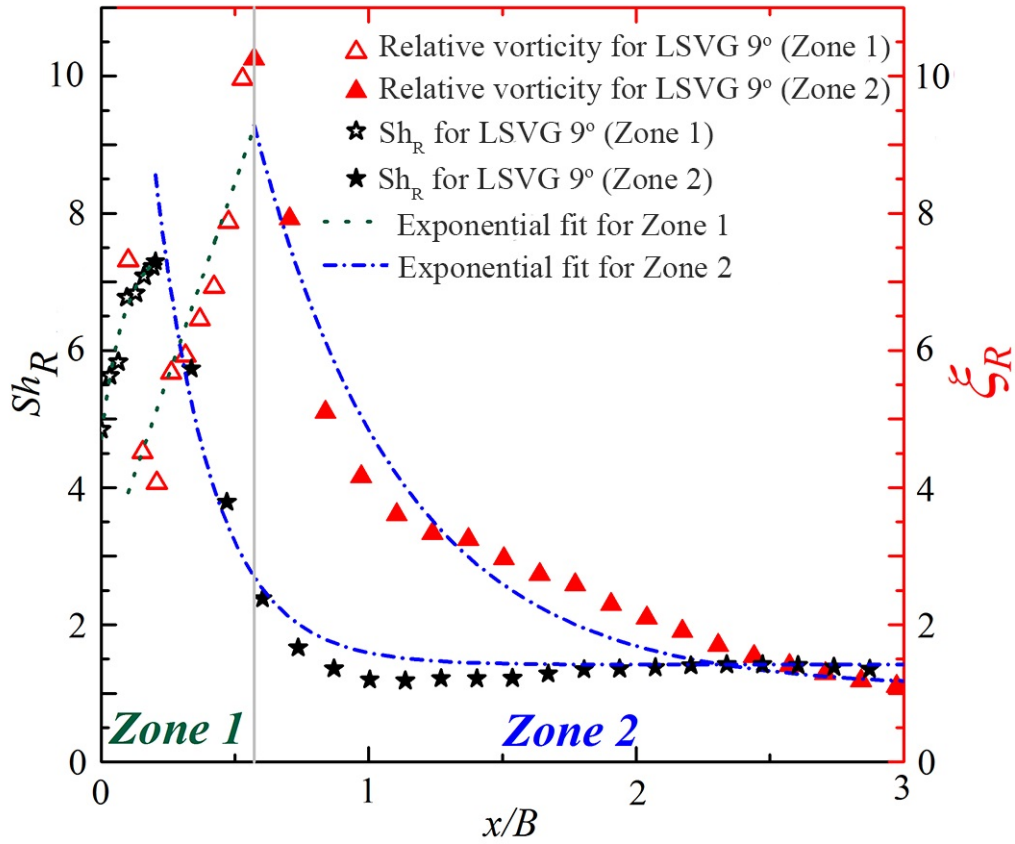
Fig. 4.13 Comparison of numerical solution and correlation for relative Sherwood number and relative vorticity along the streamwise direction for 9° LSVG

vorticity obtained in computations can be represented as,

$$\xi_R = a_1 exp(b_1 \frac{x}{B}) + c_1 \tag{4.1}$$

On rearrangement

$$\frac{1}{b_1} ln(\frac{\xi_R - c_1}{a_1}) = \frac{x}{B} \tag{4.2}$$

The variation of the relative Sherwood number also follows the similar trend,

$$Sh_R = a_2 exp(b_2 \frac{x}{B}) + c_2 \tag{4.3}$$

On rearrangement

$$\frac{1}{b_2} ln(\frac{Sh_R - c_2}{a_2}) = \frac{x}{B} \tag{4.4}$$

Equating the expressions (4.2) and (4.4), to obtain a relation between Relative Sherwood Number (Sh_R) and relative vorticity (ξ_R)

$$Sh_R = \alpha(\xi_R - c_1)^\beta + c_2 \tag{4.5}$$

where

$$\alpha = \frac{a_1}{a_2^\beta}$$

and

$$\beta = \frac{b_2}{b_1}$$

Table 4.3 Coefficients in the correlation between relative Sherwood number and relative vorticity.

		Sweep angle of VG, $\psi(o)$				Base VG
		9	7	5	3	
Zone 1	a_1	0.65	1.06	1.41	1.81	2.37
	a_2	2.69	2.75	4.35	5.06	5.27
	b_1	4.41	2.33	1.65	0.98	0.26
	b_2	1.95	1.52	1.47	1.45	1.36
	c_1	4.41	4.29	2.41	1.19	1.02
	c_2	5.97	5.22	4.02	1.57	2.49
	α	0.42	0.55	0.38	0.17	0.0039
	β	0.43	0.65	0.89	1.47	5.23
Zone 2	a_1	35.58	15.14	13.17	11.73	6.52
	a_2	18.89	12.44	8.58	7.24	5.01
	b_1	-2.41	-1.03	-0.96	-0.72	-0.65
	b_2	-4.72	-3.21	-2.84	-2.70	-2.64
	c_1	1.24	1.21	1.02	0.28	0.23
	c_2	1.42	1.17	1.03	1.08	1.16
	α	0.11	0.0058	0.023	0.007	0.0094
	β	1.96	3.12	2.96	3.75	4.06

The profiles of relative Sherwood Number and relative vorticity obtained in computations are compared with that predicted using the proposed correlation for a vortex generator with 9° lateral sweep (Fig 4.13). The proposed correlation fits well with the trends of variation of both relative Sherwood Number and relative vorticity. The same expression can be generalized for all lateral sweep angles of the vortex generator since the enhancement of mass transfer with vorticity augmentation due to the lateral sweep of vortex generator is showing a unique variation. Coefficients in this proposed correlation between relative Sherwood Number (Sh_R) and relative vorticity (ξ_R) for various lateral sweep angles of the vortex generator are

estimated and presented in Table 4.3. This correlation is applicable for the flow conditions used for the present simulation. It can be observed from the variation of Sherwood number and vorticity along the centerline in streamwise direction that the maximum Sherwood number point and maximum vorticity point is not the same. This is due to the dominance of horse shoe vortex pair over counter rotating vortex pair in the wake region adjacent to the vortex generator.
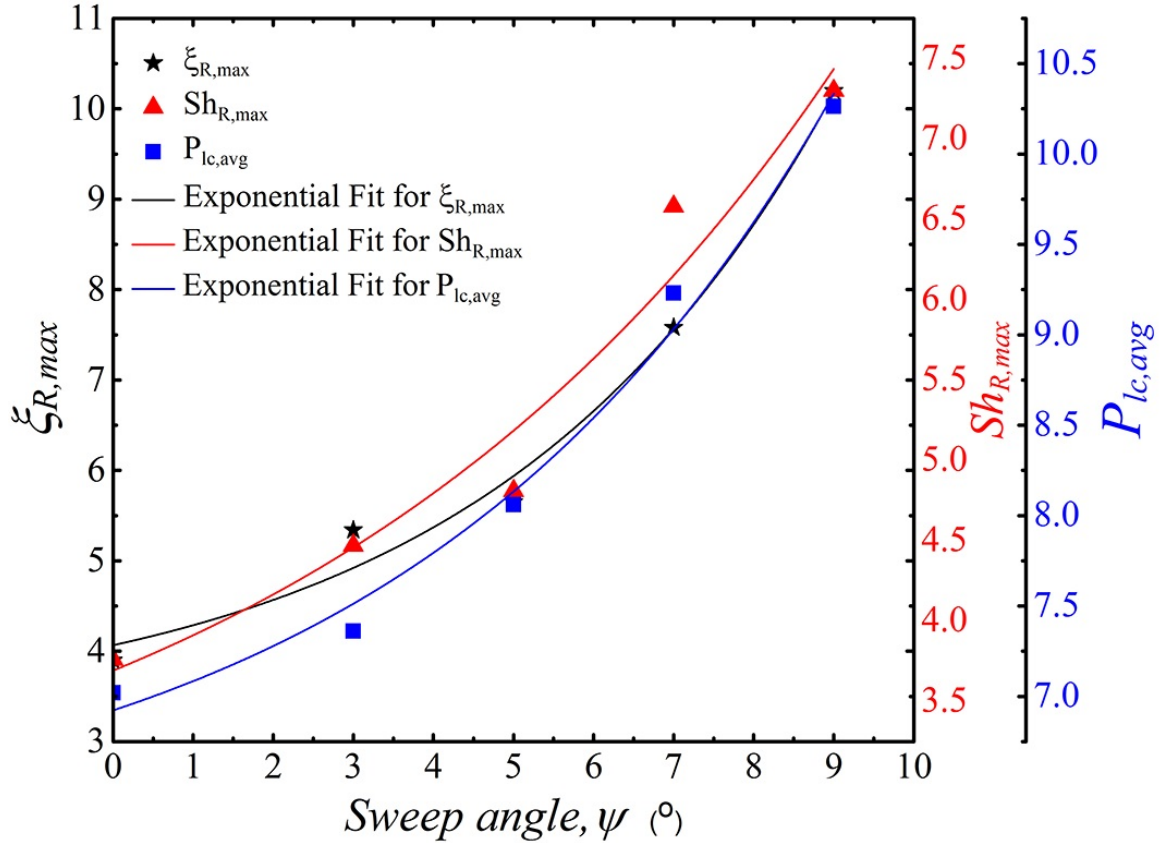
Fig. 4.14 Variation of the maximum relative Sherwood number, relative vorticity and spatial average pressure loss parameter with lateral sweep angle

Maximum values of the relative streamwise vorticity, relative Sherwood number, and the spatial average pressure loss shows a consistent rise with the lateral sweep angle of the vortex generator (Fig 4.14). Following expression is arrived at for the estimation of the maximum values of the relative streamwise vorticity ($\xi_{R,max}$), relative Sherwood number ($Sh_{R,max}$), and spatial average pressure loss ($P_{lc,avg}$) as a function of sweep angle (ψ)

$$\xi_{R,max} = 3.24 + 0.8 exp(0.24\psi) \tag{4.6}$$

$$Sh_{R,max} = 2.25 + 1.4 exp(0.14\psi) \tag{4.7}$$

$$P_{lc,avg} = 6.13 + 0.79(0.18\psi) \tag{4.8}$$

where,

$$P_{lc,avg} = \frac{1}{A} \int_A P_{lc} dA$$

evaluated from x/B=0 to 1.0 in the streamwise direction.

Now. the comparison of results obtained from the developed correlation between Relative Sherwood Number (Sh_R) and relative vorticity (ξ_R) (equation 4.5) and numerical data is discussed in detail. The average as well as maximum Sherwood number is calculated using the developed exponential power law and it is compared it with the numerical data obtained from the solver (Fig 4.15). A maximum difference of $4-6$ % is observed between the maximum Sherwood number estimated using the correlation and numerical computations. The developed correlation is found to be a useful predictive tool for estimating the peak
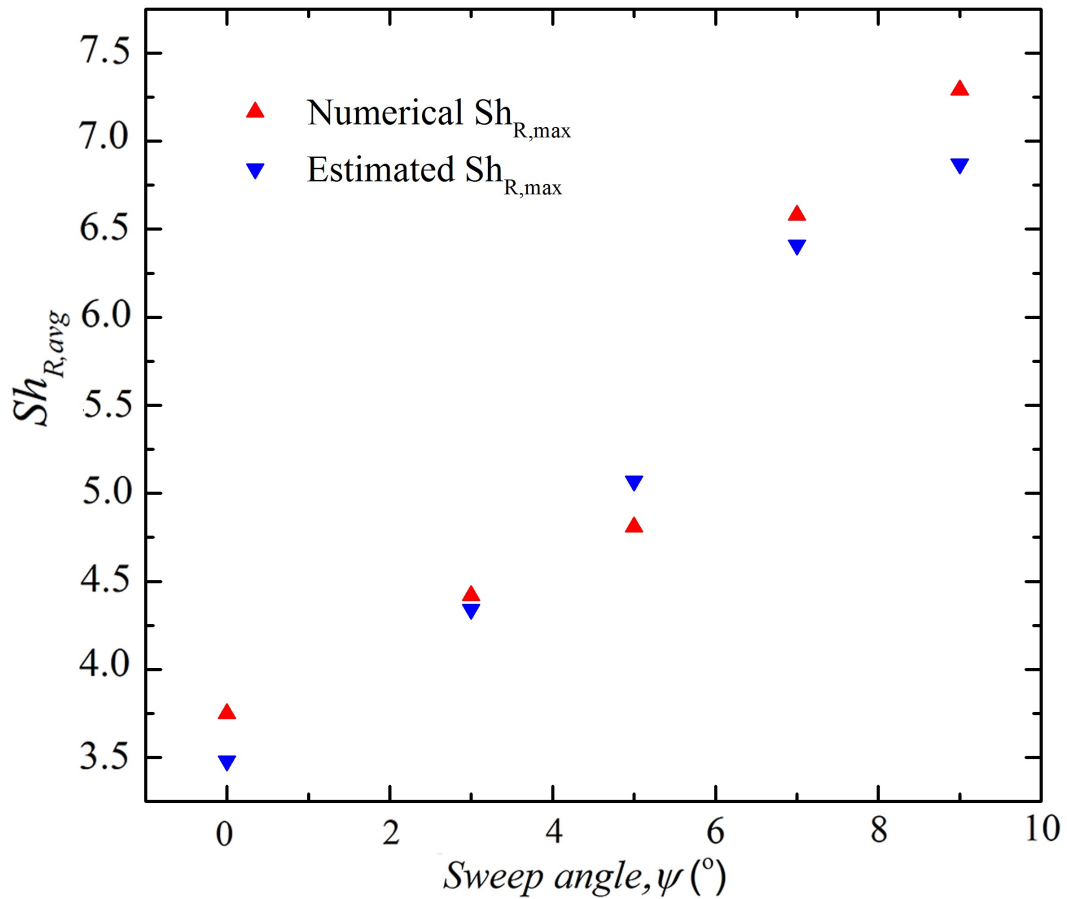
Fig. 4.15 Uncertainties in estimated and numerical maximum Sherwood number

and average mass transfer effect with sufficient accuracy. Local Sherwood number also can be determined using the developed correlation with minor deviations in zone 2 as shown in
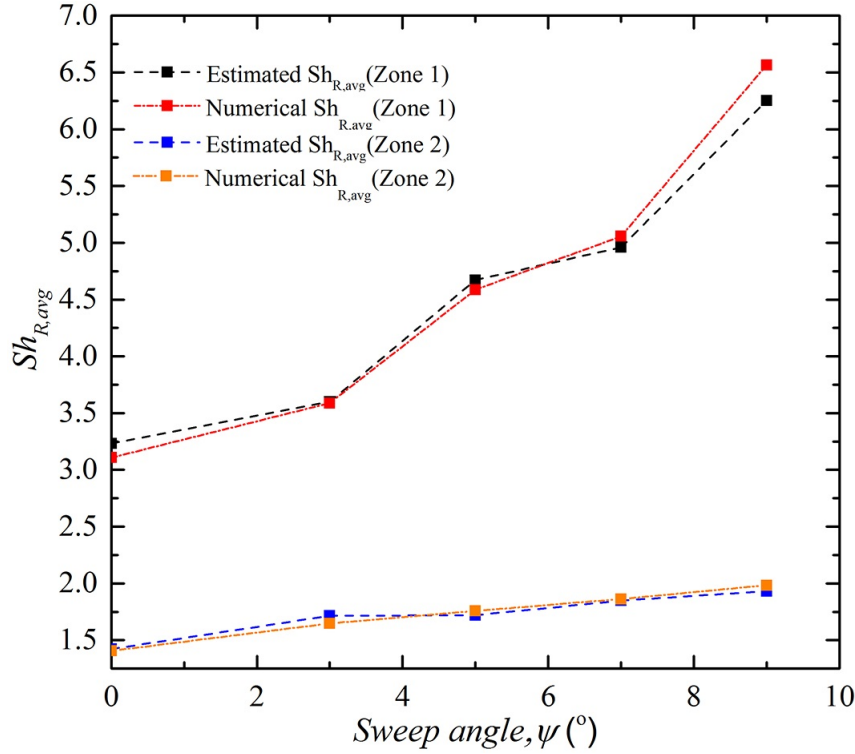
Fig. 4.16 Uncertainties in estimated and numerical average Sherwood number in both zones

Fig 4.16. These deviations are majorly attributed by the data corresponding to the region of dominant vortex interactions. Developed correlation consists of few constants resulting due to the curve fitting leading to an expression with exponential power. Presently, these constants are chosen in such a way that it shows a consistent variation with sweep angle of LSVG (Table 4.3)

4.4   Secondary flow interaction and Mass transfer

Wake regions generated in front of the vortex generators enhances the entrainment of lateral fluid streams and in turn leads to the formation of longitudinal counter rotating vortex pair. Detailed analysis of vortical fluid motion revealed the relation between longitudinal vortex interaction and location of peak mass efflux for a base VG and lateral sweep VG. Now, the focus is on trajectories of longitudinal vortices and the related mass transfer. Analysis of secondary flow field can characterize the vortices and estimate its trajectory. Geometry and dimensions of the multiple VG configuration used in the present study is given in Fig 4.17.
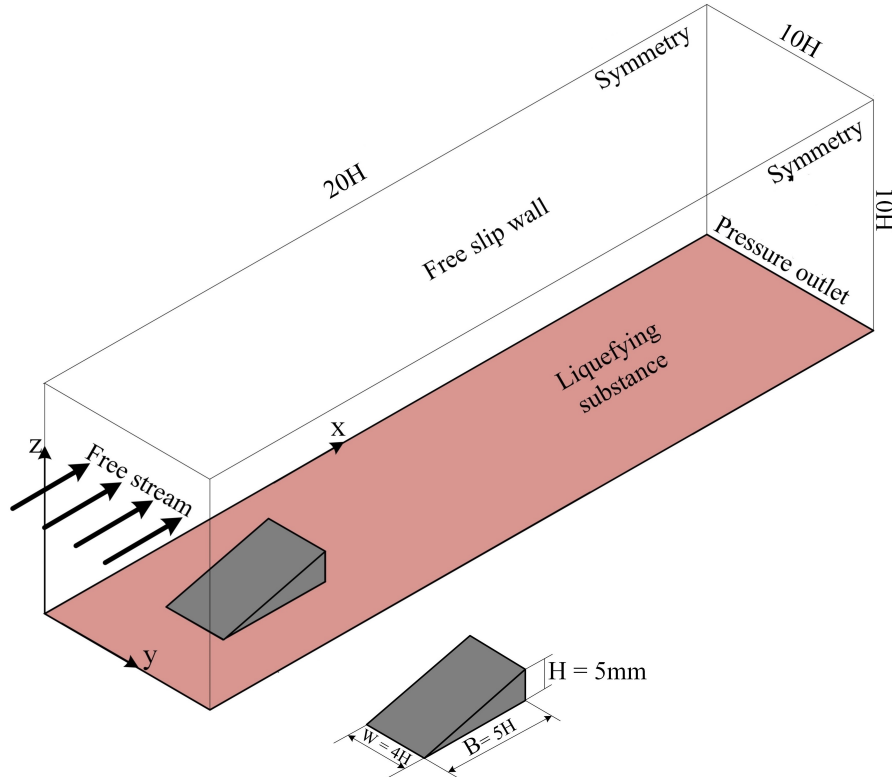
Fig. 4.17 Computational Domain with single LVG

4.4.1 Vortex theory and method of images

A few characteristic values need to be taken into account to give a representative description of a vortex. The local angular rate of rotation is defined by the vorticity ξ_x, which is a function of velocity field.

$$\xi_x = \frac{\partial v_y}{\partial z} - \frac{\partial v_z}{\partial y} \tag{4.9}$$

Another important value is the circulation (Γ). Circulation can be obtained from the numerical results either by taking the line integral for the velocity field or by taking the surface integral of vorticity over an area enclosing the vortex. A scheme of counter rotating vortex pair is shown given in Fig 4.18.

$$\Gamma = \oint_S \vec{v}\,\vec{ds} = \int_y \int_z \xi_x dy dz \tag{4.10}$$

Fundamental values for the vortex characterization are its position with respect to the wall boundary as well as the distance to existing neighboring vortices.

Gentry and Jacobi (1997) found a correlation between the circulation and the trajectory of vortices close to a wall (e.g. plate flow). The flow field induced by two counter-rotating
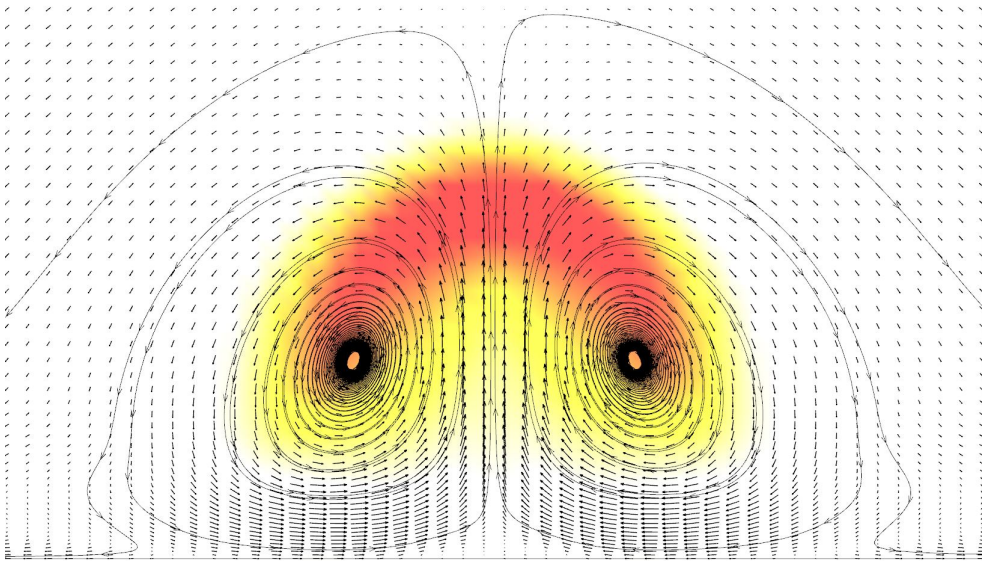
Fig. 4.18 Scheme of counter rotating vortex pair showing the circulation

vortices in a plate flow is obtained by the potential flow theory. The enhancement of heat transfer in a flow field depends on the circulation developed by the stream wise vortices. Here the vortex strength is measured by potential flow theory. The magnitude of induced core velocity for vortex 1 in x direction is given by,

$$V_{1,x} = \frac{\Gamma_0}{4\pi p} \tag{4.11}$$

which shows for a stronger vortex and nearer to the wall, induced core velocity will be more. The core-to-core (2C) and core-to-plate (p) distances were determined from images similar to Fig 4.18 and 4.19 at different stream wise locations in front of vortex generator. Referring to Fig 4.19, vortex 1 has a velocity in the y direction due to its induced velocities from vortex 3 and vortex 4. Using equation 4.11, superposition, and basic trigonometric relations, the y-velocity of vortex 1 can be written as follows:

$$V_{l,y} = \frac{\Gamma_o}{4\pi p} \left(\frac{\phi^2}{\phi^2 + 1} - 1 \right) \tag{4.12}$$

The induced velocity can also be expressed as,

$$V_{l,y} = \frac{\Delta y}{\Delta t} \tag{4.13}$$
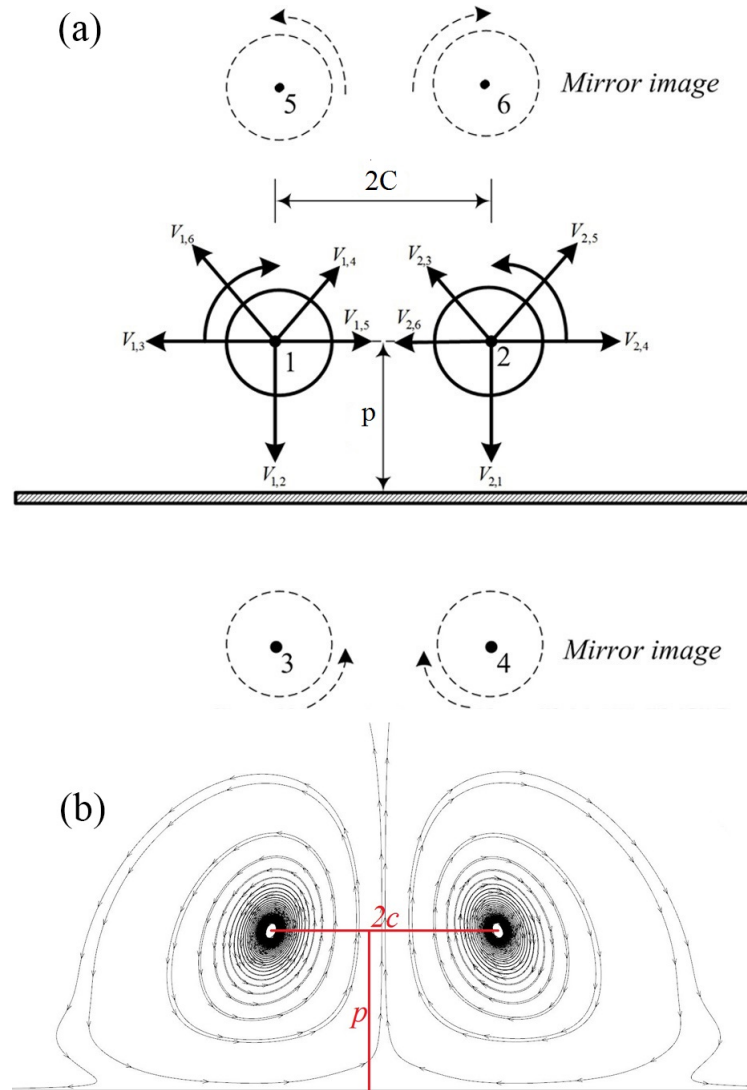
Fig. 4.19 Method of images and Secondary flow field denoting circulation

With an assumption that the vortex moves axially with a convective velocity equal to the freestream velocity, the transit time can be approximated as

$$\Delta t = \frac{\Delta x}{V_\infty} \tag{4.14}$$

Substitute and rearranging gives,

$$Circulation, \Gamma_o = 4\pi\eta(1 + \phi^2)V_\infty \tag{4.15}$$

where, $\phi = p/C$ and $\eta = \Delta y/\Delta x$

4.4.2   Vortex trajectory and locus of peak mass transfer

A rectangular boundary enclosing the vortex generated is set as the limits of integration. By assuming the vortex trajectory is directly related to the lateral location of maximum heat transfer, lateral drift ($\Delta y/\Delta x$) in vortex trajectory and location of maximum heat transfer can be compared. Table 4.4 summarizes the data values required to calculate the lateral shift, which are taken out from the numerical results. Increased circulation leads to spreading of vortex streaks. At four positions (Δx = 0.02, 0.03, 0.04, 0.05m) from the trialing edge of single VG, each vortex is directly related to one location of maximum mass transfer. Comparison between the lateral shift obtained shows there is an approximate one to one relation between the vortex trajectory by the velocity field and location of maximum mass transfer as shown in Fig 4.20. By this understanding one can easily obtain the locus of peak mass transfer by analyzing the strength of vortex path as elaborated in Appendix B.

Table 4.4 Location of maximum mass transfer and vortex trajectory

VG	x/B	Δx (m)	Γ (m^2/s)	p(m) x 10^{-3}	C (m) x 10^{-3}	Lateral drift ($\Delta y/\Delta x$)	Location of maximum mass transfer
Single	2.5	0.02	40.35	2.978	7.27	0.011	7.45
	3.0	0.03	59.52	3.013	7.02	0.016	7.05
	3.5	0.04	171.91	4.778	6.12	0.034	6.21
	4.0	0.05	188.11	4.814	5.71	0.035	4.67
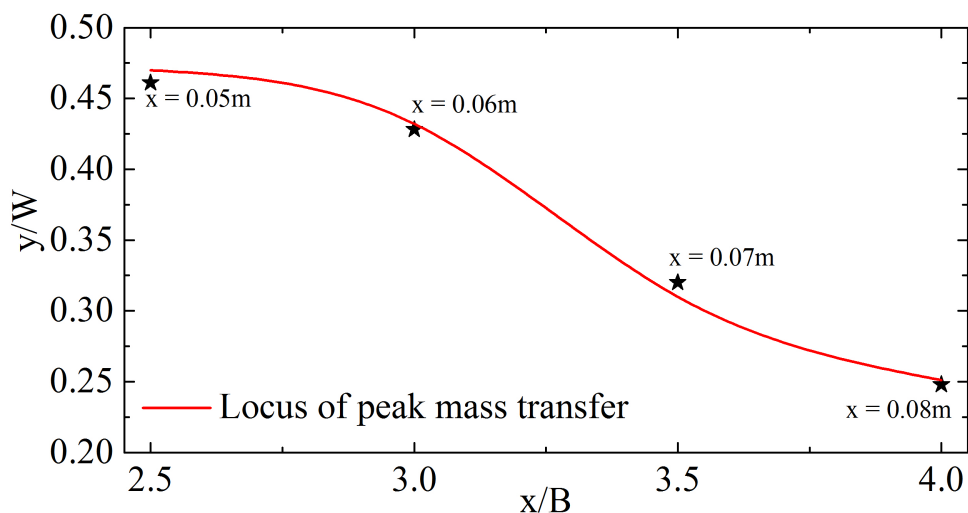
Fig. 4.20 Location of maximum mass transfer and vortex trajectory

4.5   Effect of Multiple Vortex generators

Single flow manipulator when placed in the flow field can set in a vortex system that favour mass transfer and is evident from the previous discussions. Major limitation of a single vortex generator is that it cannot sustain the enhancement effect for wider expanse beyond its vicinity. It is evident from the analysis done by the vortex trajectory and locus of peak mass transfer. The vortex strength ceases after when moving farther downstream. Enhancement in mass transfer can be significantly improved by the introduction of multiple vortex generators. This section focuses on a comparative study of mass transfer by a single VG and multiple VG configurations. Pressure losses accounting for the same is also compared in the present study. Geometry and dimensions of the multiple VG configuration used in the present study is given in Fig 4.21.

Vortex intensities and corresponding effect on heat transfer will vary with nature and extent of their interaction. Velocity magnitudes associated with regions of vortex boundary layer interaction as well as counter rotating vortex pair are observed to be relatively smaller compared to other regions. This enables the formation of gradients favouring enhancement of heat transfer. All these observations are already discussed in the previous sections. The presence of multiple VGs leads to the development of dissimilar vortices, and hence the symmetry of the flow field also becomes affected.

For single VG configuration, the effect of turbulence generated is mainly on the wake region in front of the vortex generator. However, introduction of multiple vortex generators aids in sustenance of vortices generated to farther downstream. Fig 4.22 shows the plot of streamlines superimposed on Turbulent Kinetic Energy contours for both the configuration. The TKE comparison indicate the influence of multiple vortex generators in sustenance of more turbulence in the flow field.

Fig 4.23 shows the field plot of species mass fraction superimposed on plot of streamlines for single VG configuration and multiple VG configurations at different stream wise locations. Dissimilar vortex interaction in the wake region advects more fluid laterally to the developing boundary layer. This enhancement is due to the occurrence of more than one vortex pair in the flow field. Mass transfer enhancement is more predominant in the wake regions at the trialing end of vortex generator. As the fluid passes over the VG, strong secondary vortices are produced with tangential velocities as much as two times that of free stream velocity. The high momentum fluid when passes over the sliding surface of vortex generator gets accelerated and injected into the boundary layer downstream of flow. This phenomenon results in thinning of boundary layer and more heat gets convected into the flow field. Due to the pressure difference created by the LVG, more fluid gets attracted in the lateral direction. This generates a longitudinal counter rotating vortex pair close to the lateral surfaces of VG.
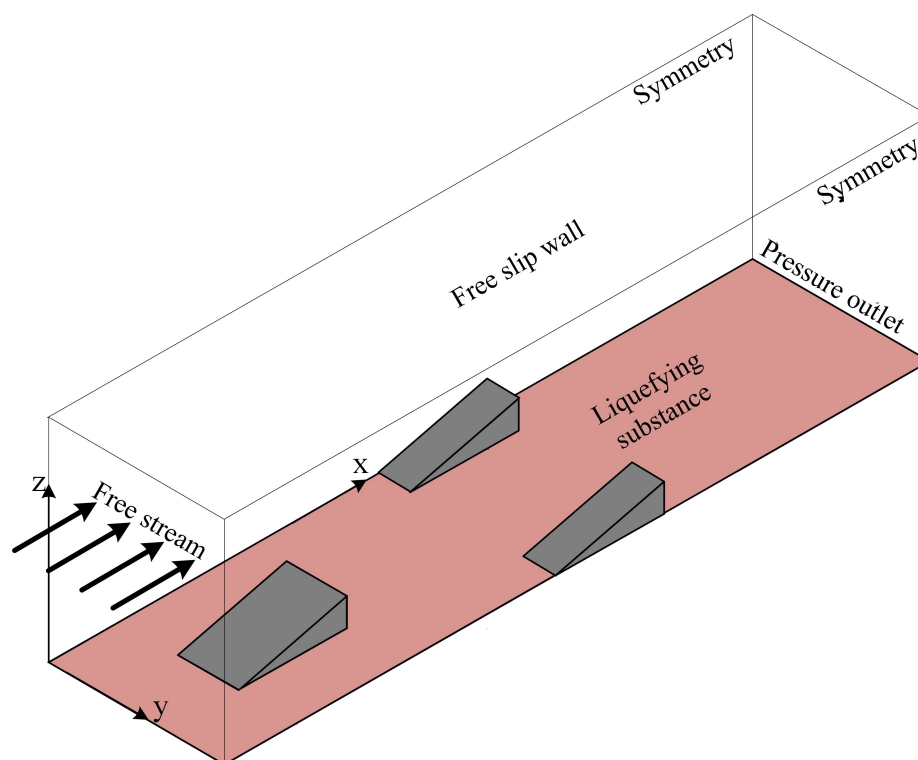
Fig. 4.21 Computational Domain with multiple LVGs

Also, horseshoe vortices are generated close to the boundary layer due flow attachment at the lateral surface of vortex generator. Velocity patterns similar to that of separated flows are observed in the present work also. Strong gradients of velocity and temperature are observed near to the wall and at the wake regions of the VG. These gradients get dominated with the introduction of multiple vortex generators in the same flow field and which in turn increase the heat transport in to the flow. The distribution of mass transfer along the span wise direction and span wise direction shows a significant increase in regions where secondary vortices and their interactions are predominant (Fig 4.23). Magnitude of velocity in the wake region of VG are much less than that of free stream velocity. Axis of the recirculation region is perpendicular to the free stream flow. Vortices generated in this recirculation regions rotates perpendicular to the main stream flow and are termed as transverse vortices. This transverse vortex is isolated from main flow, and it independently circulates in the wake region. Strong temperature and density gradients are generated as a result of secondary flows which favour convective heat transfer. Mass transfer enhancement with vorticity augmentation due to the introduction of vortex generator is quantified along the span wise direction.

Relative Sherwood number variation along span wise direction at different stream wise direction for both the configurations are as shown in Figs 4.24 and 4.25. For single VG
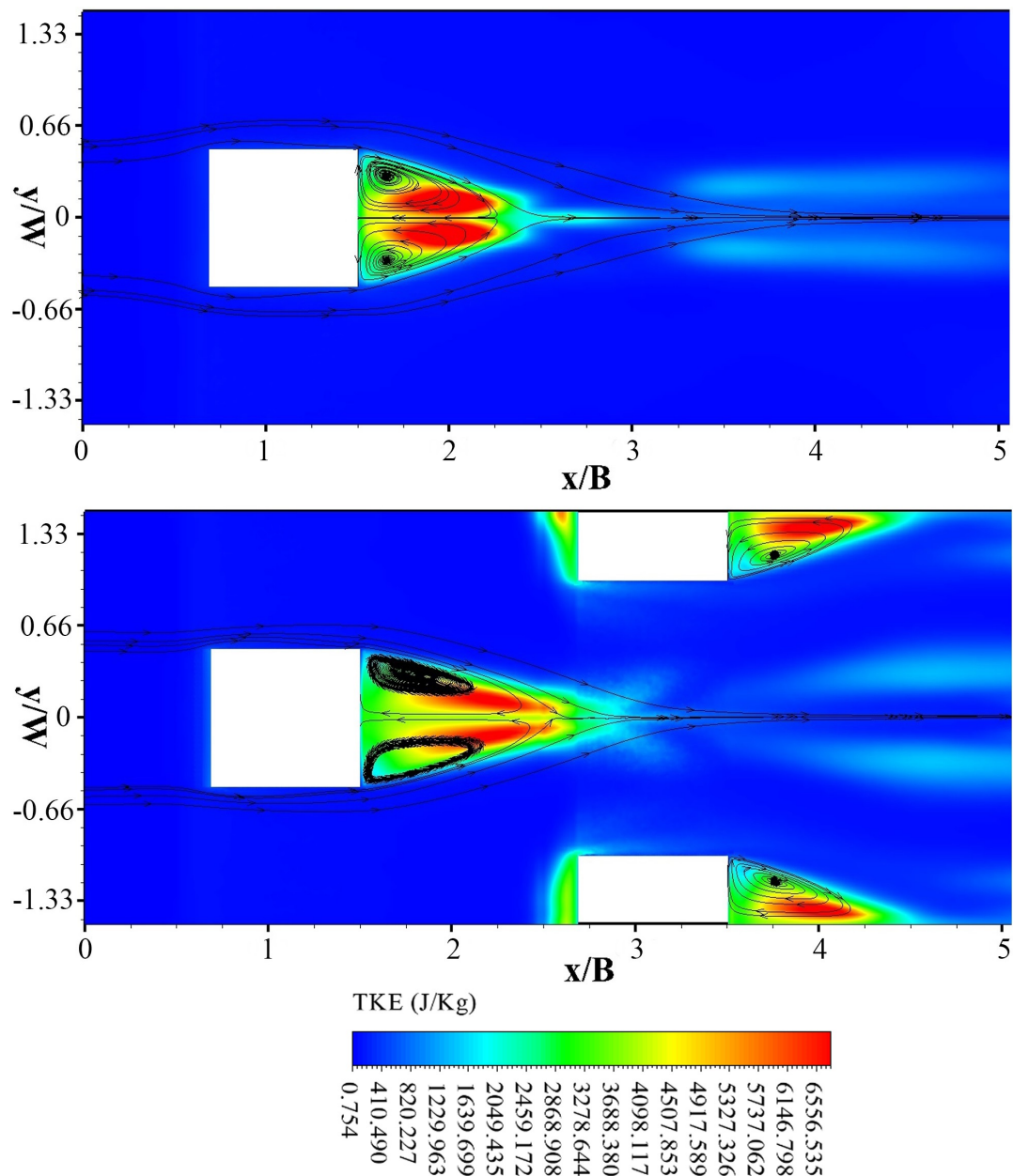
Fig. 4.22 Turbulent Kinetic Energy

configuration, the distribution of mass transfer in span wise direction depends on the vortex path. A sudden enhancement in the Sherwood number, near to the centerline, occurs in front of the vortex generator due to the vortices generated in the flow. Counter rotating vortex pair approaches towards the center further downstream, which in turn brings the peak mass transfer points to move closer to the centerline. This phenomenon is more predominant in the wake region in front of the vortex generator and becomes insignificant as moved further downstream. Whereas, for multiple VG configuration observations are somewhat different.
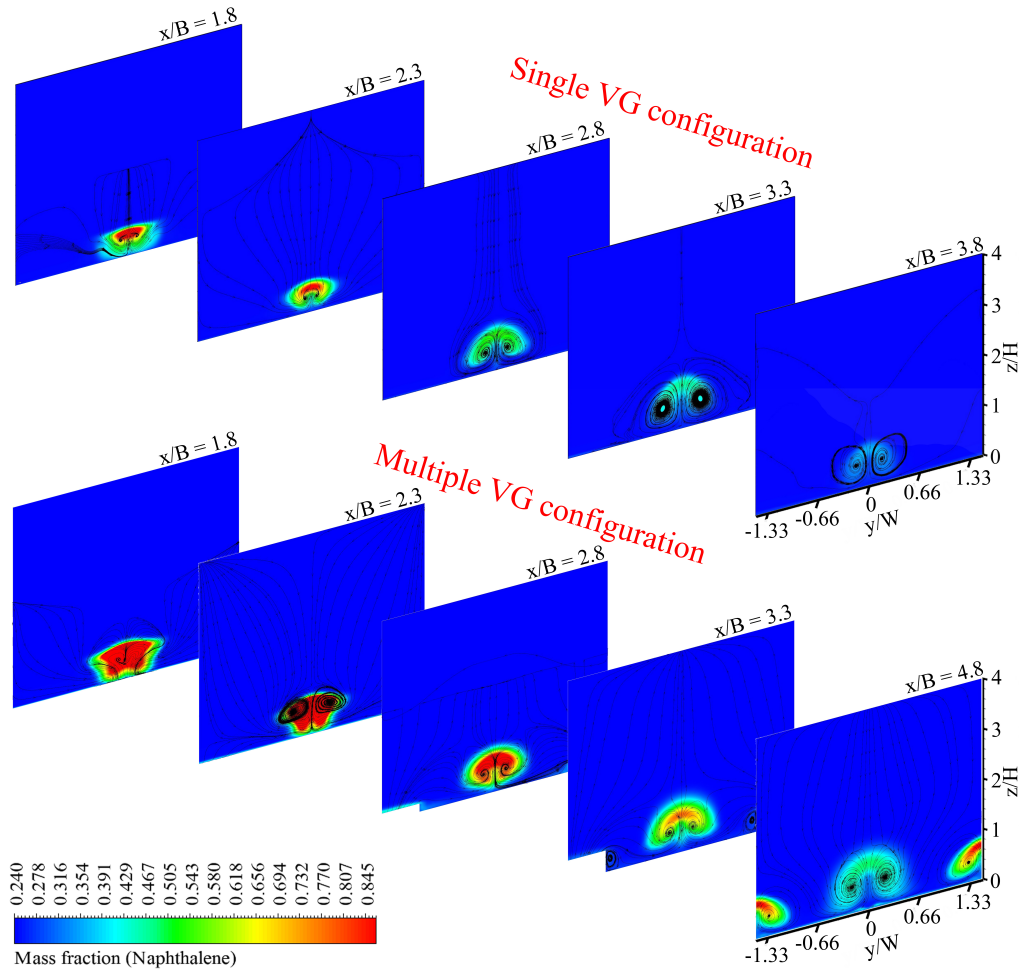
Fig. 4.23 Field plot of species mass fraction superimposed on plot of streamlines for single VG configuration and multiple VG configurations at different stream wise locations

Instead of the single peak observed in single VG configuration, multiple peaks are observed at either side of centerline. Both the number of peaks and magnitude in enhancement of mass transfer gets intensified as flow approaches and passes over the second vortex generator (x/L = 2.5 to x/L = 3.5). This phenomenon is due to the generation of more vortex pairs in the flow field. The enhancement in mass transfer diminishes further downstream as the vortex strength decreases.

4.6   Summary

Detailed analysis of vortical fluid motion revealed the mechanism of the mass transfer enhancement due to the typical flow features created by the lateral sweep of LSVG. Secondary vortices generated in the flow field can create favorable gradients that enhance convective
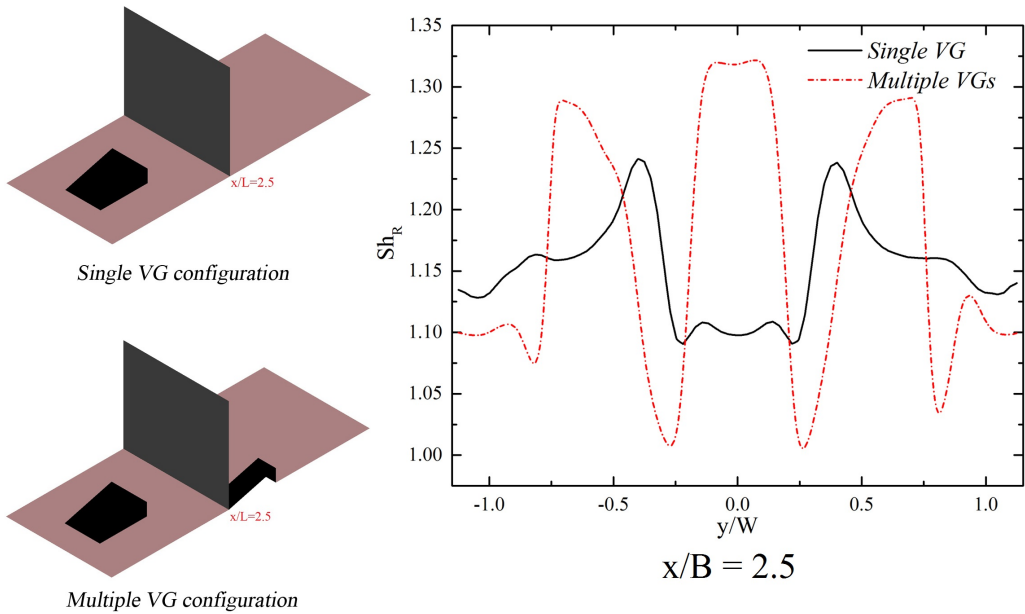
Fig. 4.24 Span wise variation of Sh_R for both configuration at x/B = 2.5
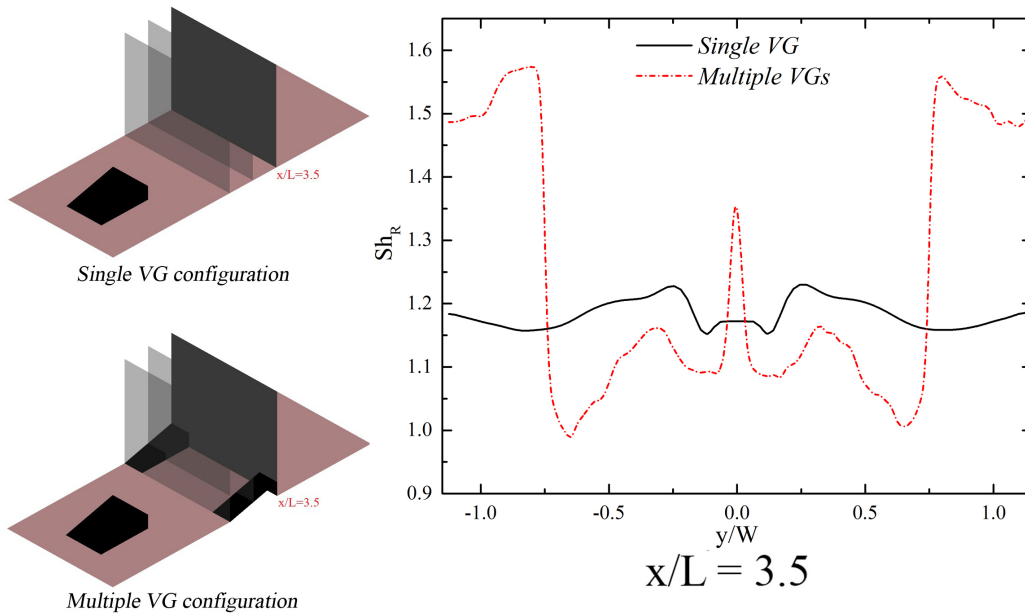
Fig. 4.25 Span wise variation of Sh_R number for both configuration at x/B = 3.5

mass transfer from the adjoining boundary. Vortices generated by LSVG enhance the entrainment of lateral fluid streams and this in turn leads to the lift-off of counter rotating vortex pair. Mass transfer enhancement is found to be dominant in these separation regions. The enhancement of mass transfer achieved by the vortex generators with the lateral sweep can be well controlled by its sweep angle, as it shows a consistent variation. The flowfield downstream of the vortex generator is divided in to two zones based on the vortex path down stream of LSVG. The first one, from the aft end of LSVG to the maximum vorticity region where both vorticity and Sherwood number shows a consistent increasing trend. Whereas in the second zone, downstream of this maximum vorticity region, vorticity and Sherwood number shows a consistent decreasing trend. A unique correlation of the form $Sh_R = \alpha(\xi_R - c_1)^\beta + c_2$ is derived for both regions to establish a relation between relative Sherwood number (Sh_R) and relative vorticity (ξ_R) along the stream wise direction. This correlation could predict average and maximum relative Sherwood number for the mass transfer enhancement created by the LSVG. The local mass transfer enhancement also can be predicted for the region close to the vortex generator using the correlation developed in this study. The locus of vortex trajectory and peak convective heat transfer has considerable agreement; hence, the role of vortices in the wake region of VGs in enhancement of convective heat transfer is established. The presence of multiple VGs introduces the interaction of dissimilar vortices in the wake region. This effect enhances convective heat transfer. The interaction of dissimilar vortices with the developing boundary layer favors injection of more mass from the lateral direction.

Though there is an enhancement of Sherwood number by 61% when multiple vortex generators are used; the pressure loss also increases up by about 78% relative to the base vortex generator. Therefore, geometrical variations to the LSVG configuration that provides asymmetrical vortex interactions and enhances mass transfer with minimal pressure loss has been attempted

Chapter 5

Mass transfer by asymmetrical vortices

The present section focuses on a unique type of vortex generator with a wedge shape, variably swept lateral edges and inclined slanting surface (VSVG) as shown in Fig 5.1. This is the modification of LSVG configuration. The different lateral sweep provided on the vortex generator found to develop large-scale asymmetrical vortices in its wake region. Flow separation at the lateral walls of the vortex generator generates asymmetric horseshoe vortices. Low-velocity regions are formed in the wake region downstream of the vortex generator, which advects more fluid in the lateral free stream to the centre. Mass efflux by the liquefaction of solid substance gets transported to the mixing zone initially by the horseshoe vortices and later carried by periodically shedding asymmetric counter rotating vortex pair. Convective mass transfer found to get consistently enhance with the increase in the asymmetry provided to the vortex generator geometry. Numerous computations have been carried out to unearth the physics of vortex interaction, their makeovers in the pattern, and consequent enhancement in mass transfer.

The temperature dependent mass efflux (TDME) condition as a user-defined function (UDF) has been invoked on the liquefying boundary as the solver can update the mass efflux with varying temperature (detailed in chapter 3). URANS have been performed in the present study for exploring flow physics and to obtain a relation between the vortex shedding and mass transfer. Effects of vortex shedding on mass evolution have been analysed for different VSVG configuration and compared with a base LSVG configuration.

Schematic of the computational domain and the various VSVG configurations studied are given in Fig 5.2. Entire domain is initialized with oxidizer inflow conditions. Present section focused on the effects of asymmetrical vortex interactions on mass evolution from a mass evolving substance when a high-speed hot oxidizer flow passes over it. Note that here the vortex generator and liquefying substance is not considered as deforming. TDME has
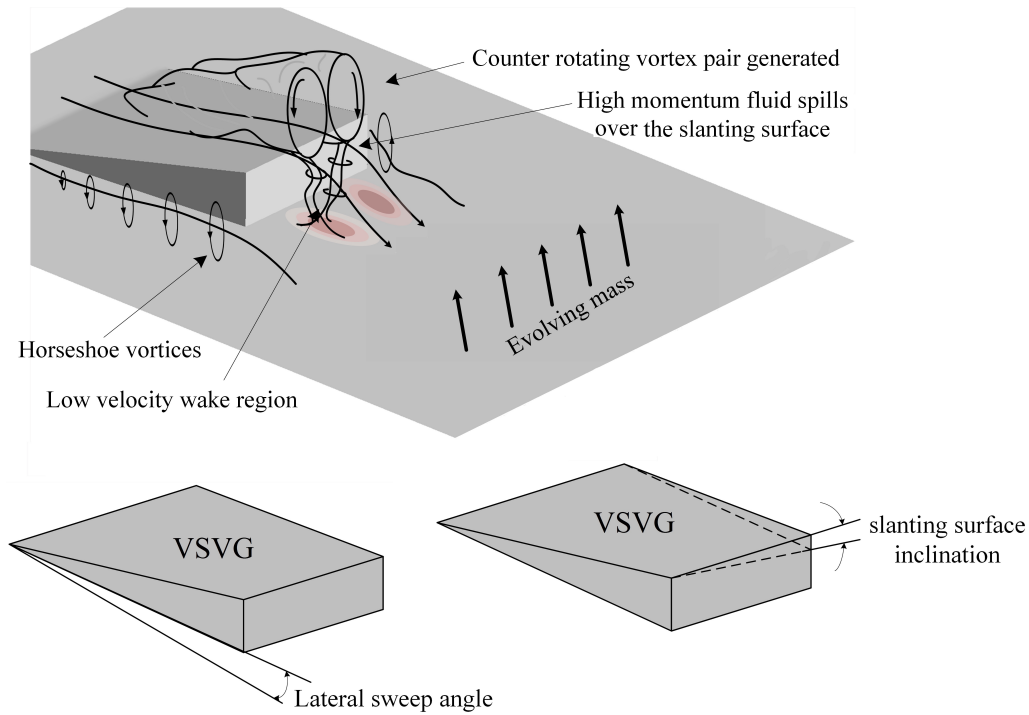
Fig. 5.1 Vortex-boundary layer interaction downstream of VSVG

been implemented at the liquefying boundary. This enables the solver to update the mass efflux with the current temperature in the flow field.

Following are the different configurations used,

Configuration 1: Flat plate with a 7° LSVG (Same lateral sweep on both sides)

Configuration 2: 3° and 7° swept VSVG configuration

Configuration 3: 3° and 7° swept VSVG configuration with slanting surface inclination

Reynolds number based on length of the vortex generator (Re_B) of the flow is set as 400000. Free slip boundary condition is given at the two sides of the computational domain.

5.1   Role of slanting surface inclination of VSVG on mass transfer enhancement

Velocity magnitudes associated with the wake regions and counter-rotating vortex pair downstream of vortex generator are comparatively less than other regions in the flow field. This low-velocity region enables favourable gradients for mass transfer augmentation. These features are rather symmetrical for a simple LSVG configuration. Pressure difference in the flow field created by vortex generator attracts more fluid from the high-speed free stream laterally and induce role up, forming the longitudinal counter-rotating vortex pair. The axis
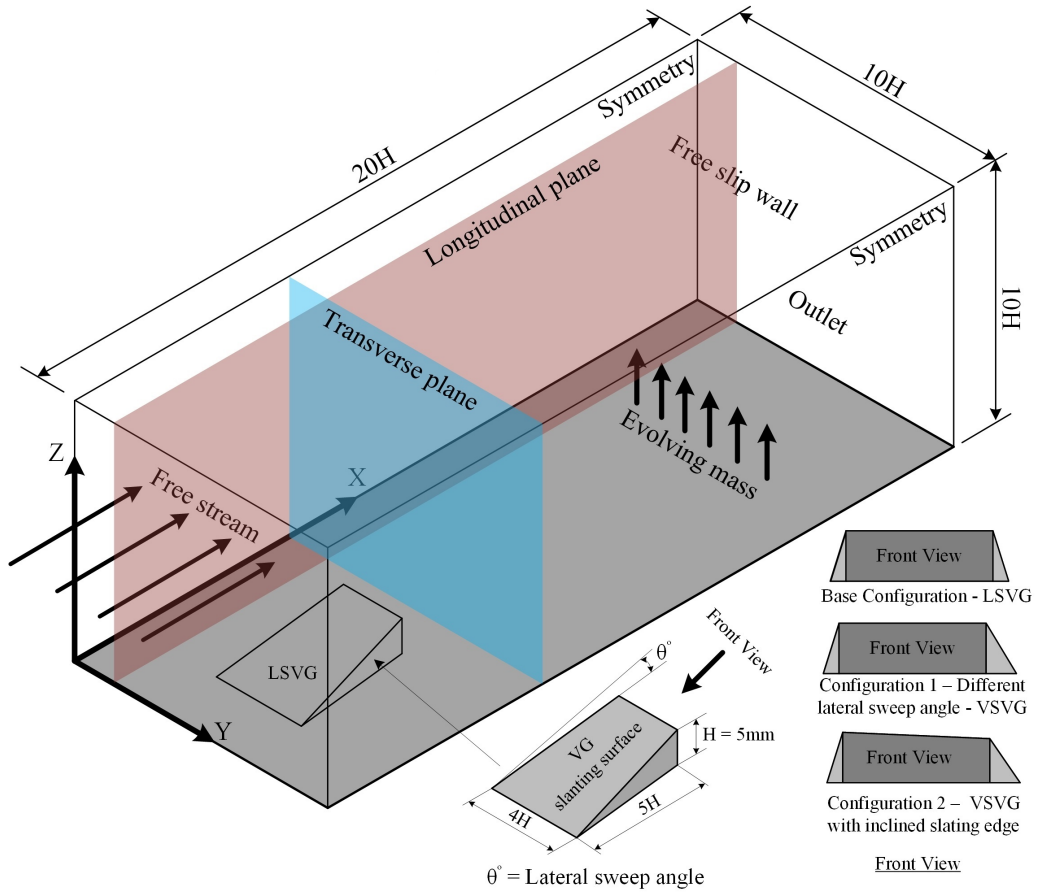
Fig. 5.2 Computational domain and VSVG geometries

of rotation of longitudinal vortices is parallel to the free stream. When a lateral sweep is introduced to the vortex generator, it creates wake vortices in the immediate downstream of the vortex generator. These wake vortices rotate independently in an axis perpendicular to the main flow. These generated vortices rotate rather symmetrical about their respective axis. However, a deliberate introduction of asymmetrical vortices can further enhance mass transfer effects. Two levels of asymmetries are deliberated in the present work by providing differing lateral sweep and slant surface inclination (Configuration 1 and 2). 3D streamlines showing recirculation zones and asymmetric wake regions in front of both VSVG configurations are shown in Fig 5.3 . These geometry manipulations given for LSVG generate pressure oscillations that bring in asymmetry to the evolving vortex structure. Streamlines superimposed on mass fraction plot in a transverse plane in front of VSVGs (configuration 1 and 2) and a plane just above the mass evolving boundary are shown in Fig 5.4a and 5.4b respectively.
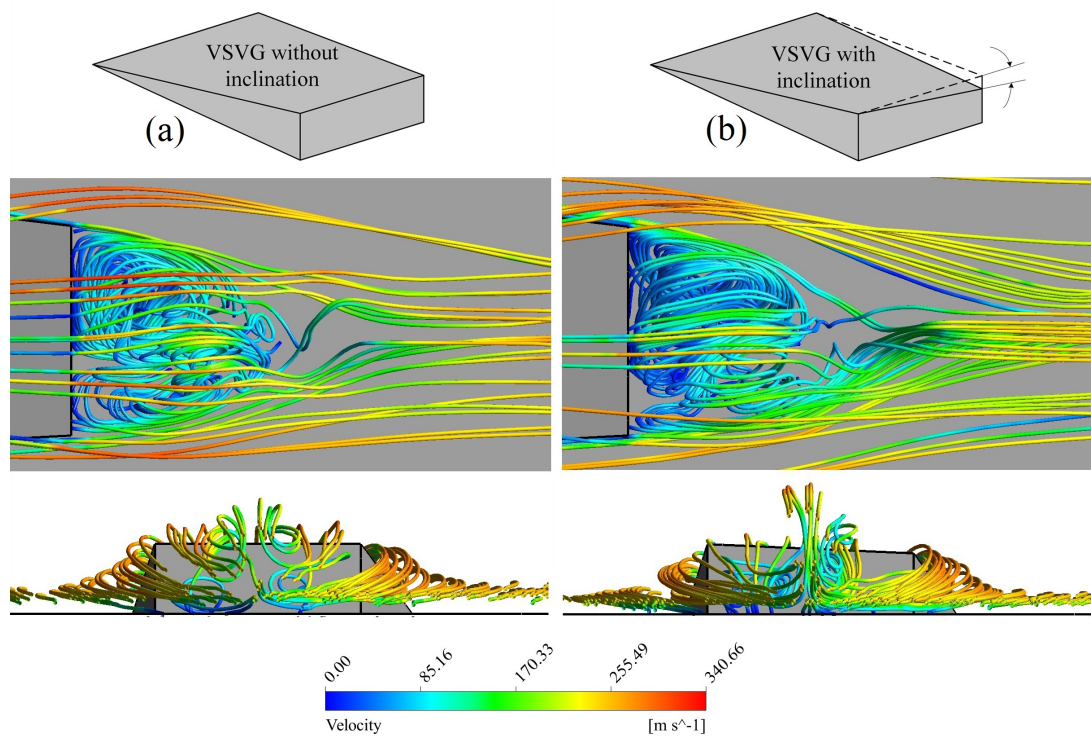
Fig. 5.3 3D streamlines showing recirculation zones and asymmetric wake regions in front of both VSVG configurations
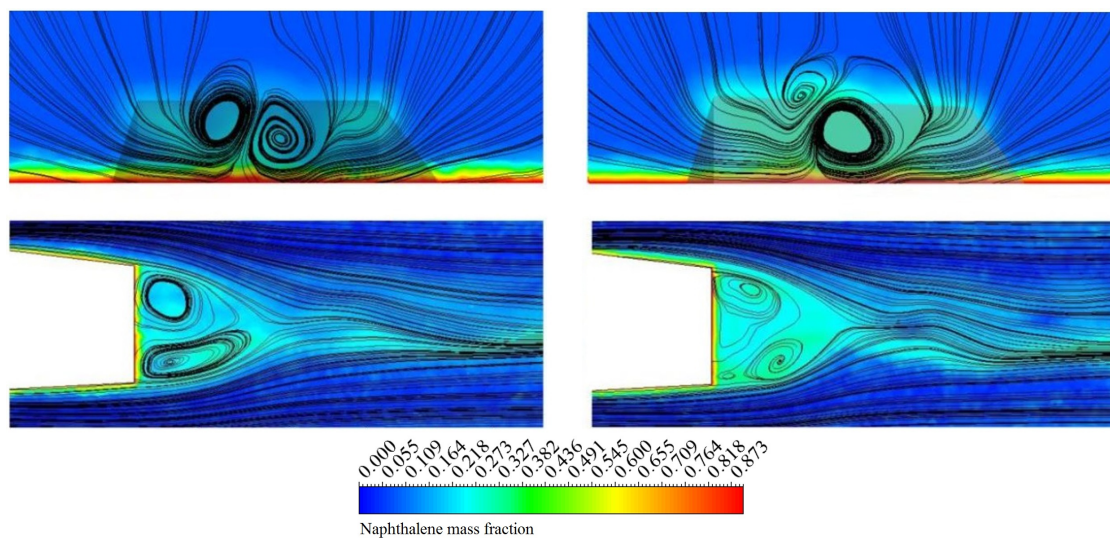
Fig. 5.4 Streamlines superimposed on mass fraction contours (t = 0.175 ms) plot after 0.175 ms

5.2   Evolution of flow structures and transfer effects

Flow attachment on the sidewall of LSVG induces lateral vortices. Counter-rotating Vortex Pairs (CVP) and horseshoe vortices deviate from its inherent symmetry due to differ in lateral sweep induced to the vortex generator. The features of large vortical structures formed downstream of the vortex generator are shown in Fig 5.5
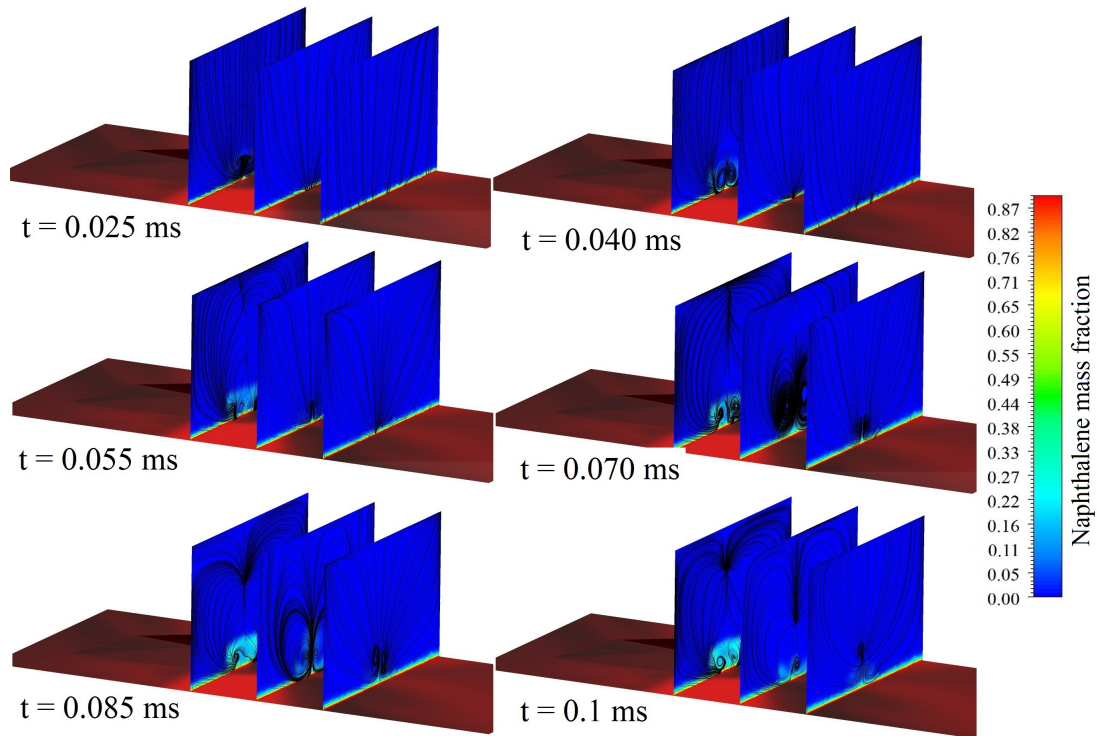
Fig. 5.5 Sequential evolution of the vortex structures and corresponding mass evolution shown on different transverse planes

Here the sequential evolution of vortex structures and corresponding mass evolution from the surface on different transverse plane downstream of VSVG with slanting surface inclination are analysed. The generated vortices get dissipated at regular time intervals and newer vortices are periodically shed from both sides of the vortex generator. The strength of vortices gets intensified downstream of vortex generator and gets dissipated farther downstream. High momentum fluid spills over the slating surface of the vortex generator and interacts with the boundary layer downstream of it. There is a stronger downwash of asymmetrical vortices due to the slanting edge inclination provided to the VSVG. This stronger asymmetry in the flow path can further disturb the developing boundary layer and release higher gradients farther downstream from the vortex generator. Dynamic vortex shedding and flow impingement are beneficial for higher mass evolution from the surface.

Periodic formation and dissipation of vortices lead to pressure pulsation and it significantly affects the mass transport
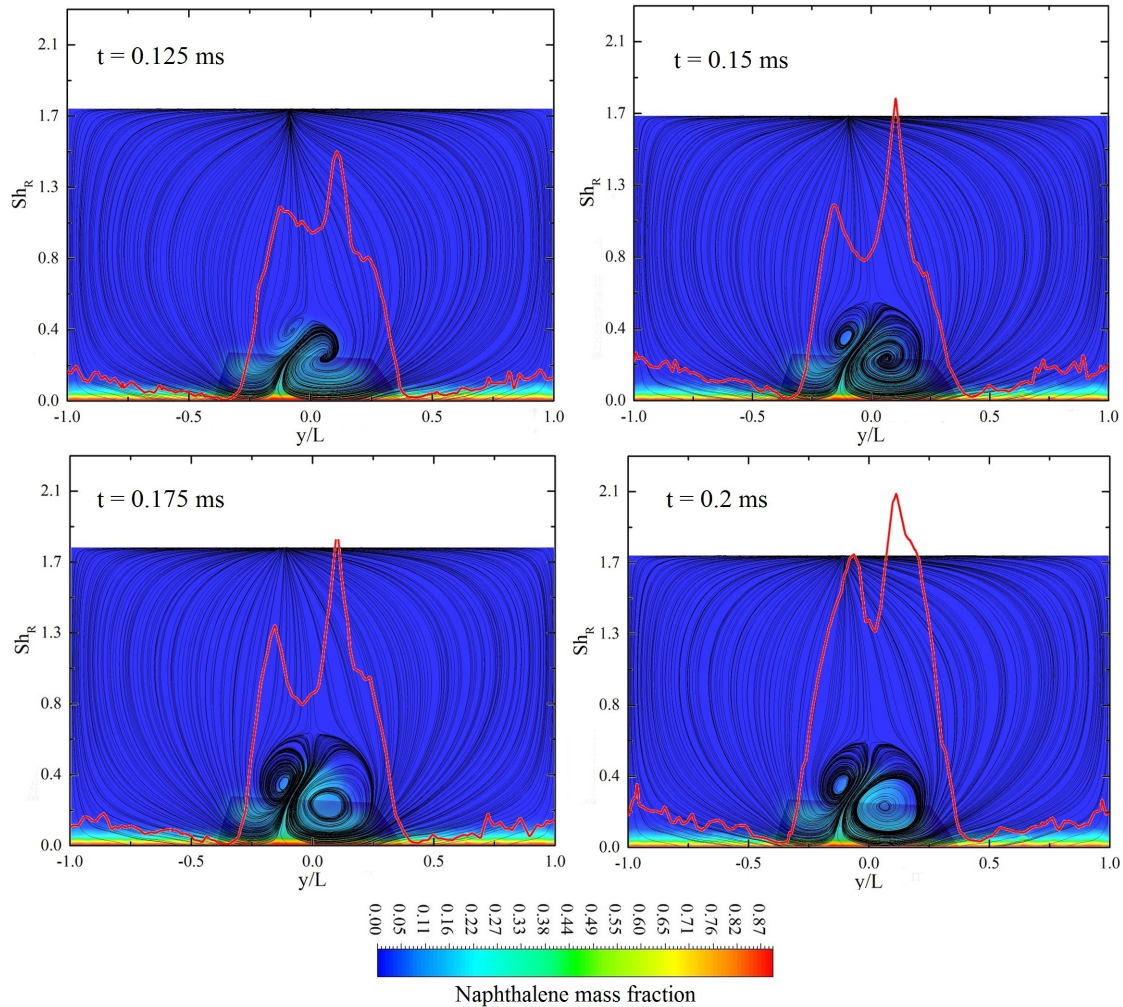
Fig. 5.6 Streamlines superimposed on species mass fraction contours at various time instances. Red curves indicate the Sherwood number profiles

Sequential evolution of strong asymmetrical vortices in front of VSVG configuration with slanting surface inclined is analysed in detail. Now the asymmetric vortex trajectories generated in the flow field are analysed in detail. There exists a correspondence of sharp gradients realized by the vortices and mass transfer effects. Fig 5.6 shows the sequential evolution of mass transfer from the surface and the streamlines on the transverse planes. The strength of counter-rotating vortices and its asymmetry gets intensified as it goes downstream of VSVG. Both the peaks observed in the Sherwood number profile (red line) is due to the interaction of vortices with the boundary. The strong downwash of the vortices lifts the mass from the surface. Due to the asymmetrical generation of vortices, the interaction of

the pair of vortices with the mass transferring surface is also different. This is evident in the Sherwood number profile shown in Fig 5.6. Interaction of CVP with the boundary decreases as it is lifted from the surface. Lifting up of CVP from the mass transferring surface leads to a better mixing up of evolved mass into the free stream. This process occurs periodically as the vortices are continuously shed from the vortex generator.
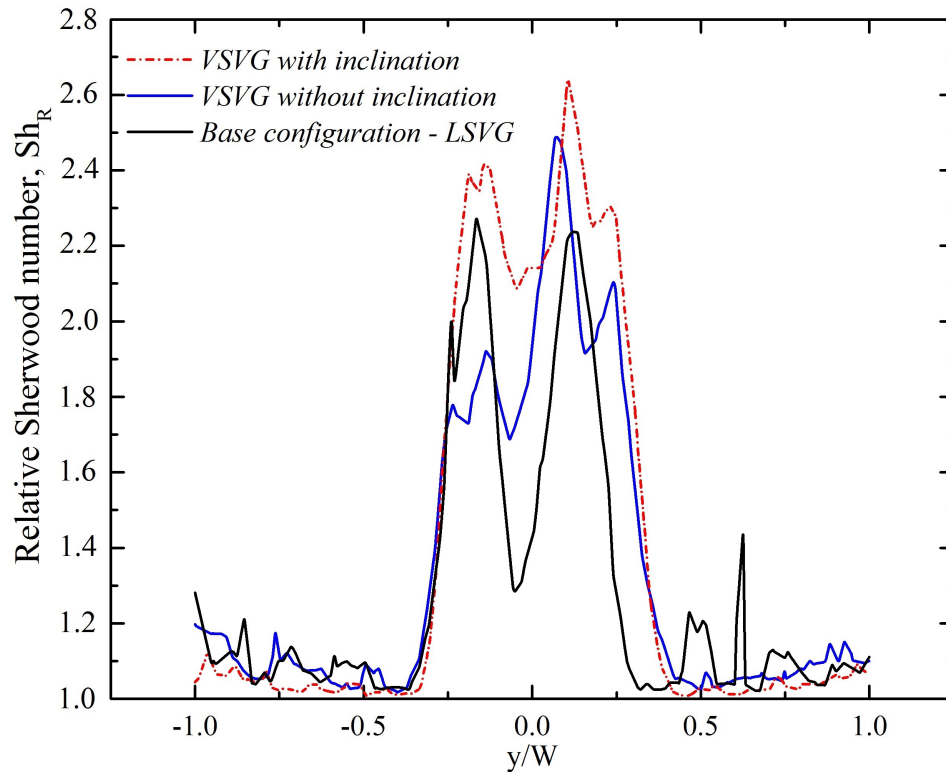
Fig. 5.7 Time-averaged relative Sherwood number in transverse directions

Asymmetrical vortical interaction near to boundary ensures sustained temperature and density gradients, which promotes mass transfer. Flow is laterally advected into the wake region downstream of the VG. The asymmetrical nature and interaction of the vortex are found to intensify with the introduction of the variable lateral sweep. Aforementioned vortical flow structures realize spatially and temporally uneven mass transfer pattern from the boundary. Comparison of relative Sherwood number variation in the transverse plane for the two VSVG configurations with the base LSVG configuration is shown in Fig 5.7. Distinct asymmetrical vortical patterns and corresponding dominant mass transfer regions are evident with VSVG configurations. The plot for Sherwood number in longitudinal direction (Fig 5.8) shows an initial peak in relative Sherwood number which corresponds to the mass transfer in the recirculation zone induced by the wake vortices. The variable lateral sweep also brings
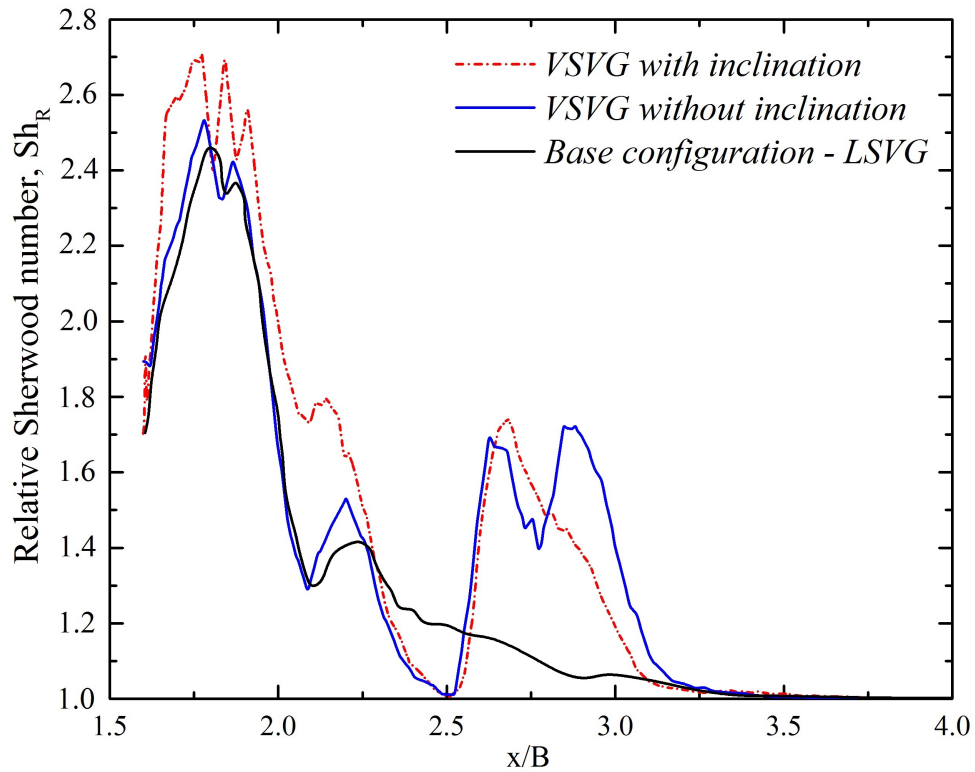
Fig. 5.8 Time-averaged relative Sherwood number in longitudinal directions

the asymmetry of transverse wake vortices and favour the generation of larger gradients that lift the evolved mass more into the free stream.

5.3   Role of the large coherent structures

Unsteady computations revealed the features of large coherent structures formed downstream of the VSVG. 3D flow visualization of the flow structure using iso-contours of the Q-criterion is shown in Fig 5.9. Longitudinal vortices are regularly distributed along the main flow field. The oscillatory nature of vortex interactions differs at various locations. Deformation of the vortical structures in the transverse direction, scalar mixing, and asymmetrical nature of rotation can be observed. Blue colour indicates the region of evolved mass from the surface and shows there is an inherent increase in mass evolution for configuration 2 than configuration 1 by the additionally induced asymmetry

Naphthalene mass fraction
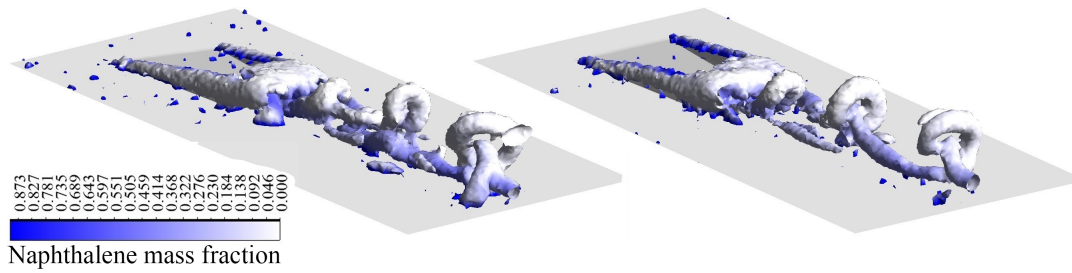
Fig. 5.9 Vortex-boundary layer interaction downstream of LSVG

5.4 Summary

Presence of variable lateral sweep provided on the vortex generator brings in unsteadiness and asymmetry to the vortices. Present URANS simulations on these configurations establishes that the mass transfer effects are enhanced by asymmetrical vortex interactions. Flow visualization using iso contours of Q-criterion reveals that mass transfer effects are dominant in the region of intense vortical motion. Present study shows that different lateral sweep and slant surface inclination can bring an enhancement of 31% and 36% relative to base VG configuration.

Chapter 6

Role of dimple cavity in promotion of mass transfer in wake region of vortex generator

Combination of passive mass transfer enhancers is emerging due to the inherent limitations of flow manipulation that a single surface feature can perform. These methods can sustain sharp gradients on the solid-fluid interface for wider expanse, thereby the effectiveness of mass/heat transfer process can be augmented considerably. A combinational flow manipulation method by placing hemispherical depression (dimple) downstream of a lateral sweep vortex generator (LSVG) has been presented in this section. Extensive unsteady computations have been performed to elucidate novel secondary flow pattern in promotion of mass transfer effects for various flow conditions and geometrical parameters. Dimpled surfaces are not protruded in to the flow and hence reduces form drag. These surfaces enhance heat/mass transfer from the surface with minimal pressure losses when compared to other methods. Dimpled arrangement ejects multiple pairs of vortices. Hence this arrangement increases local turbulence transport and secondary advection which enhances heat/mass transfer. Recirculation flows are also generated within dimples because of flow separation and reattachment of shear layer formed across the dimple. Strong temperature and pressure gradients which favours mass transport are generated due to these vortices.

Schematic of flow field resulting due to LSVG-Dimple combination and region of peak mass transfer enhancement (brown patch) are shown in Fig 6.1. It is well known that LSVG creates dominant vortex systems such as horseshoe vortices and counter-rotating vortex pairs due to lateral surface interactions and spillage over its top slanting surface respectively. Dimple placed downstream in the wake of the vortex generator alter the reattachment process as it laterally advects the fluid free-stream. This, in turn, can sustain the vortex strength for

Mass transfer augmented regions

Mixing of evolved mass in to the flow field
by counter rotating vortex pair generated

Flow impingement and reattachment at
upstream and downstream rim of dimple

Low velocity wake region

Recirculation zone inside the dimple

Fluid bends in to the dimple section
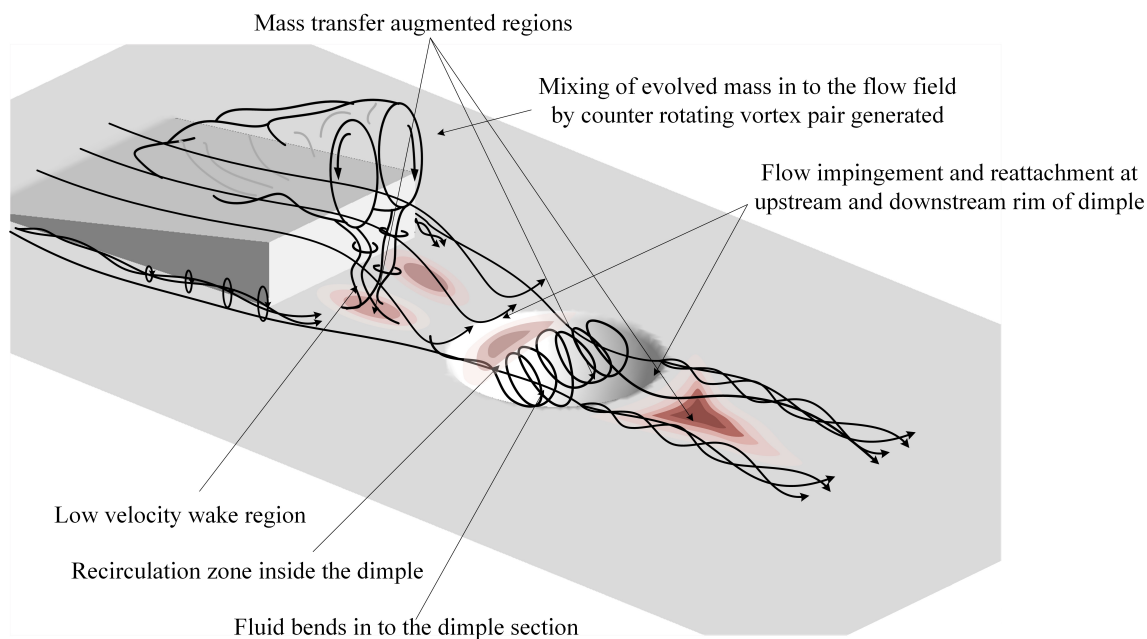
Fig. 6.1 Schematic of the vortex system downstream of LSVG in presence of a dimple

farther downstream locations. Mass transfer process from the adjoining boundary benefits due to the creation of sharper gradients on the surface and promote convective transport towards farther locations by the vortical fluid motion. In short, LSVG-Dimple combination effectively augments mass transport for a wider expanse on the solid boundary in higher Reynolds number applications. Convective mass transfer augmentation systems call for the requirement of not only the enhancement near the surface but also the evolved mass should be carried away to the farther locations in adjoining free stream. Therefore, the sustenance of the strength of the evolved vortex system in the wake of the vortex generator is a key objective while selecting combinational convective mass transfer augmenting system. Unsteady vortical fluid motion and its interaction with developing boundary layer are explored in the present study to reveal the reasons for transport process enhancement. Temperature dependent mass efflux (TDME) condition is invoked to the mass evolving boundary as a user-defined function (UDF) in agreement with adjoining fluid's thermal condition. Time-resolved analysis is performed to identify the signature of unsteadiness creates in promotion of transfer effects. Unsteady RANS has been performed in this study for a better understanding of flow physics and to obtain a relation between the frequency of vortex shedding and mass transfer. A systematic parametric study has been performed to reveal the effect of the geometry of LSVG-Dimple combination in the evolution of unsteady flow structures, which in turn can promote transfer effects. The present problem involves the flow of a hot free stream over a vortex generator and a dimpled surface placed downstream of it. The computational
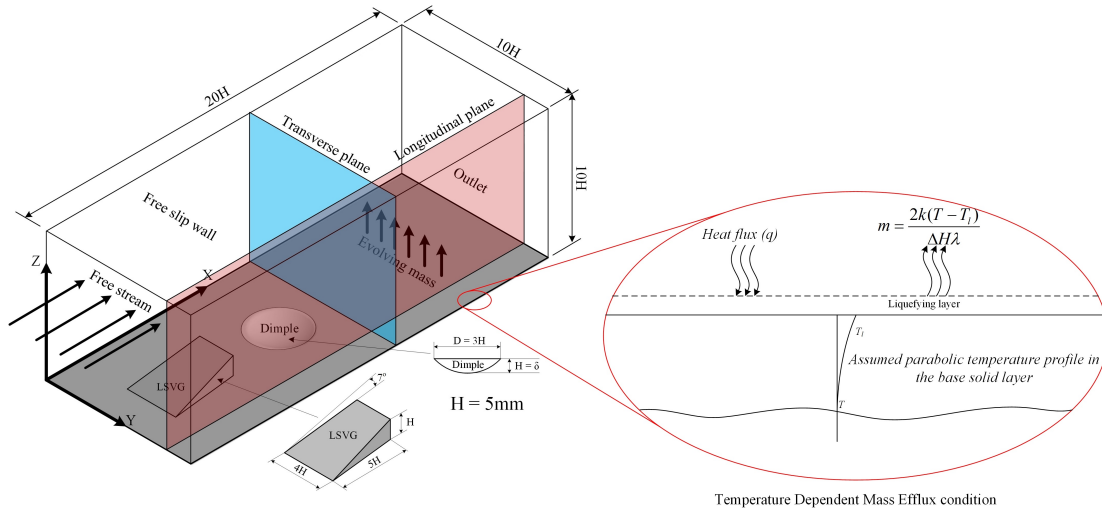
Fig. 6.2 Computational domain and boundary condition

domain used for the present analysis is given in Fig 6.2. Vortex generator is a non-deforming surface. The bottom wall of the present domain of analysis is made up of a nondeforming liquefying substance and has a surface depression. LSVG and dimpled create vortices that can enhance mass transfer from the surface. LSVG is given with a sweep angle of 7°. The distance between the LSVG and dimple is varied to study the effect of dimple location. Free stream velocity is varied such that it realizes the inlet Reynolds number (based on the dimple diameter (Re_D) of the flow to be 240000, 320000, 400000, and 480000. Boundary conditions implemented in the present section are given in Table 6.1

Table 6.1 Boundary conditions

Inlet	T = 800K, P = 1bar, Y_{O2} = 0.23
Plate	No slip, Isothermal wall, Ys = f(T_S)
Outlet	Pressure outlet
Side walls/Top wall	Free slip

The computational domain used in the present analysis is discretized mostly using hexahedral control volumes except near the lateral faces of LSVG wherein tetrahedral elements are used. Adequate grid refinement is provided near all no-slip walls by maintaining a y+ < 1. Hence adequate grid points are ensured in the laminar sub-layer and proper bias is given in the direction normal to no-slip walls. Similarly, regions expected to have sharp gradients are also given grid refinements such as areas close to the vortex generator and dimple. The present problem involves vortex interaction with developing boundary layer on a surface. Computational grid used for the present simulation is given in Fig 6.3. Computational domain is initially discretized with 0.17 million control volumes and
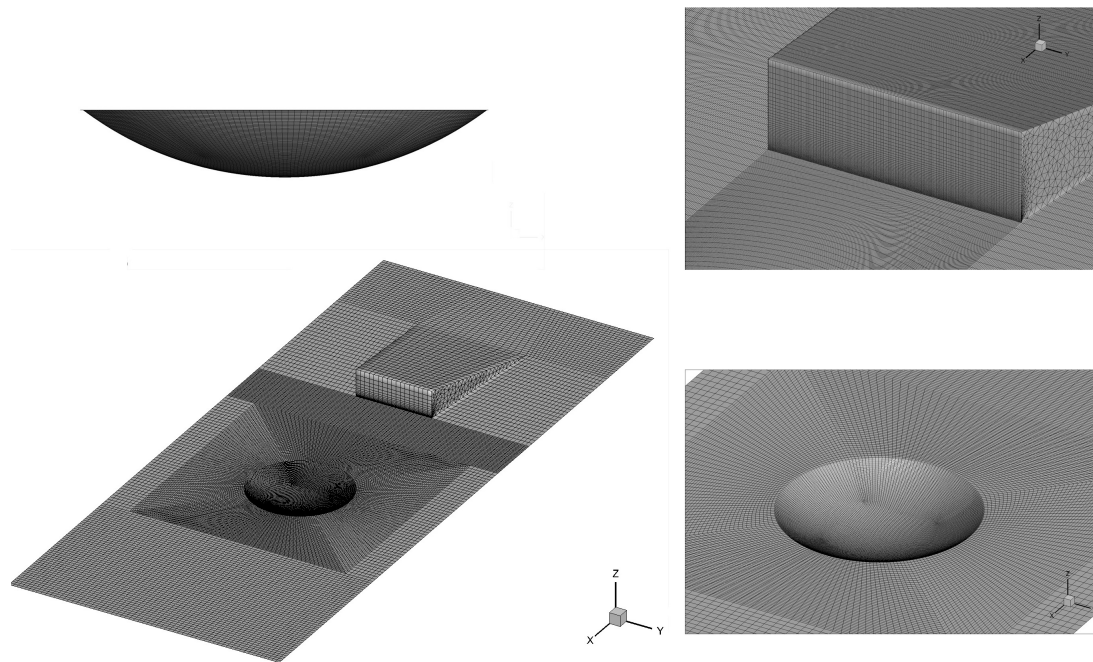
Fig. 6.3 Discretized domain

progressively refined to 0.34 million and 0.68 million control volumes. Grid independence has been assessed globally and locally by ensuring the invariance of average Sherwood number estimate and normalized local wall pressure respectively. Results for the three levels of grid refinement are summarized in Table 6.2. It can be observed that the differences in estimates fall within 1 error. Discrepancy on the second peak value of the normalized centerline wall pressure upon gird refinement has been assessed independently and ensured that the second level of grid refinement (0.34 million) provides grid independent results (Fig 6.4). Hence the grid size corresponding to the second level of refinement (0.34 million) has been selected for the further simulations y+ =0.98 and position of the first grid point above the plate is 1.4×10^{-6}m. A time independency check is performed by varying the order of magnitude of time step from $10-8$ to 10^{-10} (0.1<CFL<1). It is observed that variation in time step has negligible effect on fluctuating velocity components at salient locations taken for observation such as downstream of LSVG, fore and aft surface of the dimple. Time averaged Sherwood number obtained for time steps corresponding to 10^{-8}, 10^{-9}, and 10^{-10} are 2.3218, 2.3156, and 2.2902 respectively. Convergence is achieved for every time-steps with combination of aforementioned time-steps and number of iterations within a time-step. In the present study, 100 number of iterations per time-step is found to be adequate to ensure convergence of all conservation variables.

Table 6.2 Summary of the grid independency test

Grid refinement	No of grids (in million)	Second peak value of the normalized wall pressure along centre line	Average Sherwood number
Coarse	0.17	1.436	2.3098
Fine	0.34	1.406	2.3156
Very fine	0.68	1.397	2.3213

Sustenance of active vortical fluid motion even at farther locations away from origin is the key aspect of the present passive mass transfer enhancement method. A schematic of the vortex system developed downstream of LSVG in presence of a dimple is portrayed in Fig 6.1. A low-velocity region is created in the wake region of LSVG. Secondary flow structures are created as the flow passes over LSVG due to the introduction of tangential velocity. Longitudinal and horseshoe vortices created by LSVG disturb the developing turbulent boundary layer and lead to mass transfer enhancement on the surface near to its aft face. Vortex pairs can introduce fluid streams having higher momentum towards the developing turbulent boundary layer which can delay the separation of flow downstream of LSVG. Presence of these vortex pairs creates a low-pressure area which advects more fluid laterally towards it, which in turn can transfer the evolved mass towards farther locations in the free stream. Nature and extent of these vortical structures depend on the lateral sweep angle provided on the vortex generator. It is well known that a concave dimple cavity in isolation can advect fluid and periodically eject out vortical flow structures due to flow impingement. Dimple placed in the wake of a vortex generator produces varied periodic vortex flow structure as convoluted flow stream shed from LSVG is subjected to advection and ejection. Flow features attributed by the flow separation near to the leading rim and reattachment on the aft rim of the dimple cavity depends on free stream conditions as well as the distance between LSVG and dimple. Vortex structures emanated downstream of LSVG are further enhanced by the presence of dimple which augments large scale structures. This, in turn, can create sharper gradients on developing turbulent boundary layer downstream of the dimple. Hence a notable enhancement in the convective mass transfer is observed in the region of flow impingement inside cavity and location of amplification large scale structures past aft rim. Possession of a higher extent of tangential momentum of these vortices shed from geometrical features can transfer the evolved mass towards farther locations in free stream. Hence the LSVG-dimple combination can be regarded as an ideal choice for convective mass transfer enhancement in high-speed flows. Results of the simulation of unsteady three-dimensional flowfield with TDME condition has been post-processed so as to reveal the large vortex structures formed downstream of LSVG and at the dimpled region.
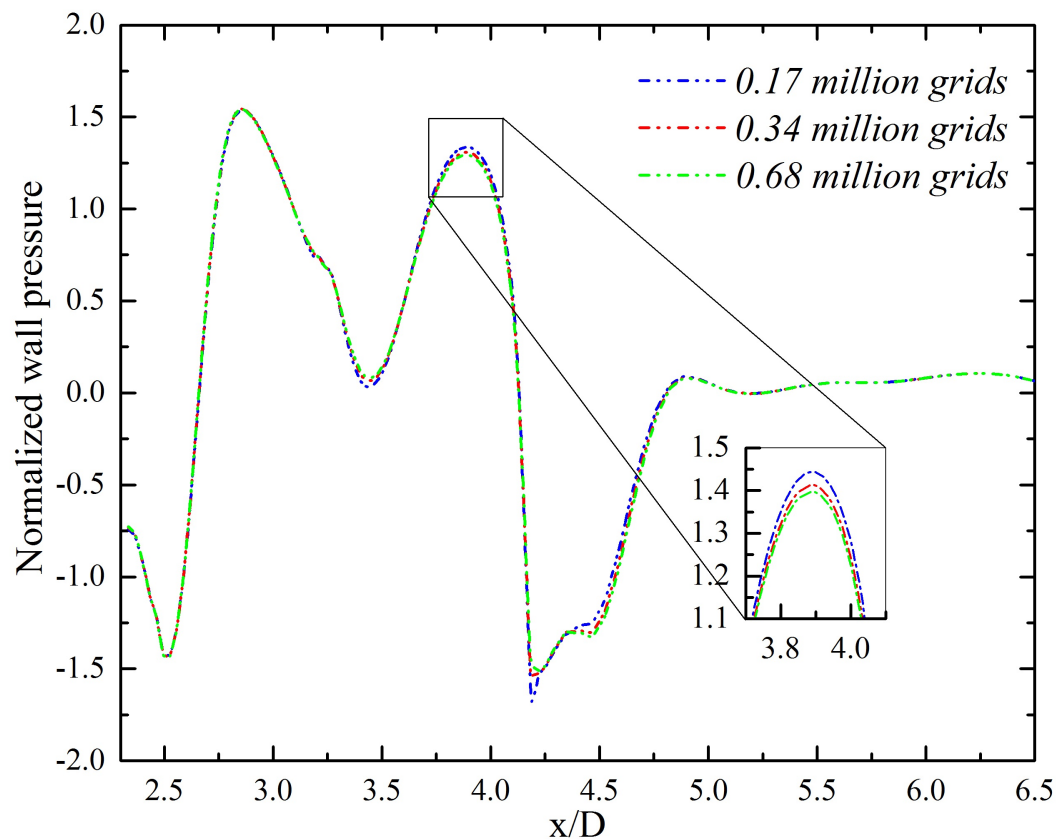
Fig. 6.4 Result of grid independence study

Iso contours of Qcriterion (Q = 0.025) are used to identify the cores of large-scale coherent vortex structures at a particular instant for two different approach velocities (Re= 320000 and 400000) as shown in Fig 6.5. Intense vortical fluid motion is evident downstream of LSVG and dimple. Advection of free stream towards the wake, suction and consequent ejection from the cavity can also be observed. Increase in approach velocity attributes a further growth in flow structures and extend mass transfer. Dimple cavity is a harmonious cohort for a combinational transfer enhancement system that can be ideally used in conjunction with vortex generator as its presence further imparts tangential momentum. Periodic ejection of vortical structure ensures the transfer of evolved mass to free stream. Choice of an ideal location for the placement of the dimple in the wake of LSVG is quite significant. Hence a detailed parametric study is taken up later in this analysis to bring about convective mass transfer profile corresponding to various options. Interaction of the asymmetric flow structures is another aspect that favors transfer process enhancement. Detailed spatiotemporal analysis of the flow structures and corresponding transport process is carried out to resolve the unsteady dynamics of a promising combinational transfer process enhancement system.
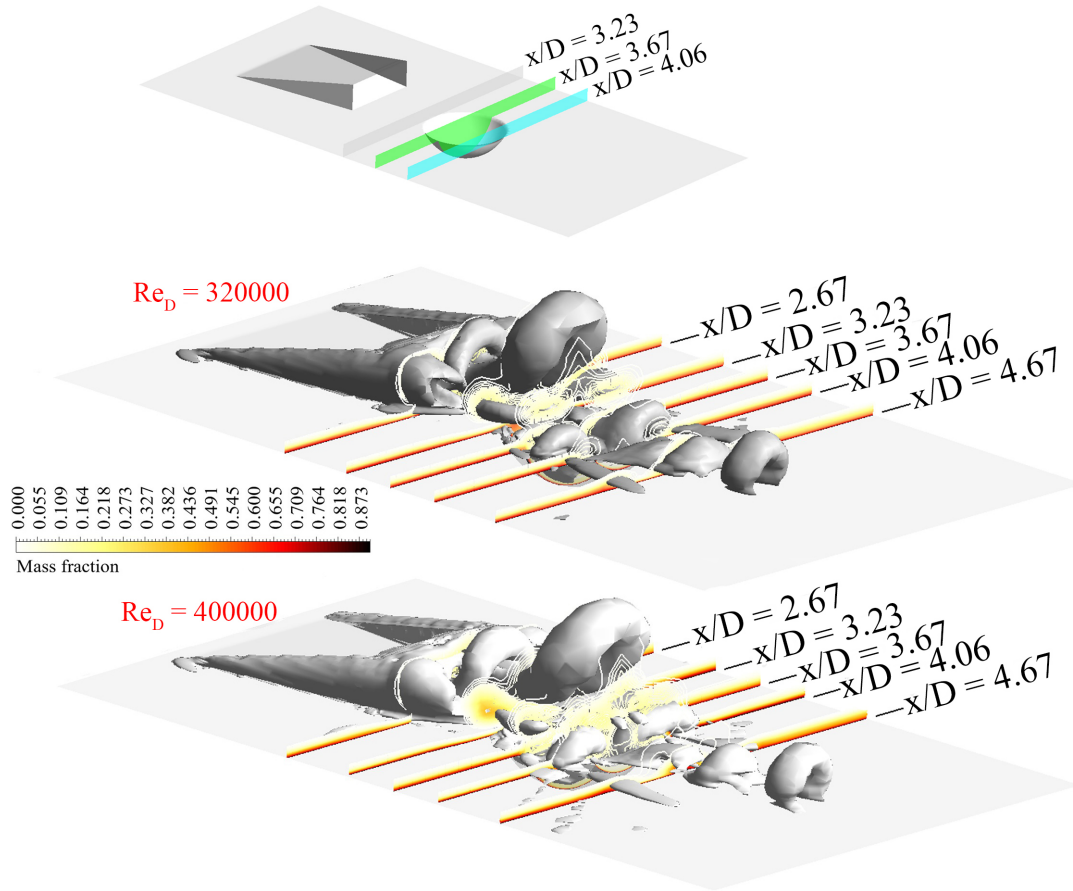
Fig. 6.5 Visualization of large coherent structures by iso contours of Qcriterion for Re_D = 320000 and 400000

6.1   Unsteady flow transitions and mass transfer effects

It is well known that any kind of lateral sweep vortex generator can set in vortex system having longitudinal and horseshoe vortices that revolve about an axis perpendicular to the freestream. Fluid stream flowing past the side wall of the vortex generator creates lateral vortices that get advected towards the center of the wake due to the low pressure. Another part of the high-speed free stream that passes over the LSVG also creates secondary flow structures. Interaction of these two sets of vortex system and consequent creation of steeper gradients on the adjoining boundary is responsible for the higher extent of mass transfer rates observed in front of LSVG. Flow of an undisturbed high-speed free-stream past a dimple cavity itself is quite unsteady due to suction and ejection processes. Hence it is vital in the present context to understand the flow transitions while the flow involving the aforementioned secondary flow structures move past dimple cavity placed in the wake of LSVG. Separation of the wake stream having vortical flow structures generates higher gradients near the rim

of the upstream half of the dimple. An independent flow recirculation is emanated inside the upstream half of the dimple due to the flow separation and this gets superimposed with existing secondary flow structures in the flow inside the cavity. Hence the present flow system exhibits a differing reattachment pattern near to the downstream half of the dimple. The nature of vortices shed from aft rim of the dimple cavity is also affected and the effect is sustained for wider expanse downstream of the dimple. Vortical fluid streams ejected out of the dimple are getting lifted off from the boundary. Hence these stream carries the evolved mass from the boundary towards the undisturbed free stream. In short, secondary flows generated and amplified by surface features favor the generation of strong temperature and density gradients near the surface which enhances the mass transfer.

Streamlines in the region of intense vortical motion are superimposed with the mass fraction of the evolved substance at various time instances are elucidated in Fig 6.1. Three-dimensional view of streamlines and mass fraction on a plane near the bottom surface is given to impart a simple understanding of the aforementioned process. Its consequent effect on unsteady convective mass transfer on two different transverse planes is also shown in detail. Creation of low-velocity area in the wake of LSVG and sharper gradients near to the boundary by the fluid streams with higher tangential momentum are quite evident.

Unsteady flow transition and corresponding mass transfer profile in terms of relative Sherwood number on a transverse plane adjacent to the LSVG are indicated in the top part of Fig 6.1. Vorticity along the streamwise direction gets augmented as more fluid passes over the LSVG and reaches a maximum level when longitudinal and horseshoe vortices interact with each other. Multiple peaks in the mass transfer profile are observed as time elapses and these are attributed by the interaction of vortices. Vortex interaction in front of LSVG is confined only in the center of the wake as more fluid is advected towards it. The counter-rotating vortex pair gets lifted off from the surface and it transfers mass towards the upper part of the free stream. Evolution of the mass transfer characteristics on a transverse plane passing through the dimple is quite different from that of the former plane. Gradients are developed near to the rim of the dimple as flow separates wherein vorticity levels are maximum. Flow separation forms a recirculation region inside the dimple and that promote mass transfer inside the dimple. It is evident that vortex interaction is favoring the local mass transfer effect. Unsteadiness in the flowfield associated with the relocation of the vortices promotes the transfer of the evolved mass towards the upper region in the free stream. Thus it is obvious from both sets of superimposed images of vorticity, mass efflux on a plot of streamlines generated for various time level that various vortical structures and its interaction are leading to steeper gradients on surfaces that enhance mass transfer. Evolution of the velocity streamlines and mass fraction field on a plane just above the surface is depicted in

Fig 6.7. Lateral spread of vortical motion relative to the size of the geometrical features and corresponding mass transfer effects are evident in this. LSVG has an inherent limitation of creating enhancement due to a limited extent of flow advection towards wake region. Dimple cavity overcomes this constraint by forming larger unsteady separation zone near the fore rim as well as pulsating ejection of flow past aft rim. Unsteady transitions of the vortices dealt in the problem is a key aspect leading to the enhancement of mass transfer.

Evolution of the cross stream normalized velocity profiles at various axial locations with time is shown in Fig 6.8. Flow separation effects are pronounced in regions near to the dimple than in front of the LSVG. Temporal growth of separation regions in front of the region is less pronounced than those near to the dimple. This evidence the role of the dimple in sustaining and augmenting the recirculatory nature of a fluid stream which contains vortical structures. Fluid streams containing recirculation in the wake region of LSVG are lifted up due to the flow oscillations induced by the dimple cavity. Low-velocity separation zones in front of LSVG and in the vicinity of the fore rim of the dimple has a decisive role in the enhancement of transfer effect in the present test case.

Unsteady flow transitions and consequent mass transfer effects pertaining to separation zones can be better visualized on the longitudinal plane. Superimposed images of velocity streamlines and mass fraction of the evolved species from the surface taken at four longitudinal planes (y/D=1.67, 1.83, 2.0 and 2.16) are shown in Fig 6.9. Interaction of the horseshoe vortices with the developing boundary layer over the surface influence the size of the trapped vortex found in front of LSVG. Low-velocity recirculation region can contain higher extents of the evolved mass. It is also evident that the ejected stream out of the dimple cavity can promote convection of the evolved mass species to the farther downstream locations.

6.2   Frequency characterization and its relation to the mass transfer effect

Frequency characterization of the large-scale structures existing in the high-speed flow past LSVG-dimple combination and its relation with mass transfer effect is envisaged. Vortices that are developed and shed in the present flow field are dependent on flow velocity as well as geometrical factors such as size and lateral sweep angle of LSVG, the ratio of depth to footprint diameter of the dimple, the distance between the aft face of the LSVG and center of the dimple, etc. Strouhal Number (St), based on dimple diameter (D) as the characteristic dimension, is used to characterize the frequency of vortex shedding triggered by the growth
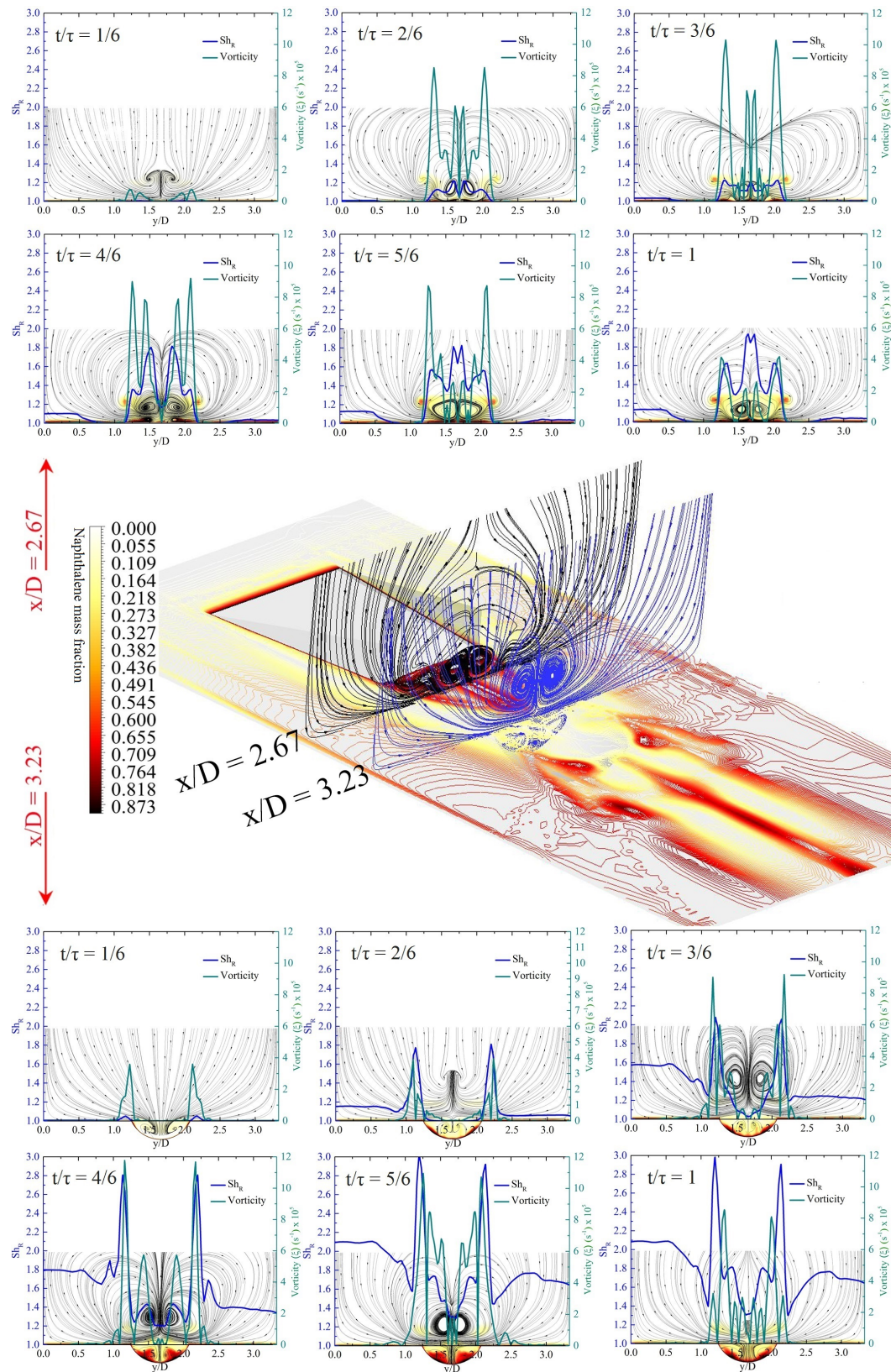
Fig. 6.6 Streamlines superimposed with mass fraction of the evolved substance on two transverse planes (x/D=2.67 (top) and x/D=3.23(bottom)) at various instances
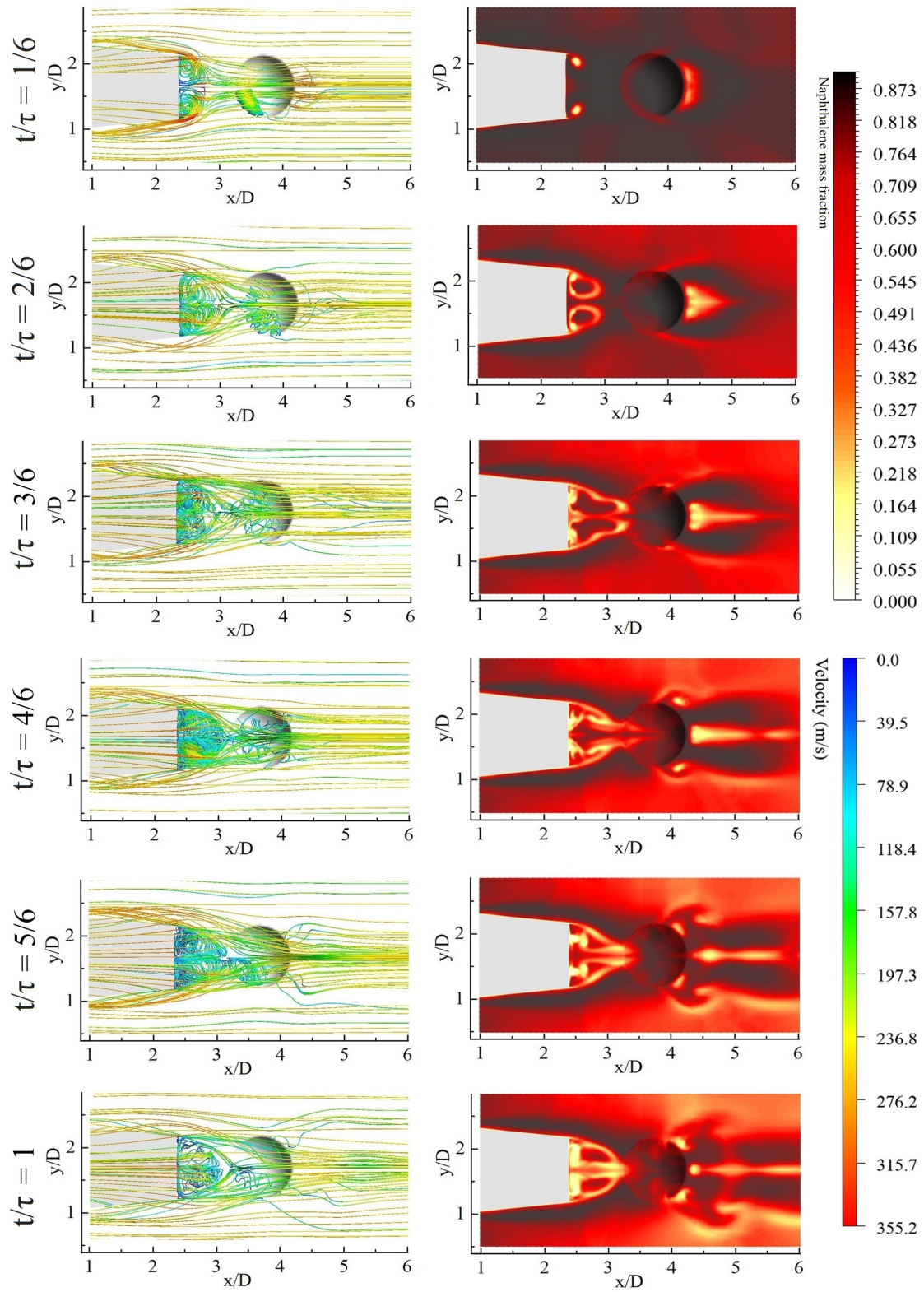
Fig. 6.7 Temporal development of the velocity streamlines and mass fraction field on a plane (z/D = 0.01) above the surface
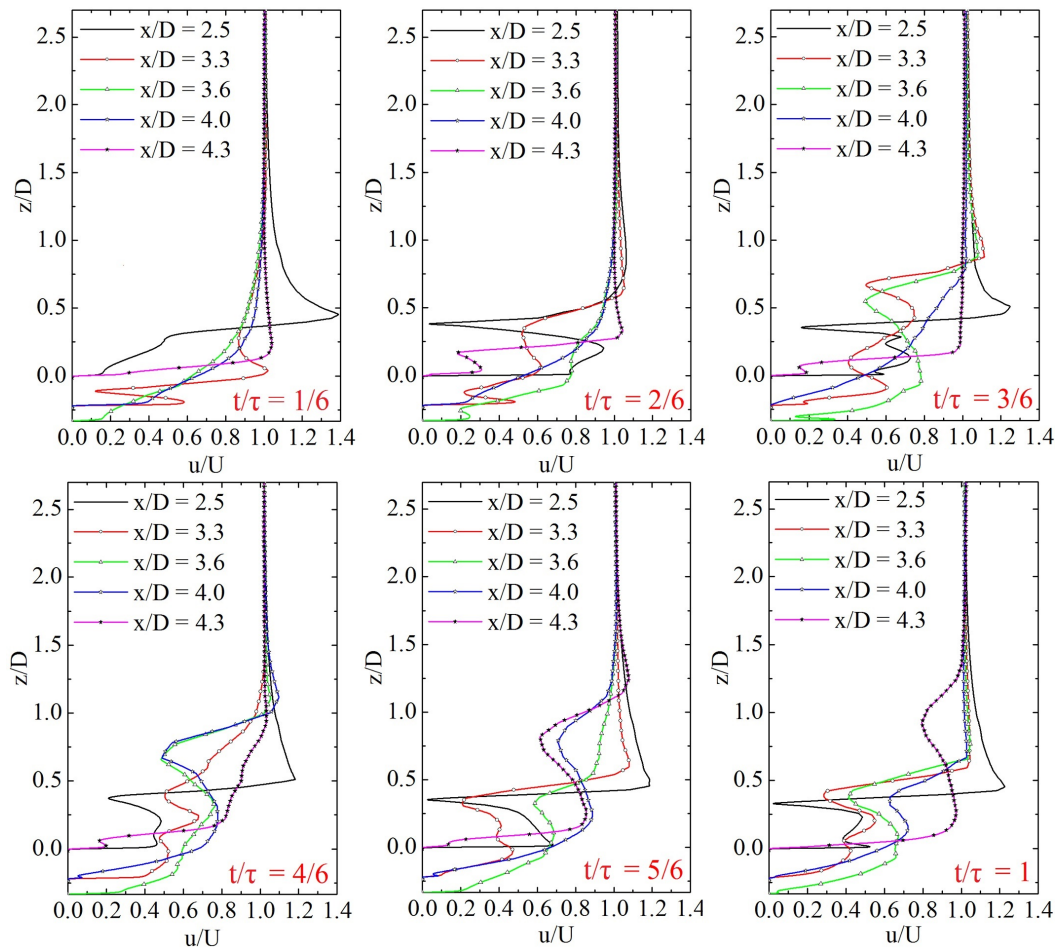
Fig. 6.8 Temporal development of the cross stream normalized velocity profiles at various streamwise locations

of instabilities in the flow field. Spatiotemporal characteristics of vortex shedding and its effect of mass transfer is assessed for various locations in the domain.

Time traces of the local mass transfer coefficients at various axial locations and their variation along spanwise directions are shown in Fig 6.10. Time traces shows predominant fluctuations in the center span of the domain and variations are minimal outside the core vortex region. It is evident from the spectra that the flow is highly chaotic in the center span and peaks have a unique dominating frequency. High amplitude fluctuations are observed in the vicinity of fore rim of the dimple than any other location in the flow field. This is attributed to the presence of active flow separation and associated recirculation. Lateral spread of fluctuations is evident in the spectra sampled for the vicinity of the dimple and is found to be less in front of LSVG and farther downstream. This is due to the cross-stream velocity attributed by the flow ejection from the dimple cavity. Time traces of the local mass transfer
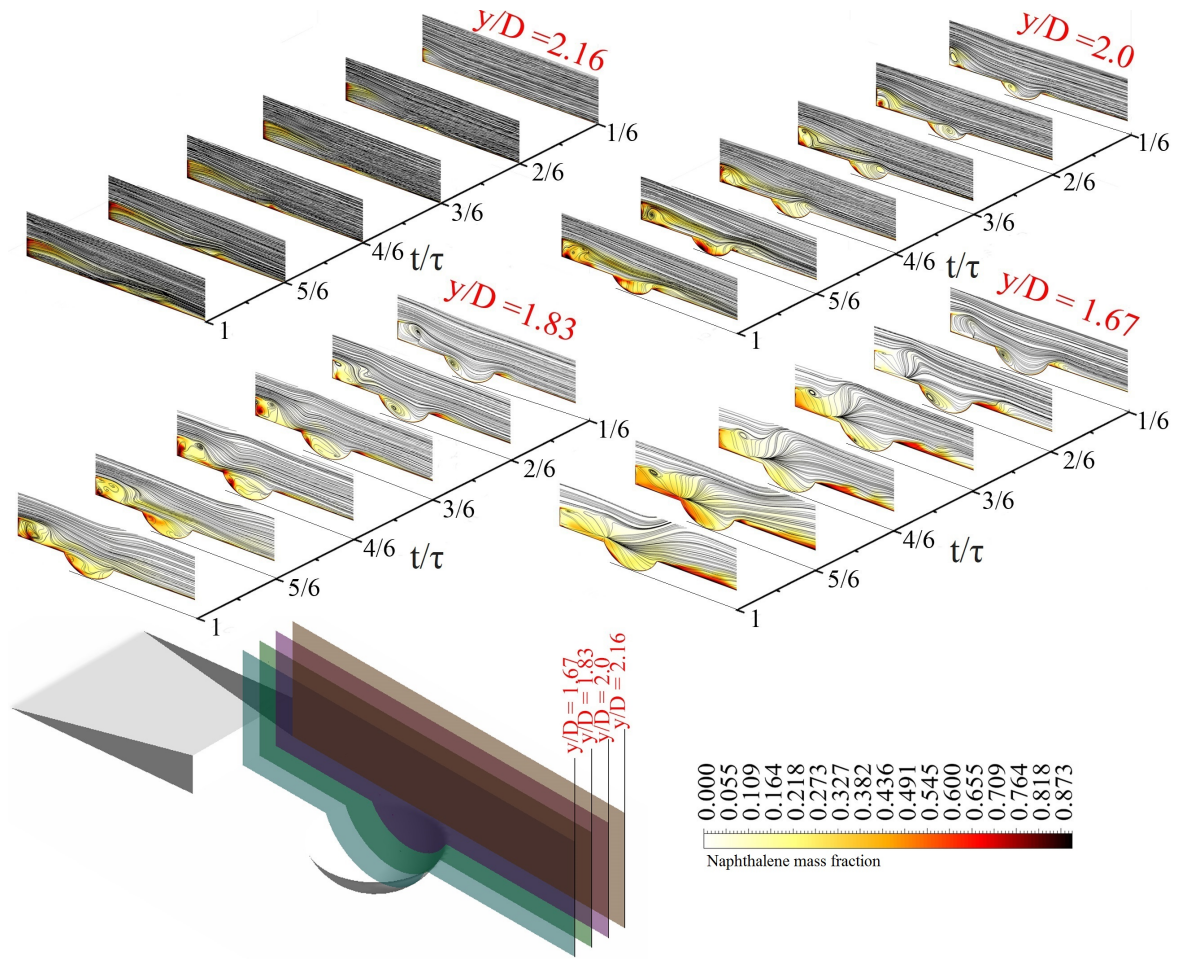
Fig. 6.9 Velocity streamlines superimposed with mass fraction field on longitudinal planes

coefficients show a unique spectrum at the downstream location of the dimple irrespective of the lateral position. Dimple can sustain oscillations for a wider locale than those created by an LSVG. An interesting modification in the spectra taken at various spanwise location can be observed in Fig 6.10b and 6.10c. Fluctuations were dominant for spectra taken for a location close to the axis (y/D=1.67) until flow gets advected in to the cavity. Later, irrespective of the lateral position, all spectra exhibit a unique kind of fluctuations. Wake region in front of LSVG is confined to the centroidal axis of the domain. This wake stream gets advected into the cavity and it spreads out laterally during ejection. This leads to the formation of a unique spectrum for all lateral location. The growth of instabilities in the flow field has a direct correlation with the mass transfer effect. Variation of the local Strouhal number with approaching free stream Re at various salient locations (such as in front of LSVG, fore edge of the dimple, center of the dimple, aft edge of the dimple, farther downstream of the dimple, etc) are plotted in Fig 6.11a. Flow instability is found to amplify with an increase
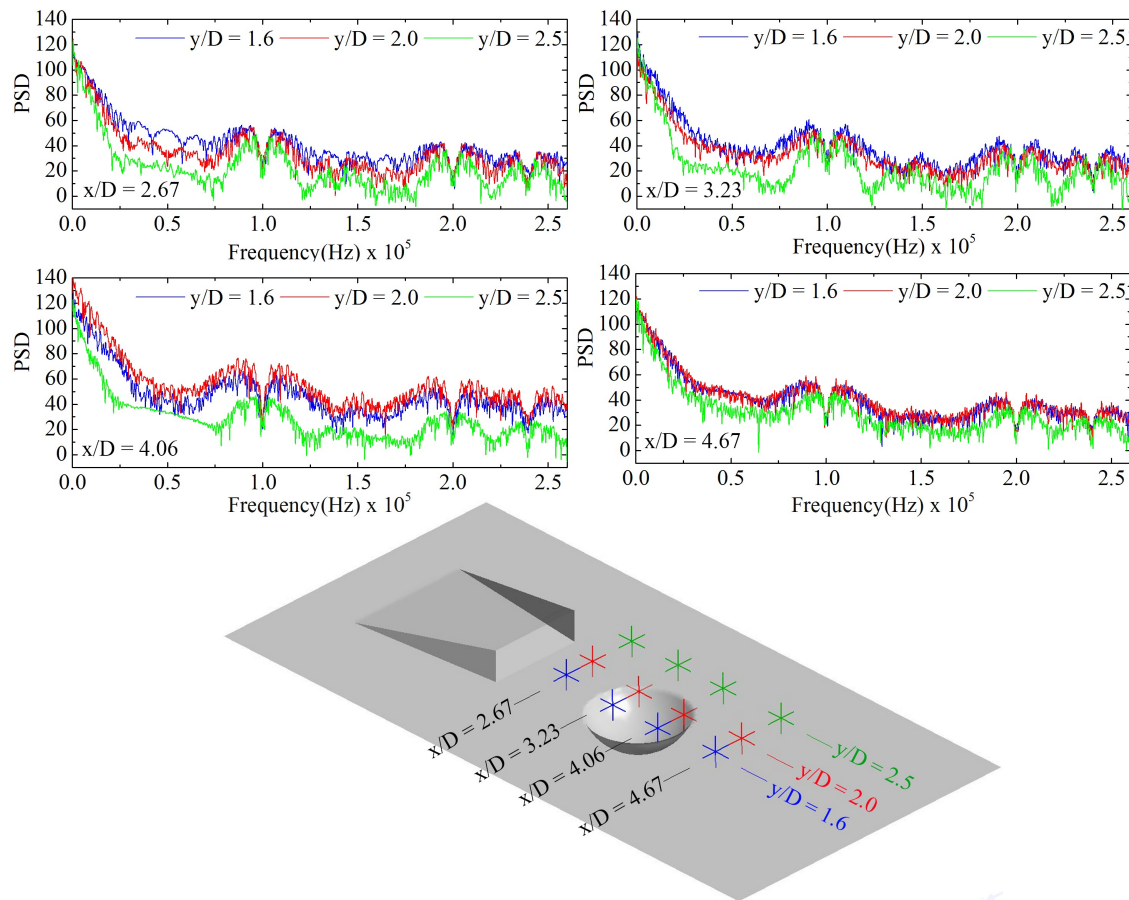
Fig. 6.10 Time traces of mass transfer coefficients at various axial locations and their deviation along the width

in approach velocity. Mass transfer effect is estimated at these transverse locations as the average of relative Sherwood number for various free stream Re. (in Fig 6.11b.)

6.3 Effect of the location and geometry of dimple placed in front of LSVG

Placement of dimple downstream of LSVG alters the wake structure significantly. Hence the distance between both geometrical features plays an important role in shaping the wake vortex structure and induced unsteadiness. Velocity streamlines on a plane close to the surface are analyzed for various extents of dimple placement (Fig 6.12). Dimple placed close to the vortex generator (d = D) is found to offer a larger amount of asymmetry to wake vortex structure leading to the generation of larger gradients in the vicinity of the aft face of the LSVG.
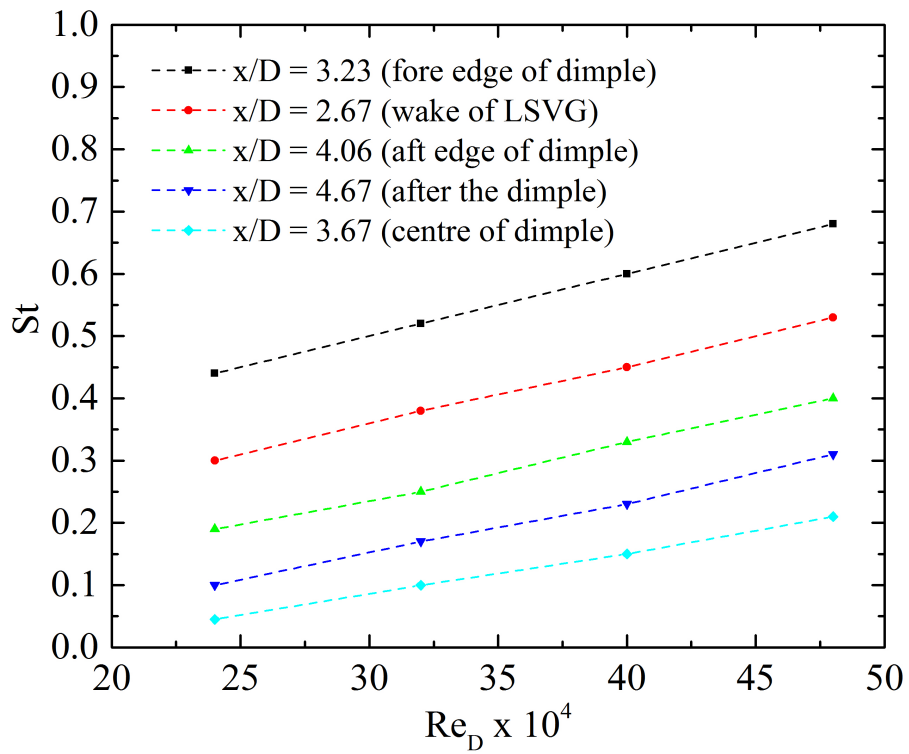
(a) Local Strouhal number variation with Re
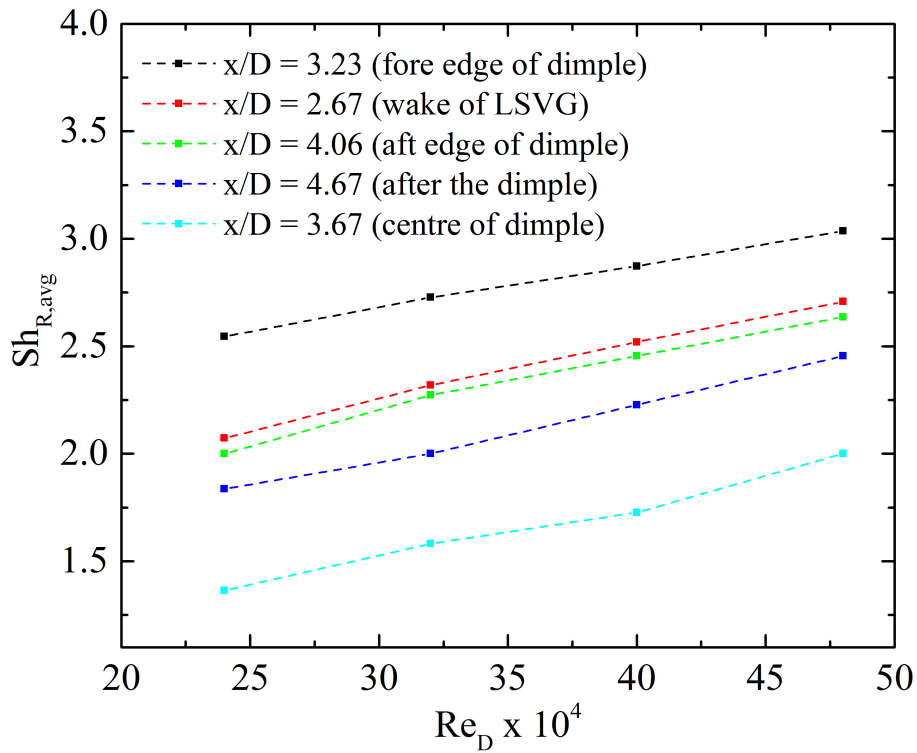
(b) Spanwise averaged Sherwood number variation with Re

Fig. 6.11 Frequency characteristics of the flow field and its effect on mass transfer
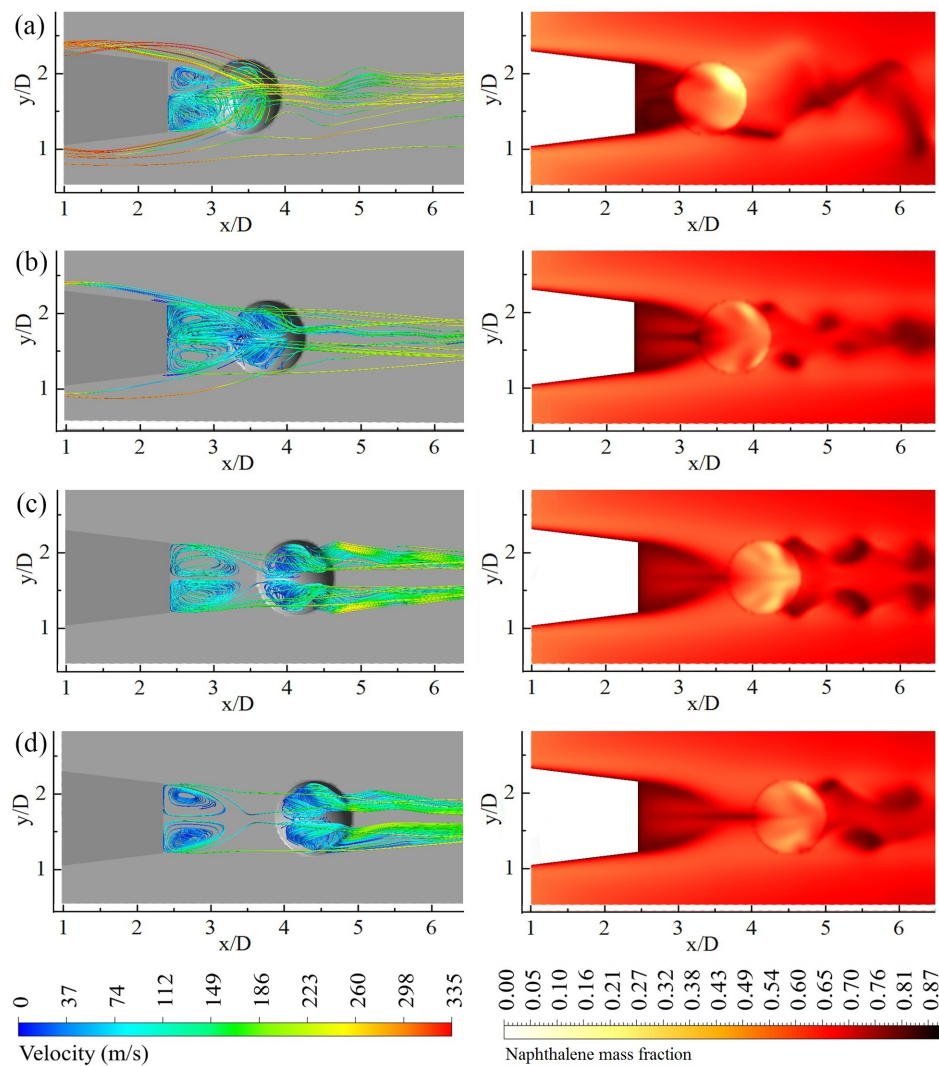
Fig. 6.12 Streamlines and mass fraction of the evolved substance on a plane (z/D = 0.01) above the surface for various dimple placement options

As a result of this, an active separation region is not created on a larger extent of the periphery of dimple rim due to the asymmetry in the wake stream that proceeding towards the fore rim of the dimple. Wake vortices attain symmetry as the dimple location is further moved downstream (d = 1.3D, 1.6D and 2D) and pronounced separation region is created in the vicinity of the dimple. Dimple is found to eject out symmetrical streams of fluid consequent to the advection of rather a symmetrical wake stream towards it. This has a significant role in promoting mass transfer effect in the downstream part of the dimple as well. Wake vortices proceeding to the dimple weakens when the dimple is placed farther from vortex generator and it adversely affects mass transfer enhancement. Span averaged relative Sherwood number variation along the axial direction for various dimple placement

options for a fixed approach Re= 400000 is shown in Fig 6.13. Dimple placed far apart from LSVG (d = 2D) is not effective in offering enhancement in downstream locations due to the weakening of incoming vortical structures in the wake. It is evident from the preceding discussion that dimple can augment and sustain the enhancement effect induced by the vortex generator and extent of augmentation depends on its location.
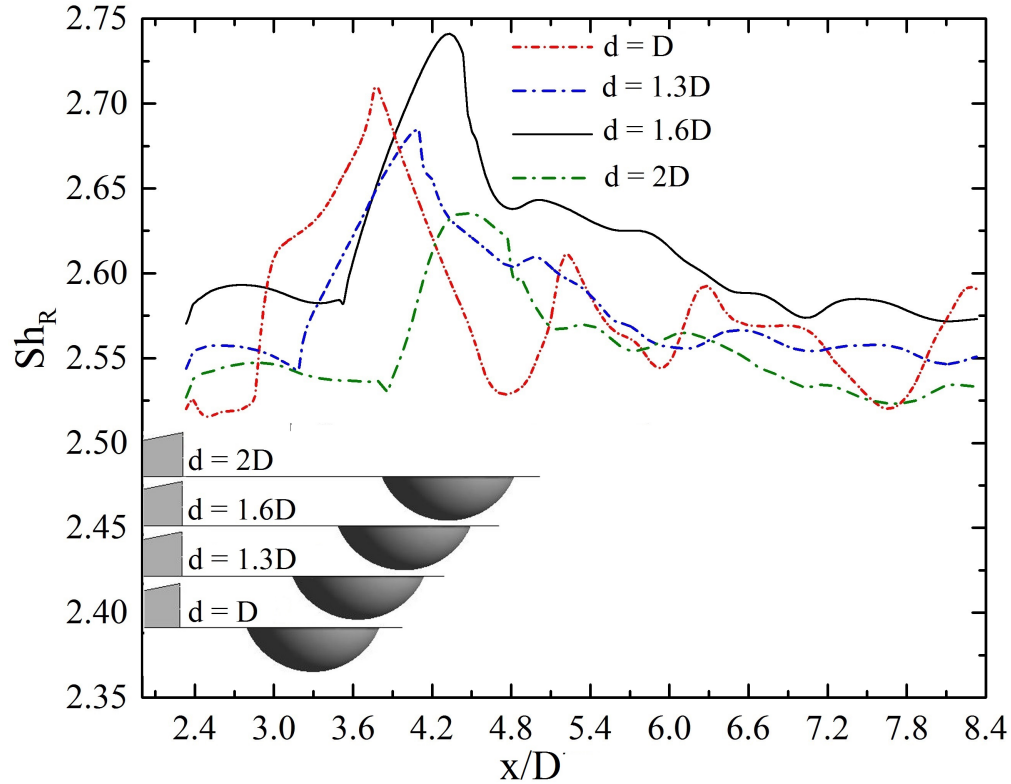
Fig. 6.13 Sherwood number variation along the axial direction for various dimple placement options (Re = 400000)

Indentation depth of the dimple has a key role in the resulting unsteady dynamics of the flow system. Hence an analysis is undertaken to reveal the effect of dimple depth to footprint diameter ratio (δ/D) in resulting mass transfer enhancement. Significant changes in the reattachment pattern of flow inside the cavity is evident as dimple depth is increased (Fig 6.14). Similarly, intense vortical structures are observed in the ejected stream from deeper cavity. Hence the deeper cavities exhibit higher mass transfer effect in the downstream region. Pronounced advection towards deeper cavities leads to the mass transfer enhancement in the separation region near the fore rim. Presence of deeper cavity in front of LSVG favor the creation of asymmetry in the wake structure that enhance mass transfer upstream of the dimple as well. Span averaged relative Sherwood number variation along the axial direction
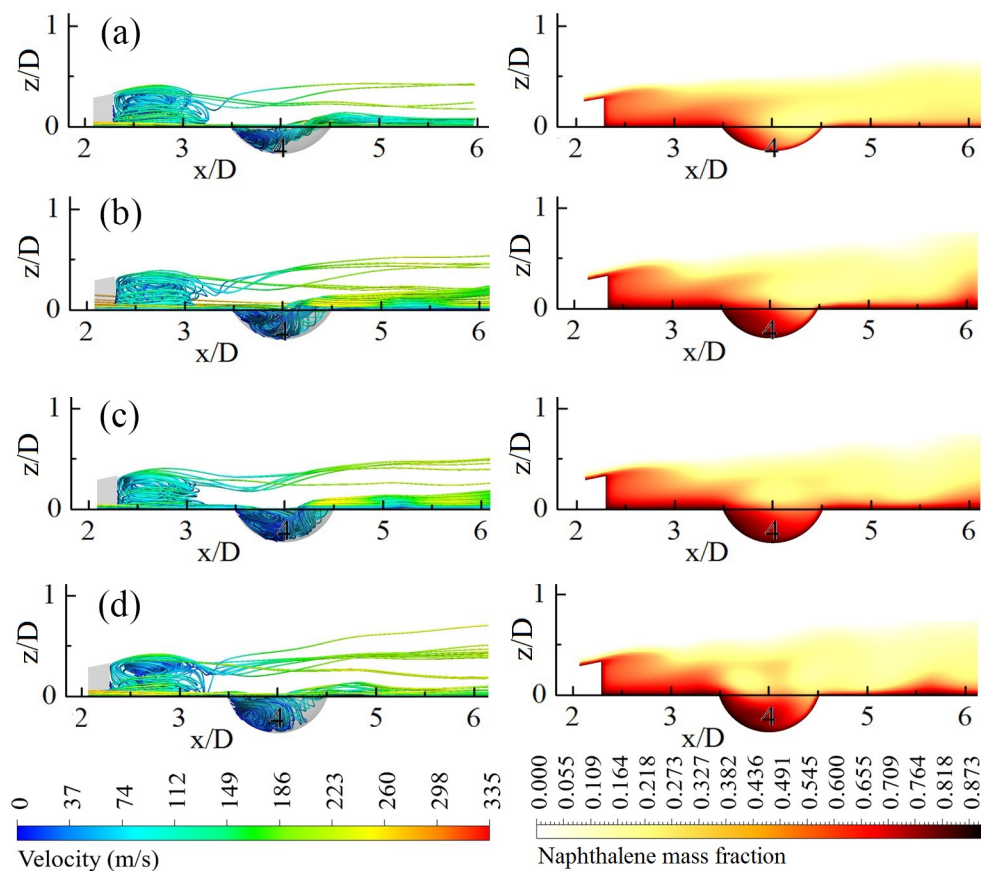
Fig. 6.14 Streamlines and mass fraction of the evolved substance on central longitudinal plane for various dimple depth to footprint diameter ratios

for various δ/D is shown in Fig 6.15. Nature of the flow ejection depends on cavity depth and this effect has a decisive role in the pattern of mass transfer effects downstream of the dimple.

High-speed flow past LSVG-dimple combinational surface features results in a complex three-dimensional flow field that promote mass transfer from the adjoining surface. Mass transfer effects are dependent on flow and geometrical aspects immensely.

As already discussed in the previous sections, the mass transfer enhancement shows a consistent increase with increase in indentation depth for fixed distance of dimple center form the trailing edge of vortex generator. This significant increase shows a consistent trend with increase in Reynolds number of the flow (Fig 6.16). However, for the case of fixed δ/D and varying distance from the trailing edge of LSVG to dimple center (d), it is observed that there is no consistent variation in mass transfer(Fig 6.17). Asymmetrical vortices are generated when the dimple is placed close to the VG. It is established that maximum mass transfer is at the upstream half of the dimple rather than at the downstream half when the
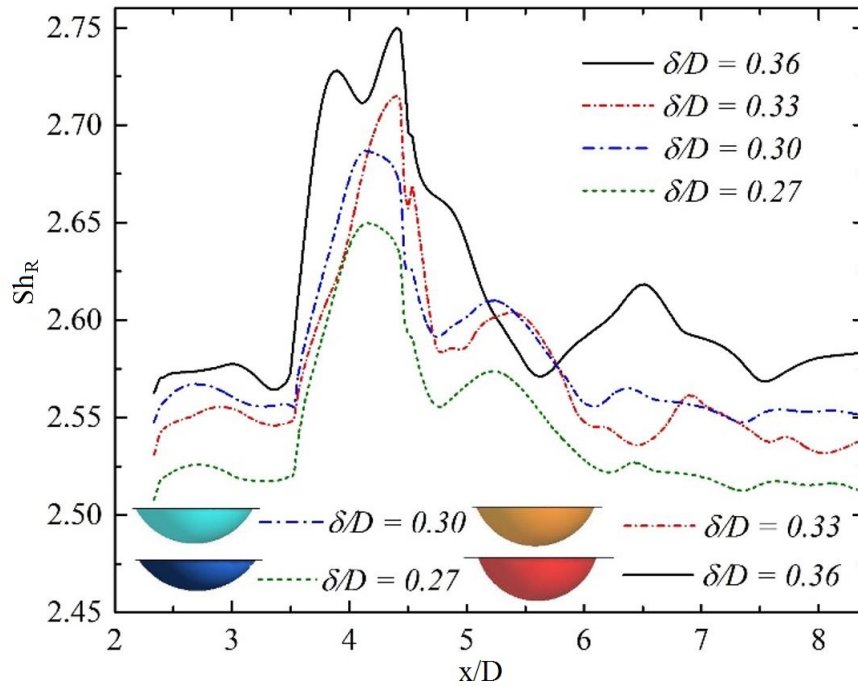
Fig. 6.15 Sherwood number variation along the axial direction for various dimple depth to footprint diameter ratios (Re = 400000)

dimple is in isolation. No active recirculation regions are generated when the dimple is either placed at the vicinity of VG or far away from the VG.

Efforts have been extended to compile the exhaustive results obtained from present computations in the form of correlations (Table 6.3) that predict mass transfer estimates as a function of geometric and flow parameters involved. Local Strouhal number, as well as relative Sherwood number at an axial location, shows a consistently increasing trend with free stream Reynolds number and a simple linear power law is used to obtain their correlation. Similarly, the mass transfer effects show a consistent improvement with an increase in dimple depth due to enhanced cavity oscillations. The dependence of sine of the location parameter (d/D) have involved the correlation for the prediction of the mass transfer effect as the asymmetry of the wake structure induced by the dimple placement is not showing a consistent trend.

6.4   Effects of dimple placed in wake of VSVG

The variable sweep vortex generator (VSVG) placed ahead of a dimple on flat surface creates asymmetrical vortex interaction of varying intensity as flow sweeps over the mass evolving

Table 6.3 Correlations developed for mass transfer estimates for various geometrical and flow conditions

Dependence of mass transfer effect on	Developed correlation	Correlation coefficients	Error estimates/ Applicability limit
Strouhal number at various axial locations	$Sh_R = A_1 Re^{0.05} + \beta(St - A_2)Re^{0.05}$	For x/D = 2.67; $A_1 = 0.77, A_2 = 0.02,$ $\beta = 1.63$ For x/D = 3.23; $A_1 = 0.65, A_2 = -0.10,$ $\beta = 1.66$ For x/D = 4.06; $A_1 = 1.13, A_2 = 0.2,$ $\beta = 1.11$ For x/D = 4.67; $A_1 = 0.80, A_2 = 0.07,$ $\beta = 1.52$	MAE = 0.114 RMSE = 0.126 $0.24 < Re_D < 0.48$ Re_D in millions
Vorticity at various axial locations	$Sh_R = \alpha(\xi - y_1)^\beta + y_2$	$\alpha = 0.3018, \beta = 1.017,$ $y_1 = 2.172, y_2 = 2.169$	MAE = 0.0575 RMSE = 0.0661 $0.24 < Re_D < 0.48$ Re_D in millions
Location of dimple (d/D) for various δ/D	$Sh_R = (1 + 0.05 Sin^2(\pi(d/D - 0.04)/0.08))Re^{1/5}$		MAE = 0.122 RMSE = 0.149 $1 < d/D < 2$
Ratio of foot print diameter to depth of the dimple (δ/D) for fixed d/D	$Sh_R = 0.05(Re)^{1/3}(\delta/D)^{1/5}$		MAE = 0.0357 RSME = 0.0403 $0.27 < \delta/D < 0.36$

Error estimates for correlation coefficients are the *MAE – Mean Absolute Error* and *RMSE-Root Mean Square Error value*
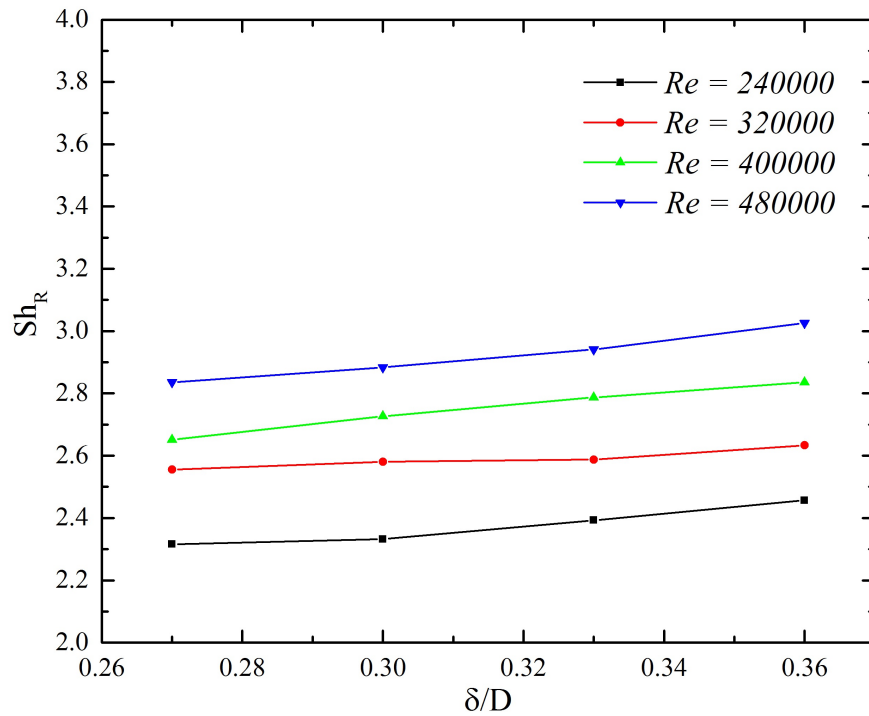
Fig. 6.16 Average Sherwood number variation for various δ/D at different Re

boundary. Extensive numerical simulations have been carried out with an objective to reveal the physics of vortex interaction, their drift in pattern, and to analyse consequent enhancement in mass transfer. It is well known from the previous discussions that the placement of LSVG generate complex three dimensional flow features downstream including large counter rotating vortex pair and horse shoe vortices. These features are rather symmetrical about a longitudinal axis passing through the centre of LSVG. Interaction of these vortices with boundary layer leads to larger gradients that can favour enhancement of transfer effects. Further augmentation is possible by the introduction of asymmetry in the evolved vortex structure. Asymmetry can be achieved by providing different lateral sweep angles on either surfaces of LSVG (already detailed in previous chapter). Unsteady numerical computations have been performed out for 7° swept LSVG and dimple combination as well as another VSVG (7° and 3° on either sides) and dimple combination.

Asymmetry in longitudinal vortex interaction favour the generation of larger gradients that lift the evolved mass more in to the free stream. Oscillatory nature of vortex interactions differ at various locations (Fig 6.18) Aforementioned distinct mass transfer pattern realized by the various types of vertical motion are further analysed to study the effect of geometry and flow effects. Average Sherwood number is computed for various transverse planes in the domain for both the configurations and compared with that of a case without the presence of
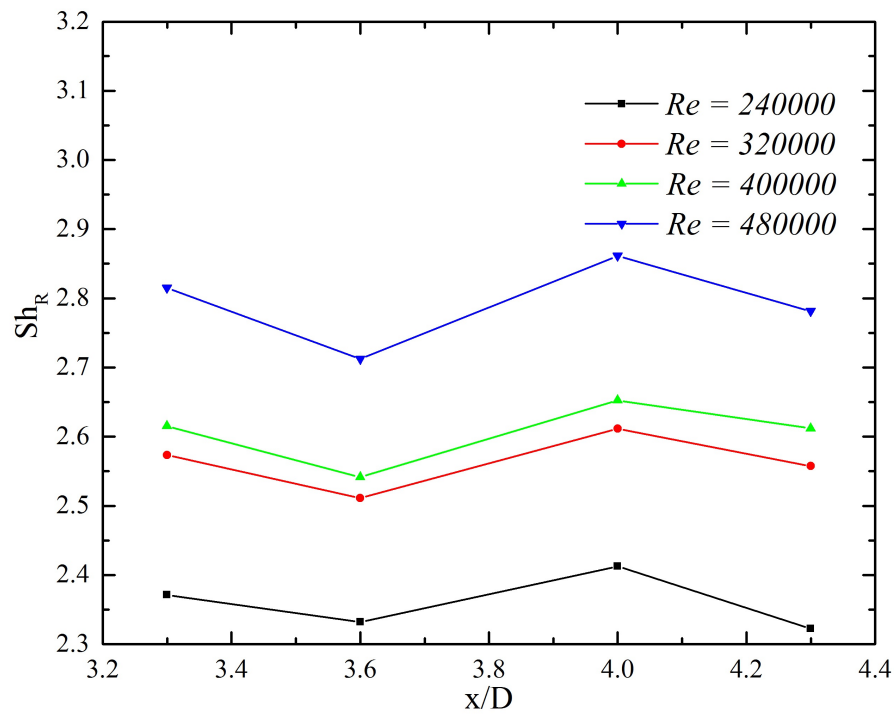
Fig. 6.17 Average Sherwood number variation for various (d/D) at different Re
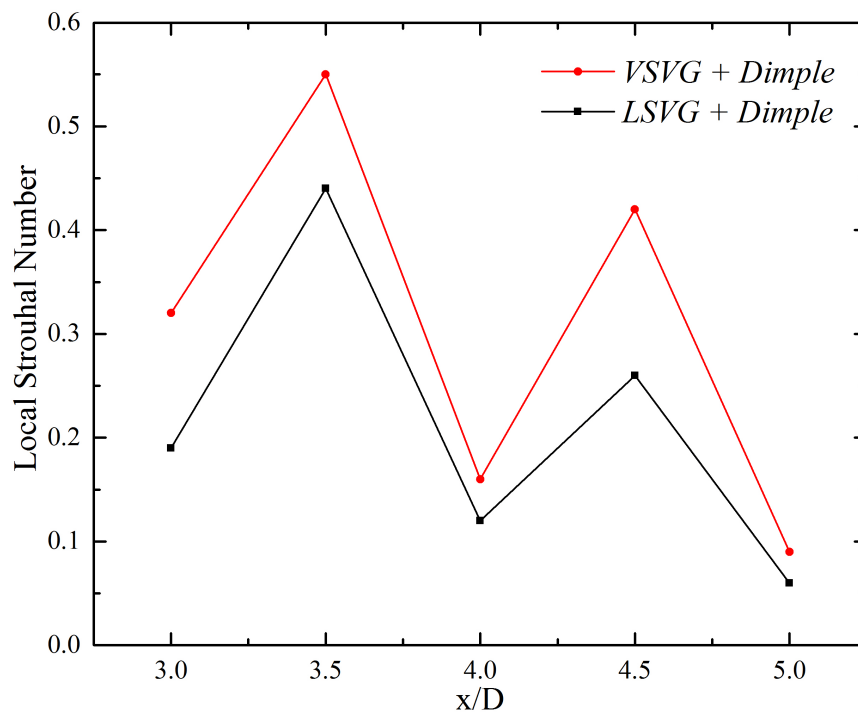
Fig. 6.18 Local Strouhal number at various axial locations

dimple. (Fig 6.19). First peak in mass transfer profile is attributed by the vortex interaction in wake region in front of vortex generator.
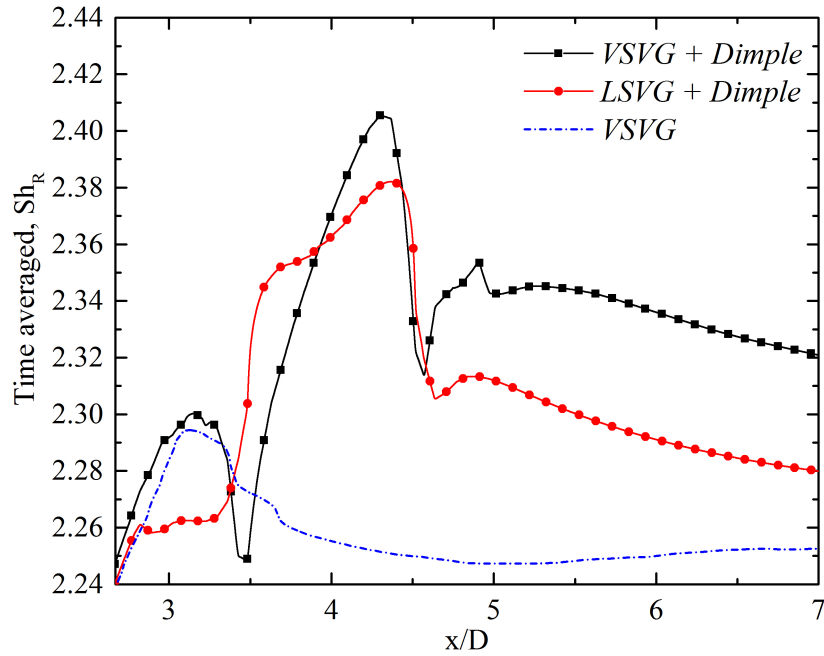
Fig. 6.19 Transverse plane averaged Sh_R along the stream wise direction for both configurations compared with that of a case without dimple

Presence of dimple realizes enhancement at the downstream locations which can further augmented by asymmetry attributed by the different sweep angles provided for the second configuration. This asymmetry can sustain improved mass transfer effects for farther downstream locations also. Enhanced vorticity and turbulent intensity in vortex affected areas favour mass transfer (Fig 6.20)

Introduction of various kinds of flow manipulators for the mass transfer enhancement generates several types of energy losses in the flow systems. Surface protuberant or depressions close to a boundary affect both mass transfer and energy losses. Total pressure loss across the flow systems are generally taken in to account for the quantification of such losses. Effectiveness of transfer enhancement is realized at the expense of pressure loss. Effectiveness of transfer enhancement is realized at the expense of pressure loss. A pressure loss parameter

$$\Delta P = \frac{P_{in} - P_{out}}{0.5 \rho V^2} \tag{6.1}$$

is used to quantify this effect. A comparison of pressure loss and mass transfer effects for various enhancement options having similar geometry and flow conditions is given in Fig
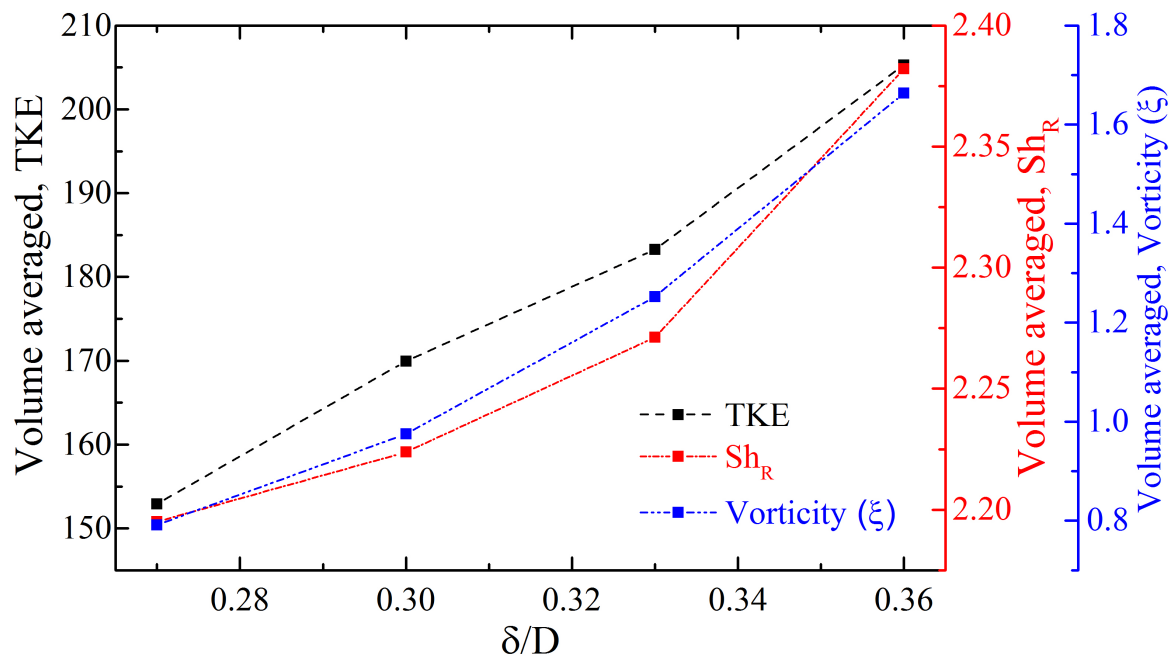
Fig. 6.20 Effect of vorticity and turbulent intensity

6.21. Vortex generator-dimple combination dealt in the present study is found to enhance convective mass transfer with minimal pressure loss.

6.5 Summary

Dimple placed in the wake of LSVG circumvents the inherent limitation of vortex generator augmenting transfer effects towards the wider and farther extent of the domain. Vortical fluid currents and their interaction create favorable gradients in the adjoining boundary that augments transfer effects. Placement of the vortex generator generate longitudinal and horseshoe vortices in the converging wake stream that gets advected into the dimple. Ejected stream out from the dimple contains vortices and gets laterally spread to a larger extent in the domain. Sharper gradients are developed near to the fore rim of the dimple and create low-velocity recirculation region within it. Sustenance of large-scale fluctuations, asymmetry of vortex interactions, and interaction of wake structures with developing boundary layer together make LSVG-dimple combination as promising mass transfer augmenting feature for high-speed flow. Dimple alters the spectral characters of large scale flow structures and thereby a unique fluctuation for the wider extent of the domain is created in its vicinity. This attributes a better passive mass transfer characteristic than a vortex generator in isolation can perform. Location of the dimple in front of the vortex generator is a vital factor that decides
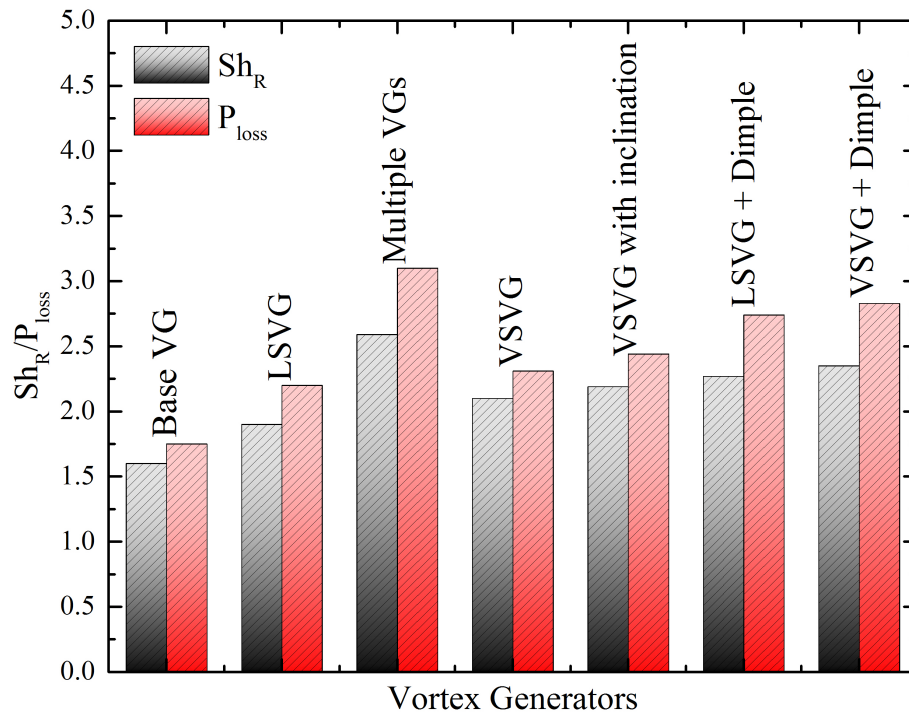
Fig. 6.21 Comparison of pressure loss and mass transfer effects for various enhancement options

the nature of asymmetry of wake vortices that head towards the fore edge of the dimple. Dimples offer greater enhancement of mass transfer when the dimple depth to footprint diameter ratio is kept higher. This is due to active sustenance of cavity induced oscillation and increase in strength of vortical structures in the ejected fluid stream with depth of the dimple.

Chapter 7

Conclusions

Exchange time available for transfer process is limited in high Reynolds number flows. Passive transfer process enhancement attained paramount research attention owing to its simplicity in implementation and versatile flow physics. Longitudinal vortices can be purposely induced into the turbulent boundary layer by geometrical variations or by the introduction of surface manipulators. Numerical analysis of passive mass transfer enhancement attributed by Lateral Sweep Vortex Generators (LSVG) and its combination with dimpled surface placed in high-speed freestream is presented in this work. Passive mass transfer enhancement methods are effective in alleviating the challenges imposed by limited exchange time available in high Reynolds number flows.

The last few years have witnessed unprecedented growth in the research publications dealing with various heat and mass transfer enhancement. A systematic review of available literature in this field has been carried out. A bird's eye view of the transfer enhancement capabilities put forward by various researchers has been compiled for each category of passive techniques envisaged in the present work. Physics of the flow field associated with transfer enhancement has been given paramount importance in such reviews as any augmentation in transfer effect is triggered by the makeovers in adjoining fluid stream. Various methods for the generation of secondary flows have been critically reviewed and the reason for transfer process enhancement has been explored in detail. A well-organized exposition of flow structures and associated transfer enhancement has formed the foundation of the present research.

Researchers have attempted various passive transfer process enhancement over the past few decades. These devices include either a single vortex generator or a combination of vortex generators or their arrays. Hemispherical and oval surface depressions are widely preferred over surface protrusions owing to their capability to enhance transfer effects with minimal pressure loss in high-speed flows. A major limitation of either surface protrusions

or depressions is that they cannot sustain the enhancement effect for wider expanse beyond their vicinity. Combinational mass transfer enhancement studies are not abundant in the literature. Convective mass transfer augmentation systems call for the requirement of not only the enhancement near the surface but also the evolved mass should be carried away to the farther locations in adjoining fluid free stream. The present research explored the sustenance of the strength of the evolved vortex system in the wake of the vortex generator and a novel combinational convective mass transfer augmenting system has been proposed.

The development of an appropriate computational methodology is essential in accurately simulating inherently involved flow physics with multiple transport phenomena. A state-of-the-art computational framework has been developed for simulating the convective mass transfer from a surface into a three-dimensional turbulent compressible flow field. A temperature dependent mass efflux boundary condition is derived and incorporated in an advection upstream splitting method based finite volume solver to simulate the mass entrainment. The computational procedure has been thoroughly validated and ensured the predictability of the solver. The advent of sophisticated visualization tools in experiments has provided an additional synergy in benchmarking. A detailed comparative estimate of flow parameters has been carried out with a test case on heat transfer characteristics of flow past a vortex generator among the validation exercises. A detailed spatiotemporal assessment of the vortical fluid motion and associated mass transfer enhancement has been carried out for various test cases. Following are the other conclusions from this study.

Secondary vortices generated in the flow field can create favorable gradients that enhance convective mass transfer from the adjoining boundary. Vortices generated by lateral sweep vortex generator enhance the entrainment of lateral fluid streams and this, in turn, leads to the lift-off of counter-rotating vortex pair. Mass transfer enhancement is found to be dominant in these separation regions. The enhancement of mass transfer achieved by the vortex generators with the lateral sweep can be well controlled by its sweep angle, as it shows a consistent variation. Also, the mass transfer enhancement consistently increases with an increase in approach velocity. A correlation of the form $Sh_R = \alpha(\xi_R - c_1)^\beta + c_2$ has been developed for the prediction of average and maximum relative Sherwood number for the mass transfer enhancement created by the LSVG. This correlation establish a relation between the relative Sherwood number and relative vorticity along the stream wise direction. Also, a relationship between the vortex trajectories and locus of peak mass transfer has been established. Presence of multiple vortex generators creates the generation of dissimilar vortices in the wake region. Interaction of dissimilar vortices favours more mass injection to the core from the lateral direction.

The locus of vortex trajectory and peak convective heat transfer has considerable agreement; hence, the role of vortices in the wake region of VGs in enhancement of convective heat transfer is established. The presence of multiple VGs introduces the interaction of dissimilar vortices in the wake region. This effect enhances convective heat transfer. The interaction of dissimilar vortices with the developing boundary layer favors injection of more mass from the lateral direction. The limitation of using multiple vortex generators is the increased pressure loss. Even though mass transfer enhancement of 61% has been achieved, the pressure loss also increases by about 78% relative to the base VG configuration. Hence, geometrical variations to the base vortex generator that generates asymmetrical vortex interactions has been attempted further.

The presence of variable lateral sweep provided on lateral sweep vortex generator is found to provide unsteadiness and asymmetry of vortices. Considerable enhancement (31% and 36%) has been obtained with different lateral sweep and slant surface inclination when compared to the base vortex generator configuration. Corresponding pressure losses are much lesser than with multiple vortex generators, 32% and 39% respectively relative to the base vortex generator. Precise control over mass enhancement is possible with the variable lateral sweep provided on lateral sweep vortex generator.

A major limitation of vortex generators observed from above analyses is that they cannot sustain the enhancement effect for wider expanse beyond their vicinity. Hence the present research has introduced a combinational passive mass transfer enhancer by placing hemispherical depression (dimple) downstream of a lateral sweep vortex generator. Enhancement is achieved by the creation of large scale vortical features, their sustenance, and spread due to the presence of the dimple cavity. This flow field encompasses vivid spatiotemporal features consisting of vortical fluid currents and their interactions, creating favorable gradients in the adjoining boundary that augments transfer effects. Placement of the vortex generator generates longitudinal and horseshoe vortices in the converging wake stream that gets advected into the dimple. Ejected stream out from the dimple contains vortices and gets laterally spread to a larger extent in the domain. Sharper gradients are developed near to the fore rim of the dimple and create a low-velocity recirculation region within it. Dimple alters the spatial and spectral characters of large scale flow structures and thereby a unique fluctuation for the wider extent of the domain is created in its vicinity. Sustenance of the large-scale fluctuations, asymmetry of vortex interactions, and interaction of wake structures with developing boundary layer together make LSVG-dimple combination as promising mass transfer augmenting feature for high-speed flow. Mass transfer enhancement of 42% and 47% has been achieved with LSVG dimple combination and VSVG dimple combination relative to the base VG configuration. Corresponding pressure losses are 56% and 61%

respectively. These are much lower compared to a multiple vortex generator configuration. The location of the dimple in front of the vortex generator is also a vital factor that decides the nature of asymmetry of wake vortices that head towards the fore-edge of the dimple. Wake vortices that are rather symmetrical are found to augment the gradients near separation region of the dimple. Also, these symmetrical wake vortices lead to the generation of unique vortical structures downstream of the dimple that augments mass transfer from a wider extent. Dimples offer greater enhancement of mass transfer when the dimple depth to footprint diameter ratio is kept higher. This is due to active sustenance of cavity induced oscillation and increase in strength of vortical structures in the ejected fluid stream with depth of the dimple. Correlations have also been worked out based on the solution for the mass transfer as a function of flow and geometry parameters involved in this analysis as well.

Possible research extension

Present study focused on mass transfer enhancement by LSVG, VSVG and its combination with dimpled cavity. Following are the possible research extensions,

- Studies can be extended for various geometry alternatives such as vortex generator combination with different dimple shapes (elliptical, tear drop or V shape dimples)

- An eccentric placement of dimples from the centroidal axis can also give another pattern of mass transfer characteristics.

- Present numerical procedure can be used to examine the mixing performance of hybrid rocket motor and solid fuel combustors

- Numerical simulation for combustion in a similar scenario can also be performed by invoking appropriate fuel oxidizer reaction mechanism.

References

Bergles, A. (2001), 'The implications and challenges of enhanced heat transfer for the chemical process industries', *Chemical Engineering Research and Design* **79**(4), 437–444.

Bergles, A. E. and Manglik, R. M. (2013), 'Current progress and new developments in enhanced heat and mass transfer', *Journal of Enhanced Heat Transfer* **20**(1).

Bergles, A., Nirmalan, V., Junkhan, G. and Webb, R. (1983), Bibliography on augmentation of convective heat and mass transfer-ii, Technical report, Iowa State Univ. of Science and Technology, Ames (USA). Heat Transfer Lab.

Bhuiyan, A. A., Amin, M. R., Karim, R. and Islam, A. (2014), 'Plate fin and tube heat exchanger modeling: Effects of performance parameters for turbulent flow regime', *International Journal of Automotive and Mechanical Engineering* **9**(1), 1768–1781.

Bhuiyan, A. A., Islam, A. and Amin, M. R. (2011), 'Numerical prediction of laminar characteristics of fluid flow and heat transfer in finned-tube heat exchangers', *Innovative Systems Design and Engineering* **2**(6), 1–12.

Biswas, G. and Chattopadhyay, H. (1992), 'Heat transfer in a channel with built-in wing-type vortex generators', *International Journal of Heat and Mass Transfer* **35**(4), 803–814.

Biswas, G., Mitra, N. and Fiebig, M. (1994), 'Heat transfer enhancement in fin-tube heat exchangers by winglet type vortex generators', *International Journal of Heat and Mass Transfer* **37**(2), 283–291.

Biswas, G., Torii, K., Fujii, D. and Nishino, K. (1996), 'Numerical and experimental determination of flow structure and heat transfer effects of longitudinal vortices in a channel flow', *International Journal of Heat and Mass Transfer* **39**(16), 3441–3451.

Bjerg, A., Christoffersen, K., Sørensen, H. and Hærvig, J. (2019), 'Flow structures and heat transfer in repeating arrangements of staggered rectangular winglet pairs by large eddy simulations: Effect of winglet height and longitudinal pitch distance', *International Journal of Heat and Mass Transfer* **131**, 654–663.

Borisov, I., Khalatov, A., Kobzar, S. and Glezer, B. (2004), Comparison of thermo-hydraulic characteristics for two types of dimpled surfaces, *in* 'ASME Turbo Expo 2004: Power for Land, Sea, and Air', American Society of Mechanical Engineers Digital Collection, pp. 933–942.

Chamoli, S., Lu, R., Xu, D. and Yu, P. (2018), 'Thermal performance improvement of a solar air heater fitted with winglet vortex generators', *Solar Energy* **159**, 966–983.

Chen, Y., Chew, Y. and Khoo, B. (2014), 'Heat transfer and flow structure on periodically dimple–protrusion patterned walls in turbulent channel flow', *International Journal of Heat and Mass Transfer* **78**, 871–882.

Chen, Y., Chew, Y. T. and Khoo, B. C. (2012), 'Enhancement of heat transfer in turbulent channel flow over dimpled surface', *International Journal of Heat and Mass Transfer* **55**(25-26), 8100–8121.

Chen, Y., Fiebig, M. and Mitra, N. (2000), 'Heat transfer enhancement of finned oval tubes with staggered punched longitudinal vortex generators', *International Journal of Heat and Mass Transfer* **43**(3), 417–435.

Chomdee, S. and Kiatsiriroat, T. (2006), 'Enhancement of air cooling in staggered array of electronic modules by integrating delta winglet vortex generators', *International communications in heat and mass transfer* **33**(5), 618–626.

Chu, P., He, Y., Lei, Y., Tian, L. and Li, R. (2009), 'Three-dimensional numerical study on fin-and-oval-tube heat exchanger with longitudinal vortex generators', *Applied Thermal Engineering* **29**(5-6), 859–876.

Chyu, M., Yen, C. and Siw, S. (2007), Comparison of heat transfer from staggered pin fin arrays with circular, cubic and diamond shaped elements, *in* 'ASME Turbo Expo 2007: power for land, sea, and air', American Society of Mechanical Engineers, pp. 991–999.

Cuevas, C., Makaire, D., Dardenne, L. and Ngendakumana, P. (2011), 'Thermo-hydraulic characterization of a louvered fin and flat tube heat exchanger', *Experimental Thermal and Fluid Science* **35**(1), 154–164.

DeJong, N. and Jacobi, A. M. (2003), 'Flow, heat transfer, and pressure drop in the near-wall region of louvered-fin arrays', *Experimental Thermal and Fluid Science* **27**(3), 237–250.

Dewan, A., Mahanta, P., Raju, K. S. and Kumar, P. S. (2004), 'Review of passive heat transfer augmentation techniques', *Proceedings of the Institution of Mechanical Engineers, Part A: Journal of Power and Energy* **218**(7), 509–527.

Donohue, J. M. and cDaniel, J. C. (1996), 'Complete three-dimensional multiparameter mapping of a supersonic ramp fuel injector flowfield', *AIAA journal* **34**(3), 455–462.

Du, W., Luo, L., Wang, S. and Zhang, X. (2018), 'Effect of the dimple location and rotating number on the heat transfer and flow structure in a pin finned channel', *International Journal of Heat and Mass Transfer* **127**, 111–129.

Du, X., Feng, L., Yang, Y. and Yang, L. (2013), 'Experimental study on heat transfer enhancement of wavy finned flat tube with longitudinal vortex generators', *Applied Thermal Engineering* **50**(1), 55–62.

Eiamsa-Ard, S., Kaewkohkiat, Y., Thianpong, C. and Promvonge, P. (2008), 'Combustion behavior in a dual-staging vortex rice husk combustor with snail entry', *International Communications in Heat and Mass Transfer* **35**(9), 1134–1140.

Eiamsa-Ard, S. and Promvonge, P. (2011), 'Influence of double-sided delta-wing tape insert with alternate-axes on flow and heat transfer characteristics in a heat exchanger tube', *Chinese journal of chemical engineering* **19**(3), 410–423.

Elyyan, M. A. and Tafti, D. K. (2009), 'A novel split-dimple interrupted fin configuration for heat transfer augmentation', *International Journal of Heat and Mass Transfer* **52**(5-6), 1561–1572.

Fluent, A. (2012), '14.5 release user guide', *Ansys Inc* .

Gentry, M. and Jacobi, A. (1997), 'Heat transfer enhancement by delta-wing vortex generators on a flat plate: vortex interactions with the boundary layer', *Experimental Thermal and Fluid Science* **14**(3), 231–242.

Gentry, M. and Jacobi, A. M. (2002), 'Heat transfer enhancement by delta-wing-generated tip vortices in flat-plate and developing channel flows', *Journal of heat transfer* **124**(6), 1158–1168.

Gholami, A., Wahid, M. A. and Mohammed, H. (2014), 'Heat transfer enhancement and pressure drop for fin-and-tube compact heat exchangers with wavy rectangular winglet-type vortex generators', *International Communications in Heat and Mass Transfer* **54**, 132–140.

Gong, J., Min, C., Qi, C., Wang, E. and Tian, L. (2013), 'Numerical simulation of flow and heat transfer characteristics in wavy fin-and-tube heat exchanger with combined longitudinal vortex generators', *International Communications in Heat and Mass Transfer* **43**, 53–56.

Gschwind, P., Regele, A. and Kottke, V. (1995), 'Sinusoidal wavy channels with taylor-goertler vortices', *Experimental thermal and fluid science* **11**(3), 270–275.

He, J., Liu, L. and Jacobi, A. M. (2010), 'Air-side heat-transfer enhancement by a new winglet-type vortex generator array in a plain-fin round-tube heat exchanger', *Journal of Heat Transfer* **132**(7), 071801.

He, Y., Han, H., Tao, W. and Zhang, Y. (2012), 'Numerical study of heat-transfer enhancement by punched winglet-type vortex generator arrays in fin-and-tube heat exchangers', *International Journal of Heat and Mass Transfer* **55**(21-22), 5449–5458.

He, Y.-L. and Zhang, Y. (2012), Advances and outlooks of heat transfer enhancement by longitudinal vortex generators, *in* 'Advances in Heat Transfer', Vol. 44, Elsevier, pp. 119–185.

Henze, M., Von Wolfersdorf, J., Weigand, B., Dietz, C. and Neumann, S. (2011), 'Flow and heat transfer characteristics behind vortex generators–a benchmark dataset', *International Journal of Heat and Fluid Flow* **32**(1), 318–328.

Hiravennavar, S., Tulapurkara, E. and Biswas, G. (2007), 'A note on the flow and heat transfer enhancement in a channel with built-in winglet pair', *International Journal of Heat and Fluid Flow* **28**(2), 299–305.

Isaev and Mityakov, A. (2003), 'Intensification of tornado turbulent heat exchange in asymmetric holes on a plane wall', *Journal of engineering physics and thermophysics* **76**(2), 266–270.

Isaev, S. A. and Leont'ev, A. I. (2003), 'Numerical simulation of vortex enhancement of heat transfer under conditions of turbulent flow past a spherical dimple on the wall of a narrow channel', *High Temperature* **41**(5), 665–679.

Isaev, S., Leont'Ev, A. and Baranov, P. (2000), 'Identification of self-organized vortexlike structures in numerically simulated turbulent flow of a viscous incompressible liquid streaming around a well on a plane', *Technical physics letters* **26**(1), 15–18.

Isaev, S., Leontiev, A., Baranov, P., Pyshnyi, I. and Usachov, A. (2002), Numerical analysis of the vortex intensification of heat transfer in a channel with a set of deep spherical dimples on one of the walls, *in* 'Doklady Physics', Vol. 47, Springer, pp. 755–757.

Isaev, S., Leontiev, A., Kornev, N., Hassel, E. and Chudnovskii, Y. P. (2015), 'Heat transfer intensification for laminar and turbulent flows in a narrow channel with one-row oval dimples', *High Temperature* **53**(3), 375–386.

Isaev, S., Schelchkov, A., Leontiev, A., Baranov, P. and Gulcova, M. (2016), 'Numerical simulation of the turbulent air flow in the narrow channel with a heated wall and a spherical dimple placed on it for vortex heat transfer enhancement depending on the dimple depth', *International Journal of Heat and Mass Transfer* **94**, 426–448.

Isaev, S., Schelchkov, A., Leontiev, A., Gortyshov, Y. F., Baranov, P. and Popov, I. (2017), 'Vortex heat transfer enhancement in the narrow plane-parallel channel with the oval-trench dimple of fixed depth and spot area', *International Journal of Heat and Mass Transfer* **109**, 40–62.

Isaev and Sergey (2003), 'The effect of rearrangement of the vortex structure on heat transfer under conditions of increasing depth of a spherical dimple on the wall of a narrow channel', *High Temperature* **41**(2), 229–232.

Jabardo, J. S., Zoghbi Filho, J. B. and Salamanca, A. (2006), 'Experimental study of the air side performance of louver and wave fin-and-tube coils', *Experimental Thermal and Fluid Science* **30**(7), 621–631.

Jacobi, A. M. and Shah, R. (1995), 'Heat transfer surface enhancement through the use of longitudinal vortices: a review of recent progress', *Experimental Thermal and Fluid Science* **11**(3), 295–309.

Jang, H. N., Park, J. S. and Kwak, J. S. (2018), 'Experimental study on heat transfer characteristics in a ribbed channel with dimples, semi-spherical protrusions, or oval protrusions', *Applied Thermal Engineering* **131**, 734–742.

Jiansheng, W., Yu, J. and Xueling, L. (2019), 'Heat transfer and flow characteristics in a rectangular channel with small scale vortex generators', *International Journal of Heat and Mass Transfer* **138**, 208–225.

Joardar, A. and Jacobi, A. M. (2008), 'Heat transfer enhancement by winglet-type vortex generator arrays in compact plain-fin-and-tube heat exchangers', *International journal of refrigeration* **31**(1), 87–97.

Katkhaw, N., Vorayos, N., Kiatsiriroat, T., Khunatorn, Y., Bunturat, D. and Nuntaphan, A. (2014), 'Heat transfer behavior of flat plate having 45 ellipsoidal dimpled surfaces', *Case Studies in Thermal Engineering* **2**, 67–74.

Ke, F., Wang, L., Hua, L., Gao, S. and Su, Y. (2006), 'The optimum angle of attack of delta winglet vortexgenerators on heat transfer performance of finned flat tube bank with considering nonuniform fin temperature', *Experimental heat transfer* **19**(3), 227–249.

Ke, Z., Chen, C.-L., Li, K., Wang, S. and Chen, C.-H. (2019), 'Vortex dynamics and heat transfer of longitudinal vortex generators in a rectangular channel', *International Journal of Heat and Mass Transfer* **132**, 871–885.

Khalatov, A., Byerley, A., Ochoa, D. and Min, S.-K. (2004), Flow characteristics within and downstream of spherical and cylindrical dimple on a flat plate at low reynolds numbers, *in* 'ASME Turbo Expo 2004: Power for Land, Sea, and Air', American Society of Mechanical Engineers Digital Collection, pp. 589–602.

Koolnapadol, N., Kaewkohkiat, Y., Promvonge, P. and Eiamsa-ard, S. (2014), Thermal behaviors in a solar air heater channel with arc-shaped baffle turbulators, *in* 'Advanced Materials Research', Vol. 1051, Trans Tech Publ, pp. 845–849.

Kwak (2005), 'Simultaneous heat transfer enhancement and pressure loss reduction for finned-tube bundles with the first or two transverse rows of built-in winglets', *Experimental Thermal and Fluid Science* **29**(5), 625–632.

Kwak, K., Torii, K. and Nishino, K. (2002), 'Heat transfer and flow characteristics of fin-tube bundles with and without winglet-type vortex generators', *Experiments in fluids* **33**(5), 696–702.

Leontiev, A., Kiselev, N., Vinogradov, Y. A., Strongin, M., Zditovets, A. and Burtsev, S. (2017), 'Experimental investigation of heat transfer and drag on surfaces coated with dimples of different shape', *International Journal of Thermal Sciences* **118**, 152–167.

Ligrani, P., Harrison, J., Mahmmod, G. and Hill, M. (2001), 'Flow structure due to dimple depressions on a channel surface', *Physics of fluids* **13**(11), 3442–3451.

Liou, M.-S. (1996), 'A sequel to ausm: Ausm+', *Journal of computational Physics* **129**(2), 364–382.

Liou, M.-S. (2006), 'A sequel to ausm, part ii: Ausm+-up for all speeds', *Journal of computational physics* **214**(1), 137–170.

Liu, H.-l., Fan, C.-c., He, Y.-l. and Nobes, D. S. (2019), 'Heat transfer and flow characteristics in a rectangular channel with combined delta winglet inserts', *International Journal of Heat and Mass Transfer* **134**, 149–165.

Liu, S. and Sakr, M. (2013), 'A comprehensive review on passive heat transfer enhancements in pipe exchangers', *Renewable and sustainable energy reviews* **19**, 64–81.

Luo (2016), 'Heat transfer and friction factor performance in a pin fin wedge duct with different dimple arrangements', *Numerical Heat Transfer, Part A: Applications* **69**(2), 209–226.

Luo (2017), 'Multi-objective optimization of a solar receiver considering both the dimple/protrusion depth and delta-winglet vortex generators', *Energy* **137**, 1–19.

Luo, L. and Wen (2016), 'Thermal enhancement by using grooves and ribs combined with delta-winglet vortex generator in a solar receiver heat exchanger', *Applied energy* **183**, 1317–1332.

Luo, L., Wen, F., Wang, L., Sundén, B. and Wang, S. (2017), 'On the solar receiver thermal enhancement by using the dimple combined with delta winglet vortex generator', *Applied Thermal Engineering* **111**, 586–598.

Lyman, A., Stephan, R., Thole, K. A., Zhang, L. and Memory, S. (2002), 'Scaling of heat transfer coefficients along louvered fins', *Experimental Thermal and Fluid Science* **26**(5), 547–563.

Mahmood, G., Hill, M., Nelson, D., Ligrani, P., Moon, H.-K. and Glezer, B. (2000), 'Local heat transfer and flow structure on and above a dimpled surface in a channel', *J. Turbomach.* **123**(1), 115–123.

Mahmood, G., Hill, M., Nelson, D., Ligrani, P., Moon, H.-K. and Glezer, B. (2001), 'Local heat transfer and flow structure on and above a dimpled surface in a channel', *Journal of turbomachinery* **123**(1), 115–123.

Mahmood, G. and Ligrani, P. (2002), 'Heat transfer in a dimpled channel: combined influences of aspect ratio, temperature ratio, reynolds number, and flow structure', *International Journal of Heat and mass transfer* **45**(10), 2011–2020.

Manglik, R. M. and Bergles, A. E. (1995), 'Heat transfer and pressure drop correlations for the rectangular offset strip fin compact heat exchanger', *Experimental Thermal and Fluid Science* **10**(2), 171–180.

Menter, F. R., Kuntz, M. and Langtry, R. (2003), 'Ten years of industrial experience with the sst turbulence model', *Turbulence, heat and mass transfer* **4**(1), 625–632.

Min, C., Qi, C., Wang, E., Tian, L. and Qin, Y. (2012), 'Numerical investigation of turbulent flow and heat transfer in a channel with novel longitudinal vortex generators', *International Journal of Heat and Mass Transfer* **55**(23-24), 7268–7277.

Modi, A. J. and Rathod, M. K. (2019), 'Comparative study of heat transfer enhancement and pressure drop for fin-and-circular tube compact heat exchangers with sinusoidal wavy and elliptical curved rectangular winglet vortex generator', *International Journal of Heat and Mass Transfer* **141**, 310–326.

Naphon, P. (2007), 'Thermal performance and pressure drop of the helical-coil heat exchangers with and without helically crimped fins', *International Communications in Heat and Mass Transfer* **34**(3), 321–330.

Oneissi, M., Habchi, C., Russeil, S., Bougeard, D. and Lemenand, T. (2019), 'Inclination angle optimization for "inclined projected winglet pair" vortex generator', *Journal of Thermal Science and Engineering Applications* **11**(1), 011014.

Oviedo-Tolentino, F., Romero-Méndez, R., Hernández-Guerrero, A. and Girón-Palomares, B. (2009), 'Use of diverging or converging arrangement of plates for the control of chaotic mixing in symmetric sinusoidal plate channels', *Experimental Thermal and Fluid Science* **33**(2), 208–214.

Prasopsuk, C., Hoonpong, P., Skullong, S. and Promvonge, P. (2016), 'Experimental investigation of thermal performance enhancement in tubular heat exchanger fitted with rectangular-winglet-tape vortex generator', *Engineering and Applied Science Research* **43**, 279–282.

Promvonge, P. (2010), 'Heat transfer and pressure drop in a channel with multiple 60 v-baffles', *International Communications in Heat and Mass Transfer* **37**(7), 835–840.

Promvonge, P. and Skullong, S. (2019), 'Heat transfer augmentation in solar receiver heat exchanger with hole-punched wings', *Applied Thermal Engineering* **155**, 59–69.

Rao, Y., Li, B. and Feng, Y. (2015), 'Heat transfer of turbulent flow over surfaces with spherical dimples and teardrop dimples', *Experimental Thermal and Fluid Science* **61**, 201–209.

Rao, Y., Wan, C. and Xu, Y. (2012), 'An experimental study of pressure loss and heat transfer in the pin fin-dimple channels with various dimple depths', *International journal of heat and mass transfer* **55**(23-24), 6723–6733.

Rush, T., Newell, T. and Jacobi, A. (1999), 'An experimental study of flow and heat transfer in sinusoidal wavy passages', *International journal of heat and mass transfer* **42**(9), 1541–1553.

Sangtarash, F. and Shokuhmand, H. (2015), 'Experimental and numerical investigation of the heat transfer augmentation and pressure drop in simple, dimpled and perforated dimpled louver fin banks with an in-line or staggered arrangement', *Applied Thermal Engineering* **82**, 194–205.

Sarmadian, A., Shafaee, M., Mashouf, H. and Mohseni, S. (2017), 'Condensation heat transfer and pressure drop characteristics of r-600a in horizontal smooth and helically dimpled tubes', *Experimental Thermal and Fluid Science* **86**, 54–62.

Shah (2016), 'Design and prototyping of a solid fuel/liquid oxidizer hybrid rocket engine'.

Siddique, M., Khaled, A.-R., Abdulhafiz, N. and Boukhary, A. (2010), 'Recent advances in heat transfer enhancements: a review report', *International Journal of Chemical Engineering* **2010**.

Singh, P., Pandit, J. and Ekkad, S. V. (2017), 'Characterization of heat transfer enhancement and frictional losses in a two-pass square duct featuring unique combinations of rib turbulators and cylindrical dimples', *International Journal of Heat and Mass Transfer* **106**, 629–647.

Skullong, S., Promvonge, P., Thianpong, C. and Pimsarn, M. (2016), 'Heat transfer and turbulent flow friction in a round tube with staggered-winglet perforated-tapes', *International Journal of Heat and Mass Transfer* **95**, 230–242.

Skullong, S., Thianpong, C. and Promvonge, P. (2015), 'Effects of rib size and arrangement on forced convective heat transfer in a solar air heater channel', *Heat and Mass Transfer* **51**(10), 1475–1485.

Song, K. and Tagawa, T. (2018), 'The optimal arrangement of vortex generators for best heat transfer enhancement in flat-tube-fin heat exchanger', *International Journal of Thermal Sciences* **132**, 355–367.

Song, K.-W. and Wang, L.-B. (2013), 'The effectiveness of secondary flow produced by vortex generators mounted on both surfaces of the fin to enhance heat transfer in a flat tube bank fin heat exchanger', *Journal of Heat Transfer* **135**(4), 041902.

Tamna, S., Skullong, S., Thianpong, C. and Promvonge, P. (2014), 'Heat transfer behaviors in a solar air heater channel with multiple v-baffle vortex generators', *Solar Energy* **110**, 720–735.

Tiwari, S., Maurya, D., Biswas, G. and Eswaran, V. (2003), 'Heat transfer enhancement in cross-flow heat exchangers using oval tubes and multiple delta winglets', *International Journal of Heat and Mass Transfer* **46**(15), 2841–2856.

T'Joen, C., Jacobi, A. and De Paepe, M. (2009), 'Flow visualisation in inclined louvered fins', *Experimental thermal and fluid science* **33**(4), 664–674.

Torii, K. and Yanagihara, J. I. (1989), 'The effects of longitudinal vortices on heat transfer of laminar boundary layers', *JSME international journal. Ser. 2, Fluids engineering, heat transfer, power, combustion, thermophysical properties* **32**(3), 395–402.

Tsynaeva, A. and Nikitin, M. (2016), 'Study of the flow in a channel with dumbbell-shaped dimples', *Procedia Engineering* **150**, 2340–2344.

Turnow, J., Kasper, R. and Kornev, N. (2018), 'Flow structures and heat transfer over a single dimple using hybrid urans-les methods', *Computers & Fluids* **172**, 720–727.

Turnow, J., Kornev, N., Isaev, S. and Hassel, E. (2011), 'Vortex mechanism of heat transfer enhancement in a channel with spherical and oval dimples', *Heat and mass transfer* **47**(3), 301–313.

Vorayos, N., Katkhaw, N., Kiatsiriroat, T. and Nuntaphan, A. (2016), 'Heat transfer behavior of flat plate having spherical dimpled surfaces', *Case Studies in Thermal Engineering* **8**, 370–377.

Wall, T., Liu, Y., Spero, C., Elliott, L., Khare, S., Rathnam, R., Zeenathal, F., Moghtaderi, B., Buhre, B., Sheng, C. et al. (2009), 'An overview on oxyfuel coal combustion—state of the art research and technology development', *Chemical engineering research and design* **87**(8), 1003–1016.

Wang, C.-C., Lo, J., Lin, Y.-T. and Wei, C.-S. (2002), 'Flow visualization of annular and delta winlet vortex generators in fin-and-tube heat exchanger application', *International Journal of Heat and Mass Transfer* **45**(18), 3803–3815.

Wang, C., Fu, W. and Chang, C. (1997), 'Heat transfer and friction characteristics of typical wavy fin-and-tube heat exchangers', *Experimental thermal and fluid science* **14**(2), 174–186.

Wang, S., Du, W., Luo, L., Qiu, D., Zhang, X. and Li, S. (2018), 'Flow structure and heat transfer characteristics of a dimpled wedge channel with a bleed hole in dimple at different orientations and locations', *International Journal of Heat and Mass Transfer* **117**, 1216–1230.

Webb, R. L. and Kim, N. (2005), 'Enhanced heat transfer', *Taylor and Francis, NY* .

Wu, J. and Tao, W. (2007), 'Investigation on laminar convection heat transfer in fin-and-tube heat exchanger in aligned arrangement with longitudinal vortex generator from the viewpoint of field synergy principle', *Applied Thermal Engineering* **27**(14-15), 2609–2617.

Wu, J. and Tao, W. (2008), 'Numerical study on laminar convection heat transfer in a channel with longitudinal vortex generator. part b: Parametric study of major influence factors', *International Journal of Heat and Mass Transfer* **51**(13-14), 3683–3692.

Wu, J. and Tao, W. (2012), 'Effect of longitudinal vortex generator on heat transfer in rectangular channels', *Applied Thermal Engineering* **37**, 67–72.

Xie, G., Liu, J., Ligrani, P. M. and Zhang, W. (2013), 'Numerical analysis of flow structure and heat transfer characteristics in square channels with different internal-protruded dimple geometrics', *International journal of heat and mass transfer* **67**, 81–97.

Xie, S., Liang, Z., Zhang, L. and Wang, Y. (2018), 'A numerical study on heat transfer enhancement and flow structure in enhanced tube with cross ellipsoidal dimples', *International Journal of Heat and Mass Transfer* **125**, 434–444.

Xie, Y., Qu, H. and Zhang, D. (2015), 'Numerical investigation of flow and heat transfer in rectangular channel with teardrop dimple/protrusion', *International Journal of Heat and Mass Transfer* **84**, 486–496.

Yang, J. S., Jeong, M., Park, Y. G. and Ha, M. Y. (2019), 'Numerical study on the flow and heat transfer characteristics in a dimple cooling channel with a wedge-shaped vortex generator', *International Journal of Heat and Mass Transfer* **136**, 1064–1078.

Yongsiri, K., Eiamsa-Ard, P., Wongcharee, K. and Eiamsa-Ard, S. (2014), 'Augmented heat transfer in a turbulent channel flow with inclined detached-ribs', *Case Studies in Thermal Engineering* **3**, 1–10.

Yoon, H. S., Park, S. H., Choi, C. and Ha, M. Y. (2015), 'Numerical study on characteristics of flow and heat transfer in a cooling passage with a tear-drop dimple surface', *International Journal of Thermal Sciences* **89**, 121–135.

Zhou, G. and Feng, Z. (2014), 'Experimental investigations of heat transfer enhancement by plane and curved winglet type vortex generators with punched holes', *International Journal of Thermal Sciences* **78**, 26–35.

Zhou, G. and Ye, Q. (2012), 'Experimental investigations of thermal and flow characteristics of curved trapezoidal winglet type vortex generators', *Applied Thermal Engineering* **37**, 241–248.

Zilliac, G. and Karabeyoglu, M. (2006), Hybrid rocket fuel regression rate data and modeling, *in* '42nd AIAA/ASME/SAE/ASEE Joint Propulsion Conference & Exhibit', p. 4504.

Appendix A

Modeling of mass efflux from boundary

In general, solid substance exposed to high temperature flow can be divided into three phases viz, preheat phase, infinite body pyrolysis phase and finite body pyrolysis phase. A fraction of external heat flux is getting absorbed into the fuel and remaining lost to the surroundings as convective and radiative losses. The net normal heat flux in to the boundary surface is obtained by subtracting surface losses from the heat flux from external ambient, wherein radiation losses can be modelled along with convective losses.

Net surface heat flux = External heat flux − Surface losses

$$q_n = q_a - h_{eff}(T_s - T_a) \tag{A.1}$$

where h_{eff} is the effective heat transfer coefficient for combined convective and radiative heat losses and the ambient temperature T_a is obtained from the solution of the external compressible turbulent ambient flow field.

As a result of this absorbed flux on the surface, its temperature increases gradually with time. Melting of fuel starts when it reaches the ignition temperature. In case of sublimating fuels/liquifying materials like naphthalene, paraffin wax or frozen methane, it directly changes from solid phase to gaseous vapour or liquid droplets.

Major assumptions in the present study are one dimensional heat conduction through the material and constant thermal properties in the domain. As a general case, decomposition of a charring material is considered here initially and later adapted for a noncharring pyrolysis model. Decomposition of charring materials can be split into char layer, pyrolysis front and virgin layer

Mathematical model for species mass efflux from the surface is developed based on energy balance at its boundary.
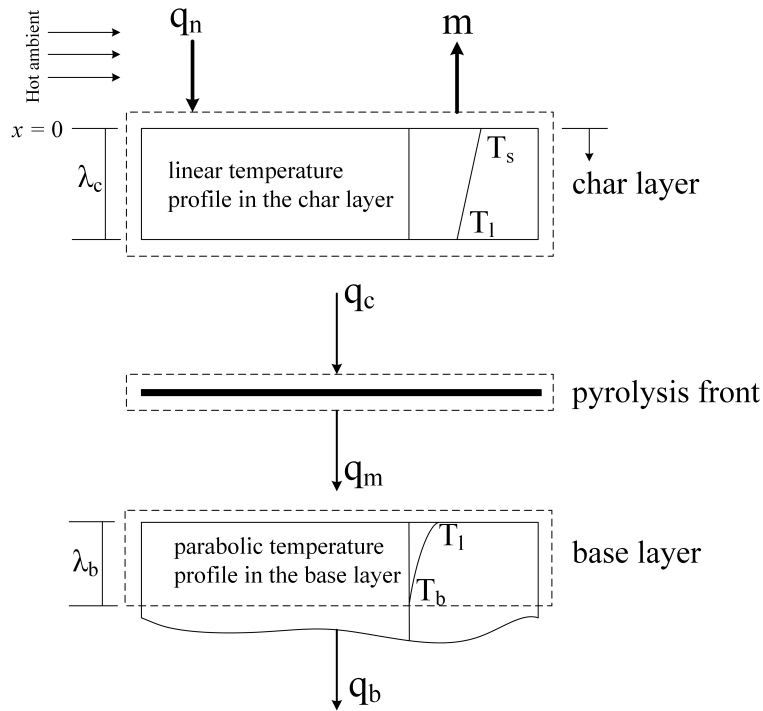
Fig. A.1 Control volumes of different decomposition layers

Mass flux of the escaping gas from the solid fuel

$$m = \rho_g v_g \tag{A.2}$$

Conservation of energy on the char layer is calculated as

$$\rho_c c_c \frac{d}{dt} \int_0^{\lambda_c} (T - T_l) dx + m c_g (T_s - T_l) = q_n - q_c \tag{A.3}$$

where λ_c is the depth of char layer formed on the boundary and q_c is the heat conducted in to the subsequent pyrolysis layer below the char layer.

Conservation of mass on the melt layer

$$(\rho_b - \rho_c - \rho_g) \frac{d\lambda_c}{dt} = \rho_g v_g \tag{A.4}$$

typically

$$\rho_g \ll \rho_c \tag{A.5}$$

So

$$(\rho_b - \rho_c)\frac{d\lambda_c}{dt} = m \tag{A.6}$$

Conservation of energy on the melt layer is calculated as

$$\rho_b \frac{d\lambda_c}{dt}\Delta H = q_c - q_m \tag{A.7}$$

where ΔH is the latent heat of fusion of the solid material and q_m is the heat conducted in to the subsequent solid layer below the pyrolysis layer.

Conservation of energy on the base solid material is calculated as

$$\rho_b c_b \int_0^{\lambda_b} (T(x',t) - T_b)dx' + \rho_b c_b \frac{d\lambda_b}{dt}(T_l - T_b) = q_m \tag{A.8}$$

Temperature profile on char layer is assumed to be linear (shown in Fig A.1)

$$T - T_l = (T_s - T_l)(1 - \frac{x}{\lambda_c}) \tag{A.9}$$

satisfying the boundary conditions $T = T_s$ at $x = 0$ and $T = T_l$ at $x = \lambda_c$

Temperature profile on base layer is assumed to second order (shown in Fig A.1)

$$T - T_b = (T_l - T_b)(1 - \frac{x'}{\lambda_b})^2 \tag{A.10}$$

satisfying the boundary conditions $T = T_l$ at $x' = 0$ and $T = T_b$ at $x' = \lambda_b$

With these temperature profiles, we get

$$\frac{m}{1 - \phi}\Delta H = \frac{k_c}{\lambda_c}(T_s - T_l) - 2\frac{k_b}{\lambda_b}(T_l - T_b) \tag{A.11}$$

Surface will be attaining the melting temperature during the process and it leads to the mass entrainment of liquefying substance

In the present case, no need to consider char fraction for a sublimating/liquefying substance as it does not develop a char layer

Therefore,

$$m = 2\frac{k_b}{\Delta H \lambda_b}(T_b - T_l) \tag{A.12}$$

This is the expression for mass efflux in gaseous form from the boundary towards the flowfield, in terms of temperature gradient developed in the solid substance, when it is exposed to a hot ambient

Appendix B

Application of the method of images

Detailed analysis of vortical fluid motion revealed the relation between longitudinal vortex interaction and location of peak mass efflux for a base VG and lateral sweep VG. Now, the focus is on trajectories of longitudinal vortices and the related mass transfer. Analysis of secondary flow field can characterize the vortices and estimate its trajectory.

Secondary flow field showing the vortices generated downstream of vortex generator from the numerical study conducted is shown in Fig B.1. From this image, two important dimensions can be determined, viz. vortex core to core distance (2C) and core to plate (p). The core to core distance is the distance between centers of counter rotating vortex pair generated. Core to plate distance is the distance between plate surface to center of vortex pairs. These two dimensions can be used along with potential flow theory to obtain the circulation of the vortices
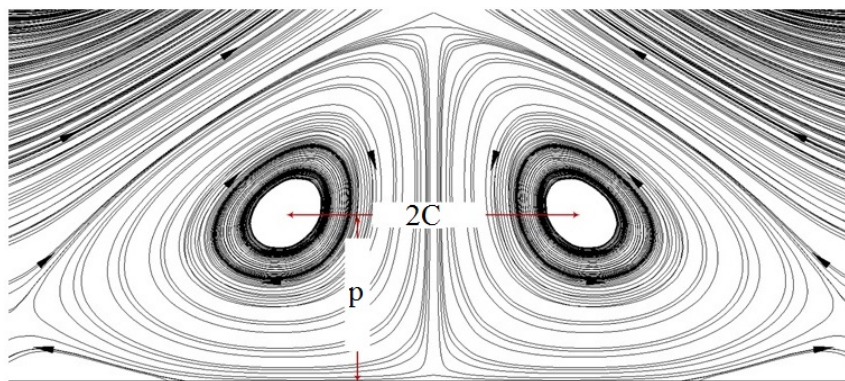

Fig. B.1 Secondary flow field to identify the circulation, Γ

The location and interaction of vortices on the boundary has significant effect on the mass transfer. Enhancement of mass transfer in a flow field depends on the circulation developed by the streamwise vortices. The circulation of vortex determines how the vortex enhances
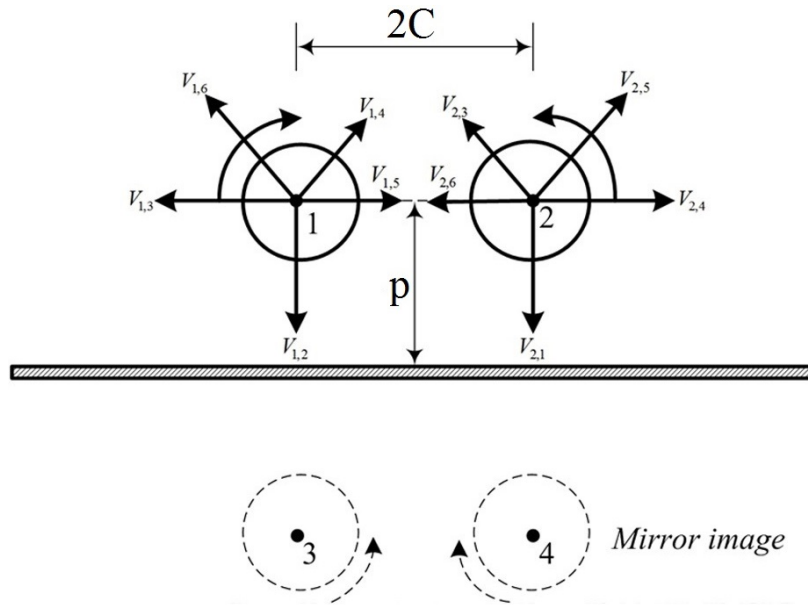
Fig. B.2 Schematic showing the induced motion of two real vortices above a flat plate

mass transfer. Higher the vortex strength, there is bulk mixing, and hence higher mass transfer. Vortex circulation can be obtained by simplified potential flow model. By using potential flow theory, the plate surface can be modeled by introducing a mirror image of vortex with circulation equal and opposite to the real vortex.

The vortex strength is measured by potential flow theory. The magnitude of induced core velocity for vortex 1 in y direction is given by

$$V_{1,y} = \frac{\Gamma}{4\pi p} \tag{B.1}$$

which shows that for a stronger vortex and one that is closer to the wall, induced core velocity will be greater. Core to- core (2C) and core-to-plate (p) distances were determined from images of vortices as shown in Fig B.1, taken at different streamwise locations in front of the VG (Fig B.1). Referring to Fig B.2, vortex 1 has a velocity in the y direction due to its induced velocities from vortices 3 and 4. Using Eqn B.1, superposition, and basic trigonometric relations, the y velocity of vortex 1 can be written as follows:

$$V_{1,y} = \frac{\Gamma}{4\pi p} \left(\frac{\phi^2}{\phi^2 + 1} - 1 \right) \tag{B.2}$$

Induced velocity can also be expressed as

$$V_{1,y} = \frac{\Delta y}{\Delta t} \tag{B.3}$$

With an assumption that the vortex moves axially with a convective velocity equal to the free-stream velocity, the transit time can be approximated as

$$\Delta t = \frac{\Delta x}{V} \tag{B.4}$$

Substitute and rearranging gives, circulation as

$$\Gamma = 4\pi\eta(1+\phi^2)V \tag{B.5}$$

where, $\phi = p/C$, $\eta = \Delta y/\Delta x$

Circulation is estimated from the numerical results either by taking the line integral for the velocity field or the surface integral of vorticity over an area enclosing the vortex, hence circulation is

$$\Gamma = \oint_S \vec{v}\,d\vec{s} = \int_y \int_z \xi_x dydz \tag{B.6}$$
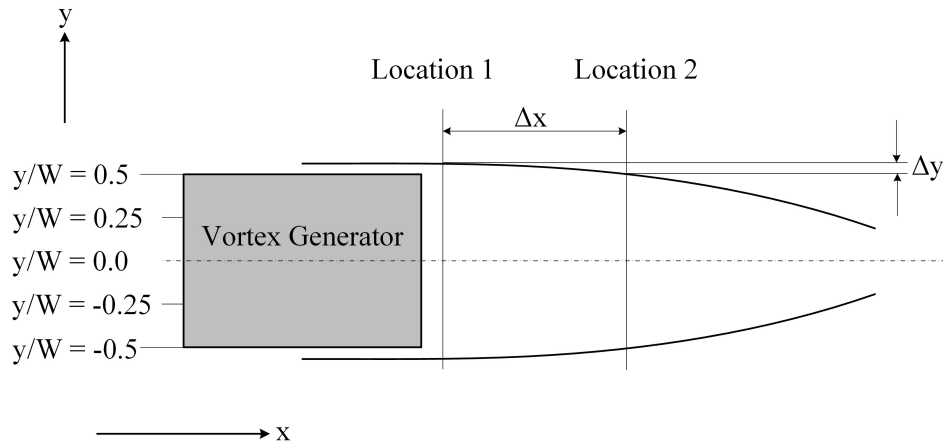

Fig. B.3 Conceptual sketch showing the path followed by the vortices downstream of the vortex generator.

Assuming that the vortex trajectory is directly related to the lateral position of the maximum mass transfer, Eqn B.5 can be validated with the present numerical results. Data required to determine the lateral drift $\Delta y/\Delta x$ can be extracted from different transverse plane infront of vortex generator (similar to Fig B.1). This lateral drift in the vortices generated is directly related to the mass transfer distribution.

With this knowledge maximum mass transfer distribution can be obtained by analyzing strength of secondary flows generated. Simple assumptions can lead to approximate characterization of flow field. Lateral drift in the vortex core and position of peak mass transfer ahas one to ne correlation and it is established in chapter 4.

List of publications

International Journals

- **Aravind, G.P.** and Deepu, M., 2017. Numerical Study on Convective Mass Transfer Enhancement by Lateral Sweep Vortex Generators. *International Journal of Heat and Mass Transfer*, **115**, pp.809-825.
  (https://doi.org/10.1016/j.ijheatmasstransfer.2017.07.104)

- **Aravind, G.P.**, Rafi, K.M. and Deepu, M., 2017. Numerical Study on Passive Convective Mass Transfer Enhancement. *In Journal of Physics: Conference Series* (Vol. **822**, No. 1, p. 012064). IOP Publishing.
  (doi:10.1088/1742-6596/822/1/012064)

- **Aravind, G.P.**, Gokul, S., and Deepu, M., 2019. Numerical Study on Convective Heat Transfer Enhancement by Vortex Interactions, *Computational Thermal Sciences*, **11**(3) 255–268
  (doi: 10.1615/ComputThermalScien.2018021278)

- **Aravind, G.P.** and Deepu, M., 2019. Convective Mass Transfer Enhancement in High Speed Flows with a Dimple Surface placed in the Wake of a Lateral Sweep Vortex Generator. *International Journal of Thermal Sciences* (Revised submission under review)

Conference Proceedings

- **Aravind. G. P.**, Deepu M, Effects of Asymmetrical Vortex Interaction by Variable Swept Vortex Generator (VSVG) on Mass Transfer Enhancement, *4th Thermal and*

Fluids Engineering Conference (TFEC), April 14-17, 2019, Las Vegas, NV, USA (doi: 10.1615/TFEC2019.hte.027755)

- **Aravind G P**, Deepu M, Effects of Unsymmetrical Vortex Interaction by Coupling Lateral Sweep Vortex Generators with Dimpled Surface on Mass Transfer Enhancement, 7th *International and* 45th *National Conference on Fluid Mechanics and Fluid Power (FMFP)*, December 10-12, 2018, IIT Bombay, Mumbai, India

- **Aravind. G. P.**, Deepu M, Numerical Study on Mass Transfer Enhancement by LSVG Coupled with Dimpled Surface, 24th *National and 2nd International ISHMT-ASTFE Heat and Mass Transfer Conference (IHMTC-2017)*, December 27-30, 2017, BITS Pilani, Hyderabad, India.

- **Aravind, G.P.**, Gokul, S. and Deepu, M, Numerical Study on Convective Heat Transfer Enhancement by Vortex Interactions, *International Symposium on Advances in Computational Heat Transfer*, May 28 - June 1, 2017, Napoli, Italy

- **Aravind. G. P.**, Deepu M, Implementation of Temperature Dependent Mass Flux Boundary Condition for Convective Mass Transfer Enhancement Computations, 6th *International and* 43rd *National Conference on Fluid Mechanics and Fluid Power*, December 15-17, 2016, MNNITA, Allahabad, U.P., India

- **Aravind. G. P.**, K M Muhammed Rafi, Deepu M, Numerical Study on Passive Convective Mass Transfer Enhancement, 15th *Asian Congress on Fluid Mechanics, organized by Institution of Engineers*, Malaysia, Nov 21-23, 2016.

- **Aravind. G. P.**, K M Muhammed Rafi, Fahd, Deepu M, Numerical Study on Convective Mass Transfer Enhancement by Baroclinic Torque Induced Vortex, *Sixth International Congress on Computational Mechanics and Simulation*, organized by IIT Bombay, June 27- July 1, 2016